UNIVERSITY OF SOUTHAMPTON

"Late Quaternary History of Red Sea Outflow"

Mia Fenton

Doctor of Philosophy

SCHOOL OF OCEAN AND EARTH SCIENCE

August 1998

This thesis was submitted for examination in August 1998. It does not necessarily represent the final form of the thesis as deposited in the University after examination.
This thesis is the result of work done wholly during registered postgraduate candidature of Mia Fenton.

UNIVERSITY OF SOUTHAMPTON

ABSTRACT

FACULTY OF SCIENCE
SCHOOL OF OCEAN AND EARTH SCIENCE

Doctor of Philosophy

LATE QUATERNARY HISTORY OF RED SEA OUTFLOW

Mia Fenton

A palaeoceanographic study is carried out on cores from the central Red Sea and western Gulf of Aden. Time stratigraphic frameworks are determined using oxygen isotope ratios, from the test of the planktonic foraminifera *Globigerinoides ruber*, and combined with AMS ^{14}C dates. Down-core variations in planktonic and benthic foraminifera, organic carbon content, and $\delta^{13}C$ and $\delta^{18}O$ are used to deliver a comprehensive history of changes in the Red Sea basin during the late Quaternary. The short time span of the Gulf of Aden core 1006 and the presence of a redepositional event in core 1005 rendered both cores unsuitable for the study of glacial Red Sea outflow. Instead the study is focussed on changes in Red Sea circulation and deep water formation relying on evidence provided in the Red Sea cores.

The Red Sea is a marginal basin of the NW Indian Ocean. Today, water exchange with the open ocean only takes place across the shallow Hanish Sill at the Strait of Bab el Mandab. River inflow along with precipitation into the basin is negligible with respect to the high evaporation rate of 200 cm yr^{-1}. Thus, the basin is extremely sensitive to global climate change and sea level variation. Circulation in the basin is anti-estuarine, with a surface water inflow compensated by a subsurface outflow. Surface flow alters seasonally according to the monsoon. During the summer SW monsoon, northwesterly winds over the entire basin drive a south flowing surface current. At this time inflow into the basin continues as a shallow, subsurface current. During the winter NE monsoon, winds are northwesterly, north of 20°N, driving a weak southward surface water flow, and southeasterly to the south, driving a strong northward surface water flow. The result is a zone of surface water convergence at around 25 °N which migrates south as intensity of the SW monsoon increases. Deep water is a 1:1 mixture of Red Sea surface water with Gulf of Suez outflow and is formed mainly in winter in the north of the basin, as well as in the Gulf of Suez.

The waters of the present day Red Sea are oligotrophic, supporting a population of tropical-subtropical, spinose foraminifera dominated by *Globigerinoides ruber* (plate 1) in the south and *Globigerinoides sacculifer* (plate 2) in the north. The species distribution is controlled by their individual dietary requirements and the seasonal availability of food (mainly zooplankton), in turn controlled by the position of the current convergence zone and monsoonal intensity. Cores 1017 and 1039 reveal sediments devoid of planktonic foraminifera (aplanktonic zones) in association with severe glacial maxima (isotope stages 2, 6 and 12). Lithified sediments, aragonitic overgrowth of pteropod tests and increase in relative abundance of Miliolids in the reduced benthic foraminiferal community are also associated with the glacial sediments, indicating elevated salinities in the basin (estimated around 50 ‰). Salinity increase is attributed to restricted communication between the basin and the open ocean, across the shallow sill, resulting from global sea level lowering combined with continued high evaporation (estimated at 200 cm yr^{-1}).

The aplanktonic zones are preceded by a systematic disappearance of planktonic foraminiferal species, where specialised carnivorous feeders (*G.sacculifer* and *Globigerinella siphonifera* (plate 6)) show earlier absence than those able to sustain themselves on limited primary productivity (*G.ruber* and *Globigerinita glutinata* (plate 7)). It is proposed that, owing to increasing NE monsoonal intensity leading up to glacial maxima, a change in primary and secondary productivity distribution in the basin resulted from prolonged inflow of Gulf of Aden waters forcing the northward migration of the surface current convergence zone. This introduced a greater diversity of food to the southern Red Sea and forced the specialised feeders northward.

An anoxic event, associated with the rapid deglaciation following glacial stage 2, is marked by a dark green, virtually foraminifera-free sediment, with elevated TOC levels. This was, likely, deposited beneath a density stratified water column. Rapid increase in relatively fresh surface water inflow from the Gulf of Aden combined with increased humidity and precipitation over the region, with possible land run-off via wadi systems on the Arabian peninsula, resulted in strong density stratification. This impeded mixing and deep water formation in the north, resulting in stagnation of the bottom waters. Dysaerobic intervals are associated with stage 3, and possibly mid-stage 6. This is inferred from $\delta^{13}C$ ratios in benthic foraminiferal tests, lack of epifauna, and the dominance of species indicative of highly saline, oxygen-poor waters. In accordance, pteropod tests imply a shallow mixed layer. Deep water formation was impeded by an intensified SW monsoon, combined with the exposure of the Gulf of Suez as dry land and consequential loss of well oxygenated Gulf of Suez outflow.

Aplanktonic zones, implying glacial Red Sea salinity around 50 ‰, and the reduction of planktonic foraminiferal numbers through time, indicating increasing isolation and salinisation of the basin, are the basis of global sea level low stand calculations. Combining the critical sill depth (18 ±5 m) required to achieve a glacial salinity of 50 ‰ (calculated using hydraulic control and conservation of mass and salt arguments) with the sill uplift rate (0.05 m yr^{-1}), sea level low stands of 120 ±5 m (stage 2), 125 ±6 m (stage 6), 120 ±8 m (stage 8), 134-122 ±9 m (stage 10) and 139 ±11 m (stage 12) are estimated.

Contents.

Chapter 7 - Discussion

Chapter 8 - Conclusions and Further Work

References

Species, plates and taxonomy

cd-rom containing raw data files

List of Figures.

Chapter 7 - Discussion

List of Tables.

Acknowledgements.

Firstly, I would like to thank Dr. Eelco J. Rohling for his excellent supervision, support and guidance throughout.

Thanks are also extended to Dr. Jean-Pierre Caulet and the National Museum of Natural History in Paris for provision of the material used in this project and support during the sampling phase.

Analytical support was provided by Dr. Philippe Bertrand and Max Dignan, at the university of Bordeaux and Shir at Southampton University during TOC analyses; Dr. Simon Troelstra, Dr. Gerald Ganssen and Hubert Vonhof at the University of Amsterdam during stable isotope analyses; Dr. Frans Jorissen, Ingride, Marianne and Mariette, at the university of Bordeaux during my training in benthic foraminiferal identification; and Dr. Richard Pearce during SEM imagery.

This research was supported by the Natural Environmental Research Council.

Personal thanks are expressed to Mum and Dad for their endless encouragement and financial support throughout, as well as to Darryl for his care and understanding, and for sacrificing the majority of his weekends to come 300 miles to Southampton without any complaints.

Special thanks go to my top house mate and landlady, Dr. Barbs, and to Ruthie sci-fi-queen Parker for being generally out of this world and my other top housemate - 5 Cambridge Road will live on in my heart (and probably in my pores)! Special thanks must also go to my favourite lab-mate: Ang, for making the trips to Paris, Amsterdam, and San Fran such a laugh, and for being the perfect picking partner in those long days behind the microscope. I do believe that without you (and the quality radio) I would have turned into a foram!

Finally to my "fancy a break?" mates: Top GT thanks must go to Mark and Jon for being ever ready to have a break from work and become "down-hill-demons" for a day (- those Sunday bikers; we certainly showed them!), and to Tracey and her endless supply of beer, wine, food and top Anne Rice novels. I must also add that lunch, coffee and Friday nights would never have been the same, or as long, without Sarah, Cathy, Craig and Tim, and the rest of the bunch at SOC. Cheers!

Chapter 1.

INTRODUCTION

This chapter introduces the scope of this thesis and sets the objectives.

The Red Sea is a marginal basin, separated from the northwest Indian Ocean by the Hanish Sill at the Strait of Bab el Mandab. Water exchange between the basin and the open ocean takes place across this shallow sill (105 km wide, minimum depth 137 m (Werner and Lange, 1975)), and through a narrow channel close to Perim Island (20 km wide, 300 m deep (Morcos, 1970)). Negligible land drainage and precipitation with respect to very high evaporation rates (200 cm yr^{-1} (Morcos, 1970; Maillard and Soliman, 1986) over the entire Red Sea, results in a convective anti-estuarine basin circulation, with surface water inflow compensated by a subsurface outflow across the sill. The restricted nature of this basin makes it extremely sensitive to global oceanographic change (eg. climate, sea-level).

This study concerns micropalaeontological, total organic carbon, and isotope analysis of two cores from the central Red Sea and two from the western Gulf of Aden, to investigate in detail the palaeoceanographic history of the region. Previously, the 120 m global sea level lowering during the last glacial maximum (LGM) (18 k BP) (Fairbanks, 1989) has been suggested to have caused great changes within the Red Sea basin through great reduction in the water exchange across the shallow and narrow sill. Sea level induced reduction of exchange transport is thought to have caused a salinity crisis in the basin throughout the last glaciation (Locke, 1984; Locke and Thunell, 1987; Thunell et al., 1988), although Deuser et al. (1976) suggest that it was caused by higher evaporation rates over the area at this time. Previous studies, using micropalaeontological and oxygen isotope data, have estimated salinities for this period at approximately 50 ‰, beyond the tolerance of planktonic foraminifera, so that an aplanktonic zone developed (Deuser et al., 1976; Schoell and Risch, 1976; Ivanova, 1985; Locke, 1984; Locke and Thunell, 1987; Thunell et al., 1988; Almogi-Labin et al., 1991; Rohling, 1994; Hemleben et al., 1996). The present study aims to compare and contrast detailed information of previous glacial maxima in the Red Sea, with

the LGM, including a deep investigation into the nature of aplanktonic zones, as well as to provide detailed information of glacial-interglacial changes in the basin.

During glacial times, as today, an anti-estuarine circulation pattern is thought to have prevailed in the Red Sea, with high salinity deep water escaping from the basin over the sill as a subsurface flow (Locke, 1984; Locke and Thunell, 1987; Thunell et al., 1988; Almogi-Labin, 1991; Rohling, 1994). The fate of the glacial Red Sea outflow in the adjacent Gulf of Aden, close to the Strait of Bab el Mandab has not before been studied. The present study was intended to highlight changes in the fate of Red Sea out flow through investigation of cores from the Red Sea and Gulf of Aden.

1.1 Specific Objectives.

- To determine variations in planktonic foraminiferal assemblages throughout cores 1017 and 1039 (central Red Sea), and cores 1005 and 1006 (western Gulf of Aden), to portray changes in surface water characteristics.
- To determine variations in benthic foraminiferal assemblages throughout cores 1017 and 1039 to portray changes in Red Sea bottom water characteristics.
- To determine oxygen isotope concentrations for the planktonic foraminiferal species *Globigerinoides ruber* in each core to create a time frame for the core sediments. Further dating evidence is obtained from AMS ^{14}C analyses. The oxygen isotope data are also used to estimate changes in the fresh water budget.
- To determine organic carbon variations within the down-core sediment as an indication of changes in productivity and / or bottom water oxygen concentrations.
- To combine these data and use them in combination with previously published results and detailed time stratigraphic assessment for each core, to portray changes in the circulation of the Red Sea basin and the influence of Red Sea outflow on the Gulf of Aden and NW Indian Ocean. (NB. Owing to unfortunate major re-sedimentation observed in the Gulf of Aden cores, this study places particular emphasis on the history of dense water formation and its fate within the Red Sea.

Chapter 2.

OCEANOGRAPHY OF THE REGION

This chapter discusses the bathymetry, climatology and oceanography of the region.

2.1 Bathymetry.

The Red Sea and Gulf of Aden are young ocean basins that initially opened around 10 million years ago (Bally, 1979), developing in two main stages. There was an initial pre-Miocene uplift and lateral extension phase, resulting in uplift and crustal thinning, volcanism and eventual formation of the Red Sea rift. This was followed by sea floor spreading during the Pliocene resulting in the formation of the axial trough (Ross and Schlee, 1973).

2.1.1 The Red Sea.

The Red Sea consists of a long, narrow basin, orientated north-northwest - south-southeast between 30° 00' N and 12° 30' N (figure 2.1). It is approximately 1932 km long and on average 280 km wide (Morcos 1970). Kossinna (1921) estimated its area to be 0.438×10^6 km^2 and its volume to be $0.215\times10^6 km^3$. This was updated by Muromtsev (1960) who estimated values of $0.450\times10^6 km^2$ and $0.251\times10^6 km^3$, respectively.

In the north the Red Sea branches into two gulfs, the Gulf of Suez and the Gulf of Aqaba. The Gulf of Suez is a shallow shelf sea with a depth of 55 to 73 m. Its entrance to the Red Sea is marked by a rapid five-fold increase in depth (Morcos, 1970). The Gulf of Aqaba is a deep basin with narrow shelves. A sill 300-340 m deep (Reiss & Hottinger 1984), divides the basin into two depressions. The northern depression is approximately 1100 m deep and the southern depression reaches 1420 m depth. Another sill, of 311 m depth, separates the Gulf of Aqaba from the Red Sea (Morcos, 1970).

The bathymetry of the Red Sea itself can be divided into four zones; the 'coral reef zone', the 'coastal shelves', the 'main trough', and the 'axial trough' (table 2.1). Within the 'axial trough' zone the so-called 'hot brine region' of the Red Sea is distinguished (Morcos, 1970).
In the south, the Red Sea is connected to the Gulf of Aden and Arabian Sea by the Strait of

Figure 2.1

Bathymetric map of the Red Sea
(depth in metres)

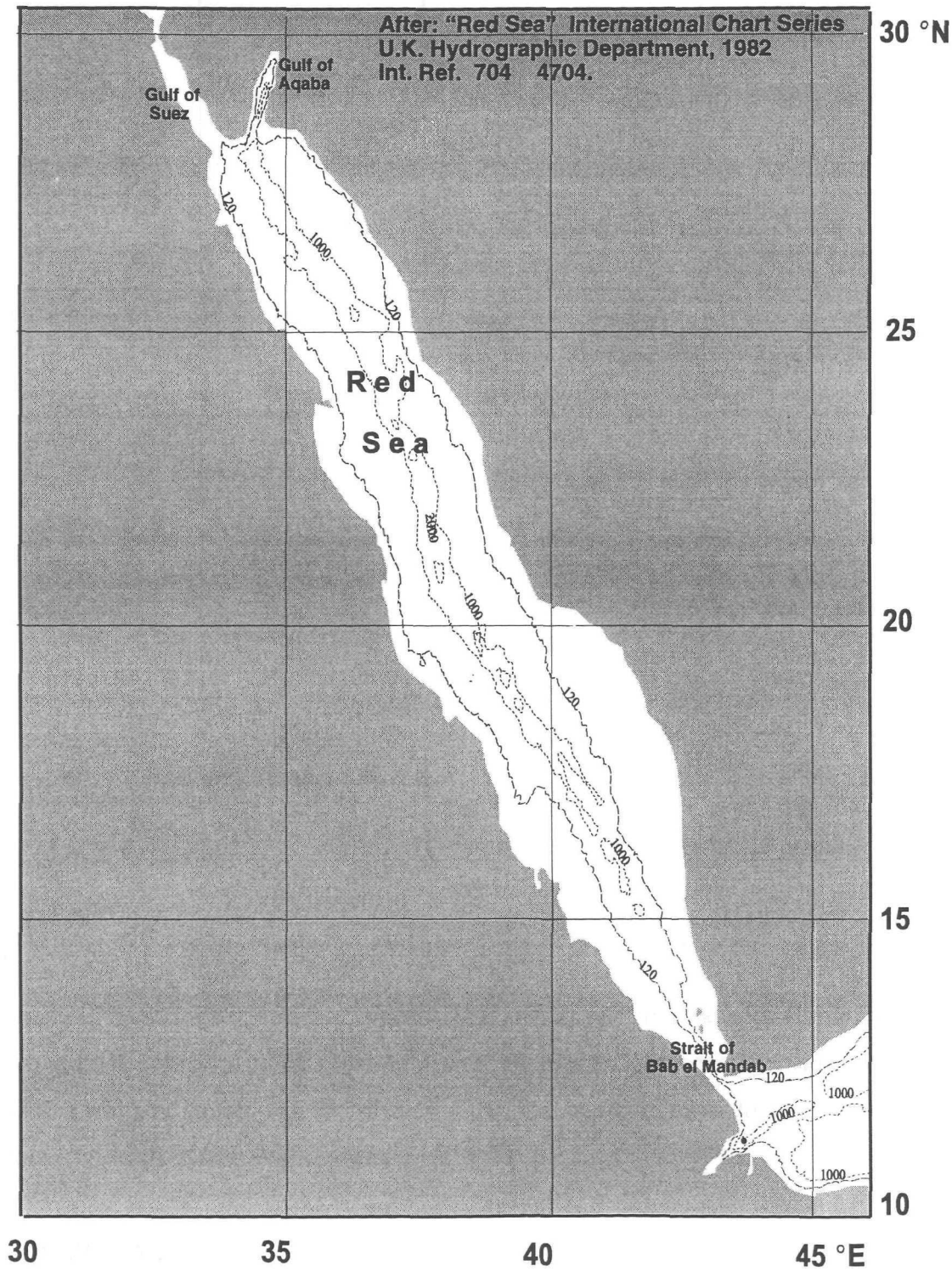

Table 2.1. Bathymetric zones of the Red Sea Proper (Morcos, 1970).

	Zone.	Depth.	Characteristics.
I	**'Coral Reef Zone'.**	<50 m.	Elevated shore reefs, barrier reefs, fringing reefs and pinnacle reefs. Southern half of the Red Sea is thickly beset with reefs leaving only a deep, narrow, central passage clear for navigation. Northern half of the Red Sea has fewer reefs, most around the entrance to the Gulf of Suez and Gulf of Aqaba.
II	**'Narrow Coastal Shelves'.**	Descend in a series of steps about 100-400 m in height.	On both sides of the northern Red Sea there are some reefless coasts which fall immediately into deep water. South of 19 ^{0}N the coastal shelves increase in width.
III	**'Main Trough'.**	>1000 m.	From 15 ^{o}N to the southern tip of the Sinai Peninsula. Isolated deeps are found between 26 and 23 ^{o}N. The deepest is the Mabahiss Deep which is >2300 m.
IV	**'Axial Trough'.**	>1100 m.	Situated between 23 and 17 ^{o}N. It is >2000 m deep and 20 km wide in places. The width of the trough increases to the south.
IVa	**'The Hot Brine Region'.**		Situated within the axial trough, between 21^{o} 10' N and 2 ^{o} 30' N. It is made up of three depressions which contain anomalously high temperature and high salinity water. The largest of the three depressions is the Atlantis II Deep. The smallest is the Chain Deep which was discovered between the Atlantis II Deep and the Discovery Deep. The depressions are connected by a narrow channel, but mixing of the hot brine solutions only occurs between the Atlantis II Deep and the Chain Deep, as the sill separating Discovery Deep from Chain Deep is too high.

Bab el Mandab (figure 2.2). The passage consists of two channels separated by Perim Island. The narrow main channel is around 20 km wide and 300 m deep. This passage widens northward to a width of around 105 km at 13°30' N but the depth decreases to a minimum of 137 m close to Hanish Island (Werner and Lange, 1975).

2.1.2 The Gulf of Aden.

Bathymetrically, the Gulf of Aden (figure 2.3) consists of three zones: the continental shelf,

Figure 2.2

Bathymetric Map of the Straits of Bab el Mandab
(depth in metres)

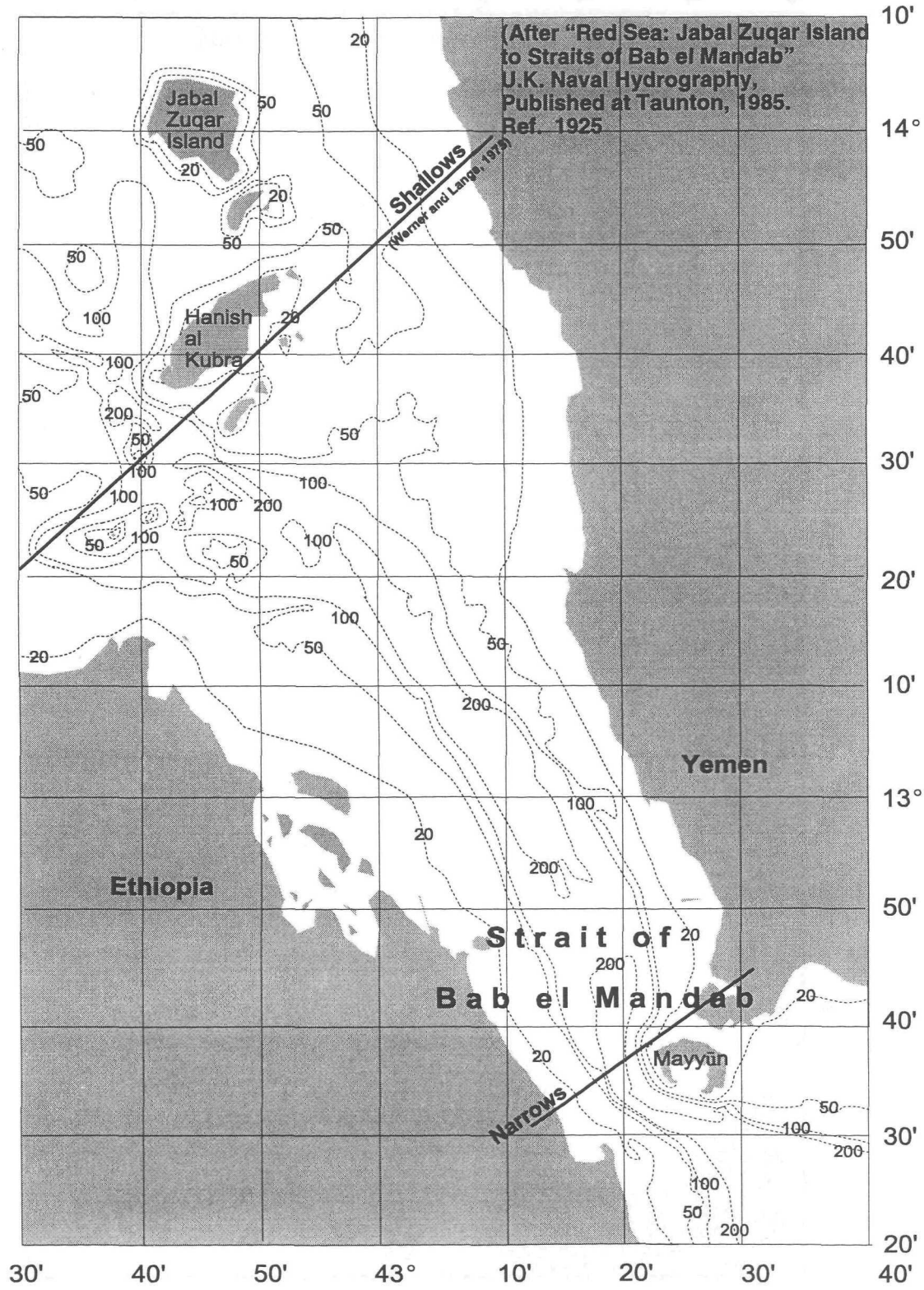

Figure 2.3

Bathymetric map of the Gulf of Aden
(depth in metres)

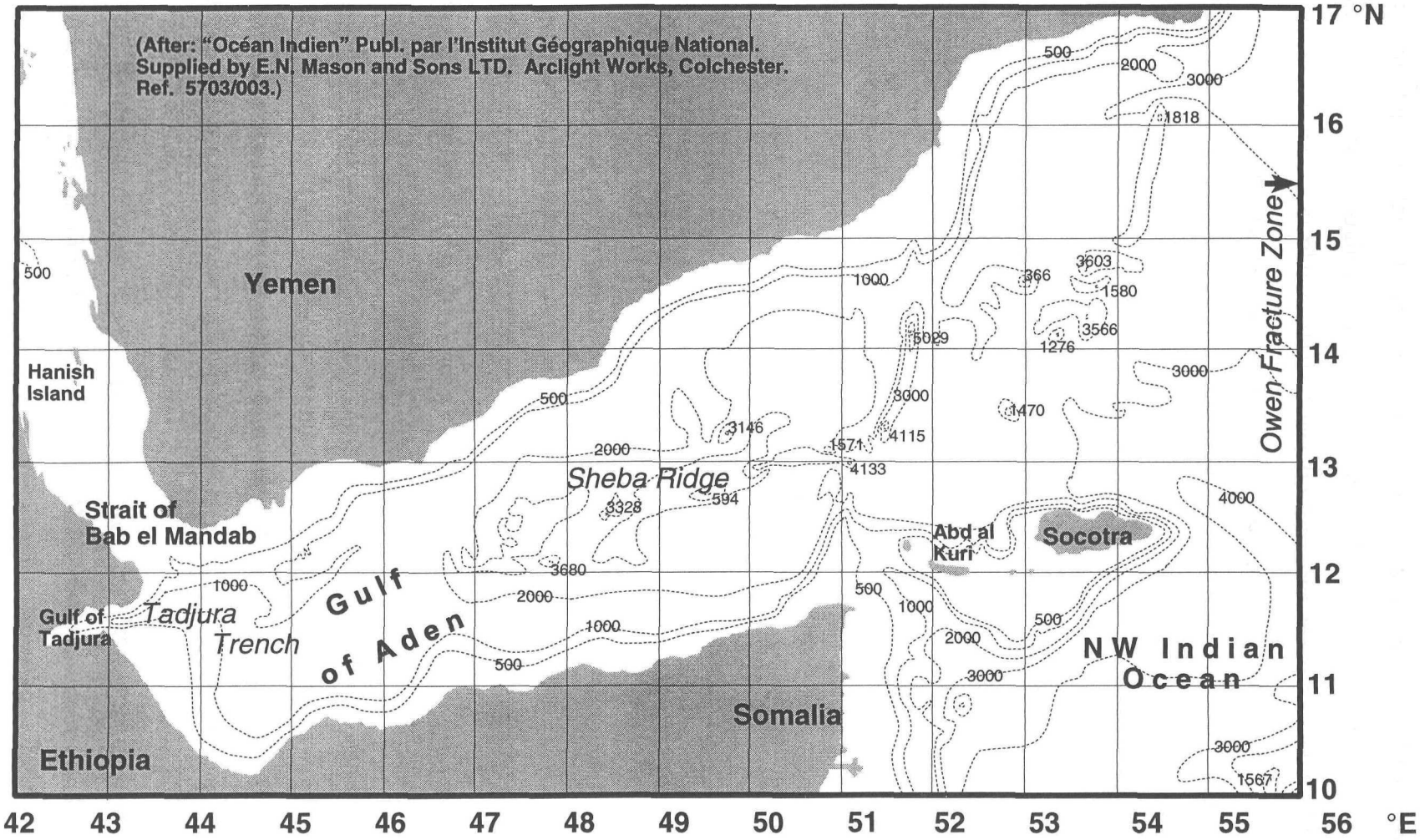

the continental slope, and the main trough. The continental shelf is narrow off the African coast, and wider along the Arabian coast, towards Oman. The slope descends steeply into the trough, which deepens eastward towards the Owen fracture zone, reaching depths >4000 m. The western sector of the trough is represented by the Tadjura Trench, reaching depths greater than 1000 m. This trench is terminated, at approximately 45° E, by the rough topography of the West Sheba Ridge and its median valley (Beydoun, 1982). The West Sheba Ridge belongs to the mid-Indian Ocean Ridge system, and links the Carlsberg Ridge to the East African Rift and the Red Sea (Schlich, 1982).

2.2 Climate and Circulation

2.2.1 The Red Sea

The Red Sea basin is situated in an arid region with very low humidity. Coastal stations record annual rainfall figures of less than 20 mm in the north and 50 to 100 mm in the south (Pedgley, 1974). Riverine flow into the basin is negligible (Morcos, 1970, Maillard and Soliman, 1986). Evaporation is very high at 2000 mm yr^{-1} resulting in a loss of 0.03 Sv ($1Sv=10^6 m^3 s^{-1}$) over the total area of the Red Sea (Morcos, 1970; Maillard and Soliman, 1986). Hence, precipitation and run-off combined are negligible with respect to evaporation over the basin (Morcos, 1970; Pedgley, 1974; Maillard and Soliman, 1986).

Circulation in the Red Sea basin is governed by thermohaline forcing, determined by evaporation, coupled with wind stress over the sea surface (Eshel et al., 1994). The resultant circulation is of an 'antiestuarine' or 'lagoonal' type, with a surface water inflow in exchange with deep water outflow (Dyer, 1973) through the Strait of Bab el Mandab (figures 2.4 and 2.5). The bottom waters of such basins tend to be young, resulting in highly oxygenated waters, usually close to calcium carbonate saturation, while surface water salinities are high as a result of the high evaporation (Dyer, 1973; Kennett, 1982).

North of 25°N, north-northwesterly winds prevail over the basin throughout the year. The wind regime over the southern Red Sea (south of 25 °N) is heavily influenced by the monsoon, as are the climate and circulation of the north Indian Ocean region (see section 2.2.2). To the south the winds remain north-northwesterly throughout the summer, SW

Figure 2.4

Schematic Circulation of the Red Sea in Winter (Northeast Monsoon).

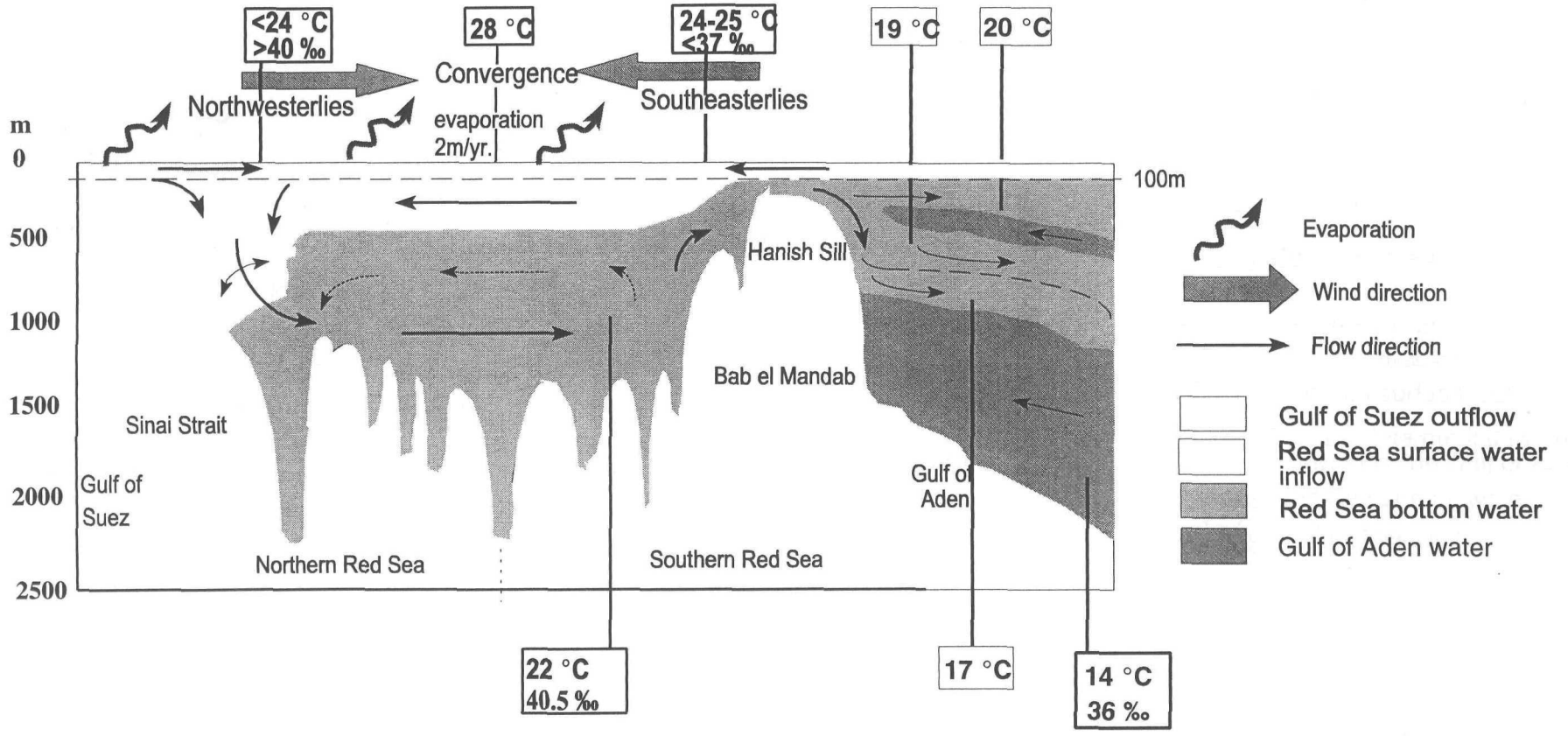

Maximum sea surface temperature is found at around 20 °N, and decreases away both to the north and to the south. Surface water salinity shows a distinguished northward increase from <37 ‰ to >40 ‰.This salinity gradient persists throughout the year.
Vertical temperature decreases with depth, and the thermocline is weak and may degenerate during winter. Vertical salinity generally increases with depth with the steepest gradient in the upper 200 m. Below approximately 200 m depth the water is isothermal and isohaline.

Data from Siedler, 1968 and Maillard and Soliman, 1986.

Figure 2.5

Schematic Circulation of the Red Sea in Summer (Southwest Monsoon).

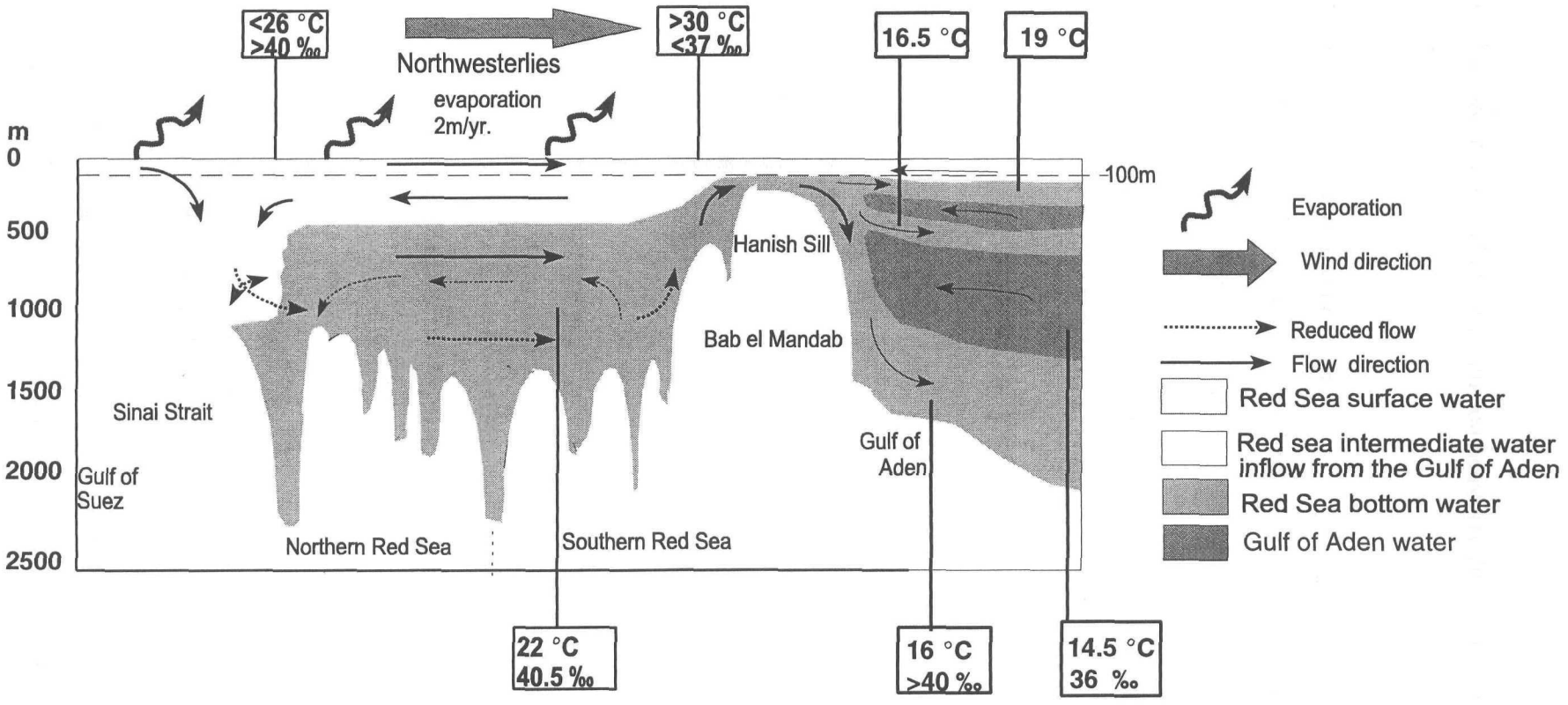

The maximum sea surface temperature is found around 20 °N and remains similar to the south. Northward the temperature decreases to <26 °C. The vertical temperature gradient is steep in the upper 200 m of the water column, distinguishing the thermocline. Below this the water is isothermal. The thermocline extends between 50 and 150-200 m depth, and is strongest around 18-25 °N, below the zone of maximum surface temperature,. Salinity remains relatively constant throughout the year, with a marked increase northward in the surface waters, and isohaline water below 200 m depth.

Data from Siedler, 1968 and Maillard and Soliman, 1986.

monsoon (June-September), but are south-southeasterly during the winter, NE monsoon (October-May).

2.2.2 The present day monsoon regime.

The monsoon is a result of the interaction of the annual cycle of solar radiation, albedo, and the differential effective heat capacities of land masses and oceans, causing a reversal in wind direction and seasonal heavy monsoonal rainfall. Land masses have a lower specific heat capacity than water, hence they warm up and cool down at a faster rate than a body of water would. Heat radiated from land and water bodies as they cool down, is known as 'sensible heat'.

During the winter season (October to May) the cold landmass of central Asia, in combination with a high albedo (reflection of insolation) resulting from snow cover over the Tibetan Plateau and Himalayas, reduces sensible heat radiation, resulting in a quasi-stable high pressure system. This system extends from Mongolia to central Europe, Turkey and Arabia. The cold, descending air leads to a radial outflow of cold dry air towards the low pressure system over the Indian Ocean. This low pressure system is the result of the higher specific heat capacity of the water body allowing sensible heat radiation to warm the air above, causing it to rise and be transported aloft, cooling along its trajectory, back to the central Asian landmass. The inter-tropical convergence zone (ITCZ) moves southward in winter, in response to the movement of the sun, to 20 °S over E. Africa, and the northeast monsoon blows across the Arabian Sea and the Gulf of Aden towards central Africa (Morcos, 1970). At this time, strong (6.7-9.3 m s^{-1}) winds blow from the south or south-southeast over the southern half of the Red Sea (figure 2.6a), channelled by the rift geometry of the Red Sea coast (Morcos, 1970; Warren et al., 1992). These winds form part of the south-easterly wind circulation between the continental depression over central Africa and the continental anticyclone extending from Asia to Arabia.

From October to December the winds converge near 20 °N. The convergence region lies north-south rather than directly across the Red Sea (Pedgley, 1974). It varies in size and is characterized by low-pressure calms (Morcos, 1970). The zone migrates south in response to

Figure 2.6 Schematic Monsoonal Wind and Current Regime in The North Indian Ocean.

a. Winter NE Monsoon

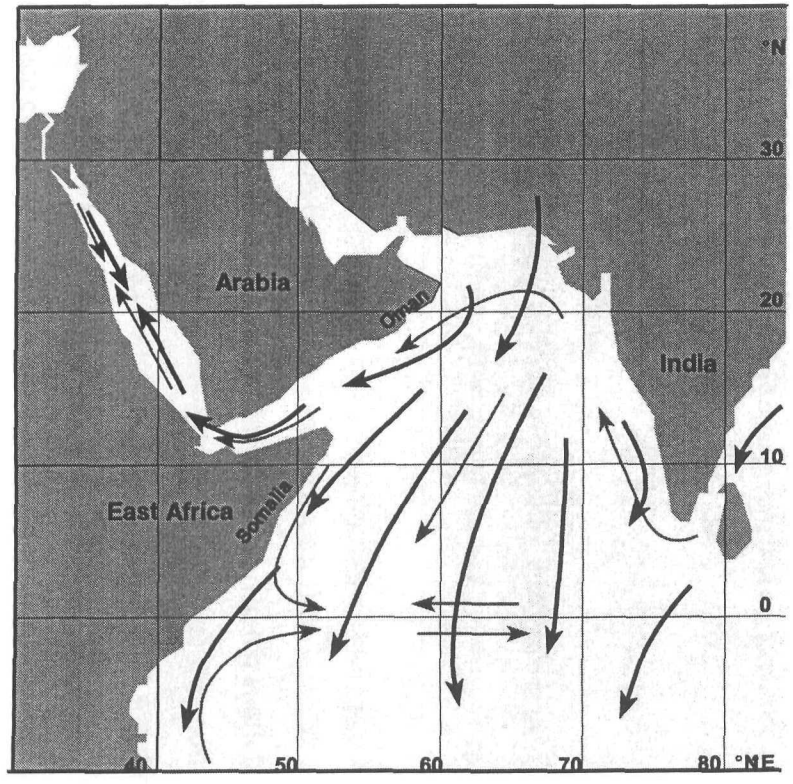

b. Summer SW Monsoon

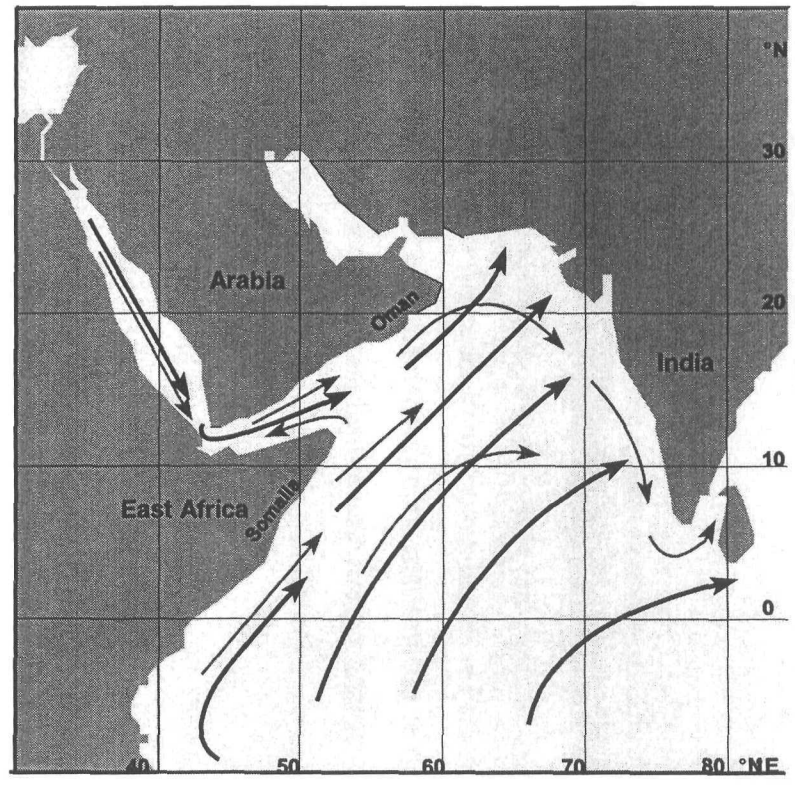

Winds Surface Currents

(Winds after Currie, Fisher and Hargreaves, 1973. Currents after Vergnaud Grazzini et al., 1995)

the monsoon regime, until by June the winds are northwesterly over the entire Red Sea (Patzert, 1974).

During the summer season (June to September) the system is reversed. The spring melt reduces albedo over the surface of central Asia, allowing the landmass to warm up. This warms the air above, causing it to rise, creating a quasi-stable low pressure system to build up over northern India (less than 995 mb (Morcos, 1970)), extending over Pakistan to the Persian Gulf. This updraught causes humid, relatively cool, maritime air to flow in from the high pressure cell over the Indian Ocean. Latent heat release from condensation/precipitation against the flanks of the Himalayas fuels further deepening of the continental low pressure cell, and consequently more inflow of maritime air, to complete this cycle. The ITCZ reaches its most northerly position (20 °N) in July and becomes identified with the front of the southwest monsoon. This passes north of Aden and the southwest monsoon flows in a clockwise direction over East Africa, the Gulf of Aden, and the Arabian Sea, towards the monsoon low of northern India (Morcos, 1970). At this time weak (2.4-4.4 m s^{-1}) north-northwesterlies or northwesterly winds dominate over the entire length of the Red Sea (Warren et al., 1992 and Morcos, 1970) (figure 2.6b). These winds are part of the north-westerly circulation on the western side of the summer Asiatic low pressure cell.

2.3 Red Sea Circulation.

2.3.1 Red Sea Surface Water (RSSW) flow

Surface water transport in the Red Sea is directly affected by wind stress over the sea surface, which changes seasonally due to the effect of the monsoon, and so causes seasonal change in the surface water flow.

In the north of the Red Sea basin the winter time surface water flow is weak and towards the south-southeast, in response to the weak southeastward winds. In the south the flow is to the north-northwest governed by the stronger northwestward winds over the southern part of the basin (Eshel et al., 1994). As a result, a two-layer flow system (surface water northward inflow, and bottom water southward outflow) is set up at the Strait of Bab el Mandab (figure 2.4). The winter surface currents converge at around 25 °N, about 5 ° further north than the

winds. This is due to the difference in the speed of the wind in the north (<3 m s^{-1}) compared to that in the south (<10 m s^{-1}).

In summer, the weak northwesterly winds drive a broad southward surface current in the centre of the basin with two northward return surface coastal currents, the western return current being broader than that in the east (Quadfasel and Baudner, 1993). This (dominantly) southward flowing surface current results, vertically, in a three-layer flow system at the Strait of Bab el Mandab, with a thin (40 m) layer of southward flowing surface water outflow, a subsurface north flowing inflow between, and a bottom water outflow below (figure 2.5).

2.3.2 Red Sea Deep Water (RSDW) formation

On the basis of a tracer study, Cember (1988) suggests that deep water forms in two ways, i) convectively, and ii) non-convectively by mixing along isopycnals.

i) Convective deep water formation:

Red sea surface water travels north, undergoing cooling and increasing salinity, hence increasing in density. In the shallow shelf area of the Gulf of Suez (<73 m deep) particularly high salinities (up to 47 ‰) are reached (Morcos, 1970). Convective deep water is a 1:1 mixture of dense winter outflow water from the Gulf of Suez with Red Sea surface water. Spring outflow water from the Gulf of Aqaba is regarded as a secondary source of low significance (Cember, 1988; Tragou and Garrett, 1997). Other, less significant sources are waters off the Sinai Peninsula, and deep convection mixing in the surface waters of the northern Red Sea (Maillard and Soliman, 1986). It has been proposed that the formation and flow of Red Sea deep water is seasonal, with formation at its maximum in winter and spring (Maillard and Soliman, 1986; Cember, 1988). Averaged, the rate of deep water formation was estimated at 0.05 +/-0.01 Sv (expressed as though flow is continuous).

ii) Non-convective deep water formation by mixing along isopycnals:

Cember (1988) discovered this process using terrigenic ^{3}He as a steady state tracer for Red Sea deep water. Terrigenic ^{3}He is primordial, mantle helium extracted from basalts in the axial rift (Lupton et al., 1977; Craig and Lupton, 1981). This mantle helium is injected

directly into the water column providing a conservative tracer for Red Sea deepwater (Cember, 1988). Isopycnals in RSDW outcrop in winter and summer in the open northern Red Sea and Gulf of Aqaba. Some 50 % of the isopycnal deep water results from Red Sea surface water mixing with outflow from the Gulf of Aqaba. The remainder is formed through deep winter mixing and convective overturning in the open northern Red Sea. The combined waters are 'injected' immediately beneath the pycnocline, at about 200 m depth, with an estimated rate of formation of 0.11 +/-0.02 Sv. The isopycnals are blocked from communication with Indian Ocean waters by the sill at Bab el Mandab. Since the isopycnally formed deep water flows southward above the Red Sea deep water flow it shows no trace of ^{3}He as it does not come into contact with the sea floor.

Combined, Cember's (1988) values for deep water formation in both modes give a total deep water renewal rate of 0.16 +/-0.03 Sv.

Deep water residence times have been calculated by several authors, varying from 72 years based on historical hydrographic observations and a continuous one-dimensional advective-diffusive model (Wyrtki, 1974); 40+/-20 years based on combined historical hydrography, tritium measurements and ^{3}He measurements to construct a two-dimensional advective-diffusive box model (Kuntz, 1985); 36 years based on C^{14}:C^{12} measurements from a reconstruction of the history of bomb radiocarbon in the source region of Red Sea deep water, with reconstruction by direct radiocarbon measurements on annual growth bands of coral in combination with ^{3}He measurements as a steady state tracer (Cember, 1988). Much longer residence times have also been proposed: 200 years based on ^{14}C dates taken from Red Sea deep water above the Atlantis II Deep (Craig, 1969) and 300 years based on historical hydrography used as parameters in a box model (Manins, 1973). Using Cember's (1988) value of deep water renewal (0.16 Sv), and an estimated 0.251×10^{6} km^{3} volume (Kossina, 1921) for the Red Sea basin, it follows that the deep water residence time (residence time = volume/deep water renewal) is about 50 years, with respect to the rate of deep water renewal. The residence time based on total Red Sea outflow (0.33 Sv (Siedler, 1969)) (residence time = volume/outflow) is approximately 25 years, half the residence time value based on deep water renewal, suggesting that there is considerable recirculation within the basin.

2.3.3 Thermohaline circulation in the Red Sea

High evaporation over the Red Sea (2000 mm yr^{-1}) increases surface water salinity and decreases surface water temperature, thus increasing the density of the surface water, as it flows north (figures 2.4 and 2.5). The warm, fresher surface water in the south, and cooler, highly saline water in the north set up a density gradient along the Red Sea axis throughout the year. This density gradient encourages the shallow inflow of fresher Indian Ocean water from the Gulf of Aden compensated by subsurface outflow of highly saline Red Sea deep water.

Figure 2.7 shows temperature profiles through the Red Sea - Gulf of Aden during winter and summer (after Wyrtki, 1971). Winter surface temperatures reach a maximum of 27 °C south of 25 °N, and >20 °C to the north. Summer surface temperatures are warmer; >30 °C in the south decreasing to 25-30 °C in the north. The annual mean sea surface temperature in the upper 40 m is 29 °C (figure 2.4). From 40 to 100 m water depth the annual mean temperature is 26 °C in the central Red Sea (between 18.2 °N and 27 °N), and decreasing to 25 °C in the north and south (Eshel et al., 1994). Water is isothermal below 200 m depth with a temperature of >21.5 and <22 °C all year round (Siedler, 1968).

Figure 2.8 shows salinity profiles through the Red Sea - Gulf of Aden during winter and summer (after Wyrtki, 1971). Surface water salinity remains almost constant throughout the year, increasing from <37 ‰ in the south, to >40 ‰ in the north. Below 200 m depth the main body of water is isohaline with a salinity of <40.6 ‰ (Siedler, 1968). However, during the summer water below 2000 m depth in the central-southern Red Sea, may achieve salinities of >43 ‰.

The density (σ_θ) of Red Sea water increases with depth, corresponding to the increase in salinity and decrease in temperature with depth. Surface water density (σ_θ) increases from 23.00 kg m^{-3} in the south, to 28.00 kg m^{-3} in the north. Bottom waters show an almost uniform density (σ_θ) below the 28.50 kg m^{-3} isopycnal (200 m depth), corresponding to the isothermal, isohaline deep water (Neumann and McGill, 1962). Hence, the vertical density gradient is well developed in the south, and weak in the north. Instability and mixing is

Figure 2.7 Temperatures in the Red Sea and Gulf of Aden (°C)

a. Winter

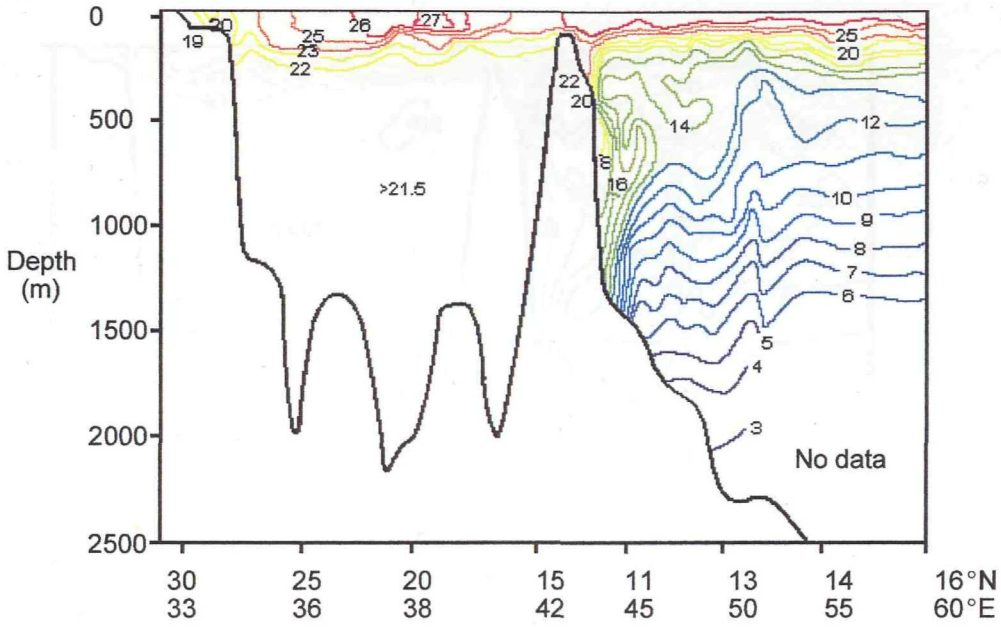

b. Summer

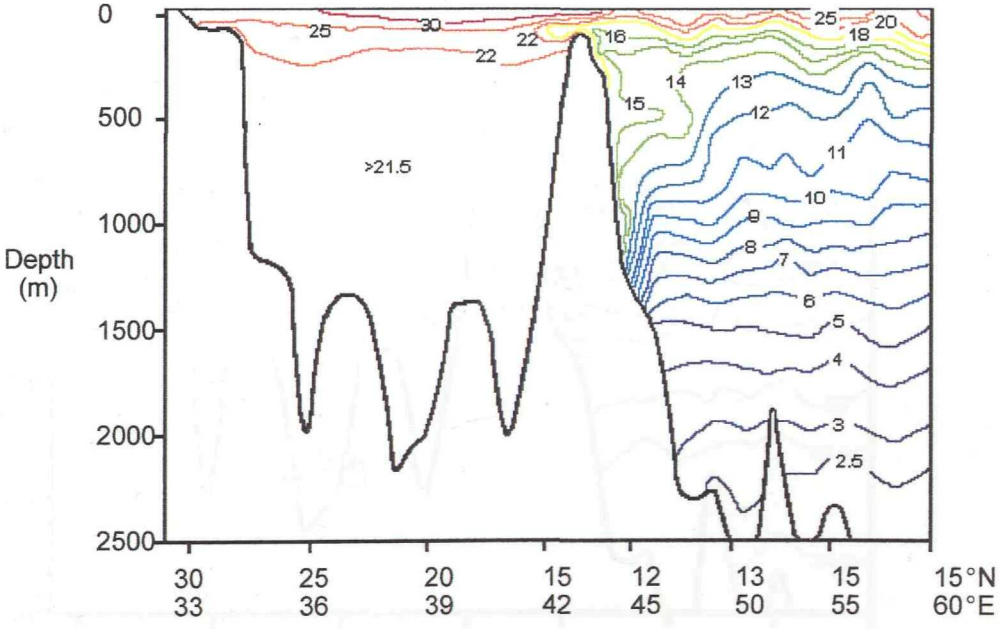

After Wyrtki, 1971.

Figure 2.8 Salinity profile of the Red Sea and Gulf of Aden (‰)

a. Winter

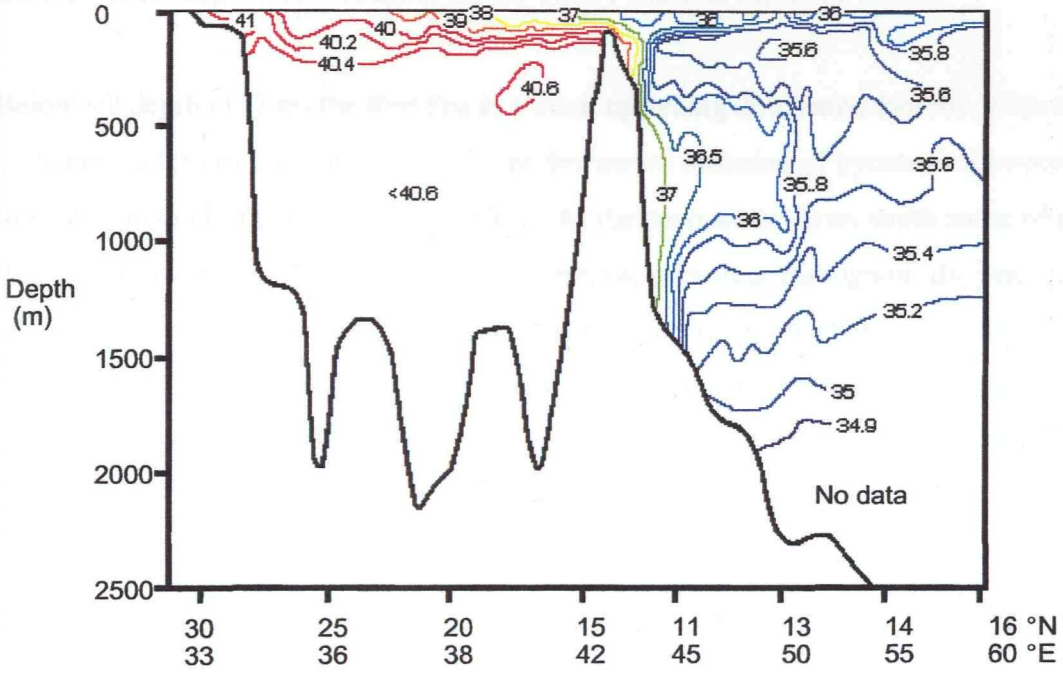

b. Summer

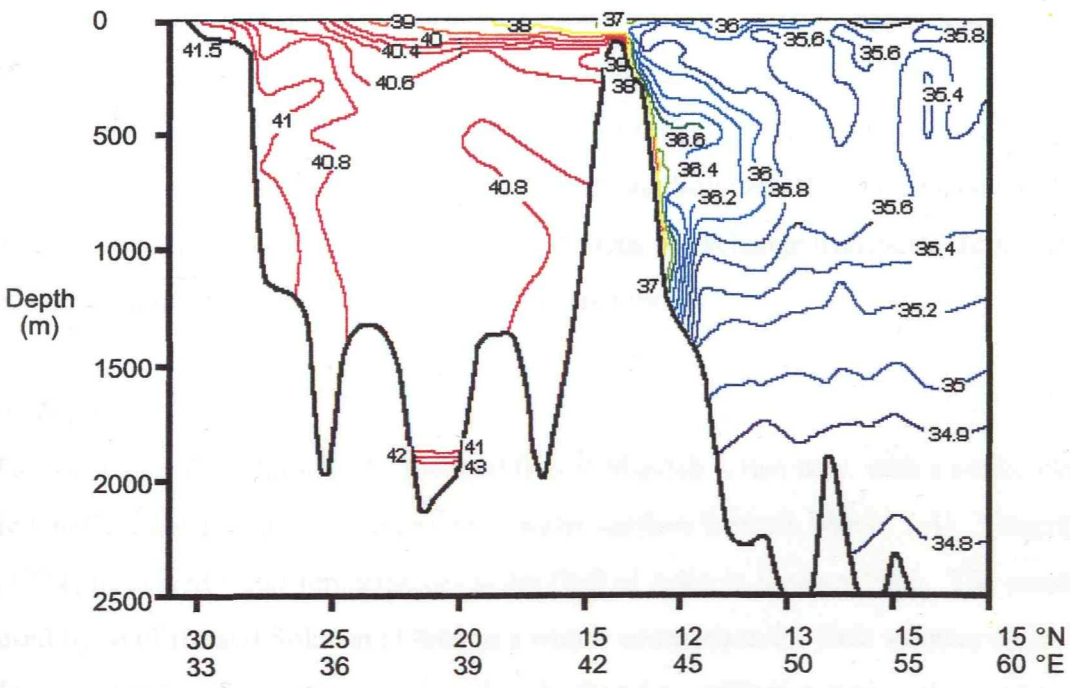

After Wyrtki, 1971

apparent in the upper 50 m, in the vicinity of Bab el Mandab, but stability rapidly increases below this depth. Stability decreases northward with the progressive increase in surface salinity and decrease in surface temperature. The northward decrease in stability culminates in the region of deep water formation off the Sinai Peninsula (Morcos, 1970).

Below sill depth (137 m) the Red Sea is a weak upwelling dominated system. This upwelling is strong enough to prevent any significant downward diffusion of pycnocline properties (temperature and salinity) (Cember, 1988). As the deep water flows south some of the upper flow is entrained into a northward mid-depth flow, persistent throughout the year, at around 500 m depth (figures 2.4 and 2.5). On reaching the northern boundary of the Red Sea, this mid-depth flow is entrained into the convective plume where it restarts the circuit (Eshel et al., 1994; Cember, 1988; Siedler, 1969). At the southern end of the Red Sea the deep water wells up to feed the outflow over the sill.

2.4 Red Sea Outflow

2.4.1 Exchange transport through the Strait of Bab el Mandab into the western Gulf of Aden.

As discussed above, exchange flow through the strait and over the sill alters seasonally due to the change in prevailing wind direction. The opposing north-northwesterly wind stress against the thermohaline flow direction (from the south-southeast) in summer causes a decrease in water exchange with the Indian Ocean. Maillard and Soliman (1986) provided a detailed discussion of the summer and winter configurations of exchange transports through the Strait of Bab el Mandab, which may be summarised as follows:

i) Winter.

During winter flow through the Strait of Bab el Mandab is two way, with a surface inflow of Indian Ocean water, and a Red Sea deep water outflow beneath (figure 2.4). Vangriesheim (1974) measured water temperatures in the Gulf of Aden in January 1963. The results were used by Maillard and Soliman (1986) as a winter comparison for their summer data. The January, 1963, temperatures measured in the Red Sea outflow waters in the western Gulf of Aden were 20 °C at 300 m and 19 °C at 500 m, warmer and deeper in comparison with the

summer (1986) values. Also the deep Red Sea layer seemed to be attached to the lowest upper Red Sea layer, and had a temperature of 17 °C (Maillard and Soliman, 1986).

ii) Summer.

During summer a three layer stratification occurs in the Strait (figure 2.5). The summer south-southeasterly wind drives a surface flow out of the Red Sea through the Strait into the Gulf of Aden. Beneath this is an inflowing layer of Indian ocean water. As this water moves up the strait towards the Red Sea the layer shoals and becomes thinner, due to the shoaling and widening of the channel. A thin bottom water outflow of Red Sea Deep Water is found beneath, which, by October, becomes confined to a narrow central channel as a thin layer of about 40 m, and is intensively mixed with the overlying relatively fresh water.

Tongues of Red Sea outflow water are found at different depths in the western Gulf of Aden (figure 2.5). In summer, the upper 30-40 m in the Gulf of Aden is warm, salty and well oxygenated (4.5 ml l^{-1}). Beneath this relatively homogeneous layer are two Red Sea layers, which each have a typical thickness of about 100 m, and are found at around 300 m (temperature 19 °C) and 450 m (temperature 16.5 °C) (figure 2.4). As summer progresses these layers sink, and by September are found 100 m deeper and are colder by about 3 °C. Maillard and Soliman (1986) suggest that the fast temperature decrease seen in summer is due to mixing with relatively cold Indian Ocean water, found beneath these Red Sea layers. A thick, homogeneous tongue of Red Sea Deep Water outflow flows at depths greater than 1000 m, with a temperature of 16 °C, and is thought to originate from the deepest part of the Red Sea outflow.

2.4.2 Red Sea Outflow and the Indian Ocean.

Red Sea outflow moves east through the Gulf of Aden, mixing with ambient waters along its trajectory, mainly at depths of 400-700 m. At 50 °E it is found to have a temperature of 11.5-12.5 °C, and a salinity of 35.9-36.1 ‰ (Shapiro and Meschanov, 1991). After leaving the Gulf of Aden the main branch of Red Sea Water (RSW) flows through a narrow (100 km) strait between Cape Guardafui and Abd-al-Kuri Island and splits into three branches (Shapiro and Meschanov, 1991) (figure 2.9):

Figure 2.9 Present Day Red Sea Outflow.

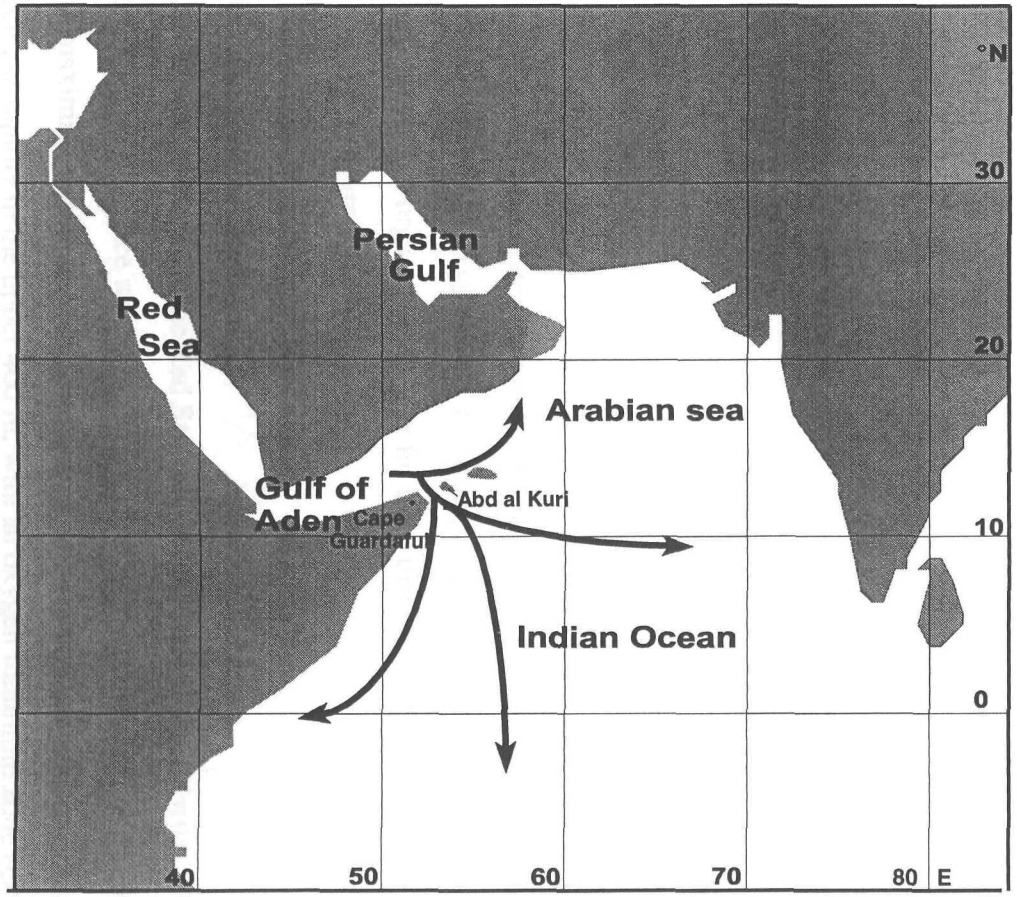

Main branches of Red Sea out flow into the Indian Ocean.

(after Shapiro and Meschanov, 1991)

- An eastward progression towards India (Shapiro and Meschanov, 1991).
- A southward flow between 55 and 65 °E, deepening progressively southward to more than 900 m at 10 °S (Shapiro and Meschanov, 1991).
- A strong southward flow along the east African margin, reaching 1100 m depth in the Mozambique Channel at 20-25 °S (Wyrtki, 1971).

The more northerly branch of Red Sea outflow spreads to the northeast along the Arabian coast (Shapiro and Meschanov, 1991). On entering the Arabian Sea, RSW sinks to a depth of 600-800 m and spreads to 17-18 °N. Difficulty in tracing the trajectory of RSW through the Arabian Sea by means of salinity maxima arise as the more saline water from the Persian Gulf enters the basin at 200-300 m depth (Shapiro and Meschanov, 1991).

The spread of RSW in the North Indian Ocean is characterised by zonal distribution of isotherms and isohalines (Rochford, 1964; Sabinin, 1964; Krause, 1968; Shapiro and Meschanov, 1991). Observations of isotherms and isohalines associated with RSW suggest that the water body has a "lenticular" distribution, that is, the RSW is found in the form of isolated patches of high salinity water with horizontal scales of 40-100 km (Cooksa, 1972; Fedorov, 1976; Belkin et al., 1986; Shapiro and Meschanov, 1991).

2.5 Dissolved oxygen distribution

The Red Sea, Gulf of Aden and Arabian Sea contain relatively low concentrations of dissolved oxygen. Bodies of ocean water with relatively low dissolved oxygen concentrations must be located either near intense oxygen sinks (consumption of free oxygen through degradation of large amounts of organic matter), or far from their sites of sea-surface oxygen renewal (Olson et al., 1993; Warren, 1994).

2.5.1 The Red Sea and Gulf of Aden.

Winter and summer oxygen profiles for the Red Sea and Gulf of Aden (after Wyrtki, 1971) are shown in figure 2.10. The surface waters of the Red Sea are rich in dissolved oxygen (>4 ml O_2 l^{-1}), with the maximum concentrations in winter, in the north (>5 ml O_2 l^{-1}). Oxygen concentrations decrease rapidly in the upper 400 m, with an oxygen minimum zone (OMZ) between 400 and 600 m depth in summer, and between 400 and 1000 m depth in winter. The

Figure 2.10 Oxygen profile of the Red Sea and Gulf of Aden (ml O_2 l^{-1})

a. Winter

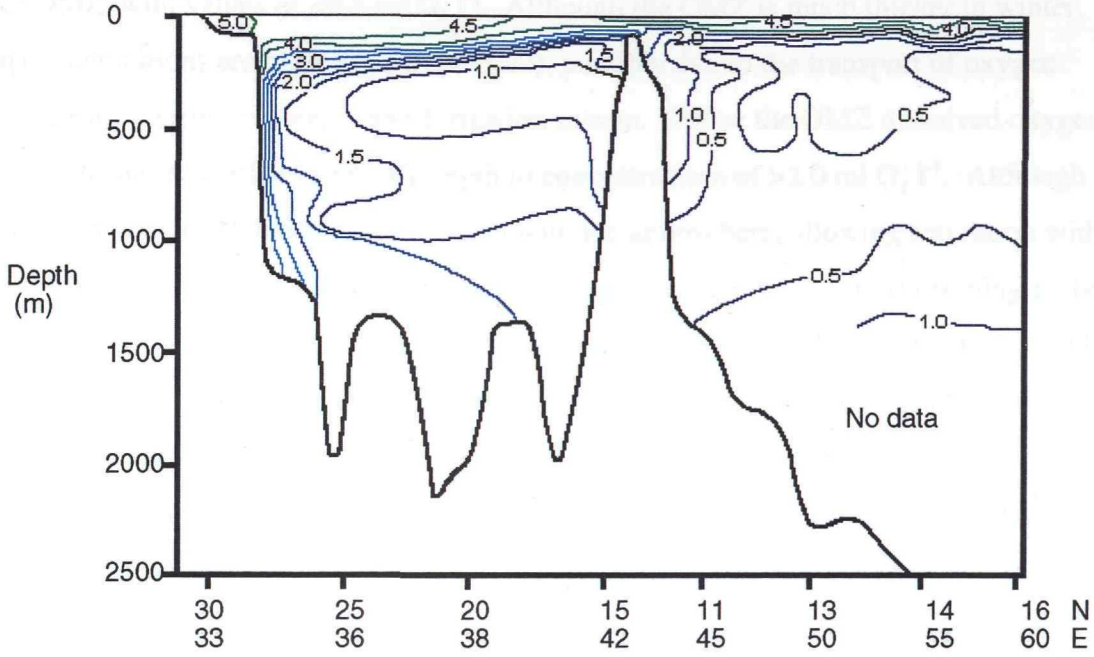

b. Summer

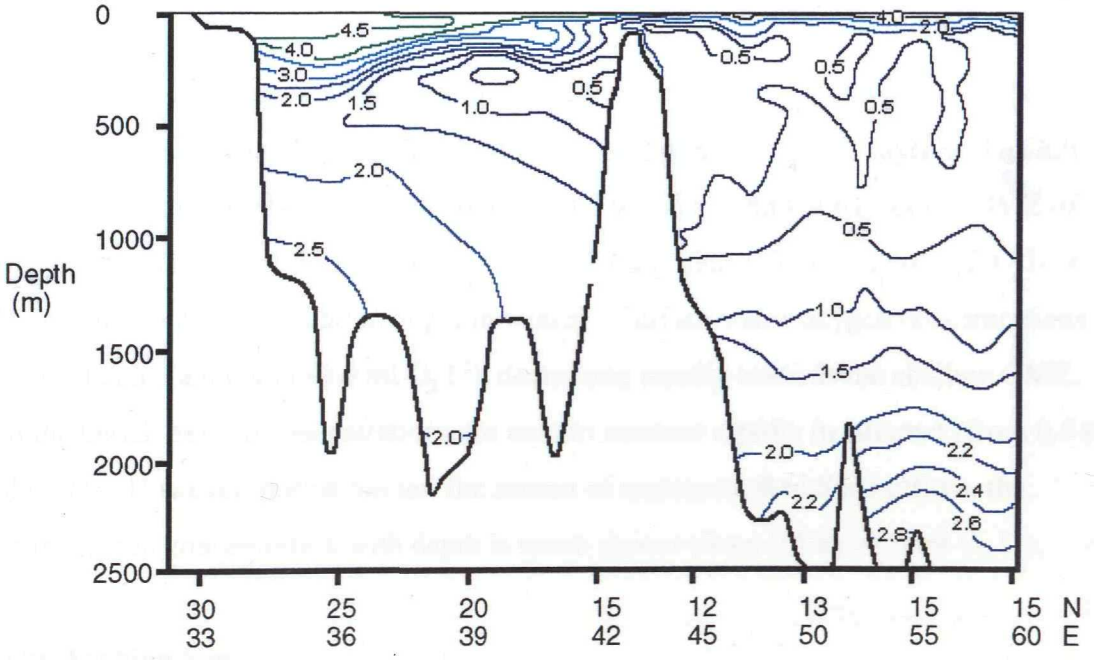

After Wyrtki, 1971

origin of this zone is suggested to be the degradation of organic matter (Morcos, 1970; Grasshoff, 1975). Since oxygen concentrations are lower in the south and the OMZ is found to be shallower it is suggested that this degradation is more rapid in the southern Red Sea (Morcos, 1970; Grasshoff, 1975). The lowest concentrations of oxygen are observed in the summer OMZ, with values of <0.5 ml O_2 l^{-1}. Although the OMZ is much thicker in winter, oxygen concentrations are higher (<1.0 ml O_2 l^{-1}), possibly due to the transport of oxygen from the surface during the deep water formation season. Below the OMZ dissolved oxygen concentrations increase with increasing depth to concentrations of >2.0 ml O_2 l^{-1}. Although the deep water was in relatively recent contact with the atmosphere, allowing saturation with oxygen, its high temperature and salinity prevent oxygen concentrations from reaching higher values like those found in intermediate and deep waters formed in cold regions (Green and Carrit, 1967; Murray and Riley, 1969, Weiss, 1970). For example, water with a temperature of 10 °C and salinity of 36 ‰ has a solubility of 6.279 ml O_2 l^{-1} from moist air at one atmosphere total pressure (Weiss, 1970). Based on the annual mean surface temperature and salinity at 40-100 m depth (26 °C, 37-40 ‰), the solubility of oxygen in Red Sea surface waters, from moist air at one atmosphere total pressure, is estimated at 4.569 to 4.518 ml O_2 l^{-1}. Red Sea deep water is estimated to have a solubility of oxygen of 4.838 ml O_2 l^{-1}, based on the annual temperature of 21.5 °C and salinity of >40 ‰ (Weiss, 1970).

Subsurface Red Sea outflow reaches the Gulf of Aden with oxygen concentrations of less than 1.5 ml O_2 l^{-1} (Grasshoff, 1975). The waters below the surface mixed layer in the Gulf of Aden that mix with the Red Sea outflow contain <0.5 ml O_2 l^{-1}, and are part of the OMZ of the Gulf of Aden (Grasshoff, 1975; Maillard and Soliman, 1986), found between 200-1000 m depth in summer and 200-1250 m depth in winter. Surface water oxygen concentrations in the Gulf of Aden are high (>4.0 ml O_2 l^{-1}), decreasing rapidly towards the shallow OMZ. Beneath the OMZ, oxygen concentrations are seen to increase rapidly in summer (from 0.5 to >2.8 ml O_2 l^{-1}). However, during winter, the season of maximum Red Sea outflow, the increase in oxygen concentration with depth is much slower (from 0.5 to >1.0 ml O_2 l^{-1}).

2.5.2 The Arabian Sea.

The Arabian Sea contains one of the most pronounced OMZs in the world ocean. This zone

is described as "disaerobic or disoxic" (Deuser et al., 1978), with oxygen concentrations of <0.1 ml O_2 l^{-1} from depths of 100 m to over 1000 m (Warren,1994). Despite the high mean annual surface productivity in the Arabian Sea (1 g C cm^{-2} day^{-1} (Olson et al., 1993), it seems plausible that too little of this particulate matter is consumed at thermocline depths to cause an inflated oxygen demand there. Since the OMZ is neither an isolated pool, nor a sluggish backwater (residence time 11±4 years (Olson et al., 1993), nor a conspicuous oxygen sink, the suboxic concentrations are attributed to the low oxygen concentration in water entering from the south, the greatest source of water to the OMZ (Olson et al., 1993). That depletion in turn is due to consumption of oxygen along the water masses long trajectory from the zone of surface renewal at 40-50° S.

Red Sea outflow (oxygen concentration: 1.5 ml O_2 l^{-1}) combined with outflow from the Persian Gulf (oxygen concentration: <0.1 ml O_2 l^{-1}, 300 m depth) (Wyrtki, 1971) constitutes a combined transport at the sills of around 0.6 Sv, providing a relatively small supply to the Arabian Sea OMZ. Their oxygen is lost rapidly downstream from the sills, presumably by entrainment of the resident oxygen poor water as they descend the continental slope (Olson et al., 1993; Warren, 1994).

2.6 Nutrients

The surface waters of the Red Sea are oligotrophic, typical of a silled basin with a negative water balance, hence productivity in the basin is low. Since land run-off and precipitation over the region are negligible, nutrients are supplied to Red Sea surface waters mainly by the inflow current from the Gulf of Aden, and by admixture and diffusion from deeper layers (Morcos, 1970).

2.6.1 Nitrate.

Winter and summer nitrate profiles for the Red Sea and Gulf of Aden (after Wyrtki, 1971) are shown in figure 2.11. During winter, nitrate concentrations in the upper 50 m in the western Gulf of Aden and southern Red Sea are five times higher (5 µg-at. l^{-1}) than those in the northern Red Sea (1 µg-at. l^{-1}), and twice as high again between 50 and 150 m depth. However, in the Strait region, values are seen to fall back to 1 µg-at. l^{-1}. The Red

Figure 2.11 Nitrate concentrations in the Red Sea and Gulf of Aden (µg-at .l^{-1})

a. Winter

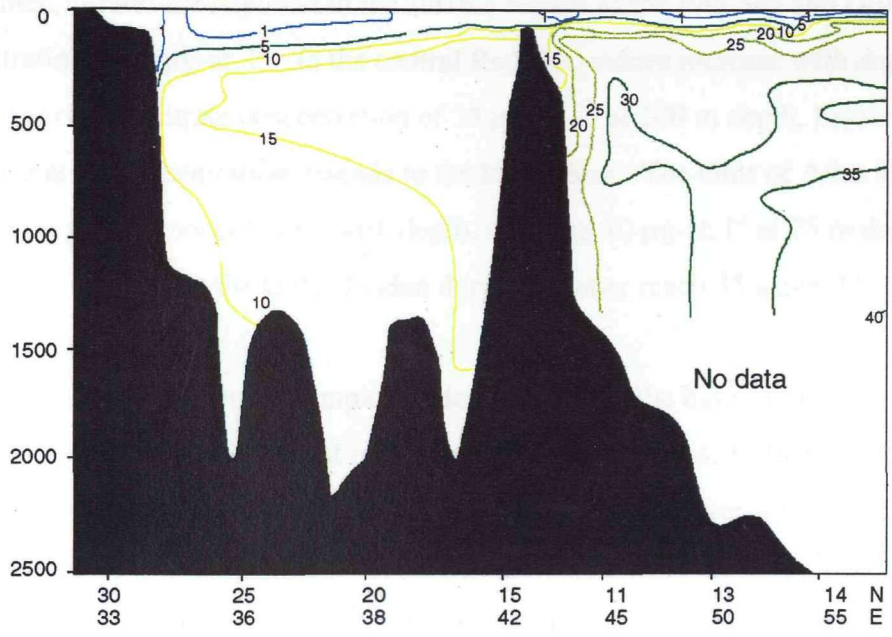

b. Summer

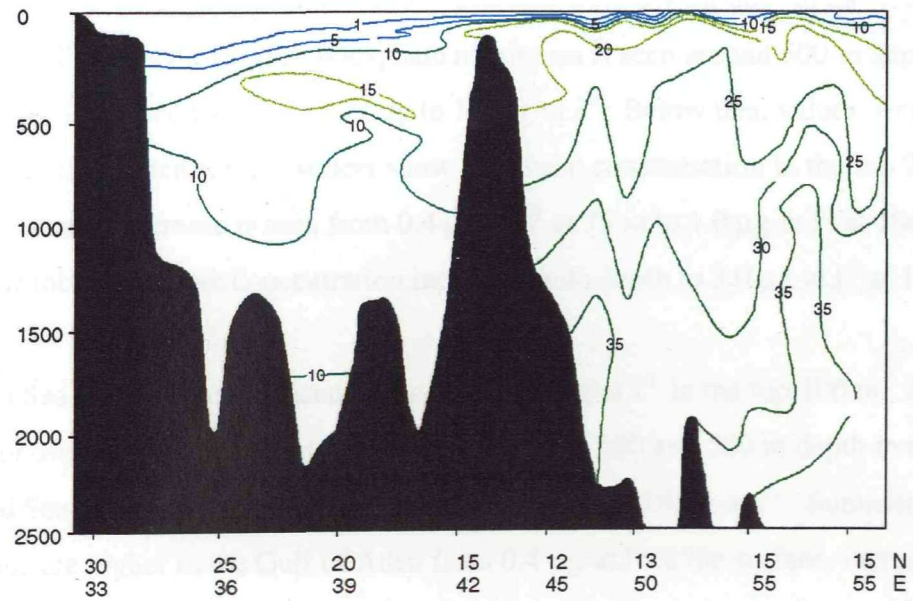

After Wyrtki, 1971

Sea intermediate waters (around 500 m depth) show a nitrate maximum of 15 μg-at. l^{-1}, falling to 10 μg-at. l^{-1} with increasing depth. Gulf of Aden intermediate waters show a maximum of 40 μg-at. l^{-1} close to 1500 m depth.

During summer, nitrates are depleted in the surface waters of the Red Sea and Gulf of Aden with concentrations of 1 μg-at. l^{-1}. In the central Red Sea, values increase with depth reaching the maximum nitrate concentration of 15 μg-at. l^{-1} at 200 m depth, below which water of 10 μg-at. l^{-1} concentration extends to the basin floor. The Gulf of Aden shows a rapid increase in nitrate concentration with depth, reaching 10 μg-at. l^{-1} at 75 m depth. Maximum concentrations in the Gulf of Aden during summer reach 35 μg-at. l^{-1}

In the Red Sea, nitrates are almost completely depleted above the base of the euphotic zone (in the basin, only 3 % of blue daylight reaches 60 m depth (Morcos, 1970)), while increasing below. High concentrations of ammonia are found in the surface layers of the Red Sea where nitrates are low. Below the euphotic zone, the concentration of ammonia is much lower and nitrate is more abundant due to the effects of nitrifying bacterial activity (Morcos, 1970).

2.6.2 Phosphate.

Winter and summer phosphate profiles for the Red Sea and Gulf of Aden (after Wyrtki, 1971) are shown in figure 2.12. Phosphate concentration is also very low in Red Sea surface waters. Winter surface water phosphate concentrations decrease from 0.4 μg-at.l^{-1} in the southern Red Sea to 0.1 μg-at.l^{-1} in the north. The phosphate maximum is seen around 500 m depth in the south of the basin, with concentrations of up to 1.5 μg-at.l^{-1}. Below this, values decrease to 0.6 μg-at.l^{-1}. Gulf of Aden surface waters show a uniform concentration in the top 75 m of 0.4 μg-at.l^{-1}. A rapid increase is seen from 0.4 μg-at.l^{-1} at 75 m to 1.0 μg-at.l^{-1} at 100 m depth. Below this, phosphate concentration increases with depth to 3.0 μg-at.l^{-1} at 1500 m.

Summer Red Sea surface water concentrations are <0.1 μg-at.l^{-1} in the top 100 m. A maximum concentration of 1.0 μg-at.l^{-1} is located between 250 and 500 m depth in the southern Red Sea. Below this, the concentration decreases to 0.6 μg-at.l^{-1}. Summer surface concentrations are higher in the Gulf of Aden from 0.4 μg-at.l^{-1} at the surface, increasing

Figure 2.12 Phosphate concentrations in the Red Sea and Gulf of Aden (µg-at.l^{-1})

a. Winter

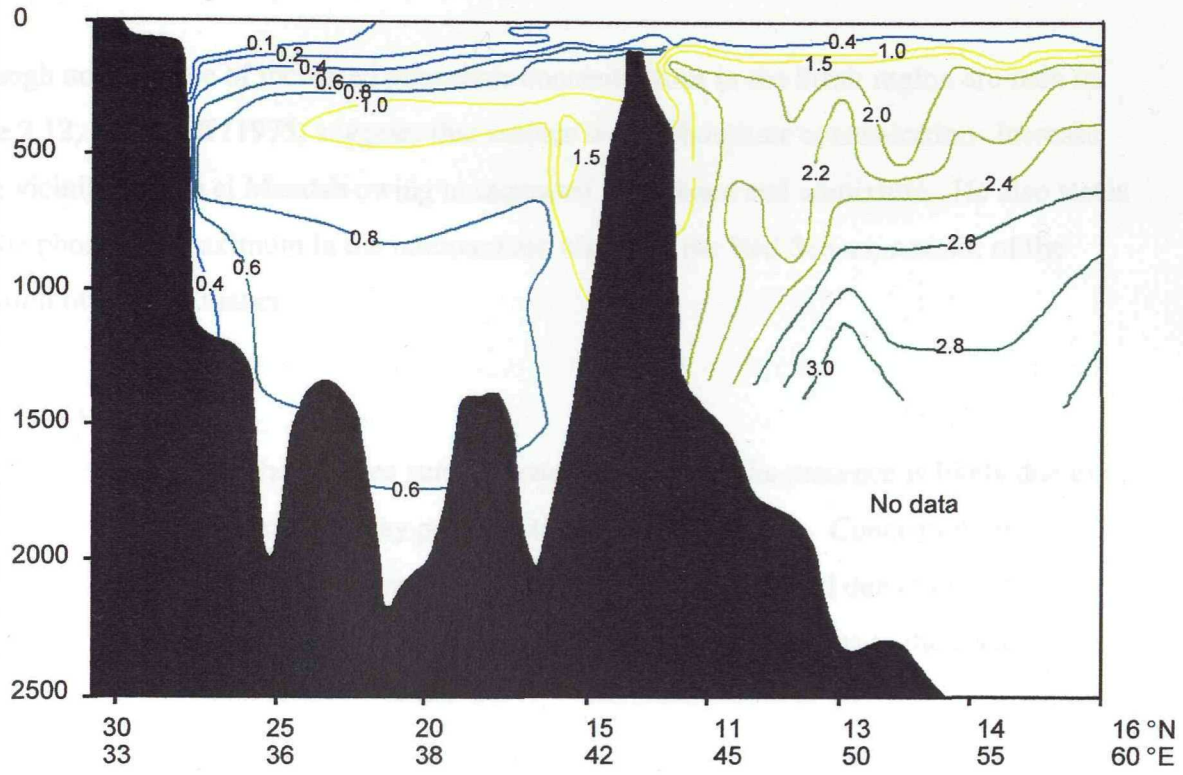

b. Summer

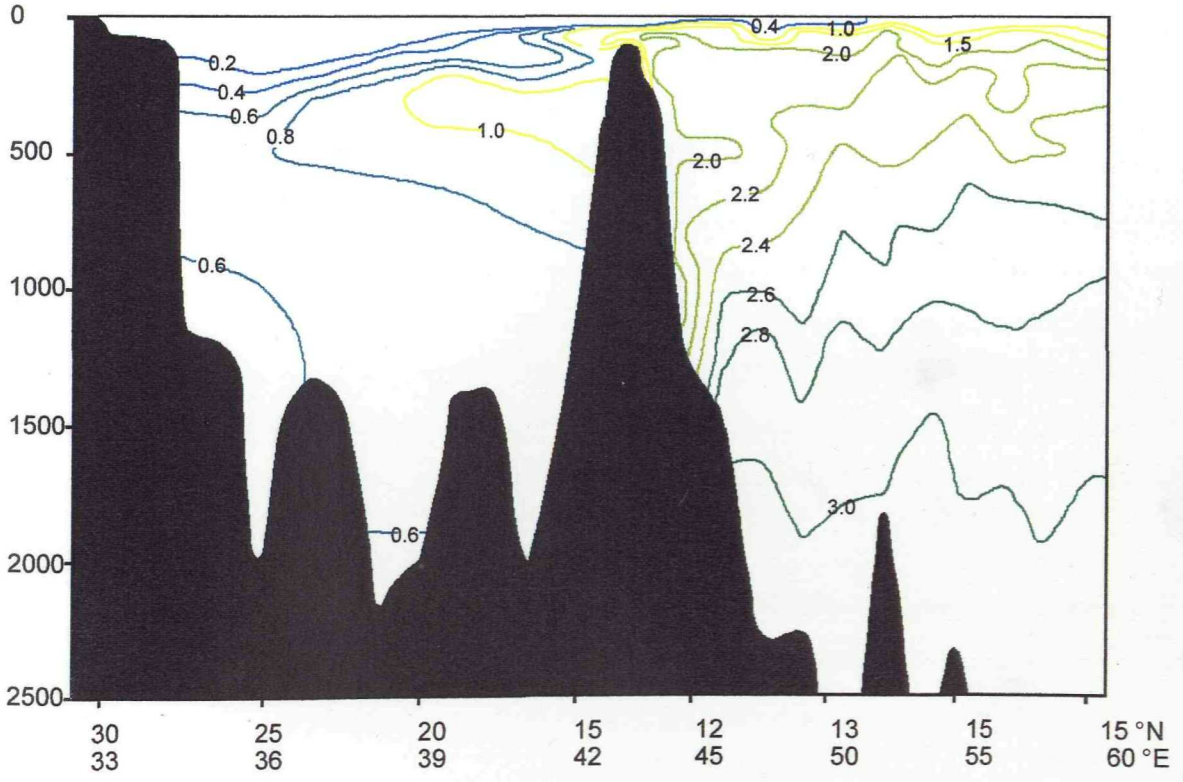

After Wyrtki, 1971

rapidly to 2.0 μg-at.l^{-1} at 100 m depth. A generally uniform increase in phosphate concentration to 2.8 μg-at.l^{-1} at 1000 m depth is seen below.

Although no evidence of increased phosphate concentrations in the Strait region are seen in figure 2.12, Grasshoff (1975) suggests that surface water phosphate concentrations increase in the vicinity of Bab el Mandab owing to increased turbulence and admixture. He also states that the phosphate maximum in the intermediate waters of the Red Sea are a result of the oxidation of organic matter.

2.6.3 Silicate.

Silicate concentration in the Red sea surface water is very low. Its presence is likely due to the partial solution of quartz and clay particles transported by storms. Concentrations increase in the upper layers due to evaporation, but decrease northward due to biological consumption. Only a very small portion of silicate on the shelves returns to the cycle (Morcos, 1970).

Chapter 3.

MODERN PLANKTONIC FORAMINIFERAL FAUNA IN THE RED SEA AND GULF OF ADEN

This chapter discusses the abundance and distribution of planktonic foraminifera in the Red Sea and Gulf of Aden.

3.1 Species distribution in the Red Sea and Gulf of Aden.

The present day planktonic foraminiferal fauna in the Red Sea is predominantly composed of spinose species (eg. *Globigerinoides ruber* (plate 1), *Globigerinoides sacculifer* (plates 2 and 3), *Globigerinella siphonifera* (plate 6), *Globoturborotalia rubescens* (plate 4), *Globoturborotalia tenella* (plate 5) and *Orbulina universa*). *G.sacculifer* is dominant north of 20 °N and *G.ruber* dominates to the south (figure 3.1). Non-spinose species (*eg. Globorotalia menardii* (plate13), *Neogloboquadrina dutertrei* and *Pulleniatina obliquiloculata*) are only present south of 20 °N in the basin during the time of winter inflow from the Gulf of Aden, decreasing in abundance northward (Kleijne et al., 1988, Hemleben et al., 1989; Ganssen and Kroon, 1991).

Table 3.1 summarises the ecological constraints for the most abundant planktonic foraminiferal species. North of 20 °N, *Globigerinoides sacculifer* dominates the living Red Sea planktonic foraminiferal assemblage (figure 3.1), accompanied by relatively low abundances of *Globigerinella siphonifera* (Auras-Schudnagies et al., 1988; Hemleben et al, 1989) . Core top sediments in the north are also dominated by *G. sacculifer*, and small planktonic foraminifera (*G. rubescens* and *G.tenella*) increase northward in Red Sea core top sediments (Auras-Schudnagies et al., 1989). In the north, sea surface temperatures are low (24-25 °C) relative to the southern Red Sea, and surface water salinity is high (>40 ‰) (Seidler, 1969; Morcos, 1970).

Globigerinoides ruber dominates the assemblage south of 20 °N (figure 3.1), with an increase in *G. siphonifera* and a decrease in *G.sacculifer* relative to the northern Red Sea abundances (Auras-Schudnagies et al., 1988; Hemleben et al., 1989). *G. ruber* also dominates

core top sediments in the southern Red Sea (Auras-Schudnagies et al., 1989). In this region surface water salinity is lower (<37 ‰), and sea surface temperature is higher (up to 30 °C), in comparison to the northern Red Sea (Siedler, 1969; Morcos, 1970).

Table 3.1 Habitat characteristics of the main Red Sea planktonic foraminiferal species based on laboratory experimental data (Anderson, 1983; Spindler et al., 1984; Hemleben et al., 1987; Hemleben et al., 1989). The experimental studies are carried out on species which have already lived part of their life in the natural environment. The species are kept under flourescent light simulating a water depth of 20-30 m (Hemleben et al., 1989). Specimens were exposed to higher and lower temperature and salinity values for observation periods of 3 hours. In order to assess the feeding behaviour of the species concerned the spinose species were maintained at a constant temperature of 26.5 °C or 29.5 °C and the non-spinose species were maintained at a constant temperature of 15 °C or 20 °C, according to the water temperature where they were found (Hemleben et al., 1989). Other comparable data has not been found in the literature.

Species	***G.sacculifer***	***G.siphonifera***	***G.ruber***	***G.glutinata***
Temperature tolerance °C	14-31	11-30	16-31	wide range
Salinity tolerance ‰	24-47	27-45	22-49	wide range
dietary preferences	Omnivore though prefers (calenoid) copepods and other zooplankton	Omnivore though prefers zooplankton	Omnivore though cannot handle strong prey, and will thrive on a herbivorous diet.	Herbivore, specialised in diatoms

The assemblage in the Strait of Bab el Mandab and Gulf of Aden is dominated by *G.ruber,* and *Globigerina bulloides* (plate 12)(figure 3.1)(Auras-Schudnagies et al., 1988; Hemleben et al., 1989), a species found to dominate eutrophic waters, often associated with upwelling

regions (Hemleben et al., 1989). *G. bulloides* occurs in the Strait and the Gulf of Aden along with *G. menardii, G. sacculifer, Neogloboquadrina dutertrei, G.tenella, G.rubescens,* and *Globigerinita glutinata* (plate 7) (Auras-Schudnagies et al., 1988; Kroon, 1988; Auras-Schudnagies et al., 1989). In the strait, *G. glutinata,* a ubiquitous species (Bé and Hamlin, 1967; Bé and Tolderlund, 1971; Tolderlund and Bé, 1971; Hemleben et al., 1989), occurs in high abundance in the core top sediments (Auras-Schudnagies et al., 1989). The Gulf of Aden shows increased abundances of non-spinose species, since nutrient concentrations are high enough to support a high primary productivity (Auras-Schudnagies et al., 1988; Kroon, 1988; Auras-Schudnagies et al., 1989).

3.2 Productivity and foraminiferal distribution.

Hemleben et al. (1989) attributed the north-south divide in spinose - non-spinose species abundance to the distribution of zooplankton and phytoplankton in the basin. The boundary at 20 °N is associated with the position of the current convergence zone (chapter 2, section 2.3.1), the position of which is dependent on the strength of the converging overhead winds, in turn controlled by the intensity of the NE monsoon. The zone provides a distinct limit to plankton productivity, with phytoplankton abundant to the south, while zooplankton dominates to the north (Hemleben and Spindler, 1983; Hemleben et al., 1989). The main food source for spinose planktonic foraminifera consists of zooplankton organisms, mainly (calenoid) copepods and their developmental stages; nauplii and copepodites. Non-spinose planktonic foraminifera feed mainly on phytoplankton (diatoms, coccolithophorids, flagellates) but non-motile, injured or dead zooplankton organisms or detrital remains are ingested as well. (Spindler et al., 1984). The oligotrophic waters of the Red Sea are unfavourable to the growth and reproduction of non-spinose foraminifera unfavourable (Hemleben and Spindler, 1983; Auras-Schudnagies et al., 1989).

The nutritional requirements of the spinose species *G.sacculifer* (dominant north of 20°N) and *G.ruber* (dominant south of 20°N) differ greatly. *G.ruber* consumes more phytoplankton in comparison to *G.sacculifer* which is specialised to feed mostly on (calanoid) copepods, as well as other zooplankton (Anderson, 1983; Spindler et al., 1984; Hemleben et al., 1989). *G.ruber* is less dependent on zooplankton consumption than any other spinose species studied,

due to its difficulty handling stronger prey (Spindler et al., 1984). Moreover, the relatively large consumption of algal protein by *G.ruber* may indicate its efficiency in utilising primary producers. Thus, the widespread occurrence of *G.ruber* in the southern Red Sea may, in part, be attributed to its capacity to establish a significant advantage in competing for energy resources in regions of limited food supply (primary and secondary productivity) (Hemleben et al., 1989).

The phytoplankton and, hence, zooplankton, distribution in the Red Sea seems to be related to the current convergence zone which is set up according to wind stress over the sea surface during the NE monsoon. During the summer southwest monsoon (figure 3.2a), northwesterly winds dominate the surface of the Red Sea and the surface circulation is governed by a southward flow (Morcos, 1970; Patzert, 1974; Pedgley, 1974). At this time chlorophyll values >40-50 mg m^{-2}, with a high of >100 mg m^{-2} around 20 °N, are restricted to the central and southern end of the basin, while there is a general rise (from <50 mg m^{-2} to >100 mg m^{-2} in places) in chlorophyll concentrations in the NW Indian Ocean (Halim, 1984) (figure 3.2b). However, during the winter northeast monsoon (figure 3.3a), southeast winds dominate the southern half of the Red Sea basin (below around 20 °N), driving a northward inflow from the Gulf of Aden, and northwesterly winds dominate the northern half (above around 20 °N), driving a southward flow. The resultant convergence of the surface water circulation of the Red Sea, is found about 5 ° further north than that of the wind field (Morcos, 1970; Patzert, 1974). During the NE monsoon, chlorophyll concentrations are maximum (65-91 mg m^{-2}) in the northern Red Sea, while chlorophyll concentrations in the NW Indian Ocean are decreased (figure 3.3b) (Halim, 1984). The higher chlorophyll concentrations in the north are attributed to deep convection mixing bringing regenerated nutrients to the surface.

Halim (1984) suggests that the Red Sea standing stock dinoflaggelate, tintinnid, copepod, euphausiid, chaetognath and appendicularian populations afford no evidence of the winter surface water inflow from the Gulf of Aden affecting their seasonal/geographic distributions. This is corroborated by Van Couwelaar (1997) and Wiebinga et al. (1987) who suggest that during the NE monsoon of 1993, the observed high zooplankton biomasses in the southern Red Sea had not resulted from import of plankton from the Gulf of Aden. Instead, they

Figure 3.2 Summer SW Monsoon

a. Schematic wind and surface current regime in the north Indian Ocean.
(Currie, Fisher and Hargreaves, 1973; Vergnaud Grazzini et al., 1995)

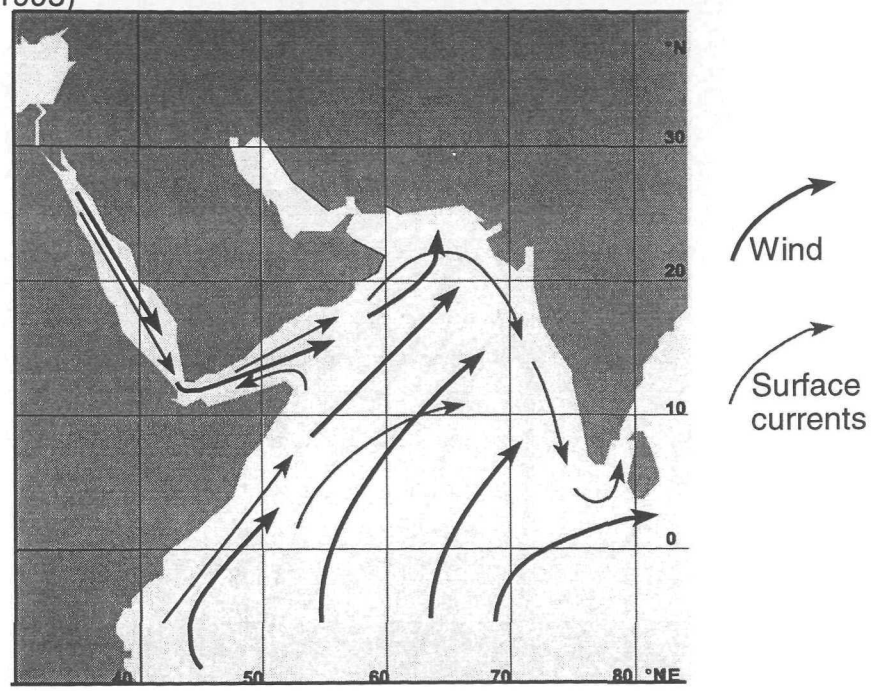

b. Schematic chlorophyll distribution (mg m-2) in the north Indian Ocean.
(Halim, 1984)

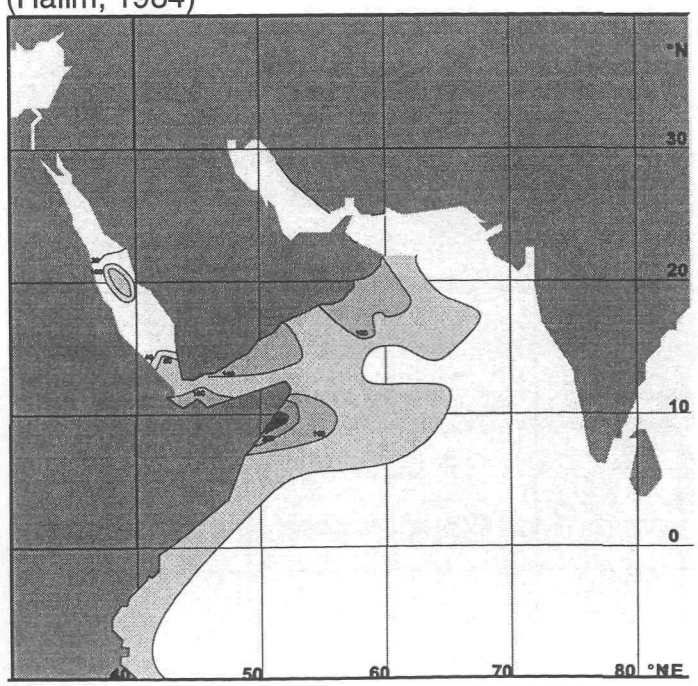

Figure 3.3 Winter NE Monsoon

a. Schematic wind and surface current regime in the north Indian Ocean.
(Currie, Fisher and Hargreaves, 1973; Vergnaud Grazzini et al., 1995)

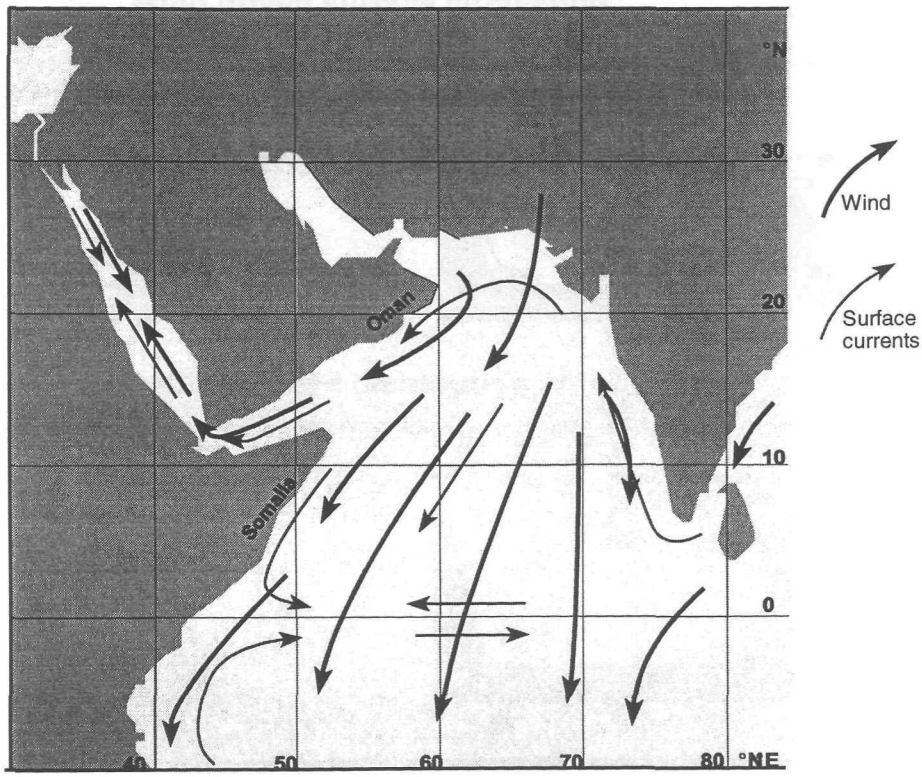

b. Schematic chlorophyll distribution (mg m-2) in the north Indian Ocean.
(Halim, 1984).

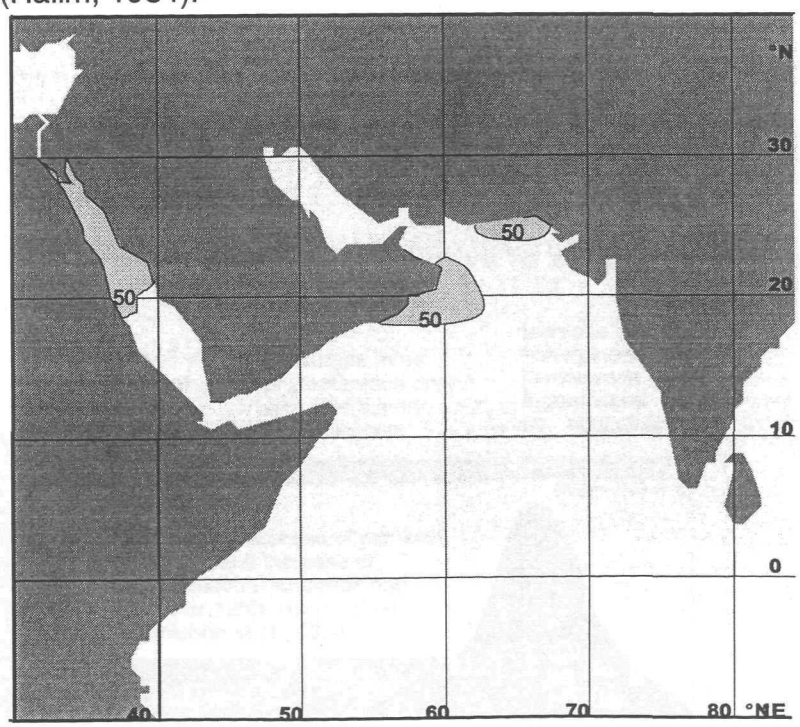

Figure 3.4 Factors in foraminiferal species distribution in the Red Sea

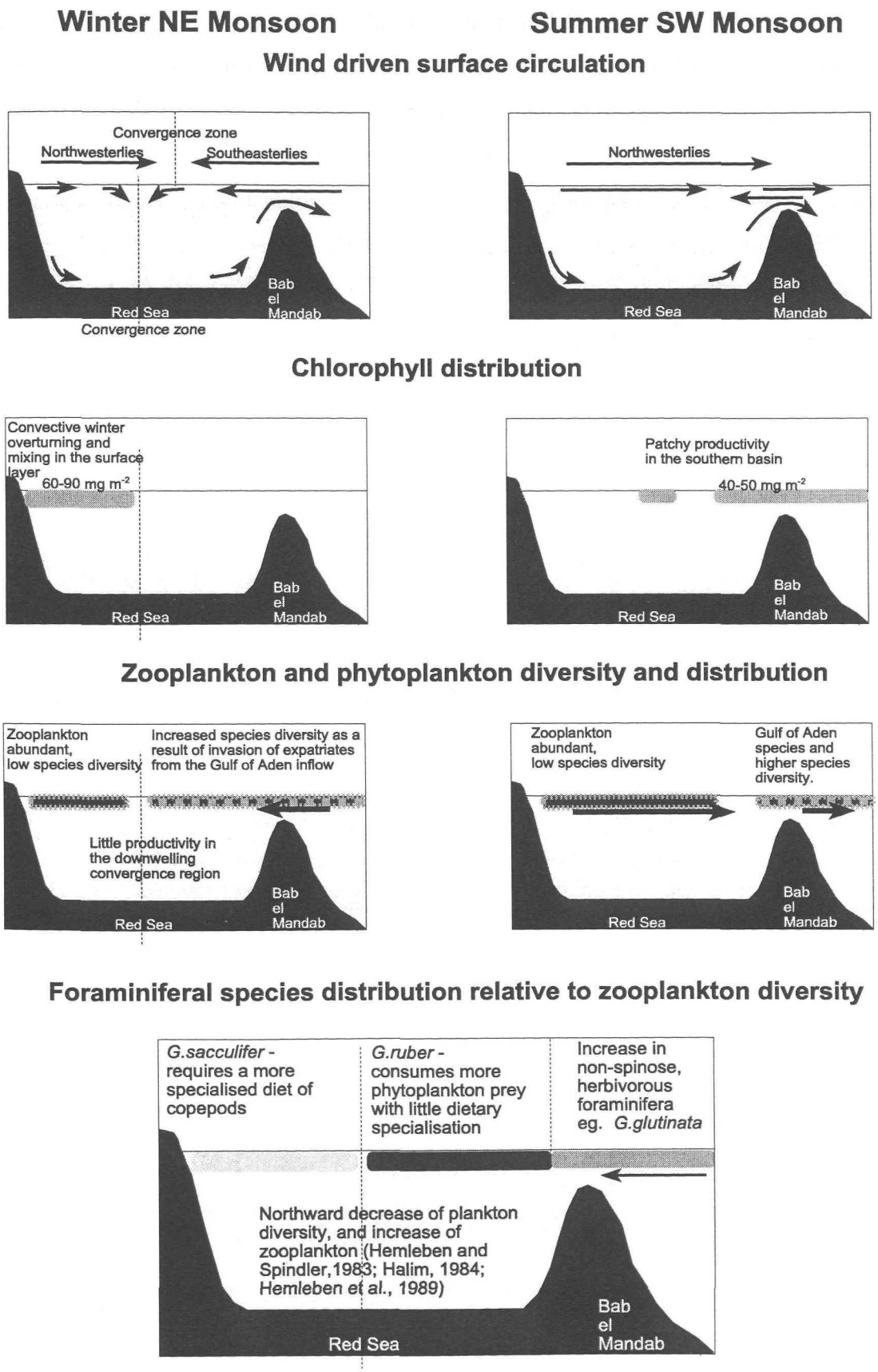

propose that the high biomass was due to local phytoplankton blooms, created by response to nutrient entrainment from the thermocline by winter cooling. However, Gulf of Aden "expatriate" zooplankton and phytoplankton species do enter the Red Sea via the inflow during the winter monsoon, diffusing northward through the basin. Although some of these expatriates remain restricted to the strait region, others penetrate northward creating a pronounced north-south plankton species gradient during winter (Halim, 1984). The southern Red Sea then shows considerably higher species diversity than the north, with the two regions being separated by the species-poor downwelling convergence zone. Although the Gulfs of Suez and Aqaba have less diverse plankton communities than the main Red Sea, they also display a significant diversity increase in winter. The plankton diversity pattern is evident from the distributions of several taxa of phytoplankton and zooplankton, of which the copepods and dinoflaggellates are the best known. For example, about 92 % of all Red Sea copepod species were recorded in winter, and only 62 % in summer-autumn (Halim, 1984).

Thus, it appears that the distribution of the planktonic foraminiferal species in the Red Sea basin is a result of the dietary requirements of the individual species and the distribution and abundance of zooplankton and phytoplankton productivity. In turn, productivity distribution seems to be governed by circulation pattern, determined by surface wind stress over the sea surface, and exchange with the Gulf of Aden (see figure 3.4 for summary).

Chapter 4.

PALAEOCEANOGRAPHY AND PALAEOCLIMATOLOGY

This chapter discusses previous palaeoceanographic and palaeoclimatic studies concerning the Red Sea.

Several studies have been carried out on the palaeoceanography and palaeoclimatology of the Red Sea using various combinations of micropalaeontological and geochemical techniques to create a comprehensive history of the basin (Herman, 1965; Berggren, 1969; Berggren and Boersma, 1969; Chen, 1969; Goll, 1969; Herman and Rosenberg, 1969; Ku et al., 1969; McIntyre, 1969; Milliman et al., 1969; Wall and Warren, 1969; Meyer, 1973; Fleisher, 1974; Reiss et al., 1974; Deuser and Degens, 1976; Deuser et al., 1976; Risch, 1976; Schoell and Risch, 1976; Levanon-Spanier et al., 1979; Reiss et al., 1980; Halicz and Reiss, 1981; Almogi-Labin, 1982; Luz and Reiss, 1983; Winter et al., 1983; Luz et al., 1984; Locke, 1984; Reiss and Hottinger, 1984; Ivanova, 1985; Almogi-Labin et al., 1986; Locke and Thunell, 1987; Thunell et al., 1988; Almogi-Labin et al., 1991; Gupta, 1994; Rohling, 1994; Almogi-Labin et al., 1996; Hemleben et al., 1996; Naqvi and Fairbanks, 1996; Rohling and Zachariasse, 1996). These studies have clearly demonstrated that the Red Sea shows great sensitivity to glacial-interglacial cycles.

4.1 Increased NE monsoonal intensity during glacial maxima.

The seasonal variation between the SW and NE monsoons has a strong influence on the present day climatology (wind regime and humidity) and oceanography (surface waters) of the Red Sea (chapter 2). As such, it is necessary to understand palaeomonsoonal variations in order to assess changing climatic variables (wind regime and humidity) and their influence on the palaeoceanography (particularly surface currents) of the basin.

Today, the dominant humid, summer southwest monsoon causes strong southwesterly winds to blow across the northwest Arabian Sea, resulting in a northwestward surface current following the coast line. This induces zones of upwelling, and consequently phytoplankton

blooms, off the coasts of Somalia and Oman . When the monsoon system is reversed and the weaker arid, winter NE monsoon dominates, the Somali and Oman upwelling slows / ceases and the zone of upwelling is shifted to the coast of Pakistan and the coast of East India (Duplessy, 1982; Prell, 1984; Fontugne and Duplessy, 1986; Prell et al., 1991; Sirocko et al., 1991).

The history of the monsoons is preserved in the form of distinct plankton assemblages and sediment facies, forming a continuous geologic record of wind driven upwelling, and thus changes in the summer southwest monsoon winds. Various studies of sediments deposited over the last 20 ky show that during the LGM the NE monsoon was dominant. The intensity of monsoon driven upwelling is influenced by precessionally driven changes in summer insolation that alter the surface low-pressure over the Asian continent, and also by glacial-interglacial climate changes that alter the land sea atmosphere pressure gradient (Duplessey, 1982, Prell, 1984, Sarkar et al., 1990; Prell et al., 1991). Evidence from patterns of accumulation rates of wind borne dolomite, lithogenic carbonate, chlorite and palygorskite from the mid-tropospheric Arabian northwesterlies (Sirocko et al., 1991), large influx of Asian pollen (van Campo et al., 1982) and quartz (Kolla and Biscaye, 1977) in Arabian Sea glacial sediments; and high Corg sediments deposited off the coast of North India, Arabian Sea and Andaman Sea, where upwelling is driven by the NE monsoon winds, (Fontugne and Duplessey, 1986) show that dry continental northwesterlies persisted over the Arabian Sea through glacial times. Off the coast of Somalia, and Oman where the productivity depends on upwelling driven by the SW monsoon, a productivity decrease is observed (Curry et al., 1992). Reduced accumulation of biogenic opal (Sirocko et al., 1991), in the glacial sediments corroborates the upwelling weakness linked to the weak glacial SW monsoon (Fontugne and Duplessey, 1986, Sarkar et al., 1990), and the probable shorter glacial summer season (Sirocko et al., 1991).

Spectral analysis of *G.bulloides*, biogenic opal abundance, number of shells g^{-1} of sediment, and $\delta^{13}C$ *N.dutertrei* records from the Somalia and Oman upwelling sites show strong peaks at 1/100 ky (eccentricity), 1/23 ky (precession), and a weak cycle at 1/41 ky (obliquity) (Prell et al., 1992; Anderson, 1993). The 100 ky band is associated with the largest variation in ice

volume, and the 23 ky band with the largest variation in summer insolation (Imbrie et al., 1984). Maximum upwelling, and hence maximum SW monsoon intensity, is in phase with interglacials and the maximum variation in summer insolation, and the NE monsoon is in phase with glacial periods and the minimum variation in summer insolation (Van Campo et al., 1982; Prell and Van Campo, 1986; Prell et al., 1992; Anderson, 1993). The prevalence of the arid winter NE monsoon during glacial maxima would induce prolonged southeasterly winds over the surface of the Red Sea resulting in a surface water inflow of Gulf of Aden waters.

4.2 Glacial salinisation of the Red Sea basin.

Planktonic foraminifera are widely used in palaeoceanographic studies to show changes in surface water characteristics. The assemblages discovered in Red Sea cores are made up of mainly spinose species typical of tropical - sub-tropical, oligotrophic waters (Hemleben et al., 1989). *Globigerinoides ruber* is found as the dominant species, along with high abundance of *Globigerinoides sacculifer*, *Globigerinella siphonifera*, and *Globigerinita glutinata* (Berggren and Boersma, 1969; Risch, 1976; Schoell and Risch, 1976; Halicz and Reiss, 1981; Luz and Reiss, 1983; Locke, 1984; Ivanova, 1985; Locke and Thunell, 1987; Thunell et al., 1988; Hemleben et al., 1996).

The main feature of the planktonic foraminiferal records is the presence of an "aplanktonic zone" found in cores throughout the Red Sea and Gulf of Aqaba, corresponding to the Last Glacial Maximum (LGM) (Berggren and Boersma, 1969; Risch, 1976; Schoell and Risch, 1976; Halicz and Reiss, 1981; Luz and Reiss, 1983; Locke, 1984; Ivanova, 1985; Locke and Thunell, 1987; Thunell et al., 1988; Hemleben et al., 1996). In each case the aplanktonic zones have been described to commence rapidly over a period of approximately 5 ky, be centred around 20 ka BP and end abruptly around 8 ka BP. Very few or no planktonic foraminifera persist through these zones. Only *G. ruber*, a euryhaline, mixed layer dweller (Bé and Tolderlund, 1971; Tolderlund and Bé, 1971; Hemleben et al., 1989), is reported to persist, albeit in negligible abundances (Locke, 1984; Ivanova, 1985; Locke and Thunell, 1987; Thunell et al., 1988; Hemleben et al., 1996). The absence of planktonic foraminiferal tests in the glacial sediments cannot be attributed to dissolution since pteropods are found in

abundance throughout the aplanktonic zones (Locke, 1984; Almogi-Labin et al., 1991; Almogi-Labin et al., 1998). If dissolution were relevant, then the aragonitic tests of pteropods would have dissolved before the calcite tests of the planktonic foraminifera.

Since LGM sea surface temperatures in the Red Sea are thought to have been only 2-3 °C lower than today while surface water temperature in the Gulf of Aden showed no significant difference (CLIMAP, 1981), high salinity is held responsible for the disappearance of planktonic foraminifera in the last glacial interval (Herman, 1965; Berggren, 1969; Berggren and Boersma, 1969; Milliman et al., 1969; Deuser and Degens, 1976; Risch, 1976; Schoell and Risch, 1976 Reiss et al., 1980; Halicz and Reiss, 1981; Almogi-Labin, 1982; Luz and Reiss, 1983; Locke, 1984; Reiss and Hottinger, 1984; Ivanova, 1985; Almogi-Labin et al., 1986; Locke and Thunell, 1987; Thunell et al., 1988; Almogi-Labin et al., 1991; Rohling, 1994; Almogi-Labin et al., 1996; Hemleben et al., 1996). *G.ruber* has a salinity tolerance up to 49 ‰ (Bé and Hamlin, 1967; Bé and Tolderlund, 1971; Tolderlund and Bé, 1971; Hemleben, 1989), yet this species is absent throughout most of the period, or present in very low numbers, suggesting that salinities in the glacial Red Sea possibly exceeded 49 ‰ (Deuser and Degens, 1976; Risch, 1976; Locke, 1984; Locke and Thunell, 1987; Thunell et al., 1988; Almogi-Labin et al., 1991; Rohling, 1994).

Further evidence for high glacial salinity in the basin is seen in the benthic foraminiferal assemblage. Glacial Red Sea sediments are marked by the increase in relative abundance of miliolids (Locke, 1984; Halicz and Reiss 1981), a group known to dwell in hypersaline lagoons and shallow water (Halicz and Reiss, 1981). Locke (1984) also reported the highest abundance of *Ammonia sp.* at this time, a genus that is also known to dwell in hypersaline lagoons and shallow water (Halicz and Reiss, 1981). Secondary aragonite over-growth on pteropod tests is found extensively throughout the last glacial interval (Halicz and Reiss, 1981; Almogi-Labin et al., 1986; Almogi-Labin et al., 1991), in conjunction with a lithified sediment horizon attributed to lithification of particles cemented by inorganically precipitated aragonite (Milliman et al., 1969; Ivanova, 1984; Locke, 1984; Almogi-Labin et al., 1991). These data imply that bottom waters were supersaturated with respect to aragonite due to very high salinity and possibly slightly higher temperature (Milliman et al., 1969; Halicz and

Reiss, 1981; Ivanova, 1984; Locke, 1984; Almogi-Labin et al., 1986; Almogi-Labin et al., 1991). High concentrations of magnesium-carbonate are found in fine sediments at this time, supporting this hypothesis (Locke, 1984). Lowering of oxygen and reduced ventilation of Red Sea deep water at this time are also apparent from the glacial benthic foraminiferal assemblage and their $\delta^{13}C$ signal (Luz and Reiss, 1983).

Glacial Red Sea salinity values have been proposed on the basis of oxygen isotope records. For example, Hemleben et al. (1996) estimated surface salinity to be 53.8 ‰, Deuser and Ross (1976) suggested that 46.4 ‰ was a minimum value and Almogi-Labin et al. (1991) estimated a value of 48 ‰. Where the planktonic foraminifera *Globigerinoides ruber* was absent, Hemleben et al. (1996) used the clean tests of the pteropod *Creseis acicula* to obtain values for the LGM. The $\delta^{18}O$ value of this species is approximately 0.3 ‰ more negative than the value of aragonite which is precipitated in isotopic equilibrium with ambient sea water temperature and isotope composition (Jasper and Deuser, 1993). Using this information, Hemleben et al. (1996) established a mean $\delta^{18}O$ offset between *C.acicula* and *G.ruber* of -1.4 ±0.12 ‰ and employed this to convert the $\delta^{18}O$ value obtained from the pteropod sample to the $\delta^{18}O$-scale of *G.ruber*. Bottom water oxygen isotope variations in the epibenthic foraminifera *Hanzawaia sp.* and *Cibicides mabahethi* suggest a very high bottom water salinity of >55 ‰ during the last glacial maximum (Hemleben et al., 1996).

It is likely that the driving force behind such high basin salinities (in the region of 50 ‰) was the glacial lowering of global sea level (Deuser and Ross, 1976; Ivanova, 1985; Locke, 1984; Locke and Thunell, 1987; Thunell et al.,1988; Almogi-Labin et al., 1991; Rohling, 1994; Hemleben et al., 1996). At approximately 18 ky BP, the last glacial maximum, global sea level stood 120 m lower than present day (Fairbanks, 1989). This would have reduced the surface area of the Red Sea by approximately 50 % of its present day value (figure 4.1) (Locke, 1984). In the north the Gulf of Suez was exposed, and in the south the broad shallow shelves were dry land. The lowering of sea level caused great changes in the strait dimensions, and since the only significant exchange between Red Sea and Gulf of Aden waters through across the narrow and shallow Strait of Bab el Mandab, a dramatic reduction in water exchange between the Red Sea and the open ocean occurred (figure 4.2). The

Figure 4.1

Glacial surface area of the Red Sea

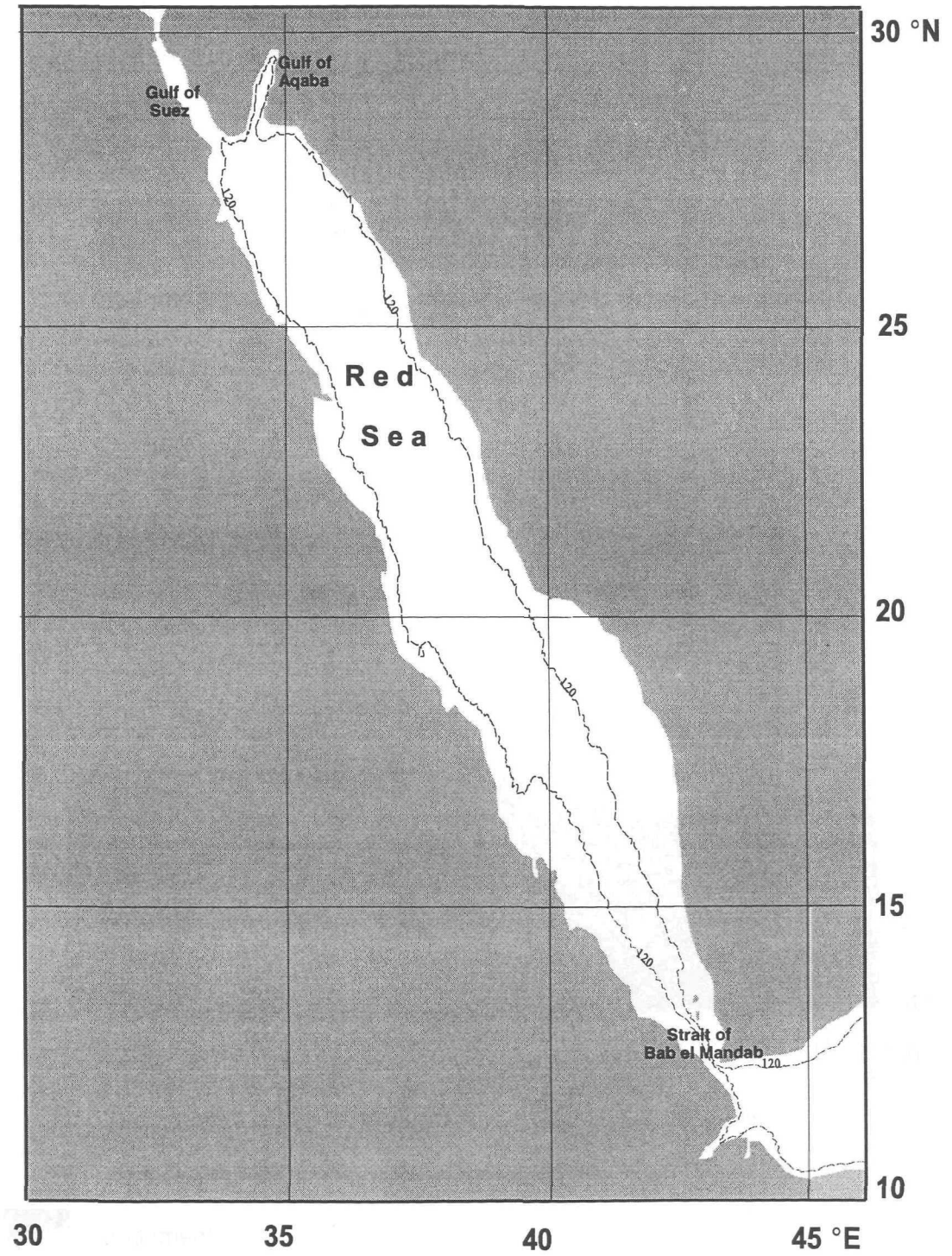

120 120 m contour (ie. sea level during the LGM)

Figure 4.2 **Cross section across the narrowest part of the Strait of Bab el Mandab (13° 44' 00" N).**

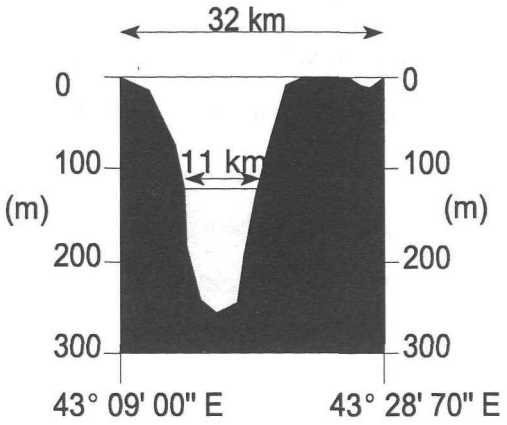

Cross section accross the shallowest part of the Strait of Bab el Mandab (12° 40' 00" N).

(After Werner and Lange, 1975)

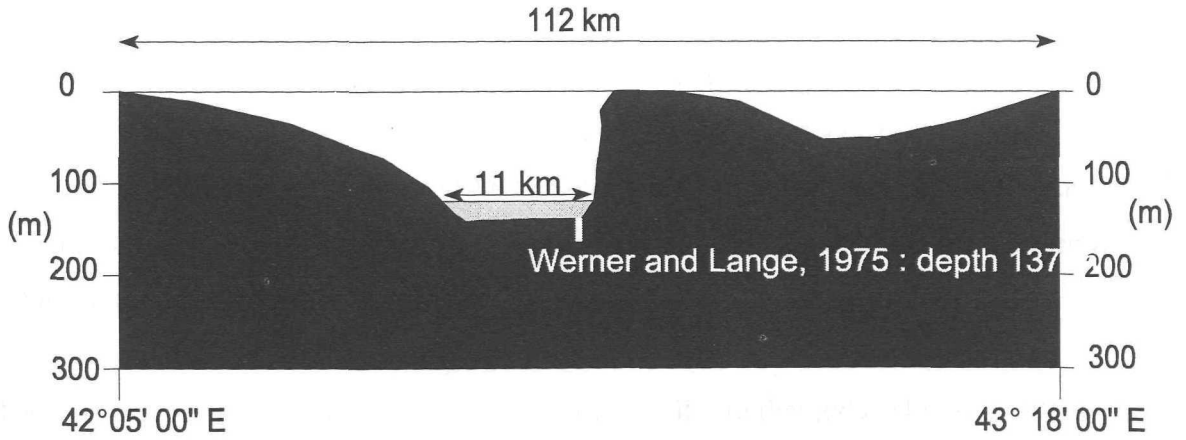

Surface area of the channel volume at present day sea level.

Surface area of the channel volume 18 ky BP.

Basement.

Depth values taken fom 'GEBCO' 5331, sheet 157a, soundings, 1981-82.

shallowest part of the sill is found close to Hanish Island with a depth of 137 m (Werner and Lange, 1975). Assuming the sill has not been significantly uplifted over the last 18 thousand years, the lowering of sea level at approximately 18 ky BP would have reduced this to 17 m depth, reducing the breadth of this channel from around 112 km to approximately 11 km, with depth values taken from GEBCO 5331 sheet 157a soundings, (1981-82), and incorporating the Werner and Lange (1975) value for the shallowest part of the sill. Hemleben et al. (1996) suggest that the sill height was deeper during glacial time and has since been tectonically uplifted. Their suggestion comes as a result of modelling the glacial flow regime over the sill at 17 m depth, using the hydraulic model of Assaf-Hecht (1974). Their results propose a two-way flow which breaks down at such shallow depths. Locke (1986) also modelled the flow over the sill using this model, however they used a glacial sill depth of 80 m. Their model, as the previous models mentioned, predicts that a reduction in width and/or depth of the Strait of Bab el Mandab, or an increase in evaporation over the Red Sea basin, will result in an increase in salinity in the basin (Thunell et al., 1988).

Present day exchange over the sill is seen as a seasonal change between a two-way flow in winter (northeast monsoon), and a three-way flow in summer (southwest monsoon). It is thought that a simple two-way flow was sustained in the shallow water column above the sill throughout the last glaciation since the prevailing wind was southeasterly due to intensification of the winter monsoon (Duplessy, 1982; Fontugne and Duplessy, 1985; Sirocko et al, 1991; Sirocko and Ittekkot, 1992), driving the surface current in a northwestward direction. Rohling (1994) suggests that continued flow in this direction would possibly set up a sea surface slope, resulting in a two-way flow system once equilibrium was achieved between the slope and the prevailing wind stress.

The evaporative loss of water from the basin was similar to that today (Locke, 1984; Rohling, 1994), so a 50 % reduction in surface area gives a 50 % reduction of evaporative volume. Hence, the reduction in Red Sea surface area by approximately 50 % resulted in reduced net evaporation from $0.88\times10^{12}\,m^3\,yr^{-1}$ to $0.44\times10^{12}\,m^3\,yr^{-1}$ (Locke, 1984; Rohling, 1994). Salinity estimates made from oxygen isotope values are dependant on whether the suggested present day increase in salinity of 1 ‰ with every 0.29 ‰ increase in $\delta^{18}O$ (Craig, 1966)

applies for the extreme hydrographic situation of the last glacial period. Rohling (1994) discussed the effects of evaporation due to increased wind stress in the last glaciation, as a result of the intensification of the northeast monsoon. His calculations showed that the surface water $\delta^{18}O$ fractionation with evaporation is -10 ‰ today, and may have been as small as -5 ‰ the LGM. This has recently been a topic of discussion by Hemleben et al., 1996, who suggest that if this fractionation indeed took place, then their salinity value of 54 ‰ for surface waters in the LGM would be a low estimate (by nearly 16 ‰).

4.3 Effects of deglaciation in the Red Sea.

A dark horizon in Red Sea core sediments, showing a relative increase in TOC content (described as "sapropelic"), immediately above the lithified horizon, has been AMS ^{14}C dated at 8 ky BP (Ivanova, 1984; Locke, 1984). This coincides with the final phase of post-glacial global sea level rise from 10 to 6 ky BP (Bard et al., 1987; Fairbanks, 1989; Bard et al., 1996).

Thunell et al. (1988) hypothesised the following explanation for the development of this horizon: The rise in sea level would have resulted in a sudden increase in volume of inflow of Gulf of Aden surface water into the Red Sea, washing the broad shallow (<100 m deep) shelves in the south as sea level rose. At the same time, 8 ky BP, the southwest (summer) monsoon was at its maximum intensity, with annual rainfall over the Arabian Peninsula higher by 100-400 mm relative to the present 25-100 mm (Prell and Streeter, 1981; van Campo et al., 1982; Fontugne and Duplessy, 1985; Prell and van Campo, 1986; Prell et al., 1992; Petit-Maire et al., 1994). Although input from permanent rivers into the Red Sea is negligible, it is possible that land run-off entered the Red Sea via wadi systems on the Arabian Peninsula (Rossignol-Strick, 1984). It is thought that the input of fresher, nutrient rich water from increased precipitation and land run off combined with the rapidly increasing volume of inflow from the Gulf of Aden into the basin at this time, decreased surface water salinity. This aided the rapid reestablishment of planktonic foraminifera communities and caused a stagnant episode in the deep waters, improving organic carbon preservation within the sediment.

Pteropod records show a completely epipelagic fauna suggesting that a strong separation between surface and intermediate waters, due to steep physical and chemical gradients, persisted at this time, impeding deep water formation off the Sinai Peninsula and, hence, ventilation of the deep waters. Maximum abundances of *Creseis chierchiae* may reflect a possible reduction in mixed layer thickness to < 50 m (Almogi-Labin et al., 1991; Almogi-Labin et al., 1998). Thus, it was inferred that circulation in the Red Sea, around 8 ky BP, was restricted to the upper part of the water column, mainly above sill depth, with surface water inflow from the Gulf of Aden and a Red Sea intermediate water outflow, and that deep waters were stagnant below (Locke, 1984; Locke and Thunell, 1987; Thunell et al., 1988).

Following approximately 1000 years of stagnation, the Red Sea underwent a drastic change over a very short time (approximately 1000 years) with salinities reaching present day values, and vertical density gradients reduced. This was noted in the increased abundance of mesopelagic pteropod species (up to 75 % of the assemblage) (Almogi-Labin et al., 1991). Between 4.6 and 2.0 ky BP it is suggested that renewal of deep and intermediate waters was invigorated as a result of down-welling of new Gulf of Suez bottom water, reactivated by the post glacial rise in global sea level, and northern Red Sea surface water (Almogi-Labin et al., 1991). Since the Gulf of Suez only reaches a maximum depth of 73 m, the Gulf of Suez source was terminated with the 120 m glacial fall in sea level (Morcos, 1979). Present day conditions were established over the last 2000 years (Almogi-Labin et al., 1991).

Chapter 5.

MATERIALS AND METHODS

This chapter introduces the core sediments used in this project and addresses the techniques used to create the data base for this study.

5.1 Material.

The sediment cores used in this study were collected by RV *Marion Dufresne*, Leg 73, in September 1992. The 10 cm diameter piston cores were split lengthwise and stored at 4 °C in PVC D-tubes with moisture saturated spongy material, at the Museum National d'Histoire Naturelle, Paris. (Core details in table 5.1, core locations on Figure 5.1 and in table 5.2).

5.2 Methods.

Table 5.3 summarises the techniques carried out on each core.

5.2.1 Foraminiferal analyses.

Samples were dried for 24 hours at ≤70 °C to prevent possible breakage of the foraminiferal tests under high temperatures. Samples were subsequently weighed (to obtain the total dry weight), then soaked in distilled water for approximately 10 minutes and wet sieved at mesh widths of 600 μm, 150 μm, 125 μm, and 63 μm. The sieved residues were thoroughly washed with distilled water, then dried at ≤ 70 °C and weighed (to obtain the dry weight per sieve fraction).

The 150-600 μm fractions were split into aliquots containing approximately 200 planktonic foraminifera using a statistically correct micro-splitter. This same size fraction was also split into aliquots containing approximately 250-300 benthic foraminifera. The foraminifera in the split fractions were speciated and sorted in a 64 cell slide and mounted. The various taxa were then counted and considered as a percentage of the total fauna (relative abundance), and also in terms of numbers per gram of sample dry weight (absolute abundance). The latter provides a means to detect possible closed sum effects in the relative abundance records.

Table 5.1. A summary of core parameters (after Caulet et al., 1992).

Core Number	**MD921017** (here after referred to as **1017**)	**MD921039** (here after referred to as **1039**)	**MD921005** (here after referred to as **1005**)	**MD921006** (here after referred to as **1006**)
Area	Red Sea	Red Sea	Gulf of Aden	Gulf of Aden
Latitude (°N).	19°23′24″	22°26′24″	11°35′13″	12°14′34″
Longitude (°E).	38°40′84″	37°13′15″	43°31′84″	43°31′84″
Water Depth (m).	570	1050	1490	480
Core Length (cm).	1540	750	1315	430
Sediment type.	Silty / sandy clay, with gradational contacts, calcareous biogenic components and shelly horizons	Silty / sandy clay, with gradational contacts, calcareous biogenic components and shelly horizons	Silty / sandy clay, with calcareous biogenic components. Lithology is uniform throughout. Occasional blocks of sharp angular basaltic material (up to 5 cm in diameter)	Inorganic silt and clay, with calcareous biogenic components. Lithology is uniform throughout. The sediment is shelly and occasional blocks of angular basaltic material (up to 5 cm in diameter) are found

Figure 5.1

Core Locations in the Red Sea and Gulf of Aden

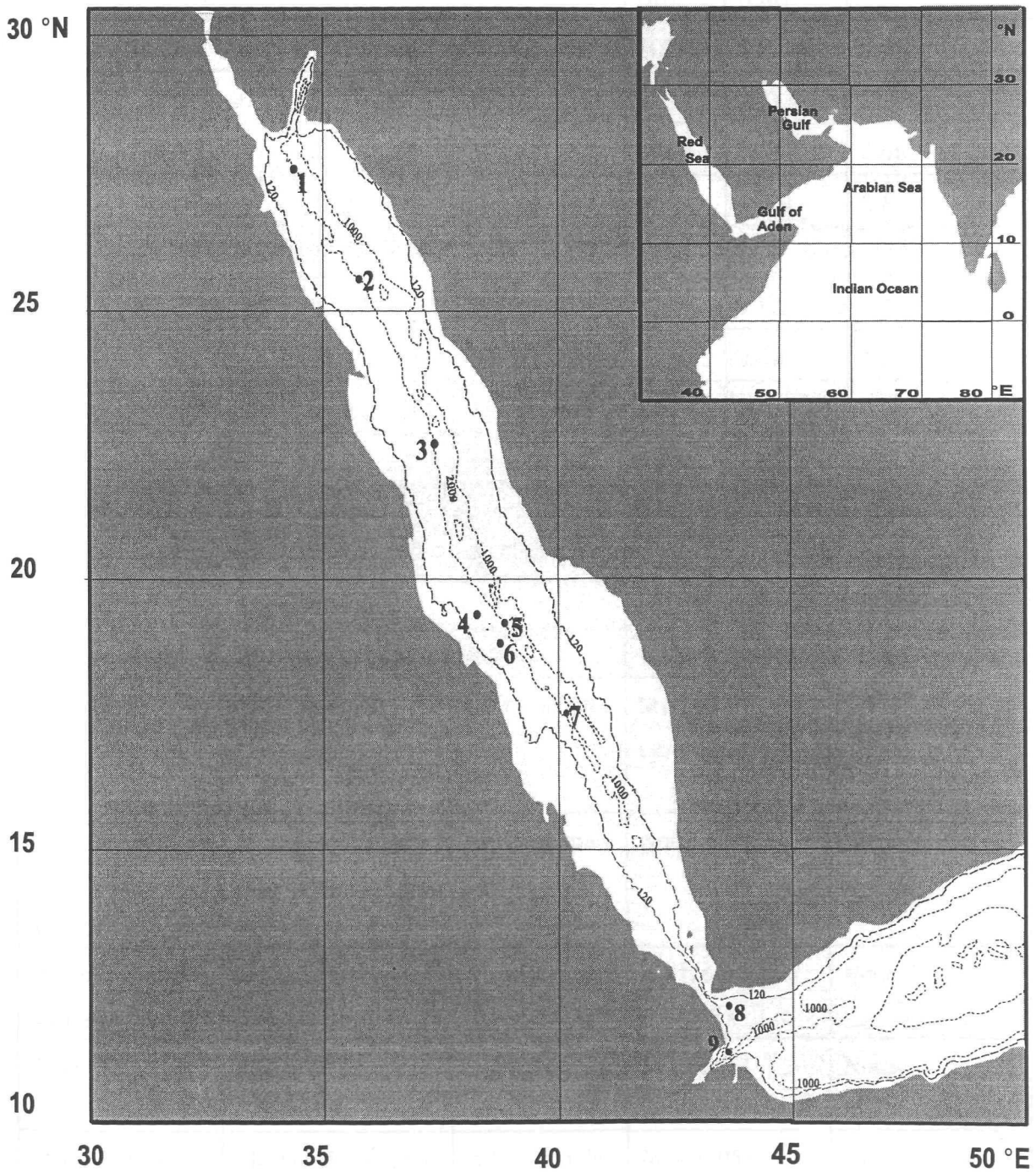

See table 5.2 for list of cores shown here.

Table 5.2 Locations of the studied cores from the Red Sea and Gulf of Aden (bold). Other cores shown are used for comparison in the study.

Refer to figure 5.1	**Core**	**Latitude**	**Longitude**	**Water Depth (m)**	**Length of Core (cm)**	**Sedimentation Rate (cm/ky)**
1	PC 68	27° 23' 02.4"	34° 16' 51"	1087	827	5-10
2	MD76-140	25° 40' 00"	35° 19' 48"	1050	450	
3	**MD92 1039**	**22° 26' 24"**	**37° 13' 15"**	**1050**	**750**	**2.66**
4	**MD92 1017**	**19° 23' 24"**	**38° 40' 84"**	**570**	**1540**	**2.8**
5	KL 13	19° 05' 09.6"	39° 04' 01.2"	1166		
6	KL 11	18° 27' 46"	39° 11' 56"	825	2093	
7	VA01-188P	17° 14' 9.6"	40° 03' 36"		1400	14-15
8	**MD92 1006**	**12° 14' 34"**	**43° 31' 84"**	**480**	**430**	
9	**MD92 1005**	**11° 35' 13"**	**43° 31' 84"**	**1490**	**1315**	

Table 5.3 Analytical techniques carried out on each core.

Analysis	Red Sea Cores		Gulf of Aden Cores	
	1017	1039	1005	1006
Planktonic foraminiferal analysis	All 157 samples	All 45 samples	Most (84) samples	All 39 samples
Benthic foraminiferal analysis	A pilot study has been carried out on 44 samples	All 45 samples	None	None
Organic carbon analysis	Most (145) samples	All 45 samples	All 126 samples	None
AMS ^{14}C	3 selected samples	3 selected samples	14 selected samples	None
Stable isotope (oxygen and carbon) analysis	Most (145) samples	All 45 samples	Most (105) samples	None

5.2.2 Total organic carbon (TOC) analyses.

Sub-samples of approximately 1 cm^3 in size were dried at a temperature no greater than 70 °C. For TOC determinations, inorganic carbon (carbonate) needs to be removed. This was done by acidification, using dilute hydrochloric acid. Normally the yield of this acidification relative to the carbonate content is between 99 and 100 %. However, in sediments that are very rich in carbonate a 50 % error may be generated in the yield, particularly if the TOC content of the sample is low. Even though a maximum of precautions may be taken to eradicate these problems (double acidification, visual control) the uncertainty is not controllable or measurable. More drastic chemical attack by acidic hydrolysis would generate organic matter hydrolysis so it is not a valid option, and the problem seems, as yet, unresolved (P.Bertrand, pers. comm. 1996).

Firstly five samples selected from core 1005 were prepared in the above manner and then split roughly in half. One of each of the samples was analysed using a Carlo Erba elemental analyser at the University of Cambridge, and a replicate analysis was performed using a Carlo Erba elemental analyser at the University of Southampton, Department of Geology. The results of these trial analyses showed high TOC values with large discrepancies between the results from the two sites (table 5.4). This was possibly due to the difference in the preparation techniques used between the sites. At Cambridge carbonate was removed by acidification using 2 M HCl in the sterile tin cups which are then put directly into the Carlo Erba. This method risks sample loss on addition of the acid through violent effervescence since the tin cups are very shallow. In Southampton carbonate was removed from the sample, again using 2 M HCl, in acid cleaned test tubes. Here there is a risk of sample contamination owing to the cleanliness of the tubes. In both cases acidification was stopped when all effervescing had stopped.

After discussion with Dr. Philippe Bertrand, it was decided that all dried samples from cores 1005, and 1017 and 1039, should be prepared and analysed in one laboratory at the University of Bordeaux, Department of Geology and Oceanography. The samples were analysed for percentage organic carbon content using a LECO 125-CS elemental analyser, with an error of detection of less than +/- 5 % of the measured value.

Table 5.4 Results of trial TOC analyses carried out in conjunction at Cambridge University and at Southampton University.

Depth in core 1005	TOC % (Cambridge)	TOC % (Southampton)
90-91.5	5.71	7.58
225-226.5	6.05	8.09
598-599.5	6.32	6.63
812-813.5	5.05	1.66
1238-1239.5	4.23	1.63

5.2.3 AMS ^{14}C dating.

Preparation for AMS ^{14}C dating involved picking 10 to 15 mg of clean, dry planktonic foraminifera. The specifically chosen samples were sent to Utrecht University for analysis. Three samples were picked from both core 1017 and core 1039 (Red Sea). It was hoped that these results would give an accurate age for the core tops and date the disappearance and return of planktonic foraminifera in the upper aplanktonic zones (see section 5.5) in each case. Initially six samples from core 1005 (Gulf of Aden) were chosen and prepared for AMS ^{14}C dating. However the results showed evidence of a redeposition event in the middle of the core. In order to ascertain the extent of this interruption a further 8 samples were prepared and analysed.

5.2.4 Stable isotope (oxygen and carbon) analysis.

Oxygen and carbon stable isotope records are based on single species pickings of 10 clean specimens of *G.ruber* per sample, from a size range 400-450 μm as determined by measurement of each specimen's longest axis. *G.ruber* is used as this species shows continuous presence throughout the cores. The use of single species records avoids complications that might arise from multi-species records due to metabolic "vital effect" fractionations. Sizes were controlled by measurement rather than dry sieving, since measurements provide vital improved control of the size fraction analysed, reducing the effects of changing fractionation through the various ontogenetic stages (Kroon and Darling, 1995).

Analyses were performed at the University of Amsterdam, using a Finnigan MAT 251 mass spectrometer combined with an automated Finnigan MAT carbonate preparation line (Bremen type). The stable isotope data were referred to the PDB standard notation and calibrated via NBS 19 and 20. The analytical precision of the carbonate standard was ±0.09 ‰ (1 sigma) and ±0.05 ‰ for $\delta^{18}O$ and $\delta^{13}C$ respectively.

Chapter 6.

RESULTS

This chapter is presented in two parts; part 1 concerns the practical results for Red Sea cores 1017 and 1039, and part 2 concerns the practical results for Gulf of Aden cores 1005 and 1006.

PART 1: THE RED SEA.

6.1 Chronology and inter-core correlation.

Time-stratigraphic frameworks have been obtained for cores 1017 and 1039 through comparison between the oxygen isotope stratigraphy (figure 6.1) and the orbitally tuned ice volume model (SPECMAP, Imbrie et al. (1984) (table 6.1)). Despite the data being less detailed and approximately 1000 years older than the more recent estimates of Martinson et al. (1987), the greater amount of time covered in the SPECMAP data (upto and including stage 22) was favoured in this study owing to the long record of core 1017. The time stratigraphic frameworks were supported by AMS ^{14}C dates (figure 6.1, table 6.2) and finally presented in comparison with the time-stratigraphic framework of the 22 m long piston core 174/KL11 (figure 6.2) (Hemleben et al., 1996), the longest Red Sea core record published to date).

The AMS ^{14}C results (table 6.2) confirm that the youngest 'aplanktonic zone' seen in cores 1017 and 1039 spans the last glacial maximum, between 10 and 30 ka BP.

On the basis of the isotope stratigraphic "datings" and the AMS ^{14}C results, age versus depth plots were prepared for the cores (figs 6.3 and 6.4). The results show virtually straight line plots ($r^2>0.9$), witnessing a continuous and steady sedimentation rate throughout the cores. A polynomial curve (of best fit) has been applied to the original curves. Although the polynomial curve is not statistically better than a linear fit, its excellent fit to the data meant that the model could be used to determine age at arbitrary depths within the cores quickly and easily. AMS ^{14}C dates were coverted to calendar ages (ka Bp_{cal}) using the Calib 3.03 program written by Stuiver and Reimer (1993). No regional effect (ΔR) was used as non has been

Figure 6.1

Oxygen Isotope Records. Cores 1017 and 1039, Red Sea.

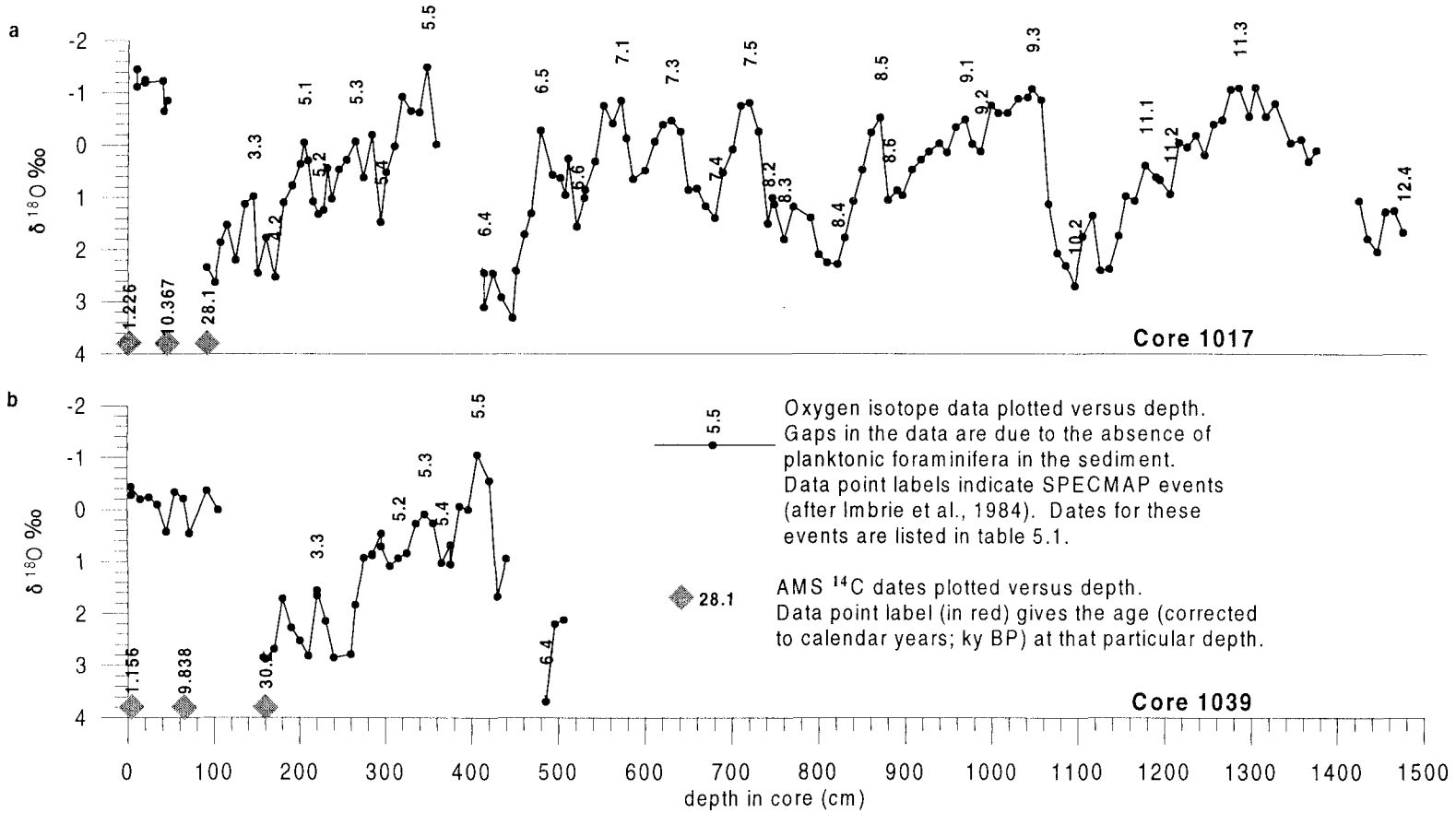

Figure 6.2 **Oxygen isotope record of core 174/KL11**

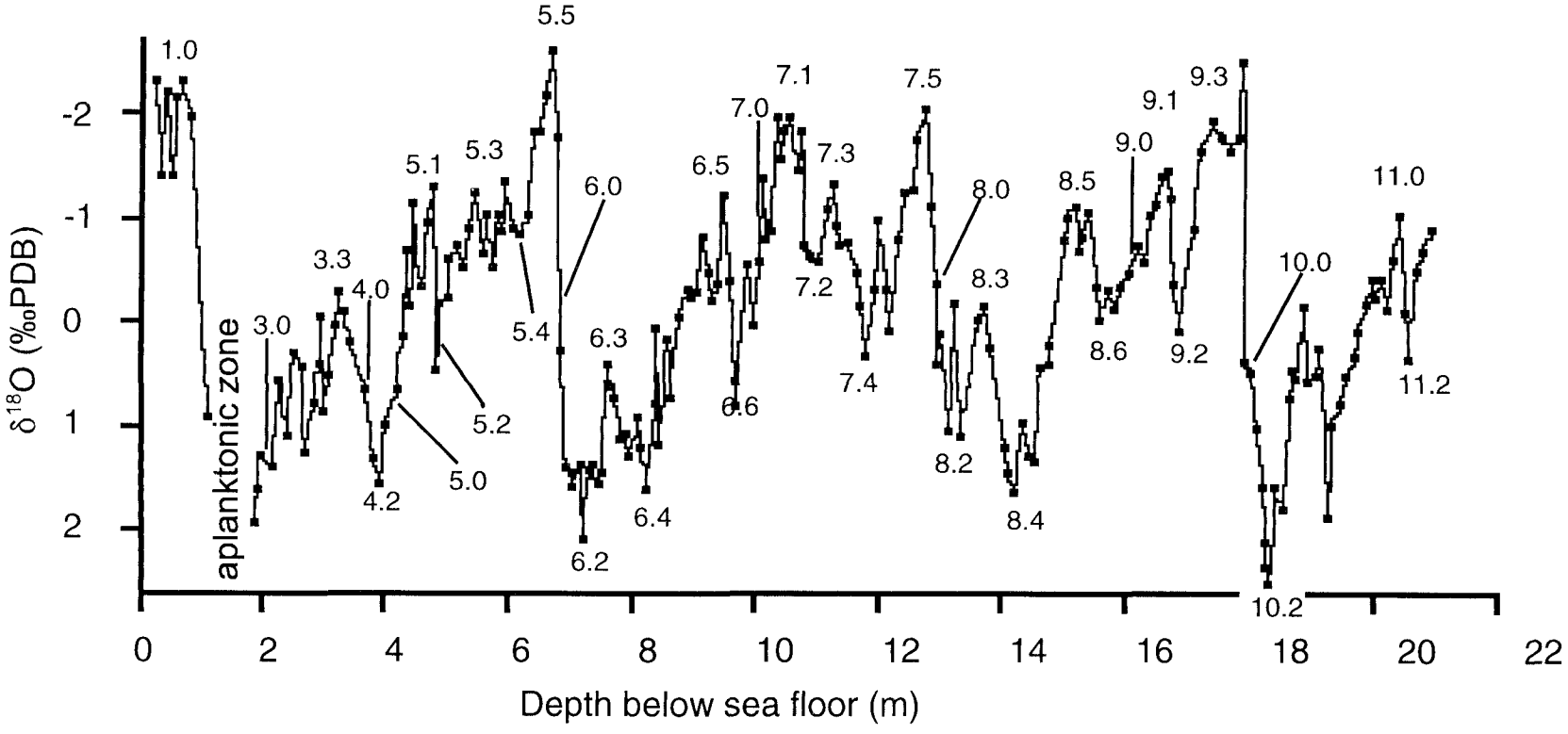

From Hemleben et al., 1996

Table 6.1 The SPECMAP time scale (after Imbrie et al., 1984). Isotopic events 2.0, 3.0 etc. (in bold text) are stage boundaries.

Event	Age ka BP	Event	Age ka BP
2.0	**12**	**8.0**	**245**
3.0	**24**	8.2	249
3.3	53	8.3	257
4.0	**59**	8.4	269
4.2	65	8.5	287
5.0	**71**	8.6	299
5.1	80	**9.0**	**303**
5.2	87	9.1	310
5.3	99	9.2	320
5.4	107	9.3	331
5.5	122	**10.0**	**339**
6.0	**128**	10.2	341
6.4	151	**11**	**362**
6.5	171	11.1	368
6.6	183	11.2	375
7.0	**186**	11.3	405
7.1	194	**12.0**	**423**
7.3	216	12.4	471
7.4	228		
7.5	238		

assigned to the Red Sea basin (Stuiver and Brazunias, 1993). These dates were used to verify the polynomial age model in the upper part of the core, showing extremely good correlation between the values (table 6.2). The polynomial model is as follows:

$y=a_0+a_1\times b+a_2\times b^2+a_3\times b^3+a_4\times b^4...+a_n\times b^n$

where y=age, a=polynomial coefficient (listed in table 6.3), b=depth in core.

Figure 6.3

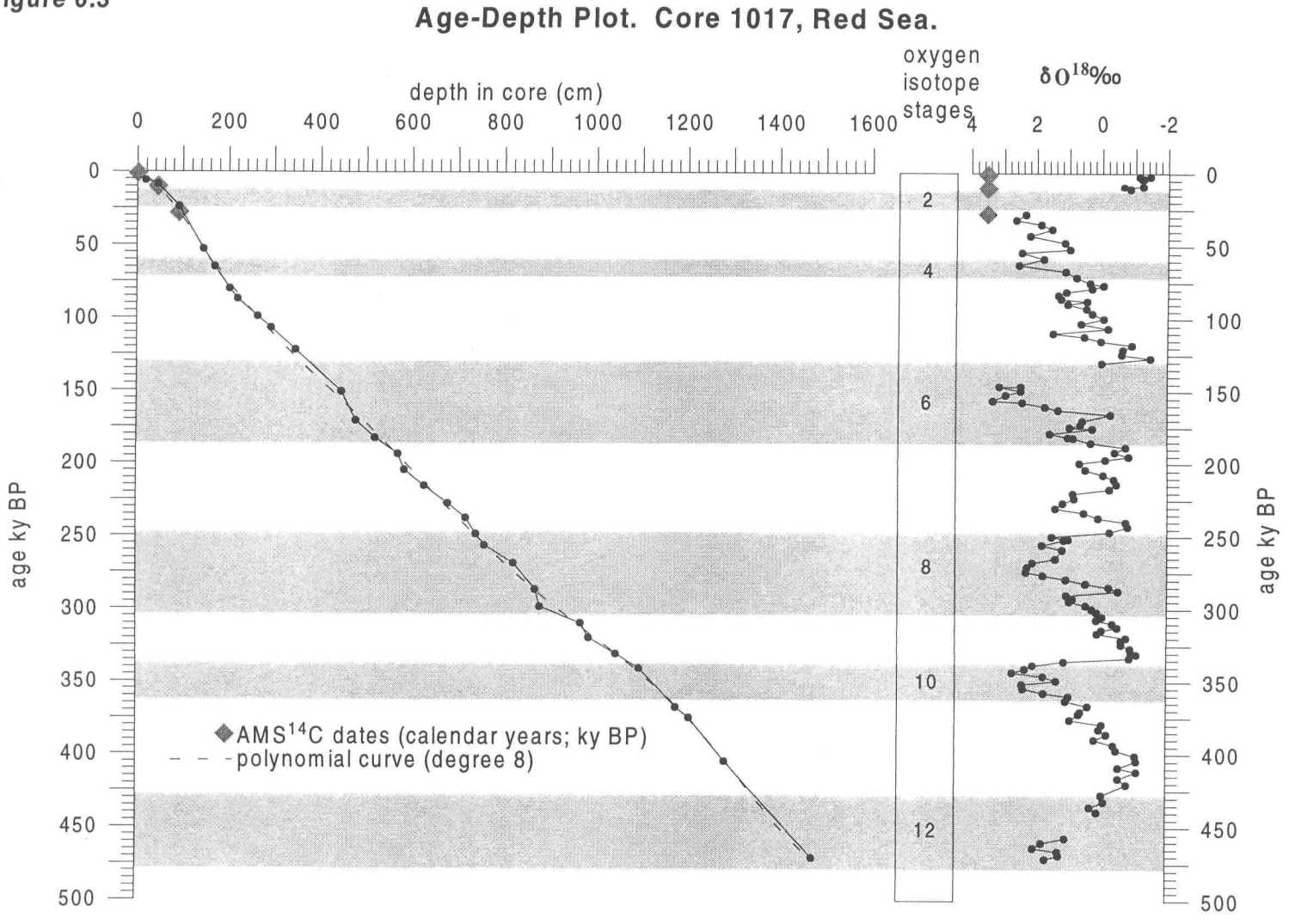
Age-Depth Plot. Core 1017, Red Sea.
depth in core (cm)
0
200
400
600
800
1000
1200
1400
1600
oxygen isotope stages
δO18‰
4
2
0
-2
2
4
6
8
10
12
age ky BP
0
50
100
150
200
250
300
350
400
450
500
AMS14C dates (calendar years; ky BP)
polynomial curve (degree 8)

Figure 6.4

Age-Depth Plot. Core 1039, Red Sea.

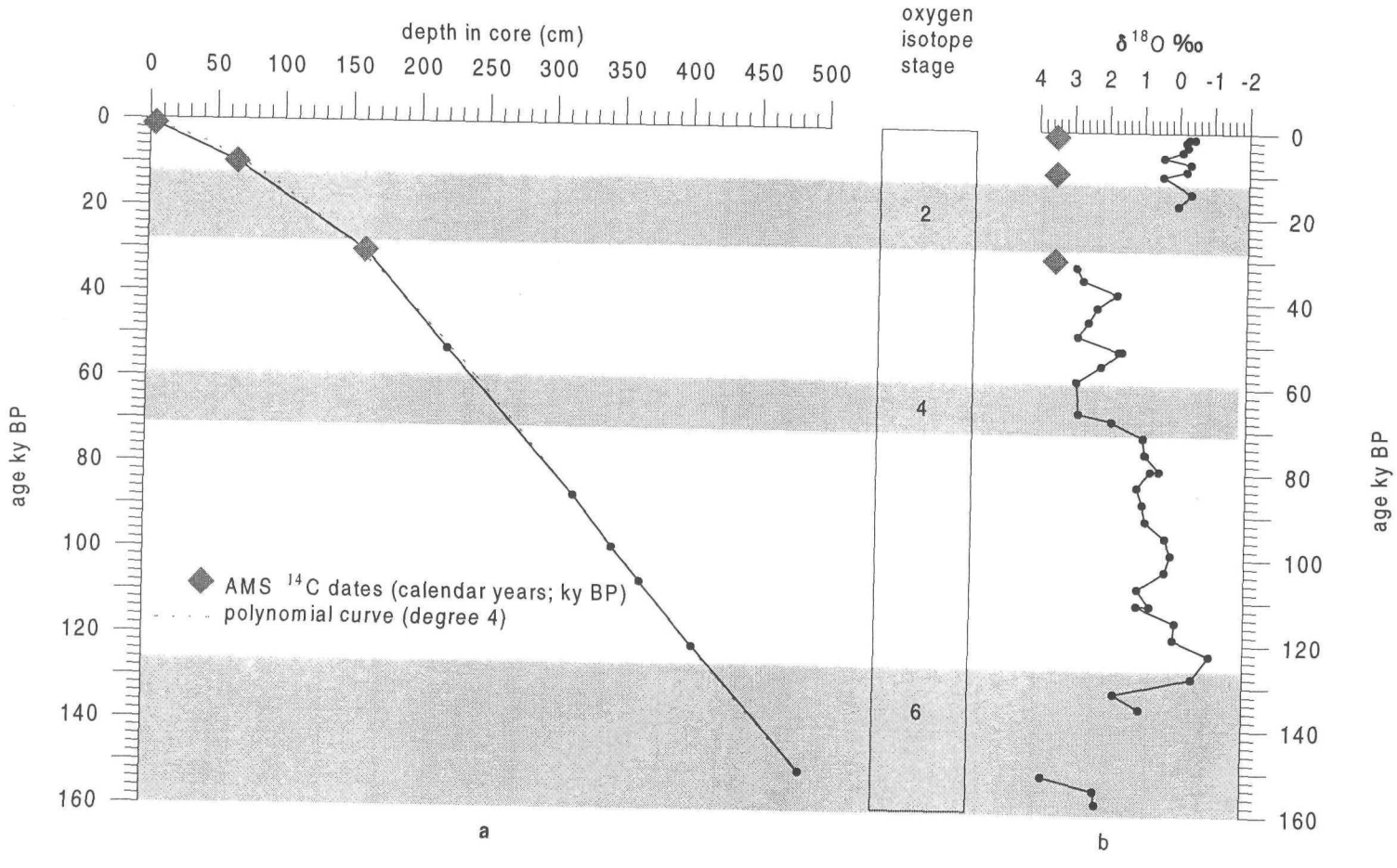

Table 6.2 AMS ^{14}C dates obtained for cores 1017 and 1039, Red Sea.

	Depth in core (cm)	**Laboratory number UtC-Nr reference**	**AMS ^{14}C date (^{14}C ka BP)**	**AMS ^{14}C corrected to calendar years (ka BP_{cal})**	**Polynomial age estimate (ka BP)**
Core 1017	1	5815	1.67 ±0.026	1.22	1.07
	45	5816	9.68 ±0.041	10.37	10.61
	91.5	5817	25.3 ±0.200	28.1	28.33
Core 1039	3.8	5818	1.61 ±0.030	1.16	1.43
	64.8	5820	9.15 ±0.047	9.84	8.98
	159.8	5819	27.4 ±0.240	30.2	31.8

Table 6.3 Polynomial coefficients of the age models used for cores 1017 and 1039, Red Sea.

polynomial coefficient number (a)	**Core 1017 polynomial 8 coefficients**	**Core 1039 polynomial 4 coefficients**
a_0	0.982952	1.17553
a_1	0.0809173	0.0635054
a_2	0.00363979	0.000929681
a_3	-1.6847×10^{-5}	-7.66183×10^{-7}
a_4	3.78095×10^{-8}	-2.15688×10^{-10}
a_5	-4.61693×10^{-11}	
a_6	3.11153×10^{-14}	
a_7	-1.08144×10^{-17}	
a_8	1.50462×10^{-21}	

Summarising, core 1017 provides an uninterrupted record of over 471 ky of deposition in the central Red Sea. Core 1039 also contains an uninterrupted sedimentary record that covers a shorter time span of over 171 ky and provides excellent comparative material for the sediments down to that age, as found in core 1017.

6.2 Down-core sedimentary variations.

Figures 6.5 and 6.6 show down-core sedimentary variations for cores 1017 and 1039 respectively. Both cores contain clay sediments that are beige in colour. Core 1039 contains an olive green clay horizon between 70-74 cm depth around (10.5 ka BP). This corresponds to a similar olive green clay horizon at 41-48 cm depth (around 11.5 ka BP) in core 1017, however, the boundaries of this horizon are not as sharp as those seen in core 1039. The main feature of the cores is a coarse zone with abundant carbonate concretions (up to 80 % of the sediment is in the 600 μm size range) corresponding to glacial isotope stage 2 (12-24 ka BP) in both cores. Above this, to core top, there is a small but distinct increase in the 150-600 μm sediment fraction in both cores. Core 1039 also shows an increase in the >600 μm fraction in core top sediments. The dominant sediment size fraction throughout the rest of the core is <63 μm, with an abundance generally greater than 70 %.

6.3 Down-core organic carbon (TOC) variations.

Both cores 1017 and 1039 show generally low values of TOC % within the sediment (<0.5 %) (figs 6.7a and b).

The down-core variation in the TOC content (weight %) for core 1017 (figure 6.7a) is very noisy. A peak value (0.97 %) occurs at 11.58 ka BP, at the end of glacial isotope stage 2. This value is preceded by variable, but predominantly low TOC values (approximately 0.25 %). Following this peak, values are variable but fall to between 0.30 - 0.45 % up to present day.

Core 1039 shows a low amplitude down-core variation of TOC (figure 6.7b), with general values around 0.25 %. At 10.2 ka BP, the TOC % peaks at 2.8 %, following isotope stage 2. This correlates well with the peak TOC value in core 1017, although deposition of the high TOC sediment in core 1017 is implied to be 750 years earlier. This peak corresponds to the "sapropelic" horizon, dated at around 8 ka BP, found in Red Sea sediments (Ivanova, 1984; Locke, 1984). Hereafter, the organic carbon rich layer will be termed as the "sapropelic horizon".

Figure 6.5

Down-Core Variations in Sediment Grain-Size Classes, Core 1017, Red Sea.

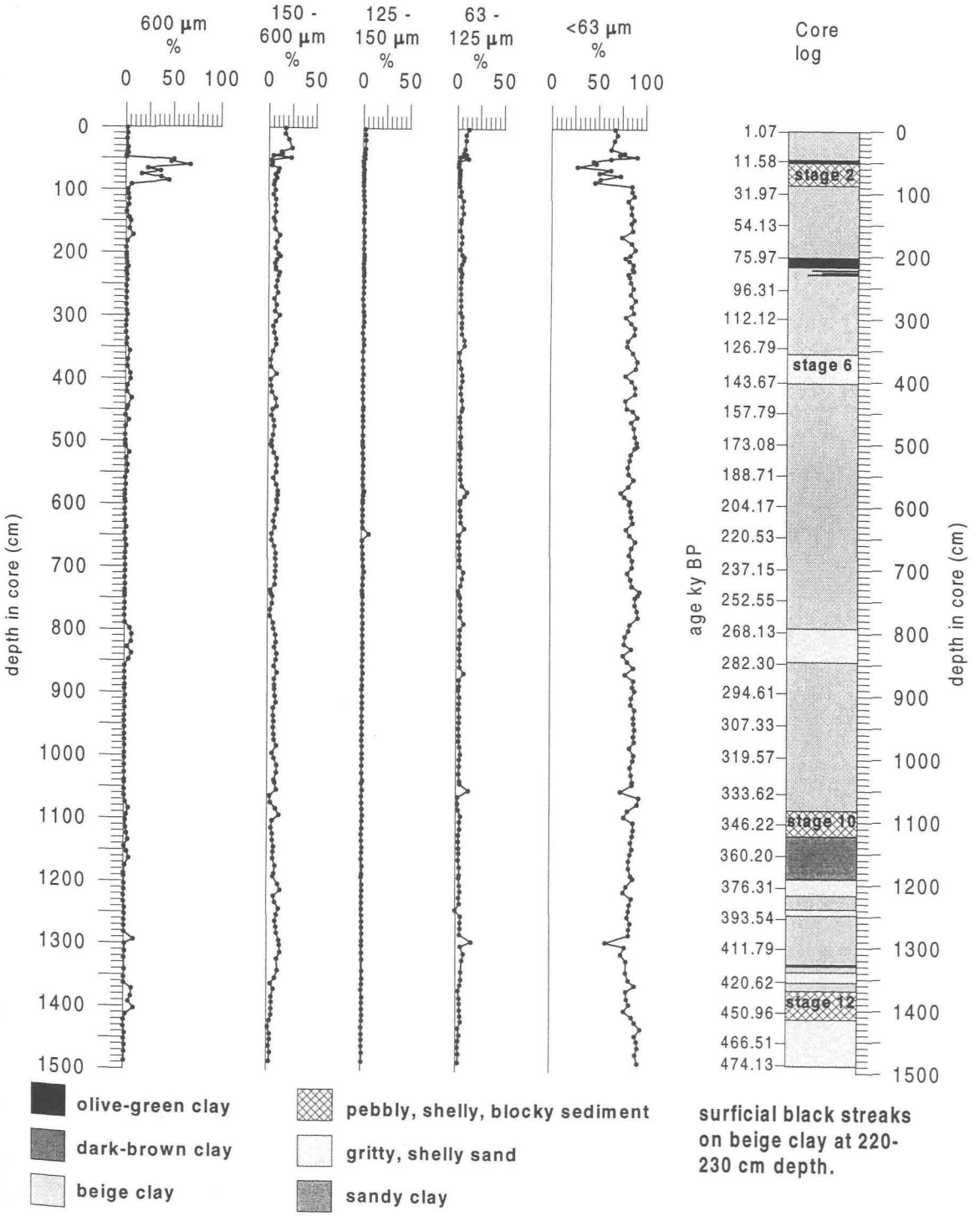

surficial black streaks on beige clay at 220-230 cm depth.

Figure 6.6

Down-Core Variations in Sediment Grain Size Classes, Core 1039, Red Sea.

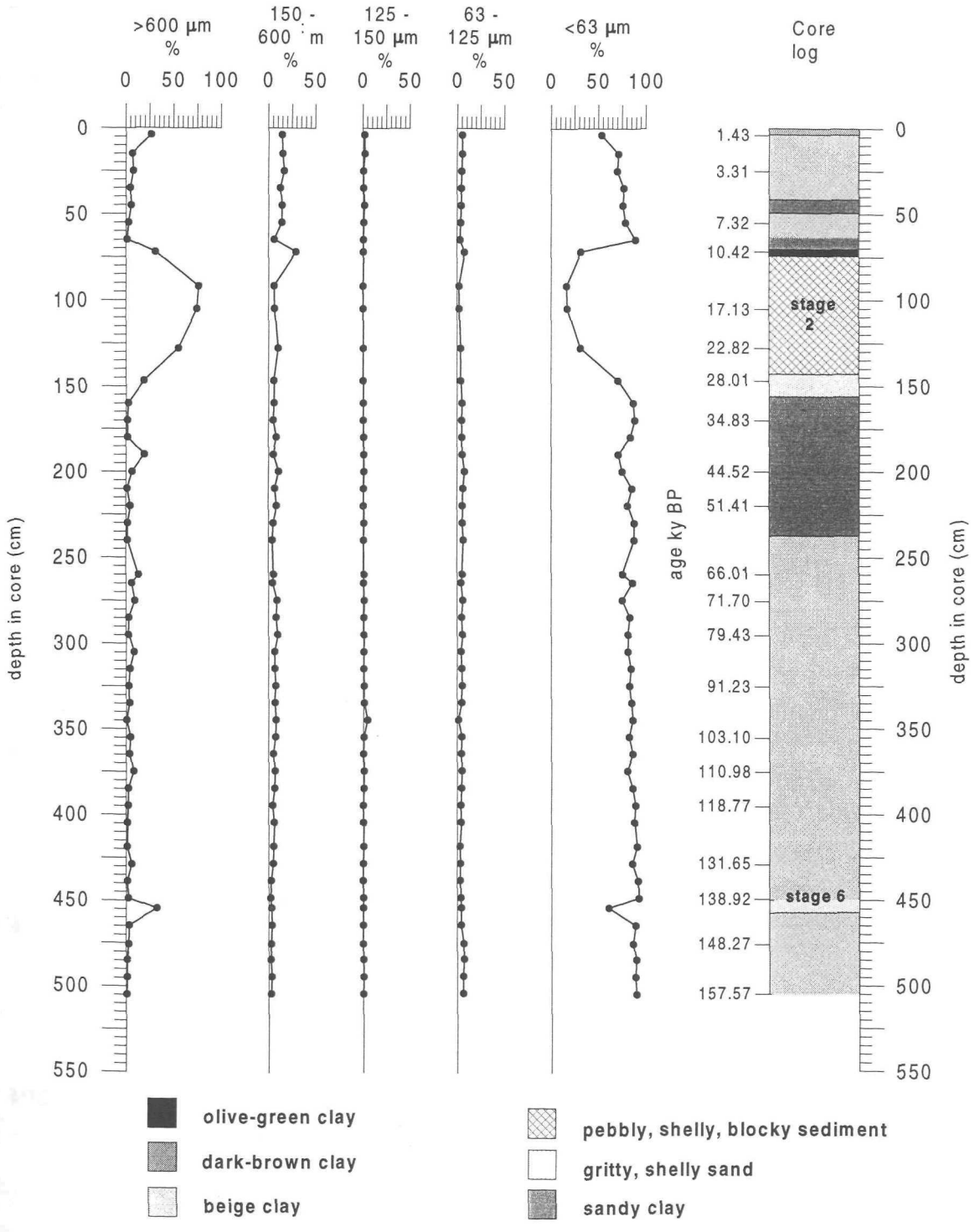

Figure 6.7

Down-Core Geochemical Variations. Cores 1017 and 1039, Red Sea.

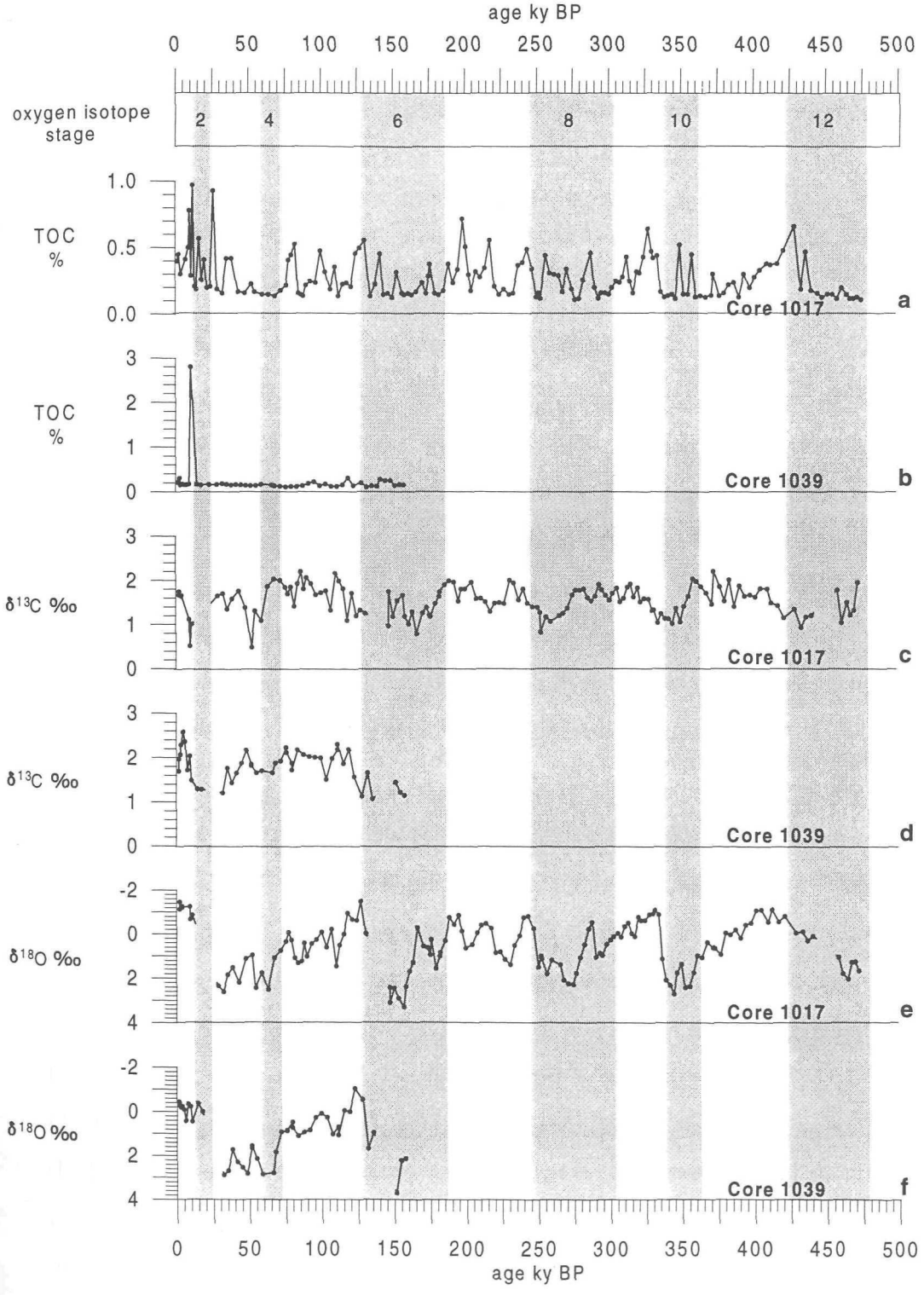

6.4 Down-core isotope variations.

Stable oxygen and carbon isotope analyses on *G.ruber* from the 400 to 450 μm size fraction were carried out on both cores 1017 and 1039 (figures 6.7c,d,e and f).

The down-core variations in $\delta^{13}C$ and $\delta^{18}O$ show a predominant glacial-interglacial influence. Enriched $\delta^{13}C$ values are found in both cores during interglacial periods and lower values are found during glacial intervals. Values range between 1 ‰ and 2.6 ‰ in core 1039 and 0.5 ‰ and 2.2 ‰ in core 1017. Normal oceanic glacial-interglacial $\delta^{13}C$ variations are also in the order of 2 ‰ (Libes, 1992). No obvious change in $\delta^{13}C$ values is seen in conjunction with the TOC enriched sediments.

High $\delta^{18}O$ values are found during glacial intervals (where samples were available) in both cores 1017 and 1039. Values are spread over a wide range, spanning 5-6 ‰, (3.8 ‰ to -0.9 ‰ in core 1039 and 3.4 ‰ to -1.5 ‰ in core 1017) which strongly exceeds normal oceanic ranges of $\delta^{18}O$ variability which span 1 ‰ to 2 ‰ (Kennett, 1982; Libes, 1992; Rollinson, 1993). This high amplitude variation found in the Red Sea is attributed to the concentration effect of the basin, owing to the high evaporation (2 m yr^{-1}) and restricted communication with the open ocean, so that the basin functions as an amplifier of normal climate/ocean variability (Rollinson, 1993). The observed Red Sea oxygen isotope variation pattern is very similar to that of the open ocean and its amplification provides detailed isotope stratigraphy.

6.5 Down-core planktonic foraminiferal variations.

Cores 1017 and 1039 have provided an excellent record of planktonic foraminiferal history in the central Red Sea. Both cores contain mainly tropical-subtropical spinose species typical of oligotrophic, gyre centre surface waters. *Globigerinoides ruber* (plate 1) is the most common species found in the sediment of both cores. It is accompanied by high abundances of *Globigerinita glutinata* (plate 7), and *G.sacculifer* (plates 2 and 3), *G.rubescens* (plate 4), *O.universa*, *G.tenella* (plate 5) and *G.siphonifera* (plate 6) combined as the SPRUDTS group (Rohling et al., 1993) (figures 6.8, 6.9, 6.10 and 6.11). Total planktonic foraminifera per gram of sediment versus age for both 1017 and 1039 (figure 6.12) show obvious dominance of full glacial influences on these records, marked by distinct aplanktonic zones with no or

Figure 6.8

Relative abundance of the most common planktonic foraminiferal species. Core 1017, Red Sea.

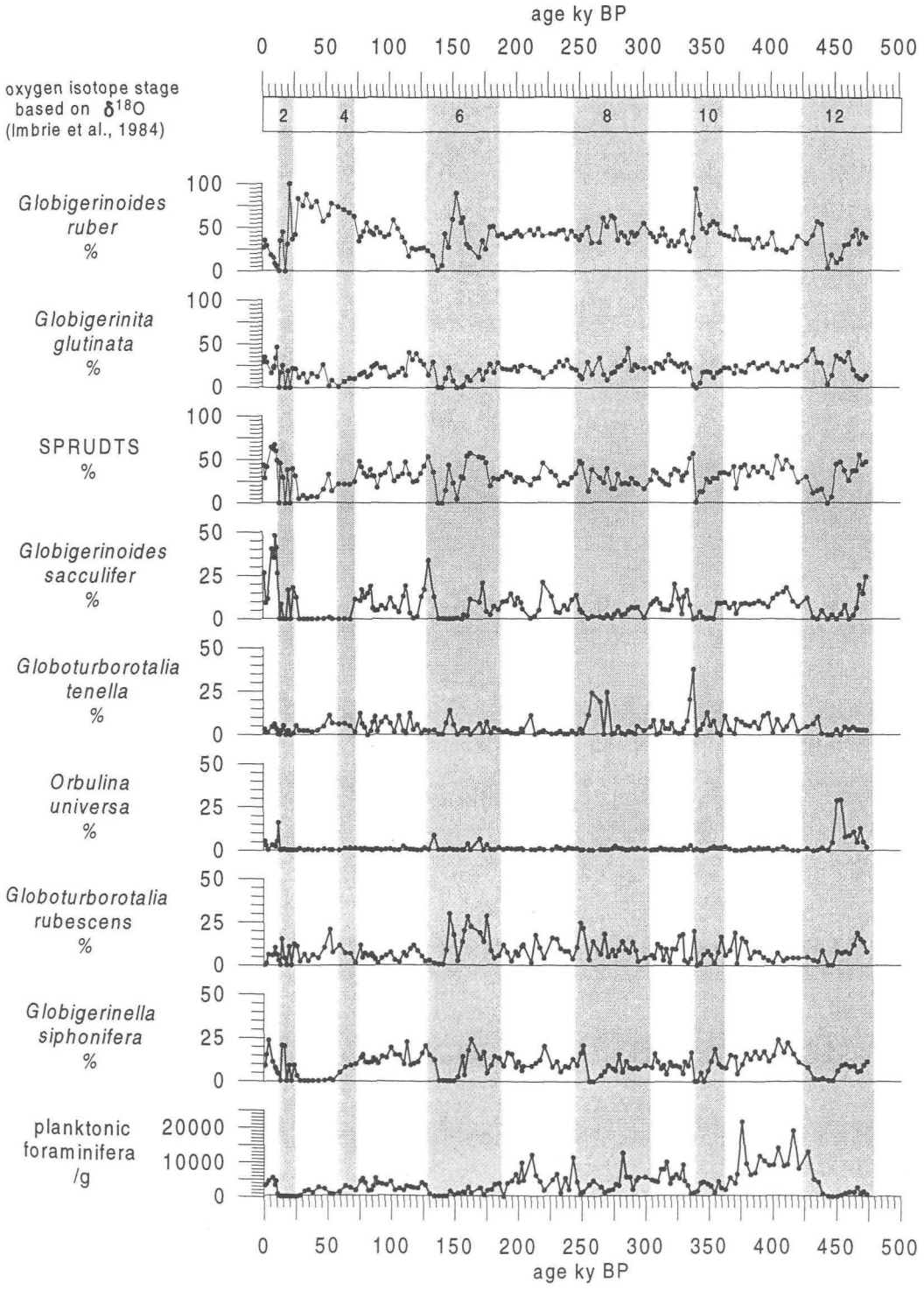

Figure 6.9

Relative abundance ofthe most common planktonic foraminiferal species. Core 1039, Red Sea.

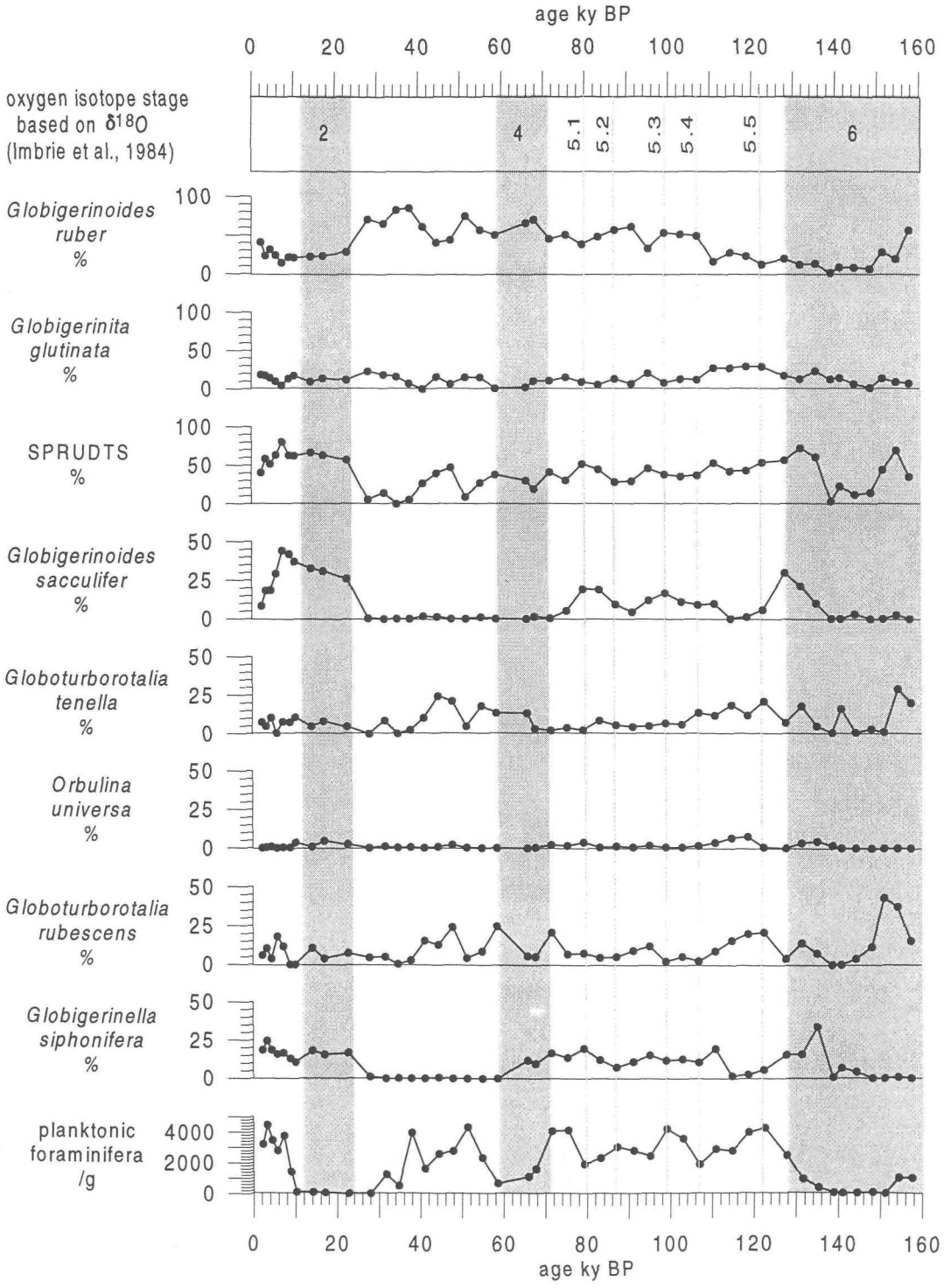

Figure 6.10

Absolute numbers of the most common planktonic foraminiferal species. Core 1017, Red Sea.

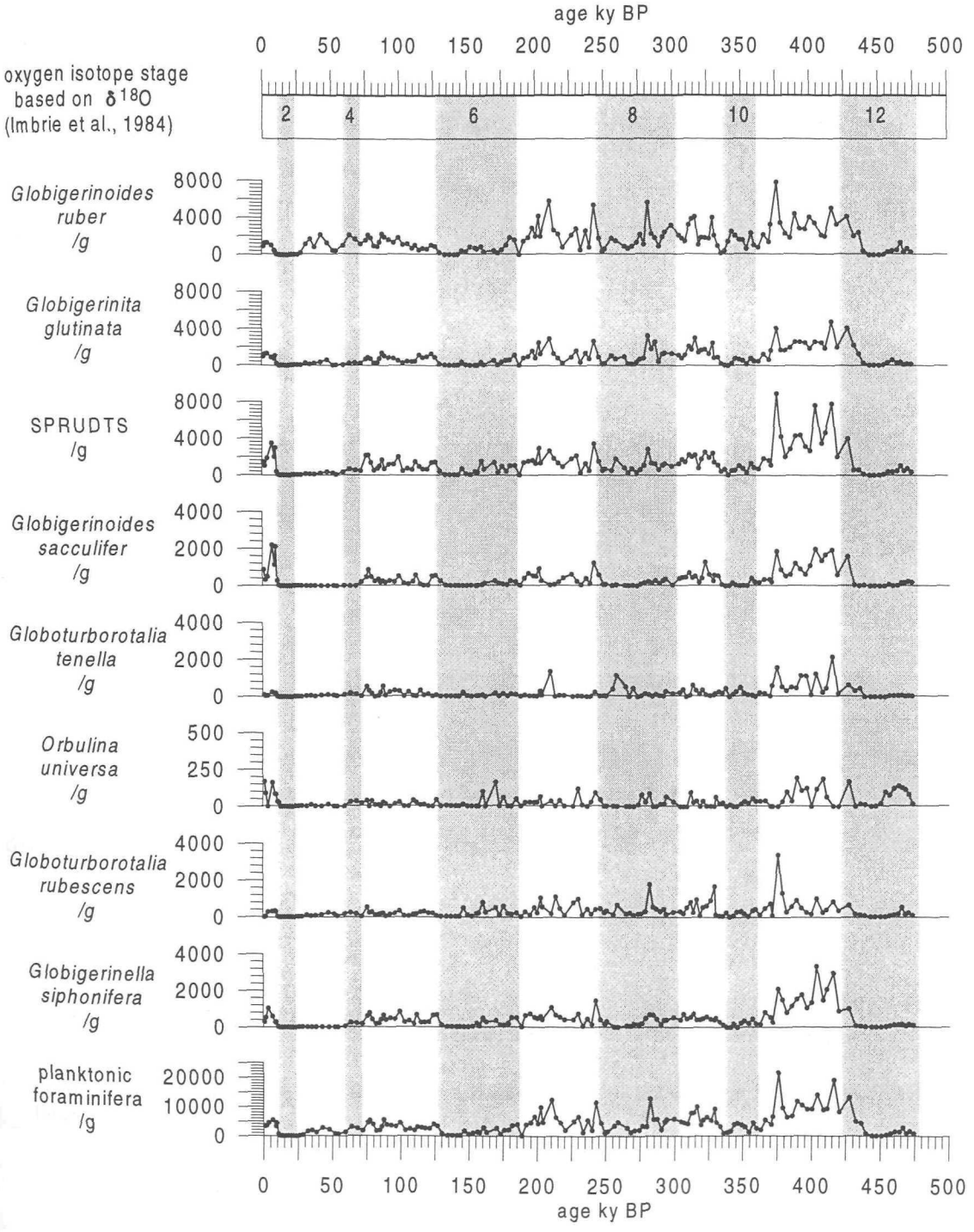

Figure 6.11

Absolute numbers of the most common planktonic foraminiferal species. Core 1039, Red Sea.

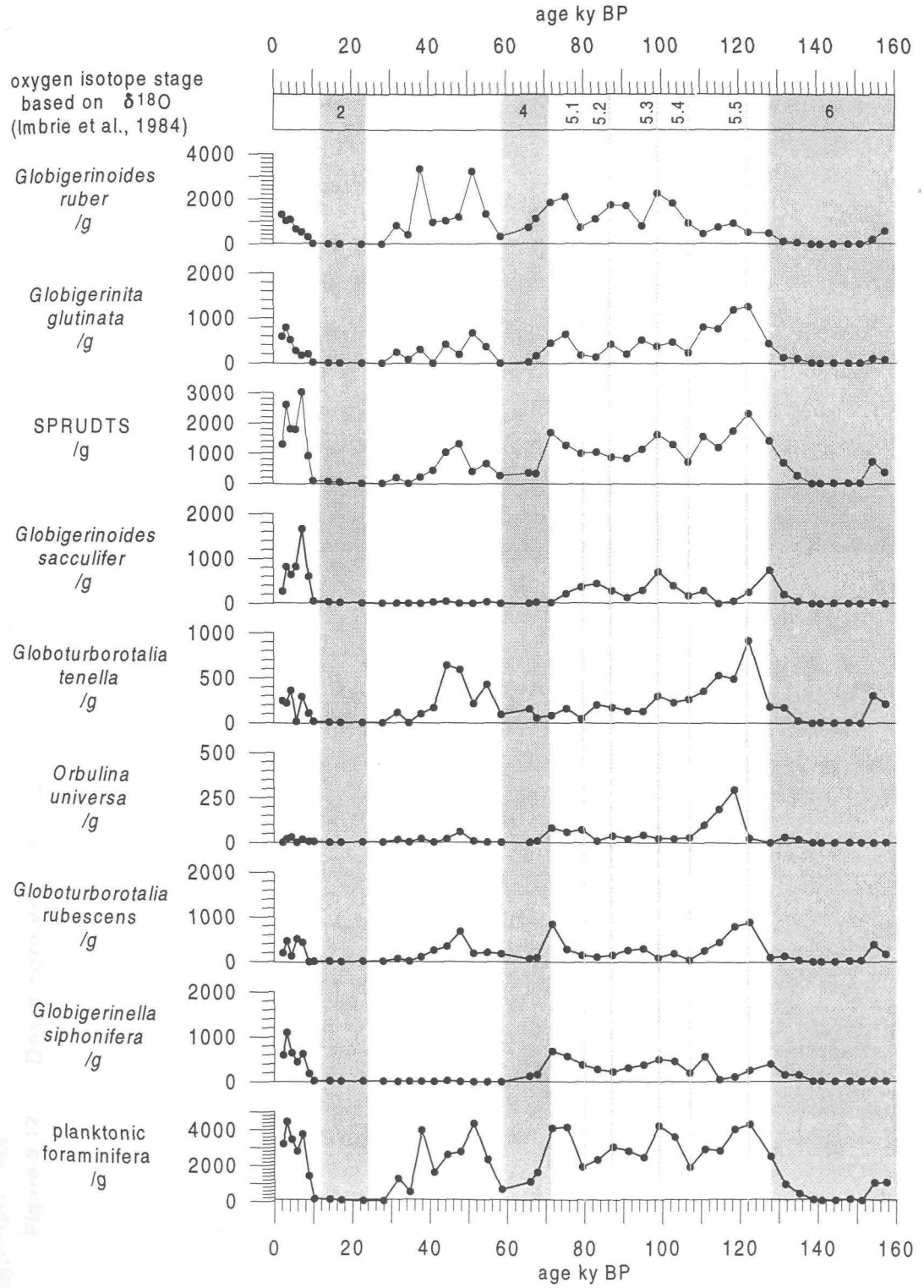

Figure 6.12 **Down core variation of planktonic foraminiferal numbers per gram of sediment. Cores 1017 and 1039, Red Sea.**

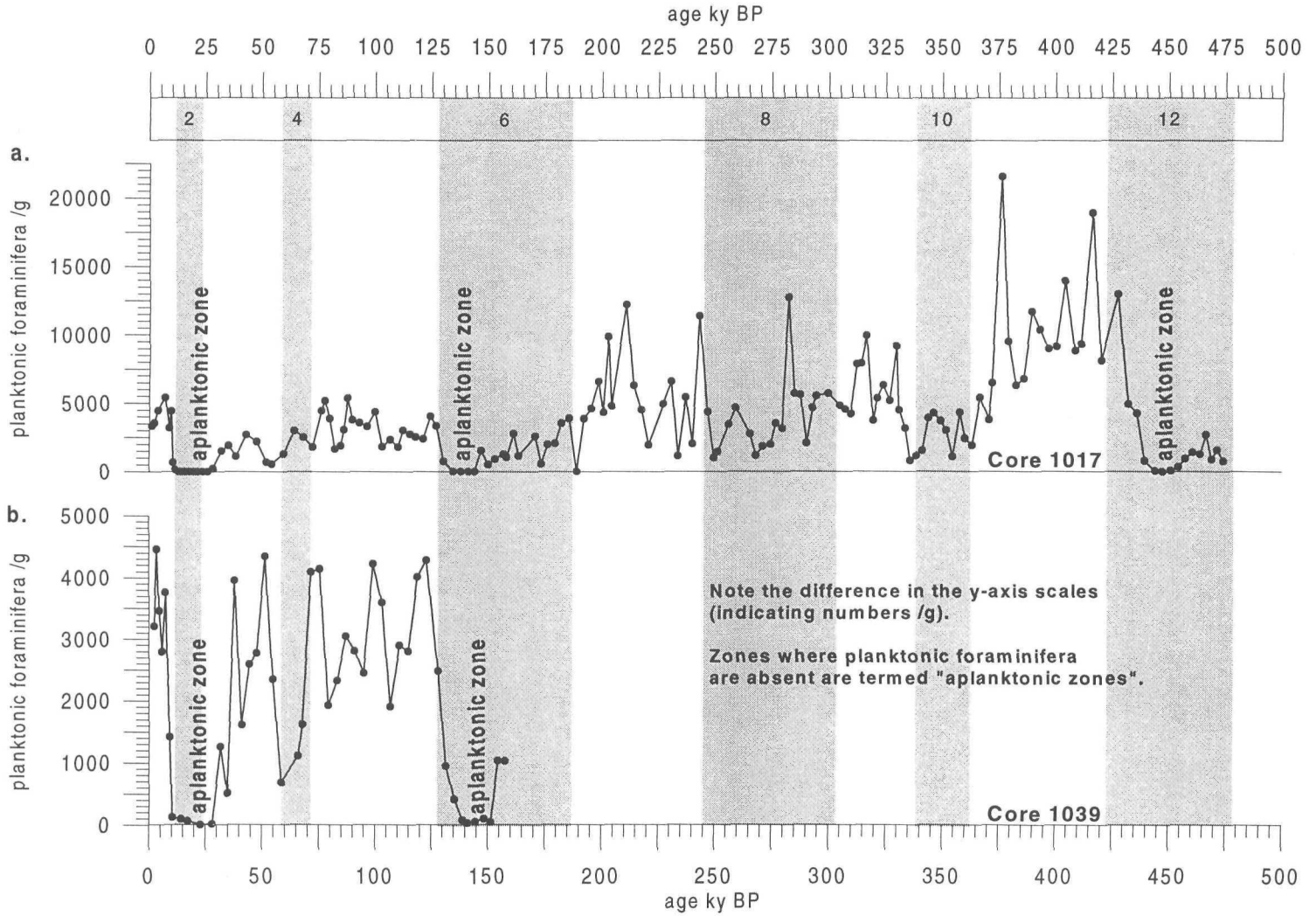

very few planktonic foraminifera. In addition, the curve for core 1017 shows a distinct decrease in planktonic foraminiferal numbers towards the present day. The aplanktonic zones correlate with glacial isotope stages 2, 6 and, in core 1017, stage 12. They are characterised by a relatively rapid onset and an abrupt ending and are preceded by a weak succession of species disappearance (figures 6.13 and 6.14) commencing around 15 ky before. The first species affected is *G. sacculifer*, followed by *G. siphonifera*. These species are dramatically reduced in numbers long before *G. rubescens* and *G. tenella* (omitted from figures 6.13 and 6.14 owing to their low absolute abundance) whose decline is rapidly followed by the abrupt decline in numbers of *G. glutinata* and *G. ruber*.

Relative abundance curves show which species are present in the aplanktonic zones. Often the absolute numbers curves show that only very low abundances persist (Berggren and Boersma, 1969; Locke, 1984; Ivanova, 1985; Thunell et al., 1988; Hemleben et al., 1996), making the significance of relative abundance rather doubtful. There is one exception however, namely the 100 % peak of *Globorotalia anfracta* (plate 8), an opportunistic species (Hemleben et al., 1989), in core 1017 at 136 ka BP, isotope stage 6 (fig 6.15a). Conversely the high percentages of *G. anfracta* in isotope stage 2, (core 1017) are not matched by significantly increased absolute abundances (fig 6.15b). The increased relative abundance of *T. quinqueloba* (plate 9) (a cold water species) corresponds also to a slight increase in absolute numbers of this species in stage 6 (cores 1017 and 1039) and stage 12 (core 1017) (figs 6.15 and 6.16c and d). Also in core 1039, an increase in the abundance of *G. anfracta* is observed between 140 and 148 ka BP, again in stage 6 (figs 6.16a and b) corresponding to an increase in absolute numbers of this species.

6.6 Down-core benthic foraminiferal variations.

The benthic foraminiferal fauna discovered in cores 1017 and 1039 is, apparently, endemic with no known analogues. Only a pilot study was carried out on the benthic foraminiferal content of core 1017, giving a broad impression of faunal changes over the last 500 ky. However, a meticulous study was carried out on core 1039, revealing detailed faunal variations over the last 160 ky. Benthic foraminiferal numbers per gram of sediment for cores 1039 and 1017 are shown in figure 6.17.

Figure 6.13 **Successional disappearance of planktonic foraminifera. Core 1017, Red Sea.**

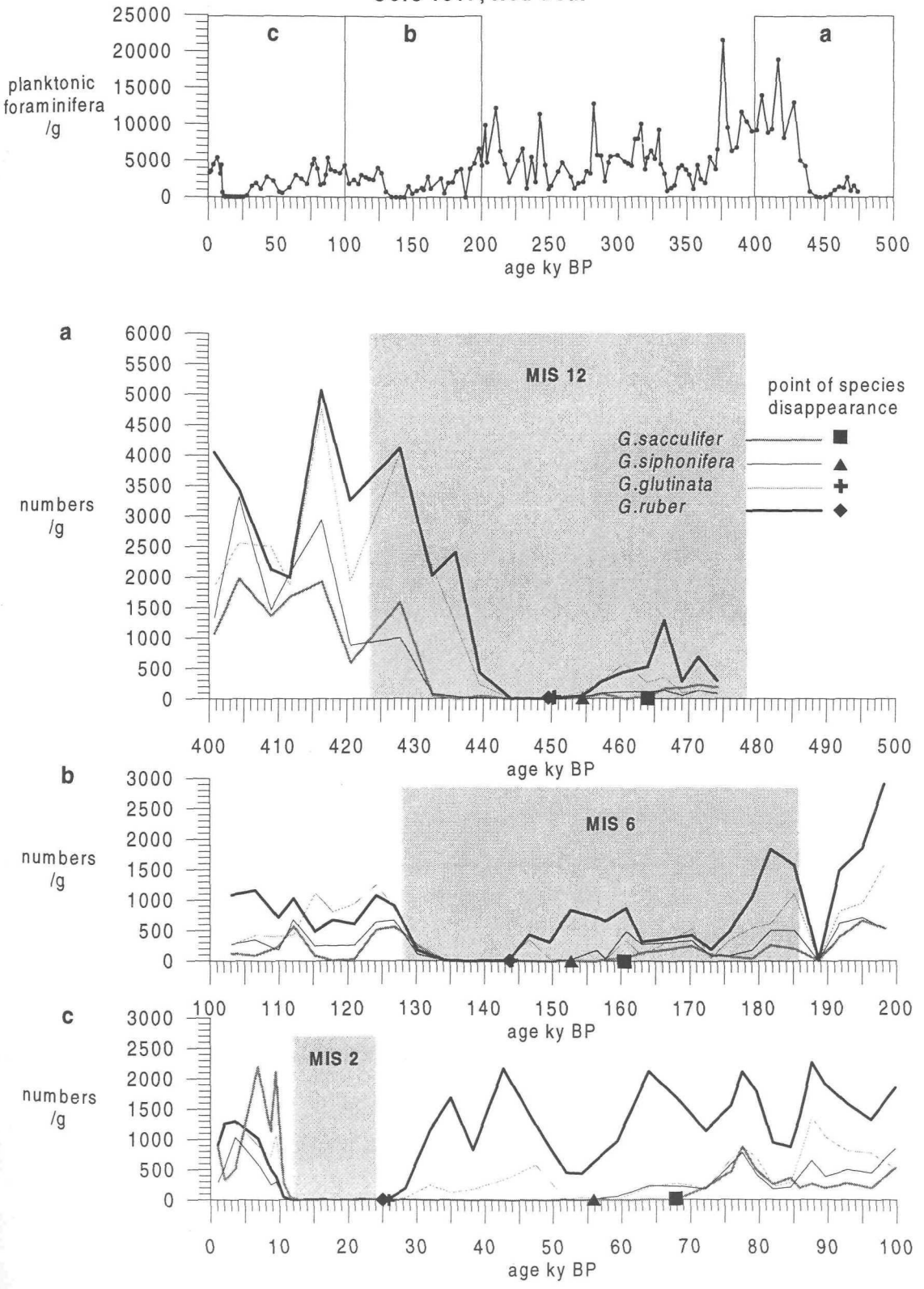

Figure 6.14 **Successional disappearance of planktonic foraminifera. Core 1039, Red Sea.**

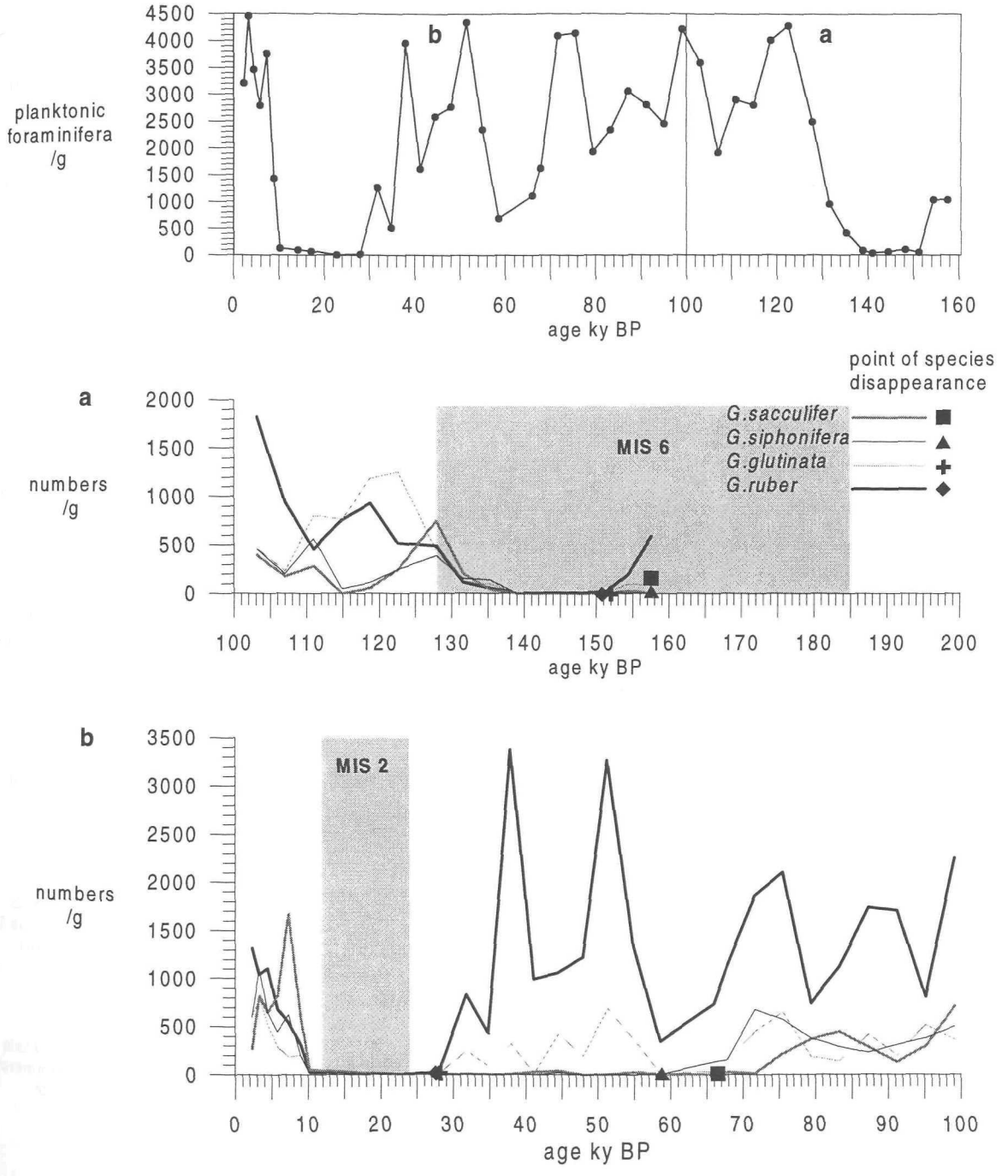

Figure 6.15 Variation of *G.anfracta* and *T. quinqueloba* versus Age. Core 1017, Red Sea.

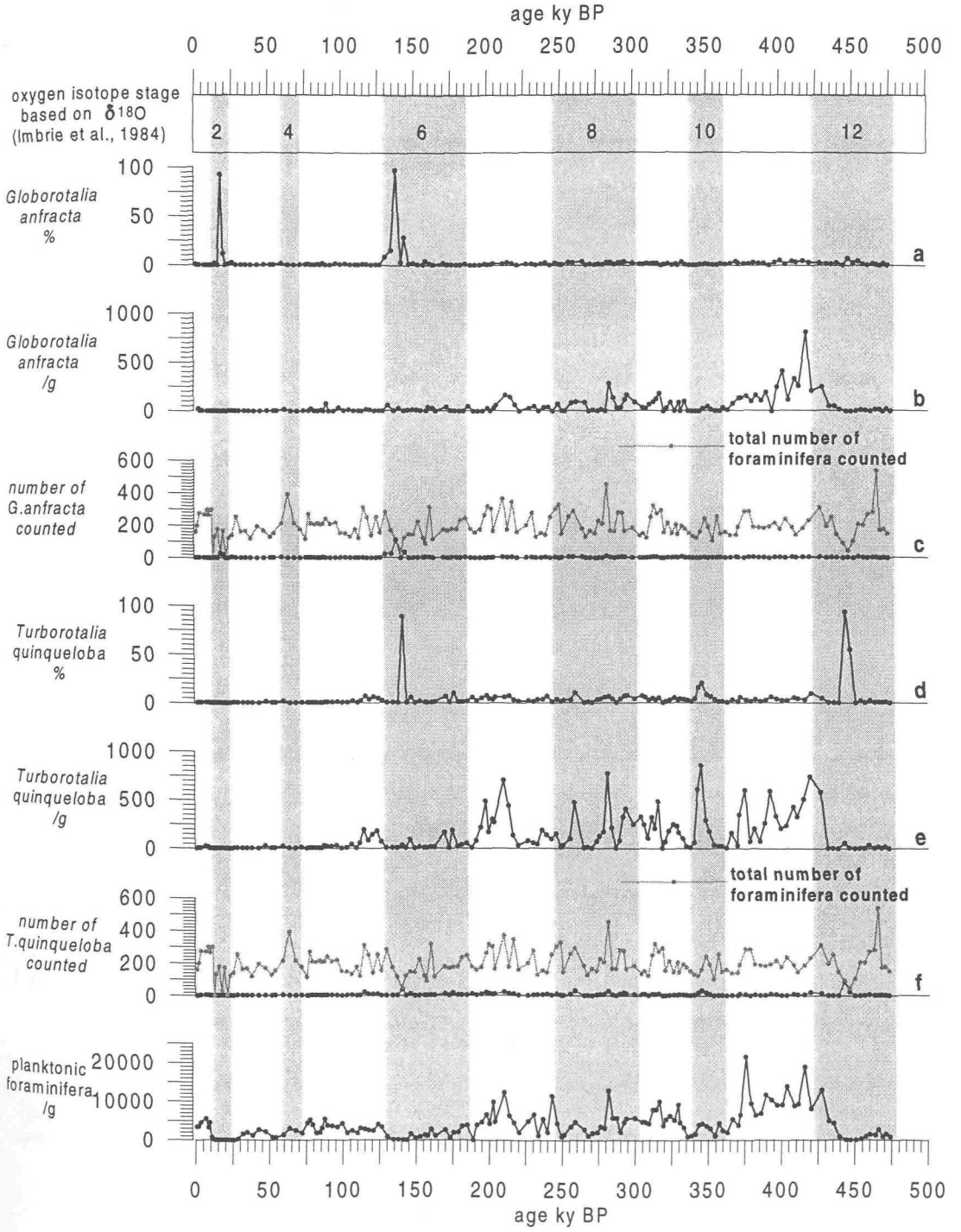

Figure 6.16

Variation of *G.anfracta* and *T.quinqueloba* versus age. Core 1039, Red Sea.

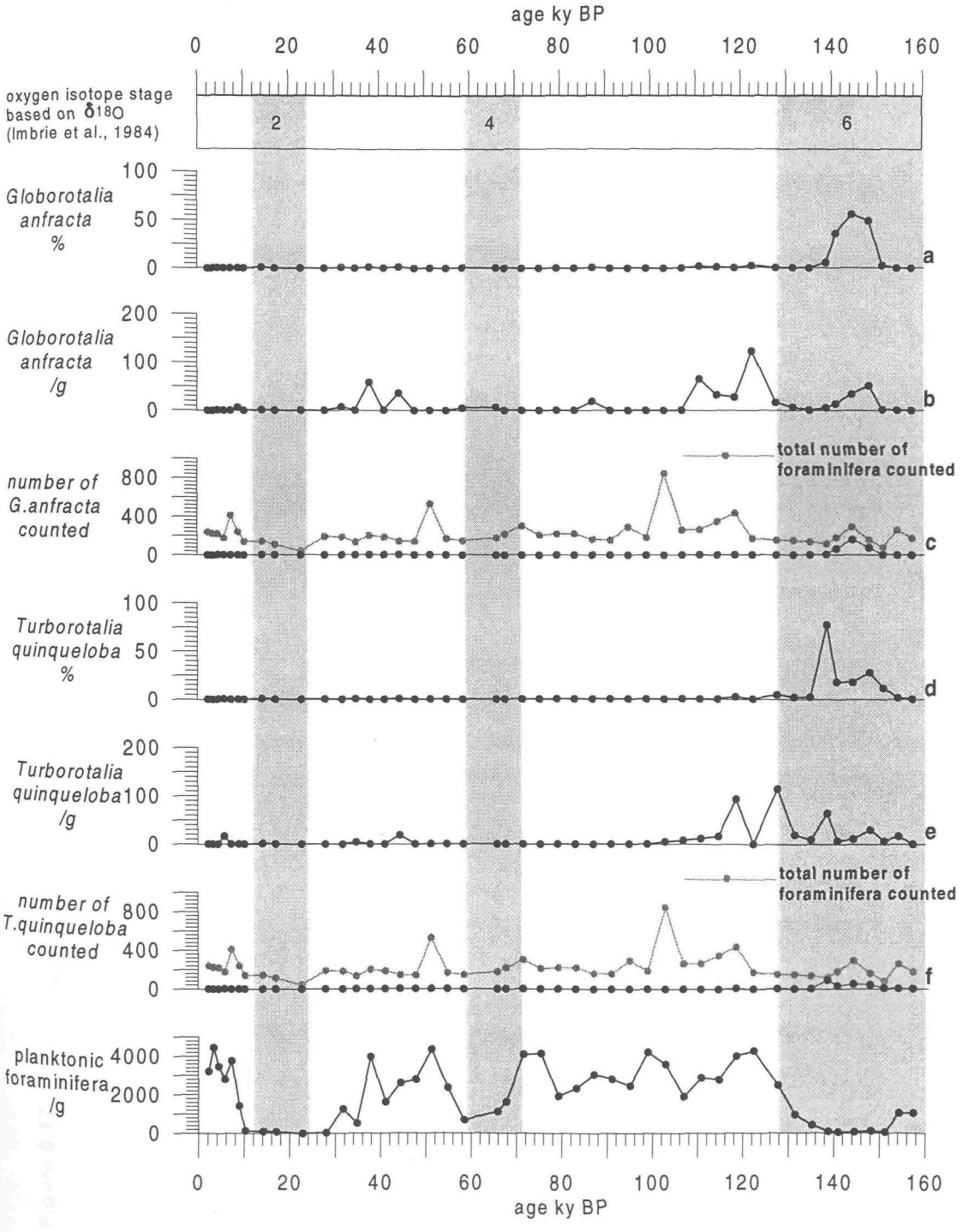

Figure 6.17

Benthic foraminiferal Numbers versus Age. Cores 1017 and 1039, Red Sea.

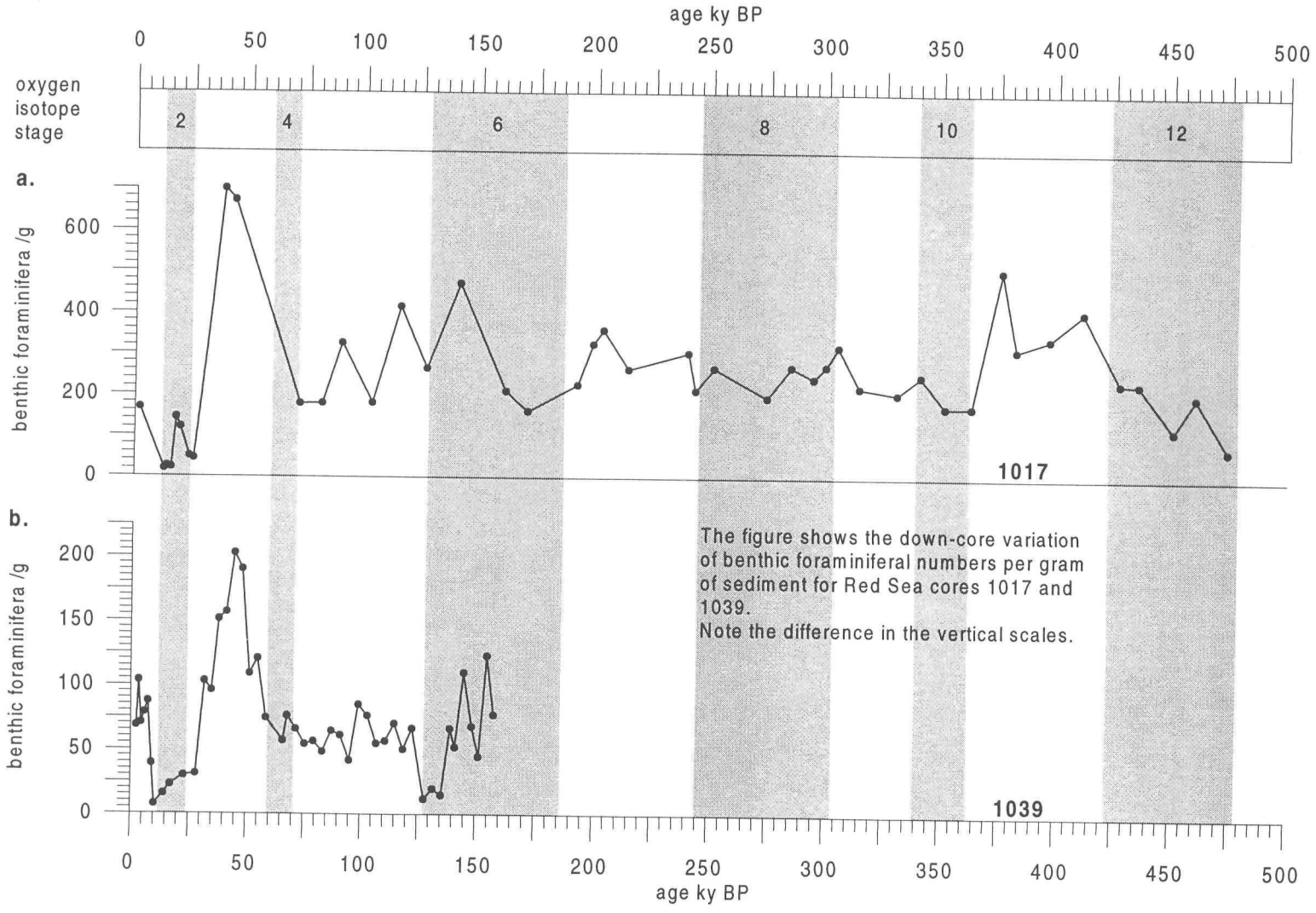

6.6.1 Principal component analysis:

Non standardised principal component analysis (PCA), based on Davis (1986), was carried out on the benthic foraminiferal relative abundance results of cores 1039 and 1017, both as individual data sets and as one combined. The aim of the analysis is to highlight statistical subdivisions of the faunas into principal assemblage components which may assist the identification of environmental control on the fauna. The main results of each analysis are shown in table 6.4.

i) PCA of core 1039.

The result of the analysis showed only two significant factors accounting for 32.54 % (principal component (PC) axis 1) and 21.72 % (axis 2) of the total variance of the data set. The most positive and negative species loadings on axes 1 and 2 are given in table 6.4. The dominance of *B.subreticulata* (plates 22 and 23) (figure 6.18) in PC axis 1 (loading +0.79) is clearly displayed in the shape of the resulting curve (figure 6.19a), which peaks positively in stage 5, remains positive in stage 4 and reaches its most positive peak in mid stage 3 (around 40 ka BP). This peak is followed by a rapid decline, reaching the most negative peak towards the end of stage 3 (around 30 ka BP). A comparable negative peak is also noted in mid stage 6 (around 160 ka BP). The tendency towards negative values in stages 2 and 6, and to a lesser extent in stage 4, suggests a glacial-interglacial influence on the fauna.

The most positive and negative loadings on PC axis 2 are shown in table 6.4. PC axis 2 (figure 6.19b) again shows strong negative peaks towards the end of stage 3 (around 30 ka BP) and during mid stage 6 (around 150 ka BP). The highest positive values are seen in the Holocene and slightly lower values persist throughout interglacial stage 5. The strongest negative values are seen throughout glacial stages 2-4 and stage 6. Thus a distinct glacial-interglacial influence is identified in PC axis 2.

ii) PCA of core 1017.

Non standardised PCA analysis of the pilot study of core 1017 also reveals a glacial-interglacial influence on the benthic foraminiferal fauna, though these results are not so reliable owing to the low resolution of the data. The main results are given in table 6.4. PC

Table 6.4 Results of PCA carried out on the Red Sea benthic foraminiferal data

Axis	A.				B.				C.				D.			
	Most positive (+ve) and negative (-ve) species (sp) loadings on each axis:															
	sp	**+ve**	**sp**	**-ve**	**sp**	**+ve**	**sp**	**-ve**	**sp**	**+ve**	**sp**	**-ve**	**sp**	**+ve**	**sp**	**-ve**
PC 1	**1**	0.79	**7**	0.474	**1**	0.916	**4**	0.188	**1**	0.88	**4**	0.202	**6**	0.318	**7**	0.798
	3	0.136	**9**	0.246	**2**	0.126	**5**	0.188	**3**	0.189	**6**	0.184	**3**	0.309	**9**	0.205
	8	0.089	**4**	0.151	**3**	0.078	**6**	0.163			**5**	0.175	**10**	0.152	**12**	0.112
							7	0.106			**7**	0.171	**11**	0.145	**4**	0.109
	representing 32.54 % of the total variance				**representing 33.03 % of the total variance**				**representing 30.97 % of the total variance**				**representing 22.24 % of the total variance**			
PC 2	**7**	0.618	**6**	0.58	**7**	0.384	**3**	0.612	**6**	0.393	**7**	0.684	**3**	0.487	**6**	0.62
	1	0.359	**10**	0.238	**5**	0.29	**11**	0.332	**3**	0.385	**9**	0.223	**8**	0.351	**12**	0.173
	14	0.155	**12**	0.093	**4**	0.28	**13**	0.219	**10**	0.18	**1**	0.135	**2**	0.302	**10**	0.166
	8	0.128	**3**	0.093	**12**	0.251	**2**	0.131	**11**	0.137	**14**	0.134	**14**	0.182	**9**	0.144
					1	0.201					**4**	0.12			**4**	0.127
	representing 21.72 % of the total variance				**representing 19.60 % of the total variance**				**representing 15.86 % of the total variance**				**representing 13.83 % of the total variance**			
PC 3													**4**	0.37	**3**	0.601
													8	0.347	**7**	0.412
													9	0.192	**6**	0.243
													2	0.178	**15**	0.142
													representing 12.70 % of the total variance			

A. PCA results for core 1039 only

B. PCA results for core 1017 only

C. PCA results for the combined data of cores 1039 and 1017

D. PCA results for the combined data of cores 1039 and 1017, excluding *Bolivina subreticulata.*

1 *Bolivina subreticulata*
2 *Eherenbergina trigona*
3 *Uvigerina porrecta*
4 *Hanzawaia boueana*
5 *Hoeglundina elegans*
6 *Cibicides ungerianus*
7 *Bulimina marginata*
8 *Cassidulina laevigata*
9 *Bolivina subspathulata*
10 *Anomalina ammonoides*
11 *Gyroidina altiformis*
12 *Biloculina irregularis*
13 *Hyalinea balthica*
14 *Uvigerina hollicki*
15 *Astrononion echolsi*

Figure 6.18

Down-core variation of *Bolivina subreticulata* versus age. Cores 1017 and 1039, Red Sea.

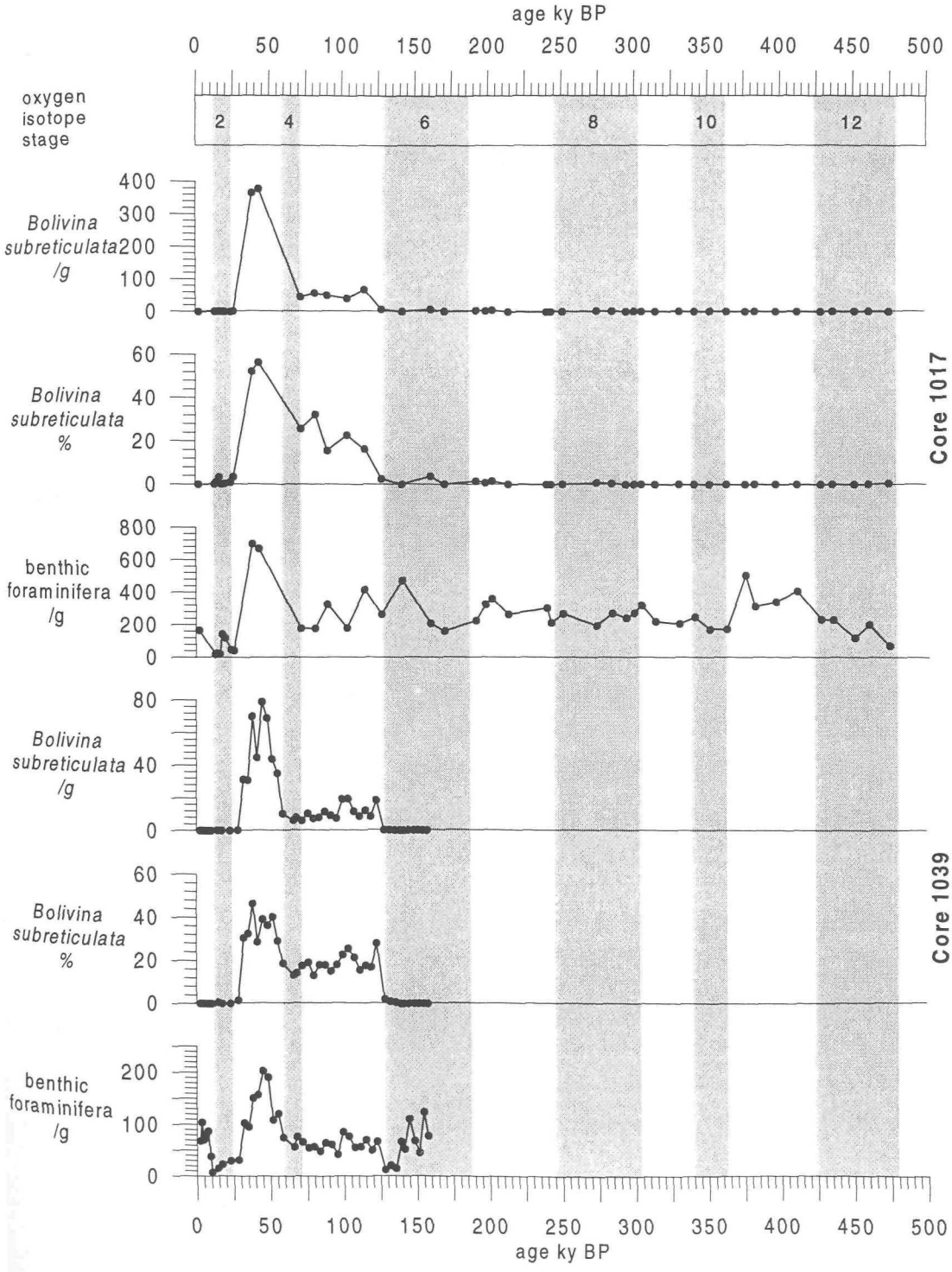

Figure 6.19 **PCA results of the individual benthic foraminiferal data sets of cores 1017 and 1039, Red Sea.**

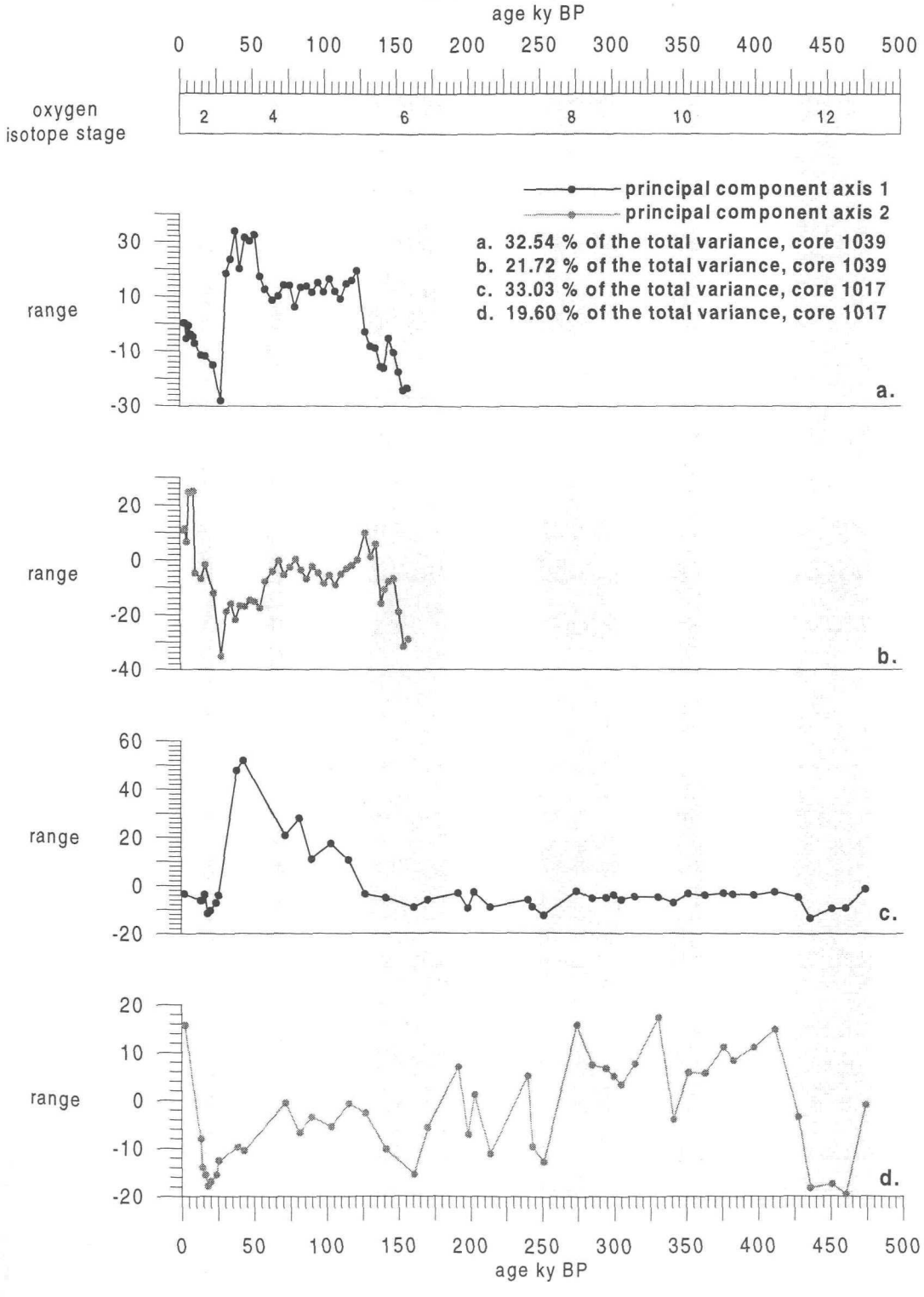

axis 1 (figure 6.19c) represents 33.03 % of the variance of the data, and PC axis 2 (figure 6.19d) represents 19.60 % of the variance of the data. The strong influence of *B.subreticulata* is again obvious in PC axis 1, with the highest positive loading (0.916). The curve highlights a glacial-interglacial influence with the most negative values associated with glacial stages 2, 6, 8 and 12. Glacial stage 4 shows reduced positive values and stage 10 shows a slight decrease in values, in agreement with this.

PC axis 2 shows a clear glacial-interglacial influence with highest positive values in interglacial stages 1, 9 and 11. Stages 5 and 7 also show a tendency towards more positive values, in agreement with this. Glacial stages 2-4, 6, 8 and 12 show the most negative peaks.

iii) PCA of core 1039 and 1017 combined.

Owing to the similarity of the two data sets, the benthic foraminiferal relative abundance data were combined and PCA was performed on this in order to further assess environmental parameters with a larger data set, thus increasing the significance of the results. The main results are shown in table 6.4. Two PC axes were seen to be significant, PC axis 1 representing 30.97 % and PC axis 2 representing 15.86 % of the total variance. The PC axes were plotted for each core (figure 6.20).

PC axis 1 for both cores 1039 and 1017 (figure 6.20a and c) is extremely similar to that of their individual PCA analysis (figure 6.20a and c). The dominance of *B.subreticulata* (+0.88) is again clear, as is the glacial-interglacial influence. PC axis 2 (figure 6.20b and d) also shows great similarity to PC axis 2 of each of the individual analyses (figure 6.20b and d), showing the distinct glacial-interglacial influence.

iv) PCA of the combined data set excluding *B.subreticulata.*

Owing to the dominance of *B.subreticulata* in the previous analyses, this species was removed from the combined data set and PCA was carried out on the resultant relative abundances, in order reveal any species associations not yet highlighted. The results are shown in table 6.4. Three significant PC axes resulted. PC axis 1 represents 22.24 % of the total variance, PC axis 2 represents 13.83 % and PC axis 3 represents 12.70 %. The

Figure 6.20 **PCA results of the combined benthic foraminiferal data sets of cores 1039 and 1017, Red Sea.**

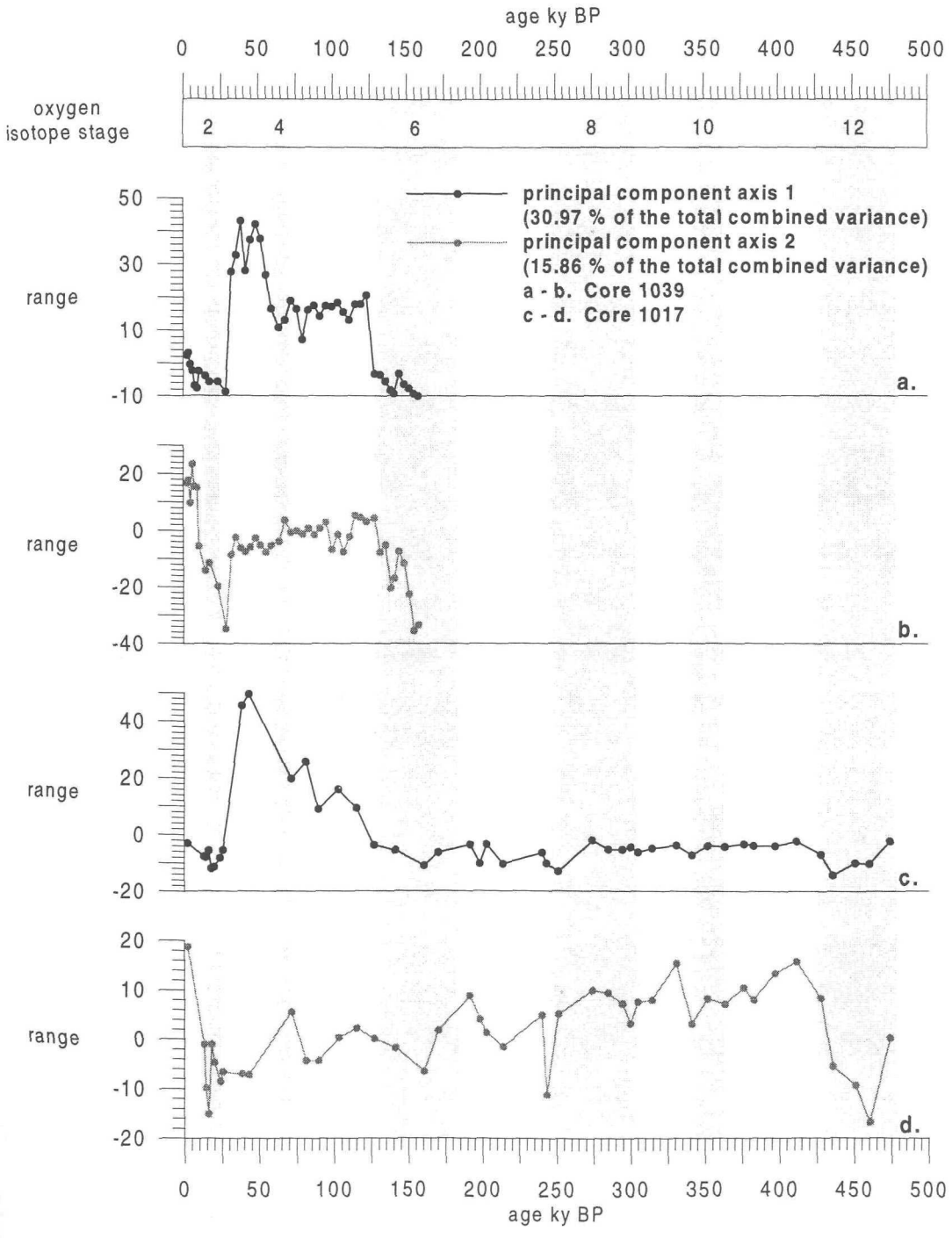

exclusion of *B.subreticulata* has improved the shape of the curves, which now show distinct events associated stage 3, and with the glacial-interglacial relationship (figure 6.21). PC axis 1 (figures 6.21a and c) is dominated positively by *C.ungerianus* (plate 24) (0.318) and negatively by *B.marginata* (plate 18) (-0.798). PC axis 1 peaks positively in the Holocene and interglacial stages 9 and 11. The values are seen to remain relatively high through stages 5 to mid stage 3. At around 30 ka BP the curve reaches its most negative value in core 1039 (figure 6.21a), comparable only to the negative values of mid stage 6 (160 ka BP), and in core 1017 (figure 6.21c) at the onset of stage 7 (245 ka BP) and during mid stage 12 (460 ka BP). Core 1017 also shows a comparable negative value in stage 2, although corroborating evidence of this is not seen in core 1039.

PC axis 2 (figures 6.21b and e) is dominated positively by *U.porrecta* (plate 33) (0.487) and negatively by *C.ungerianus* (-0.62). In core 1039 (figure 6.21b), the most distinct aspect of this PC axis is the peak in negative values throughout stage 3, a low oxygen period in the Red Sea basin (Almogi-Labin et al., 1998). No other period of time shows such negative values, although mid stage 6 shows a fall in values and stage 5 shows a steady fluctuation between more positive and negative values throughout. The end of stage 2 is also marked by a fall to negative values before rapidly rising to the highest positive values. Core 1017 (figure 6.21e) also shows the most negative values in stage 3 with no other comparable values. Both cores show positive values associated with the glacial maxima of stages 2 and 6, and core 1017 shows positive peaks in stage 8 and 12 also.

PC axis 3 (figure 6.21c and f) is dominated positively by *H.boueana* (0.37 %) and negatively by *U.porrecta* (-0.601 %). Core 1017 shows no particular variation along this axis (figure 6.21f), with the most negative peaks seen in the Holocene and mid stage 8 (around 270 ka BP). The highest positive values appear to be associated with glacial maxima (stage 2, 6, late in stage 8 and 10, and stage 12). Core 1039 (figure 6.21c) also shows more positive values associated with glacial stages 2, 4 and mid-late stage 6). Most negative values are apparent in stage 1 and during the latter half of stage 3 (40 - 30 ky BP). Values are noted to increase abruptly in mid stage 6 (around 160 ka BP).

Figure 6.21 **PCA results of the combined benthic foraminiferal data sets, excluding *B.subreticulata*, of cores 1039 and 1017, Red Sea**

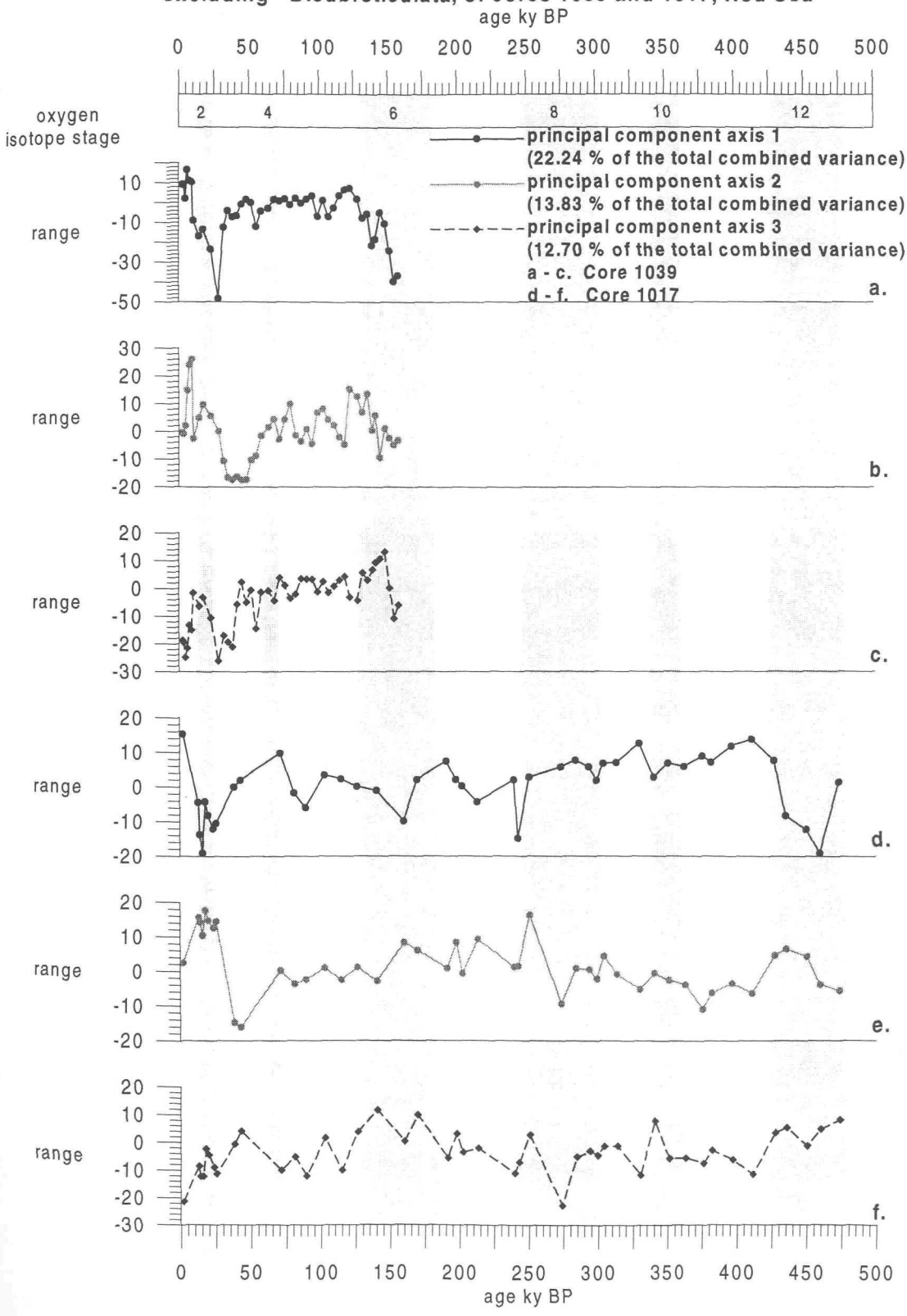

v) Summary.

Although no particular species assemblages were identified by the PCA analyses, it is apparent that the faunal change is dictated by glacial-interglacial influence, and possibly by periods of poor ventilation in the basin, for example, the Red Sea low oxygen period, stage 3 (Almogi-Labin et al., 1998). To explore this further, a closer investigation of individual species abundance variations in cores 1017 and 1039 is carried out.

6.6.2 Down-core benthic foraminiferal species variations.

Since the study carried out on core 1017 was of limited resolution, the results are not discussed in great detail, but are used as a helpful, long-term comparison to the more detailed study of core 1039.

i) Core 1017.

The graph of absolute abundance of benthic foraminifera per gram of sediment (fig 6.17a) shows an abrupt drop to approximately 20 benthics g^{-1} in conjunction with glacial isotope stage 2. Absolute numbers are also seen to fall in stages 12, 10 and 6, though not so abruptly and to around 200 benthics g^{-1}. Maximum numbers are seen in mid-stage 3 (around 30 ka BP), reaching the order of 700 benthics g^{-1}.

Relative abundance curves of the more prominent species (figure 6.22 and 6.23) show that isotope stage 2 is marked by an increase in miliolids (particularly *Biloculinella irregularis* (plate 45)), *Bulimina marginata*, and *Cibicides spp.* (particularly *C.ungerianus*). The increase in miliolids in core 1017 reaches about 40 %. *Bolivina spp.* are most abundant (up to 65 %) in the sediments deposited during isotope stage 3, with *B.subreticulata* being the dominant species. Stage 1 sediments above the aplanktonic zone are dominated by *Uvigerina spp.*, mainly *U.porrecta* (up to 25 %). *Cibicides ungerianus* is also present in abundance (up to 20 %).

ii) Core 1039.

Contrary to the low-resolution style of the pilot study on core 1017, benthic foraminifera have been studied in detail from core 1039. These results provide a comprehensive record of

Figure 6.22

Abundance of benthic foraminiferal species.
Core 1017, Red Sea.

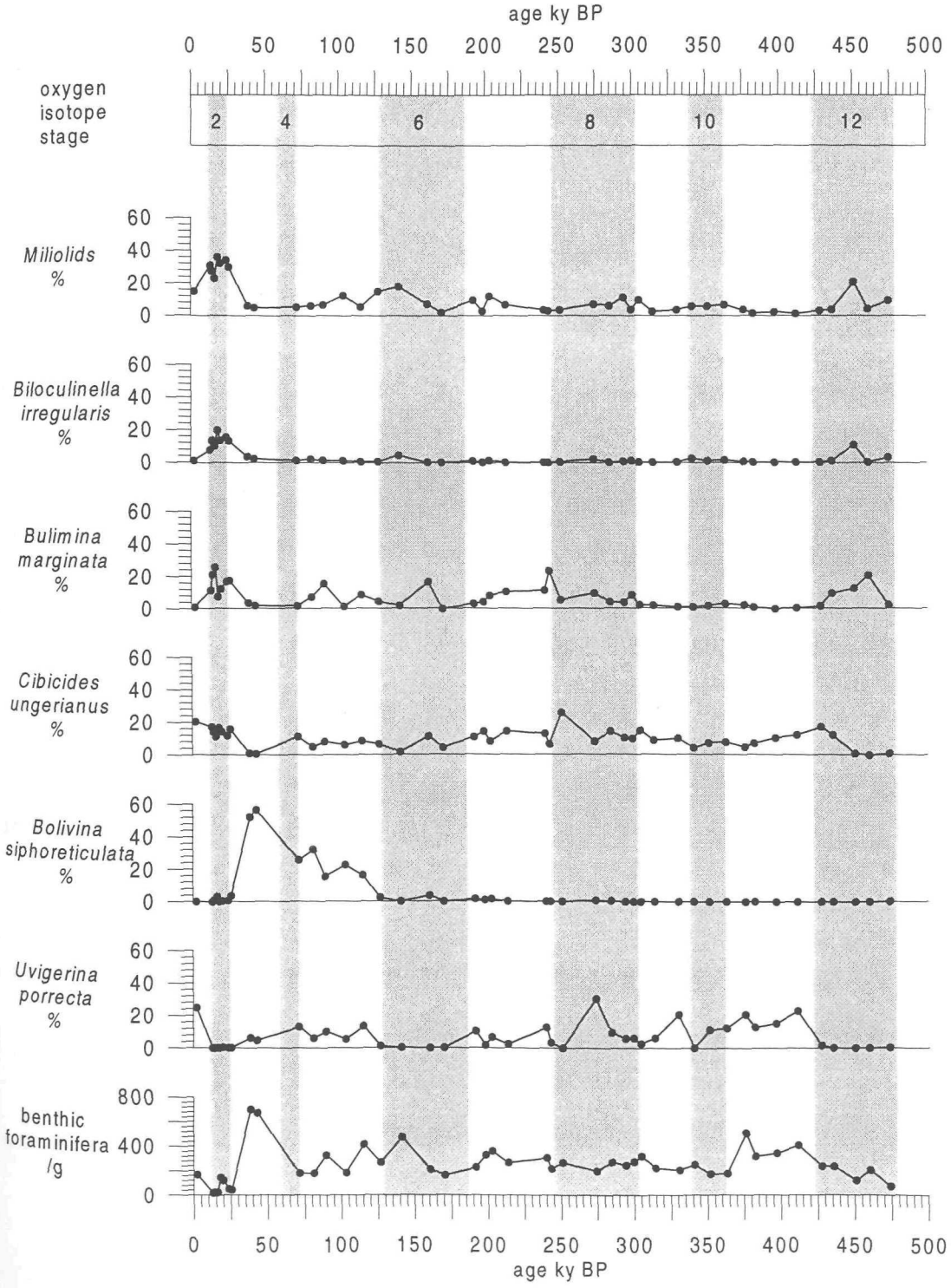

Figure 6.23

Absolute numbers of benthic foraminifera versus age.
Core 1017, Red Sea.

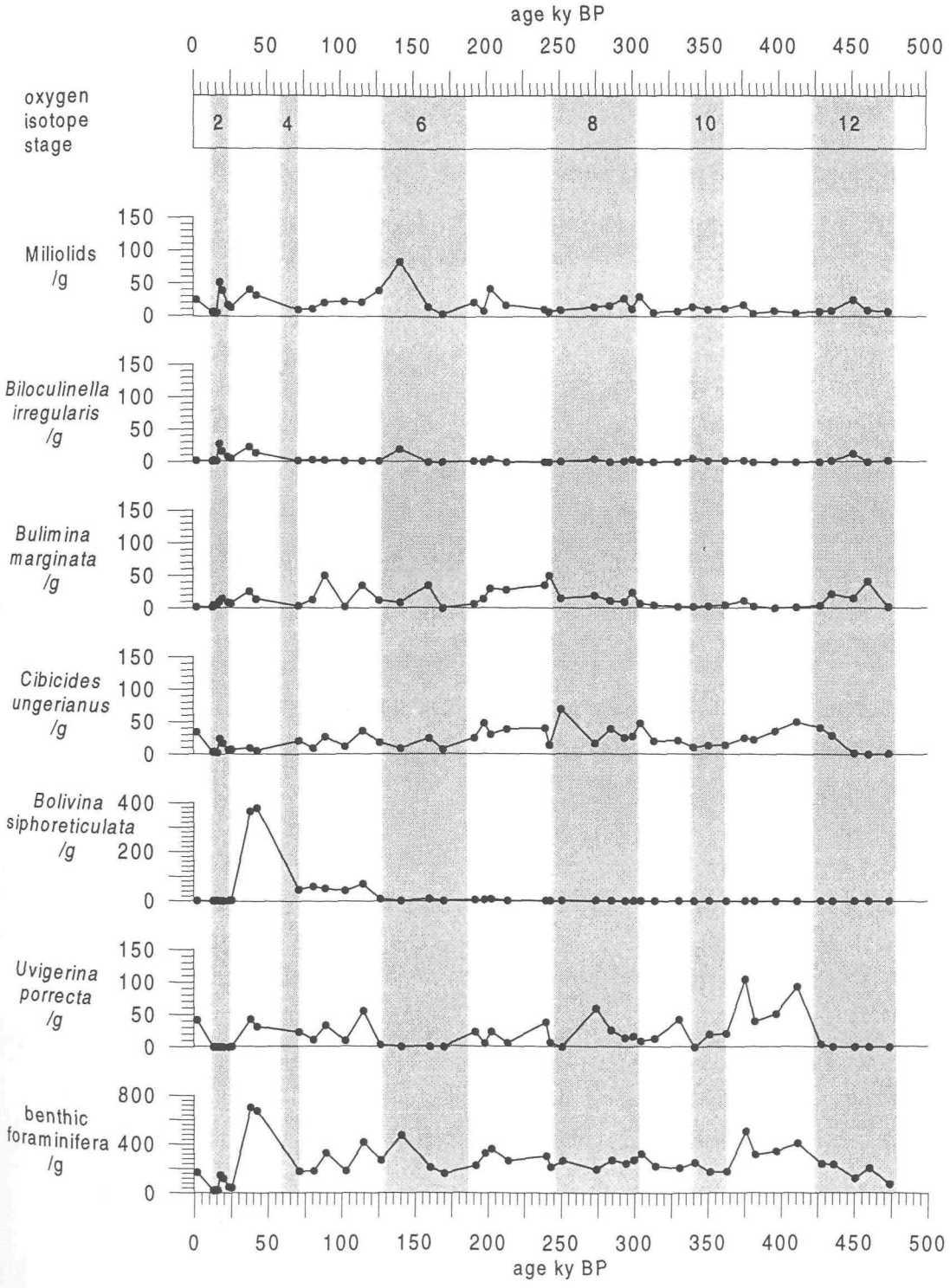

changes in the fauna over the last 160 ky. Benthic foraminiferal numbers per gram are shown in figure 6.17b. The most abundant (generally greater than 8 % relative abundance) foraminiferal species are discussed here. Owing to the nature of the PCA results (section 6.6.1), the fauna has been grouped into those dominating stage 3 (possible low dissolved oxygen indicators? (Murray, 1991; Gupta, 1994)), and those dominating glacial (possible high salinity indicators? (Halicz and Reiss, 1981; Locke, 1981)) and interglacial periods. In combination with the stage 3 groupings, an assessment of species present in the sapropelic sediment has been carried out. These species are also thought to represent a poorly ventilated environment since it is suggested that the sapropel developed beneath a density stratified, stagnant, and consequently oxygen depleted water column (Ivanova, 1984; Locke, 1984; Almogi-Labin et al., 1991).

a) Sapropel-type and stage 3-dominant fauna:

The fauna depicted in figures 6.24 have been grouped on account of their presence through the sapropelic horizon. The TOC record for core 1039 shows low values throughout the core with the exception of a peak value of 2.8 % at 10.24 ka BP. The benthic foraminiferal numbers per gram of sediment show very low values (<5 g^{-1}) coinciding with this peak. It is noted that only 15 specimens could be counted from the whole sample at this horizon. Species present at this time include *Cancris auriculus* (plate 16)(40 % (6 counted)), *Brizalina spathulata* (27 % (4 counted)), *Bolivina italica* (plate 15) (14 % (2 counted)), and *Eponides punctulatus* (plate17) (7 % (1 counted)). These four species are also found together in stages 3 and 6, although in lower relative abundances (generally <5 %). This suggests the possibility of similarities between stages 3 and mid-stage 6, and the environment of deposition of sediment rich in TOC at 10.24 ka BP. It is speculated that the differences in relative abundances may be a function of the degree of oxygen deficiency which would have been strongest during the deposition of the sapropel.

Other species with high relative abundances in both stages 3 and 6 (figure 6.25) include *Bulimina marginata* (stage 3 maximum, 62 %; stage 6, 50 %), *Uvigerina hollicki* (plate 19) (stage 3, 16 %; stage 6, 38 %), *Cassidulina laevigata* (plate 20) (stage 3 maximum, 18 %; stage 6, 16 %) and *Ehrenbergina trigona* (plate 21) (stage 3, 8 %; stage 6, 6 %) (figure 6.21).

Figure 6.24

Sapropel type benthic foraminiferal fauna. Core 1039, Red Sea.
(note differences in the Y-axes)

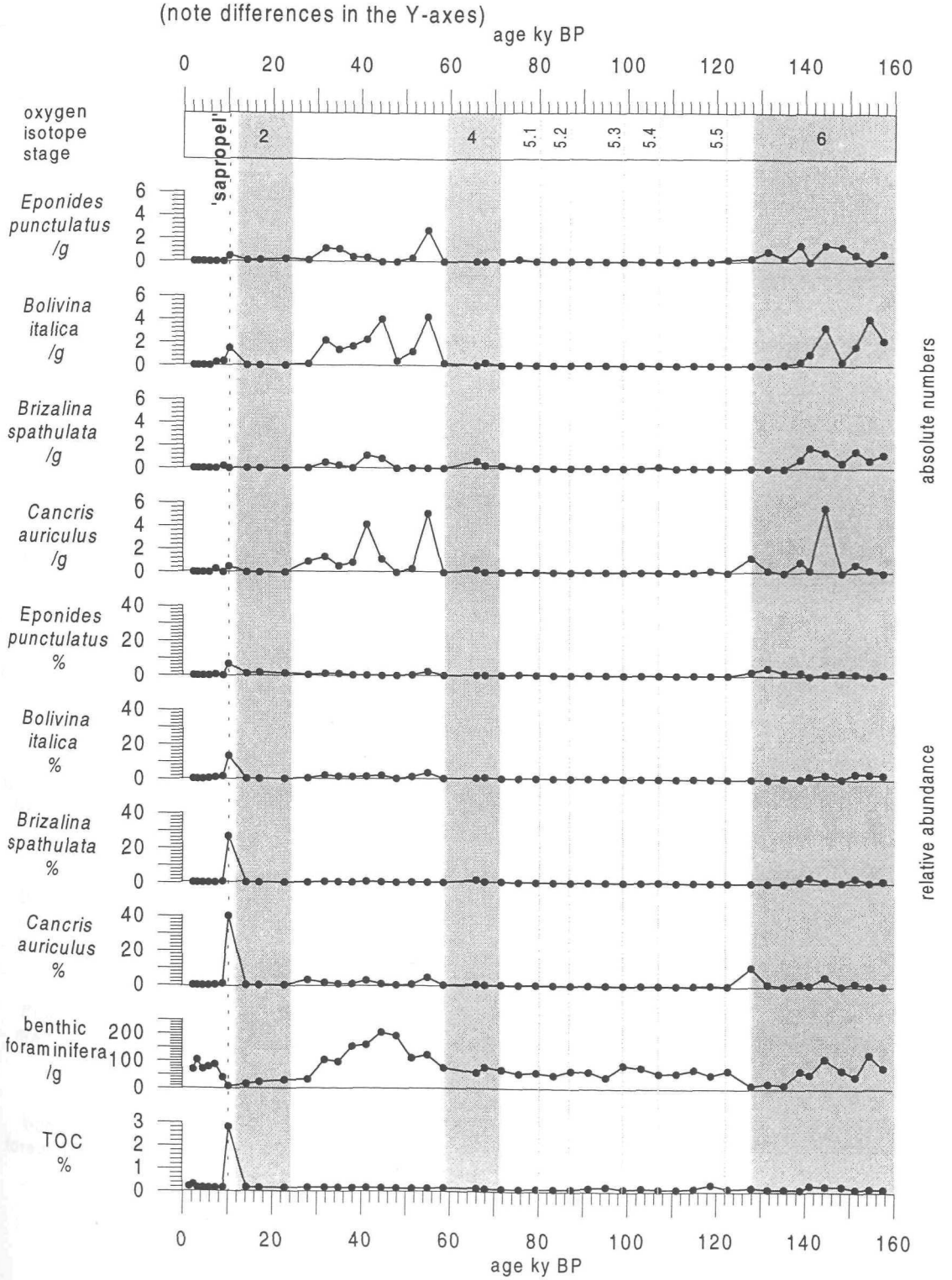

Figure 6.25 **Benthic foraminifera abundant during isotope stages 3 and 6. Core 1039, Red Sea.**

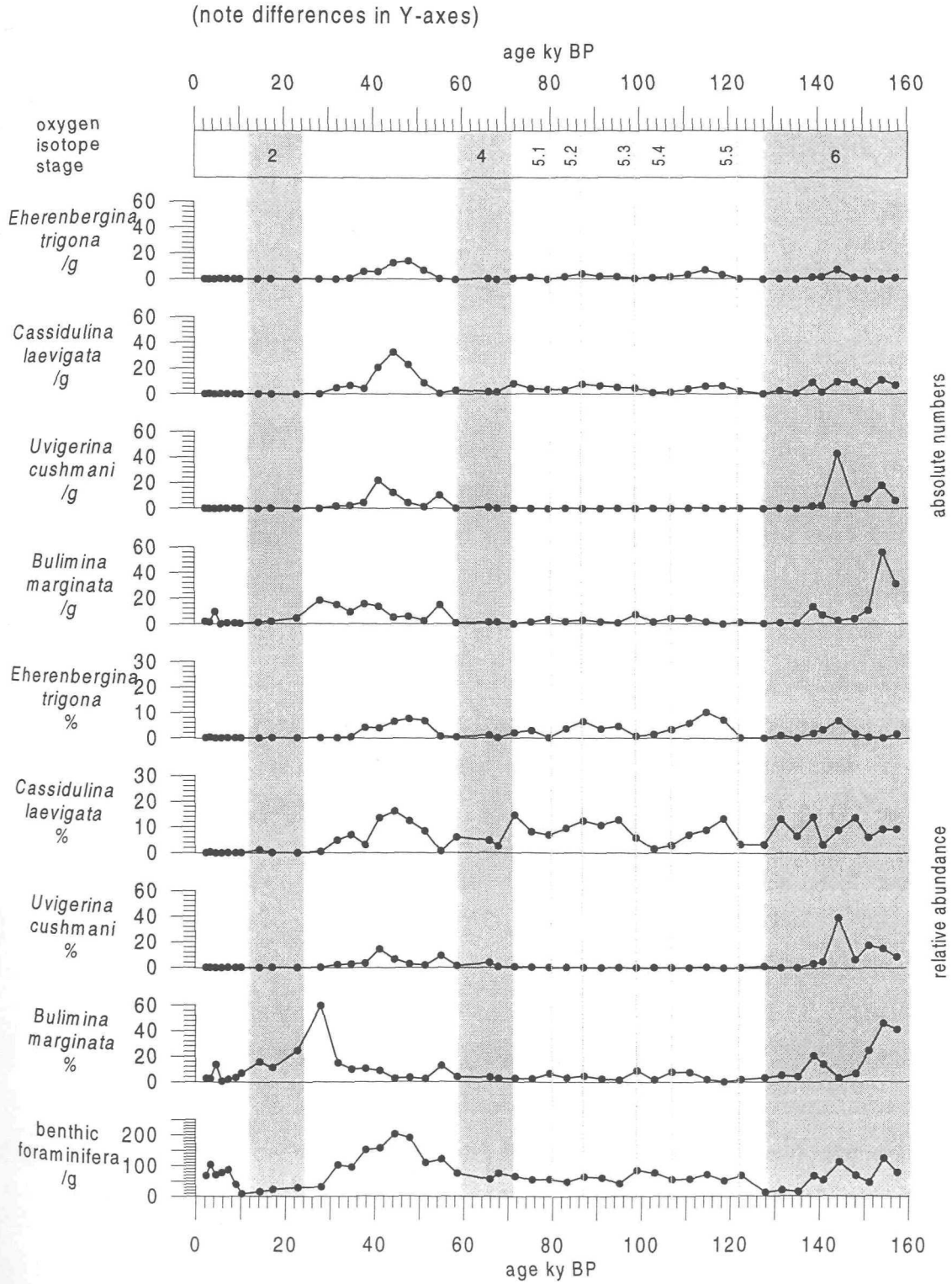

Although relative abundance curves of *Cassidulina laevigata* and *Ehrenbergina trigona* depict values for stage 5 which are similar to those seen in stages 3 and 6, the absolute numbers show much lower values for stage 5. Stage 3 benthic foraminiferal fauna is dominated by the high abundance of *Bolivina subreticulata* (figure 6.18). The predominance of this species can be seen clearly in the shape of the total benthic foraminifera g^{-1} curve (figure 6.17). The high abundance of *B.subreticulata* in the sediments is also apparent throughout stages 4 and 5, and its absence in stages 1,2 and 6 is clear. The benthic foraminiferal data from core 1017 (figure 6.18) also shows dominance of *Bolivina subreticulata* in stage 3 and its generally elevated abundances throughout stages 4 and 5. It also depicts the virtual absence of this species through stages 1, 2, 6, 7, 8, 9, 10, 11 and 12. A slight, yet significant, increase in abundance is seen in core 1017 around mid stage 6, suggesting a possible environmental similarity between this time and stage 3.

b) Interglacial dominant fauna:

Stages 5 and 1 are true interglacial periods. Stage 3 is not a true interglacial phase, but is regarded as a warmer interstadial within the last glacial cycle which extends through stages 4 to 2. Here, stage 3 is grouped as an interglacial stage. Benthic foraminiferal species with high relative abundance at these times are grouped as interglacial indicators (figure 6.26). *Cibicides ungerianus*, *Uvigerina proboschidia* (plate 25), *Hyalinea balthica* (plate 26), *Anomalina ammonoides* (plate 27), *Glandulina laevigata* (plate 28) and *Gyroidina altiformis* (plate 29) are considered as "true" interglacial indicators, all peaking in interglacial stages 1 and 5. It is noted that *C. ungerianus*, *A. ammonoides*, *G. laevigata* and *G. altiformis* also show relatively high abundance in early stage 6. *Siphotextularia sp.* (plates 30 and 31) is seen to have a high abundance in isotope stage 5 alone. *Astrononion echolsi* (plate 32) and *Uvigerina porrecta* are also grouped with the interglacial indicators since they only show significant abundance in stages 1, 3 and, to a lesser extent, stage 5. *Textularia fistulosa* (plate 34) and *Rosalina elegans* (plate 35) show a gradual increase through stage 1 to present, as do *U. proboschidia*, *H. balthica*, *G. altiformis*, *A. echolsi* and *U. porrecta*, although *T. fistulosa* and *R.elegans* show a slight occurrence in stage 3. *C. ungerianus*, *A. ammonoides* and *G.laevigata* show abrupt abundance peaks around 9 ka BP and tail off towards present day. Figure 6.27 shows absolute numbers of interglacial indicating species.

Figure 6.26 **Relative abundance of species common during interglacial periods. Core 1039, Red Sea**

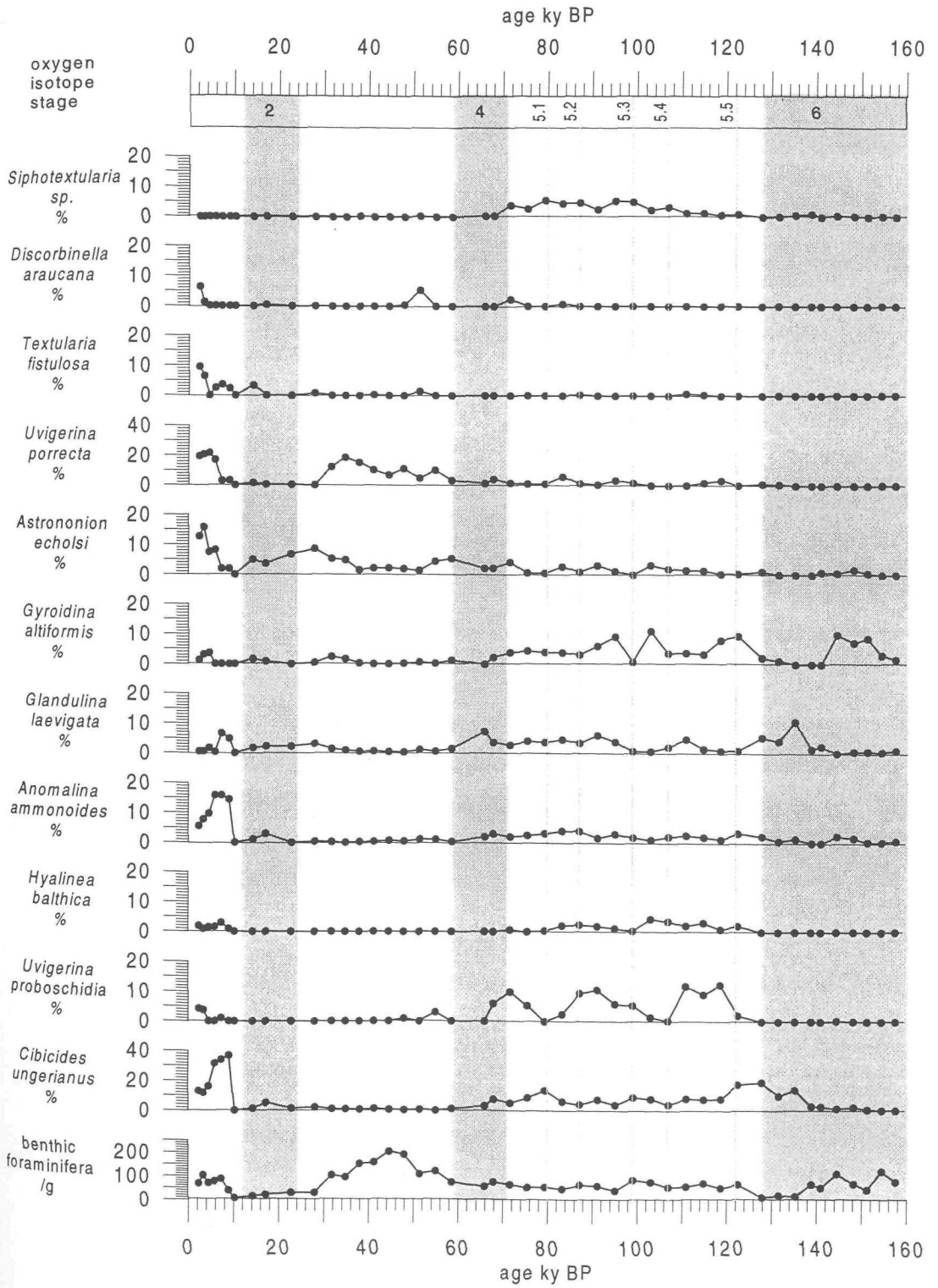

Figure 6.27 Absolute numbers of benthic foraminiferal species common during interglacial periods. Core 1039, Red Sea.

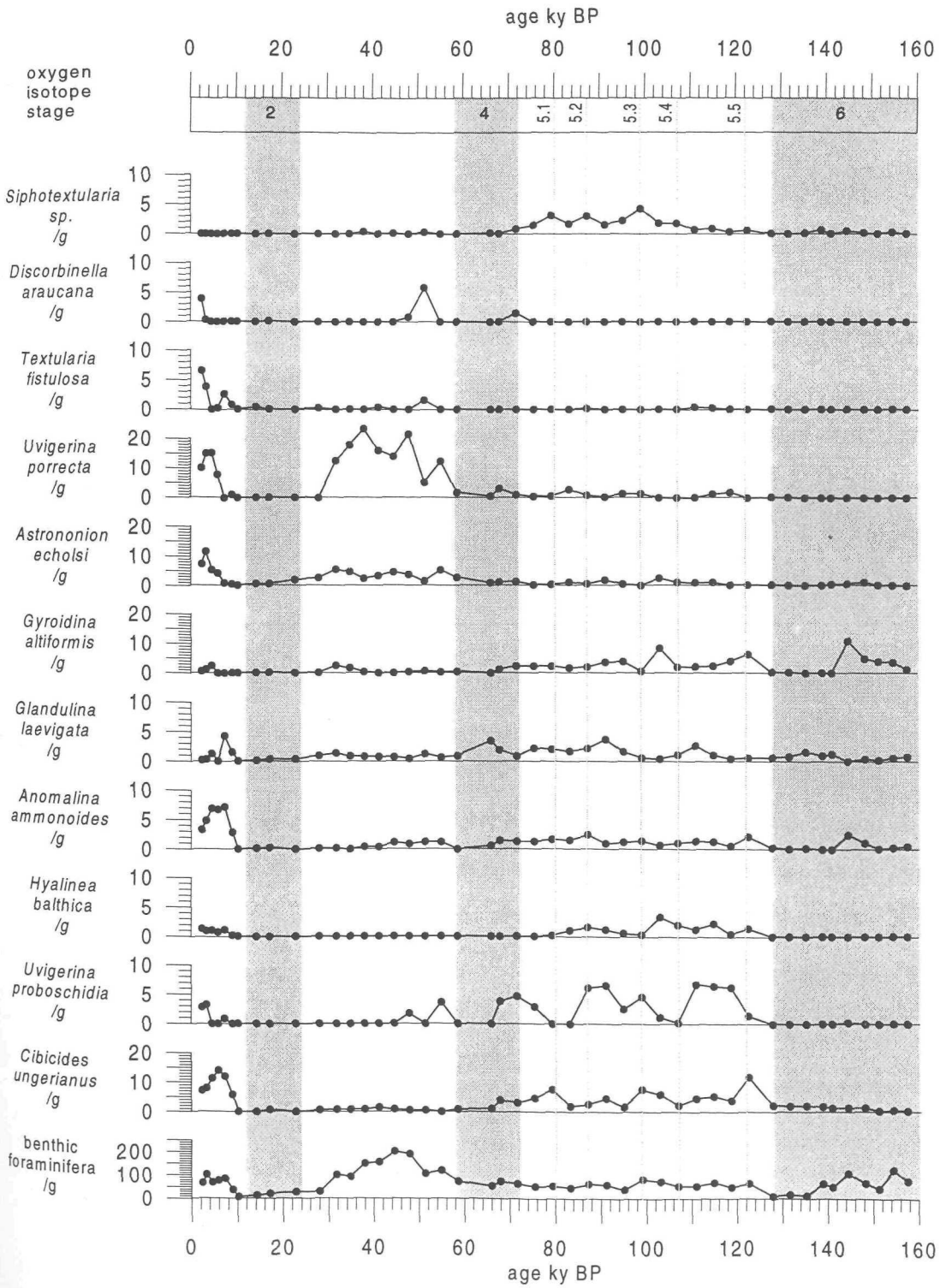

c) Glacial dominant fauna:

Benthic foraminifera species showing higher relative abundance during stages 2 and 6, and to a lesser extent stage 4, are regarded as glacial indicators (figure 6.28). *Bolivina subspathulata* (plate 36) is a true glacial indicator, peaking in stage 2 and late stage 6 only, although their absolute numbers (figure 6.29) are low throughout stage 2. *Eponides punctulatus* is also considered to be a glacial indicator owing to its greater persistence in stages 6 and 2, despite the large peak in abundance at 10 ky BP and its presence in stage 3 which was discussed in section 6.6.2.ii.a. *Gyroidina umbonata* (plate 37) peaks in stage 4 alone, and *Gyroidina subsoldanii* (plate 38) peaks in stages 4 and 2 although the absolute numbers show high values throughout interglacial stage 5. Salinity tolerant miliolids (Halicz and Reiss, 1981) also appear to be glacial indicators with relative abundance peaks in stages 2, 6 and 4. The more abundant miliolids found in the sediment (*Spiroloculina communis* (plate 39), *Spiroloculina depressa* (plate 40), *Miliolinella subrotunda* (plate 41), *Quinqueloculina multimarginata* (plate 42), *Quinqueloculina lamarkiana* (plate 43), *Triloculina tricarinata* (plate 44) and *Biloculina irregularis* (plate 45)) are shown in figures 5.19a and b. *Biloculina irregularis* shows the highest relative abundance of the miliolids (up to 20% in stages 2 and 6), proving to be a true glacial indicator. However, absolute numbers (figure 6.29) show greater abundance of miliolids in interglacial stages 1, 3 and 5, owing to generally lower benthic absolute abundances in glacial maximum intervals.

6.6.3 Epifaunal-infaunal species and temperature tolerance of species groups.

The significantly abundant benthic foraminiferal species mentioned for core 1039 may also be grouped, on the basis of genus descriptions (Murray, 1991; Gupta, 1994), into epifaunal and infaunal species and cold, temperate-cold and temperate-warm species (table 6.5). Figure 6.30 presents the down-core variation of these groups, based on the accumulated values of the relative abundance and absolute numbers according to the whole data set, hence the summed percentage values depicted in the curves do not total 100 %.

i) Epifauna versus infauna

Species known to be epifaunal and infaunal (table 6.5) have been combined into epifaunal and infaunal species groups. The relative abundance of epifauna (figure 6.30a) shows a

Figure 6.28 **Relative abundance of benthic foraminiferal species common during glacial periods. Core 1039, Red Sea.**

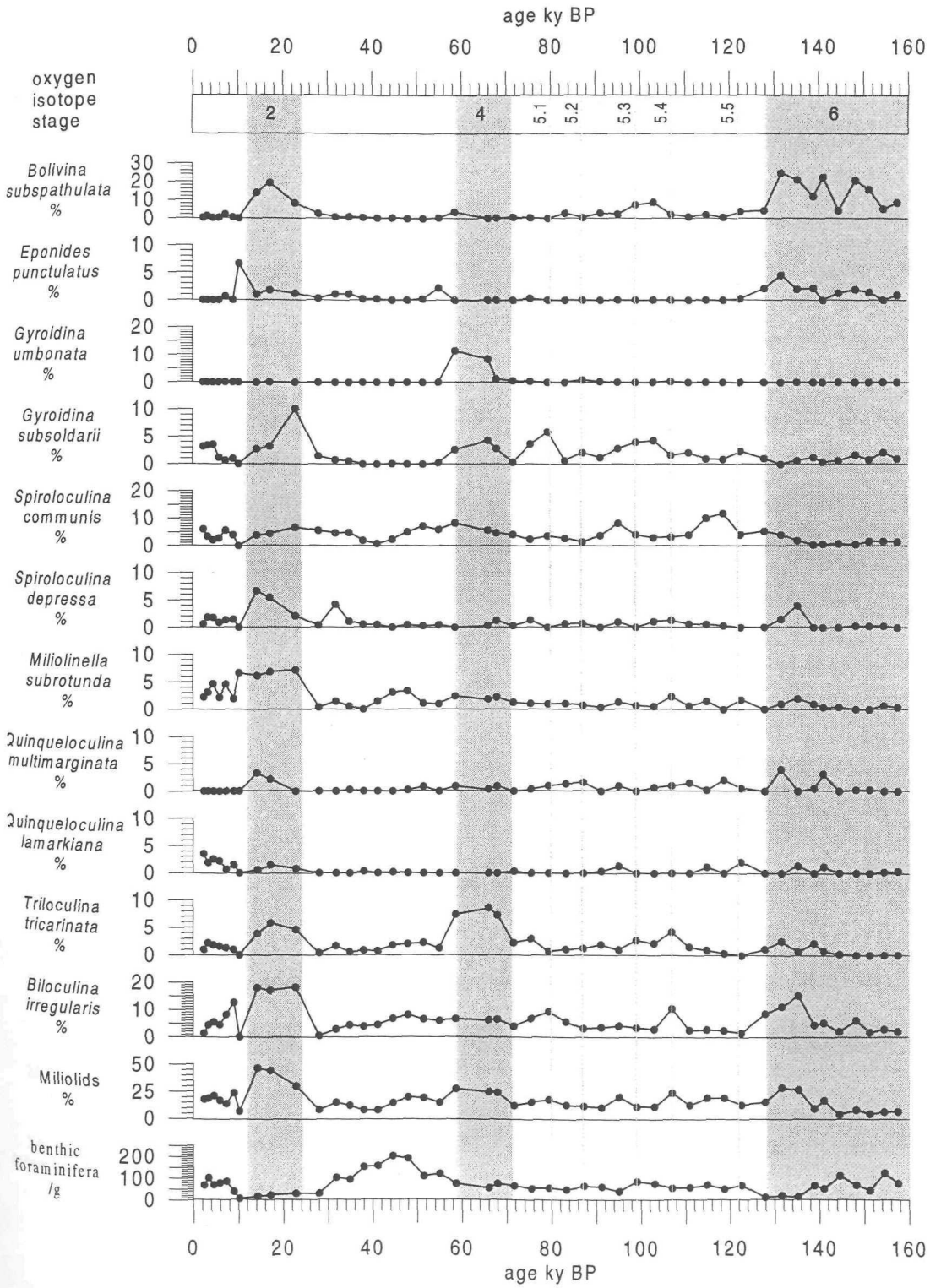

Figure 6.29 **Absolute numbers of benthic foraminiferal species common during glacial periods. Core 1039, Red Sea.**

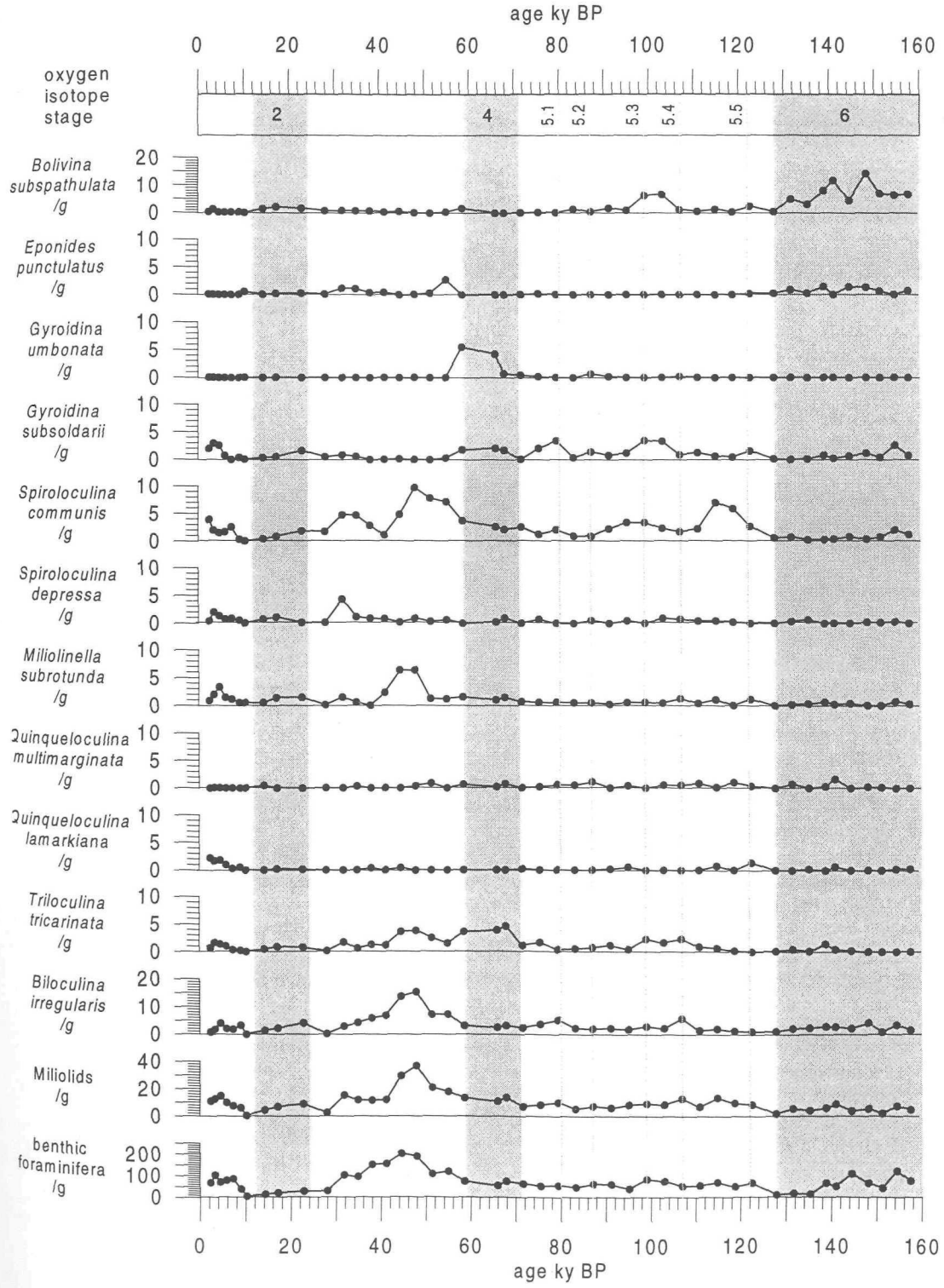

Table 6.5 Ecological parameters of significant benthic foraminiferal species found in core 1039 (Murray, 1991; Gupta, 1994)

Species	Epifaunal	Infaunal	Possible temperature tolerance:		
			Cold	Temperate	Sub-tropical
C.auriculus	✓			✓	✓
B.spathulata		✓	✓	✓	✓
B.italica		✓	✓	✓	✓
E.punctulatus	✓		✓	✓	
B.marginata		✓	✓	✓	
U.cushmani		✓	✓		
C.laevigata		✓	✓	✓	
E.trigona	✓		✓		
B.subreticulata		✓	✓	✓	✓
C.ungerianus	✓		✓	✓	✓
U.proboschidia		✓	✓		
H.balthica	✓		✓	✓	
A.ammonoides	✓				
H.boueana	✓			✓	✓
G.laevigata		✓			
G.altiformis	✓		✓		
Siphotextularia	✓		✓	✓	✓
A.echolsi		✓	✓		
U.porrecta		✓	✓		
T.fistulosa	✓		✓	✓	✓
D.araucana	✓			✓	✓
B.subspathulata		✓	✓	✓	✓
G.umbonata	✓		✓		
G.subsoldarii			✓		
Miliolids			✓	✓	✓

Figure 6.30 **Epifaunal and infaunal, and temperature indicating species down-core variation**

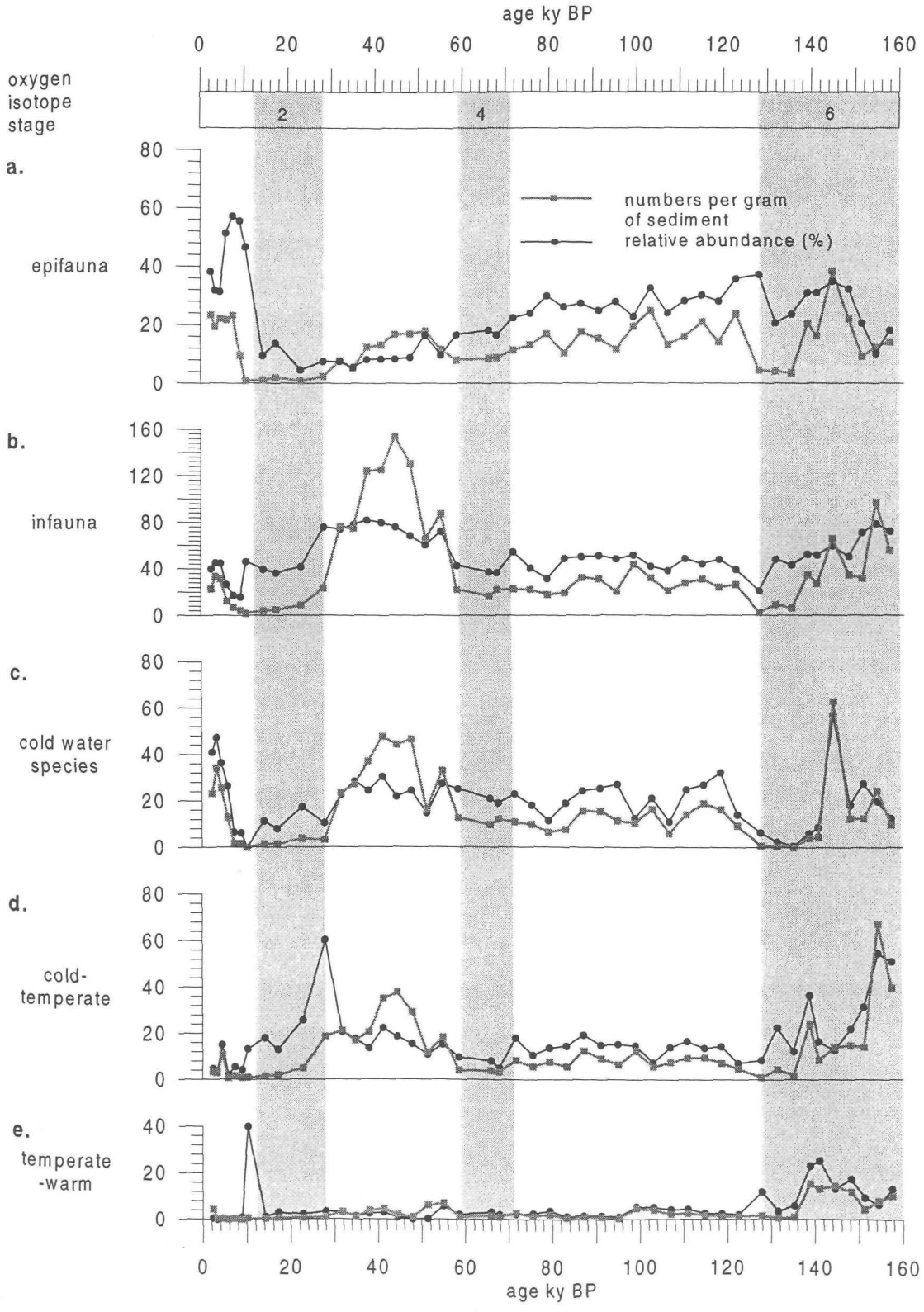

maximum peak (approximately 60 %), immediately following the deposition of the "sapropelic" horizon around 10 ka BP, maintaining a high abundance throughout stage 1. This is corroborated by the peak seen in absolute numbers (approximately 25 g^{-1}) at this time. The abundance of infauna (figure 6.30b) falls abruptly in conjunction with the epifaunal peak and recovers slowly towards present day. High epifaunal abundance is also seen in stage 5 (30-40%) and in mid stage 6 (>30 %) where absolute numbers peak at approx 35 g^{-1}. Infaunal benthic foraminifera show a distinct peak in stage 3 (approximately 80 %) and mid-late stage 6 (approximately 75 %). Stage 5 also has a high infaunal abundance (approximately 50 %). The glacial maxima (stages 2 and 6) are associated with a fall in relative epifaunal abundance (stage 6 approximately 20 % and stage 2 approx 4 %), and comparably low infaunal relative abundance (approximately 38 % stage 2 and 20 % stage 6). Thus it would seem that the infauna is relatively more tolerant of glacial conditions in comparison to the epifauna. The results also imply that the environment was particularly suited to the infauna during stage 3 and mid-stage 6 (around 150-160 ka BP), suggesting a significant alteration of the bottom water environment took place at these times.

ii) Cold-temperate-warm species

The fauna has also been split into cold, cold-temperate and temperate-warm categories (table 6.5) on the basis of genus tolerances (after Murray, 1991) (figures 6.30c, d and e). No truly warm species were found. Cold species peak in abundance in mid stage 6, stage 3 and stage 1, as do cold-temperate species although the relative peaks are staggered. Temperate-warm species show low abundance in glacial maxima. The maximum abundance peak is at the time of sapropel deposition. Plots of cold versus temperate warm, and temperate-cold versus temperate-warm species showed no relationship and as such are not included here. The results imply that any temperature variation in the bottom water was not great enough to significantly influence the benthic foraminiferal fauna.

6.6.4 Summary

The benthic foraminiferal investigation carried out on cores 1017 and 1039 has shown that:

- It is difficult to group the fauna into specific assemblages showing systematic abundance variations

- *Bolivina subreticulata*, a species tolerant of high salinity and low oxygen conditions (Gupta, 1994) is the most significant species in the core, dominating the sediments from the stage 6-5 boundary to the end of stage 3.
- Benthic foraminiferal species present within the sapropelic horizon, deposited beneath a stratified, stagnant water column (Locke, 1984; Ivanova, 1984), also show increased abundances during stage 3, a period thought to have been characterised by poor ventilation in the Red Sea (Almogi-Labin et al., 1998), and during mid-stage 6.
- Infaunal species are dominant (upto 80 %) in stage 3 and mid-late stage 6.
- The total benthic fauna shows clear responses to glacial-interglacial cycles with a great reduction in foraminiferal numbers associated with glacial maxima.
- During glacial maxima miliolid species, known to tolerate extreme salinities (Halicz and Reiss, 1981) are abundant.
- Any bottom water temperature variation did not significantly affect the benthic foraminifera.

6.7 Pteropod preservation in cores 1017 and 1039.

The occurrence of pteropod tests and their preservation state, according to Almogi Labin et al. (1986) (table 6.6), were noted throughout the cores (table 6.7). The general state of preservation and abundance of pteropods is seen to decrease down-core. The presence of pteropod tests continues throughout the aplanktonic zones, displaying secondary aragonite overgrowth (figure 6.31) in that of isotope stage 2. Their persistence indicates that the decline in planktonic foraminiferal numbers cannot be attributed to dissolution since the aragonitic pteropod tests would have dissolved before the calcite tests of the foraminifera.

Table 6.6 Five modes of preservation of pteropod shells recognised in core sediment from the northern Red Sea suggested as a tool for past glacial cycle identification (Almogi-Labin et al., 1986)..

	Pteropod Shell Condition	**Preservation**	**Conditions necessary for type of preservation**	**Glacial / Interglacial**
I	Transparent.	Perfect.	Oligotrophic surface waters with a low supply of organic matter to the sediment.	Aragonite preservation indicates **glacial** interval.
II	Opaque-white.	Well preserved. Transparency may have been lost due to slight shell corrosion.		
III	Shell with secondary aragonite overgrowth.	Original shell is preserved and secondary overgrowth takes place.	Aragonite encrustation is thought to be a rapid, subsurface process.	
IV	Internal mould with remnants of the original shell.	Extensive aragonite dissolution leads to shell destruction and fragmentation.	Precipitation-lithification process is rapid and occurs while the shells are completely filled with sediment. This enhances preservation.	Aragonite loss and moulding indicates **interglacial** interval.
V	Internal mould.	Entire original shell is missing. Moulds are often composed of fine grained sediment with more than 90% Mg calcite.		

Table 6.7. Pteropod preservation in sediments from from core MD76-140 (after Almogi-Labin et al., 1986), and from cores 1017 and 1039, Red Sea.

Core MD76-140, Red Sea (Almogi-Labin et al., 1986)				**Core 1017, Red Sea.**			**Core 1039, Red Sea.**		
Oxygen isotope stage		**Pteropod preservation.**	**Comments.**	**Oxygen isotope stage and distance down-core**	**Pteropod preservation**	**Relative abundance**	**Oxygen isotope stage and distance down core.**	**Pteropod preservation.**	**Relative abundance.**
Core top sediments		60% transparent shells		**core top sediments**	transparent	abundant	**core top sediments**	mainly transparent	very abundant
1. Int.	**Middle**	Opaque-white shells dominant.		**Isotope stage 1 9.5-48cm.b.s.f.**	transparent	abundant	**Isotope stage 1 14.8-71.8cm.b.s.f.**	opaque-white shells	very abundant
	Base	>40% internal moulds with remnant aragonite.							
2. Glac.		Secondary aragonite overgrowth dominates.	Minimum abundance of pteropods is observed in indurated layers	**Isotope stage 2 48-70.5cm.b.s.f.**	secondary aragonite overgrowth	very abundant	**Isotope stage 2 71.8-146.8cm.b.s.f**	Secondary aragonite overgrowth.	abundant
3. Glac.		Transparent shells dominate.	Highest abundance of pteropods, particularly in mid-stage.	**Isotope stages 2-5 70.5-369.5cm.b.s.f.**	opaque white shells	abundant	**Isotope stages 3-5 146.8-450 cm.b.s.f**	mainly opaque shells and molds	abundant
4. Glac.		Increase in opaque-white shells.	Significant loss of pteropods	**Isotope stage 6 369.5-466cm.b.s.f.**	moulds with remnant shell	very abundant	**Isotope stage 6 450-480 cm.b.s.f.**	molds with remnant shell	Less abundant
5. Int.	**a,b,c,d.**	Mostly internal moulds.	Minimum abundance of pteropods.	**Isotope stage 7 466-746.5cm.b.s.f.**	opaque white shells	abundant			
	e.	Most original aragonite is lost.	Lithification more intense. Numerous nodular fragments.	**Isotope stages 8-9 746.5-996.5cm.b.s.f.**	moulds, some with remnant shell	not abundant			
6. Glac.		Poor preservation continues.		**Isotope stage 9 996.5cm.b.s.f.**		ABSENT			
7. Int.		Poor preservation.	Minimum abundance of pteropods.	**Isotope stages 9-12 996.5-base of core**	moulds, some with remnant shell	not abundant			
8. Glac.		Some secondary aragonite is preserved.							

Figure 6.31

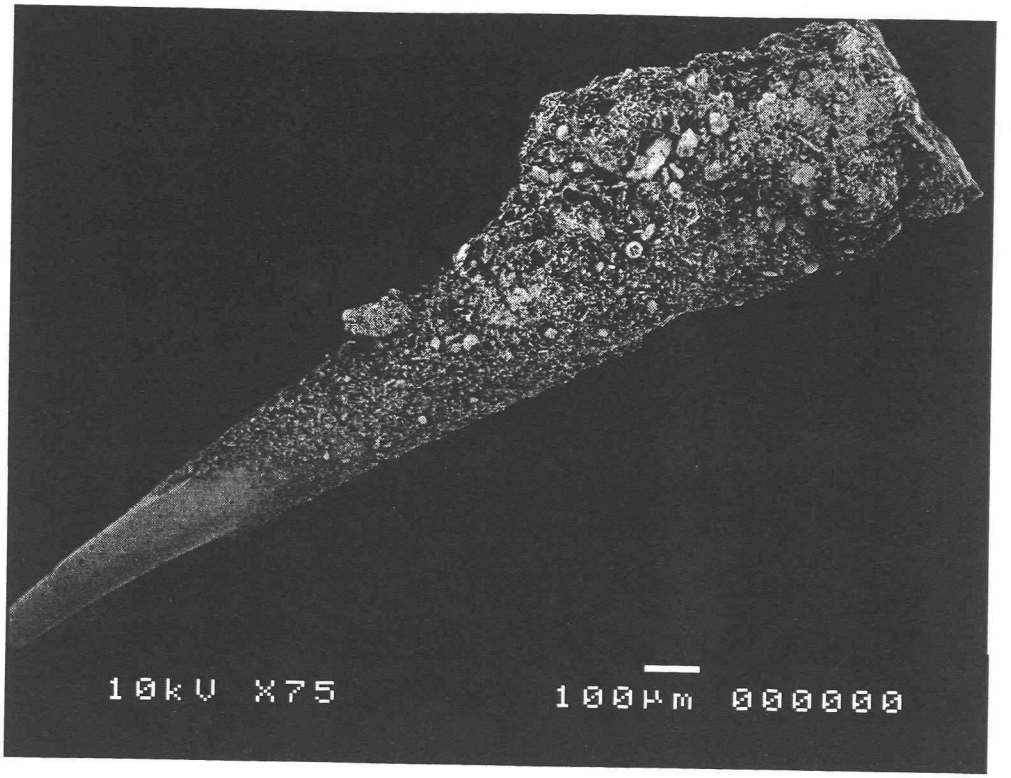

a. Pteropod test with secondary aragonite overgrowth

b. Acicular (needle-like) crystals of secondary aragonite

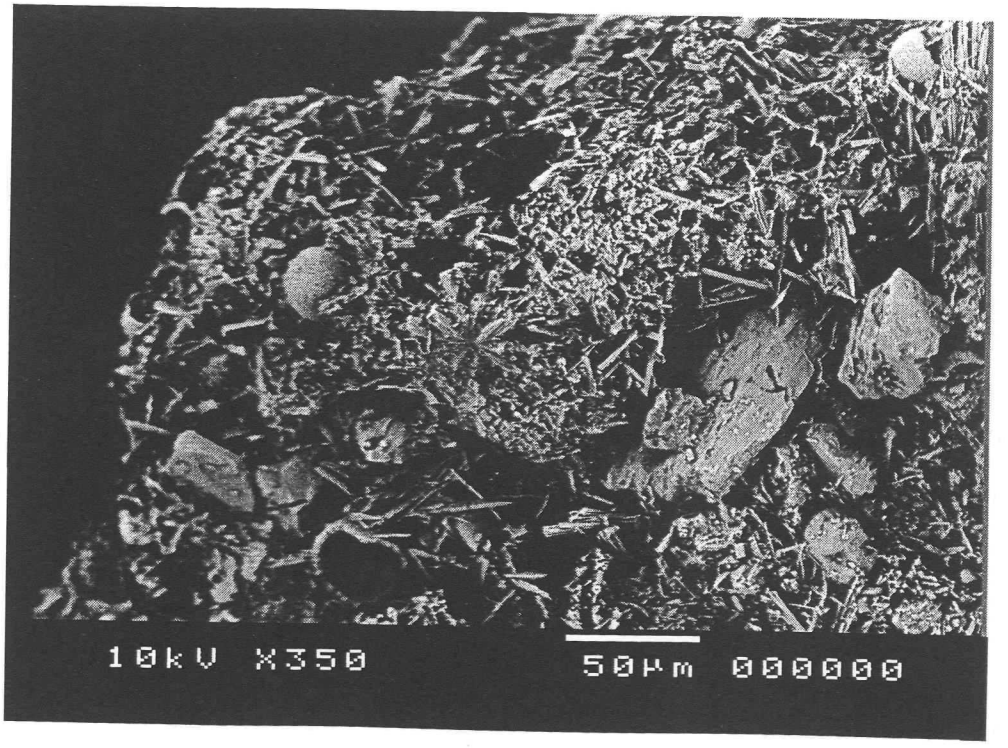

PART 2: THE GULF OF ADEN.

6.8 Down-core sedimentary variations, cores 1006 and 1005.

Both cores 1005 and 1006 show little variation in sediment size down-core. Core 1006 consists of a monotonous olive green clay throughout, with no significant variations (figure 6.32). The sediment is dominated (up to 75 %) by particles <63 μm in size. Particles of size 125-63 μm make up the majority (up to 25 %) of the remaining sediment fraction. A sharp, angular block of basalt, of 5-6 cm in diameter, was found at 331 cm depth within the core.

Core 1005 consists of olive-green clay (figure 6.33). The most significant variation is that concerning an increase in percentage of material of 125-63 μm between 475 and 400 cm depth, corresponding to a peak in total foraminiferal numbers (figure 6.34a) and low organic carbon values (figure 6.34b). This is immediately preceded by a sharp, high percentage peak of coarser, pebbly-shelly material (>600 μm), around 490 cm depth. There is a general decrease in fine sediment (<63 μm) in the upper 700 cm of the core, corresponding to increased TOC values (figure 6.34b). Sharp, angular blocks of basalt were found at arbitrary depths below 630 cm depth in the core.

6.9 Down-core planktonic foraminiferal variations, cores 1006 and 1005.

6.9.1 Core 1006

Figures 6.35 and 6.36 show down-core planktonic foraminiferal variations in core 1006. No significant down-core variation was observed in the down-core records of planktonic foraminifera in this core. The absolute numbers of planktonic foraminifera (g^{-1}) (figure 6.35) show higher values around 50 cm, 200 cm, 300 cm and 375 cm depth . These peaks (up to 2000 foraminifera /g) are reflected in the absolute numbers of all the individual species. Figure 6.36 shows relative abundance of the most abundant species in core 1006. The dominant species in the sediments are *G.bulloides* (plate 12) (up to 60 %), *G.glutinata* (up to 30 %) and *G.ruber* (up to 30 %).

6.9.2 Core 1005

The down core variations in core 1005 little resemblance to those of core 1006. Figure

Figure 6.32 **Down-Core Variations in Sediment Grain-Size Classes. Core 1006, Gulf of Aden.**

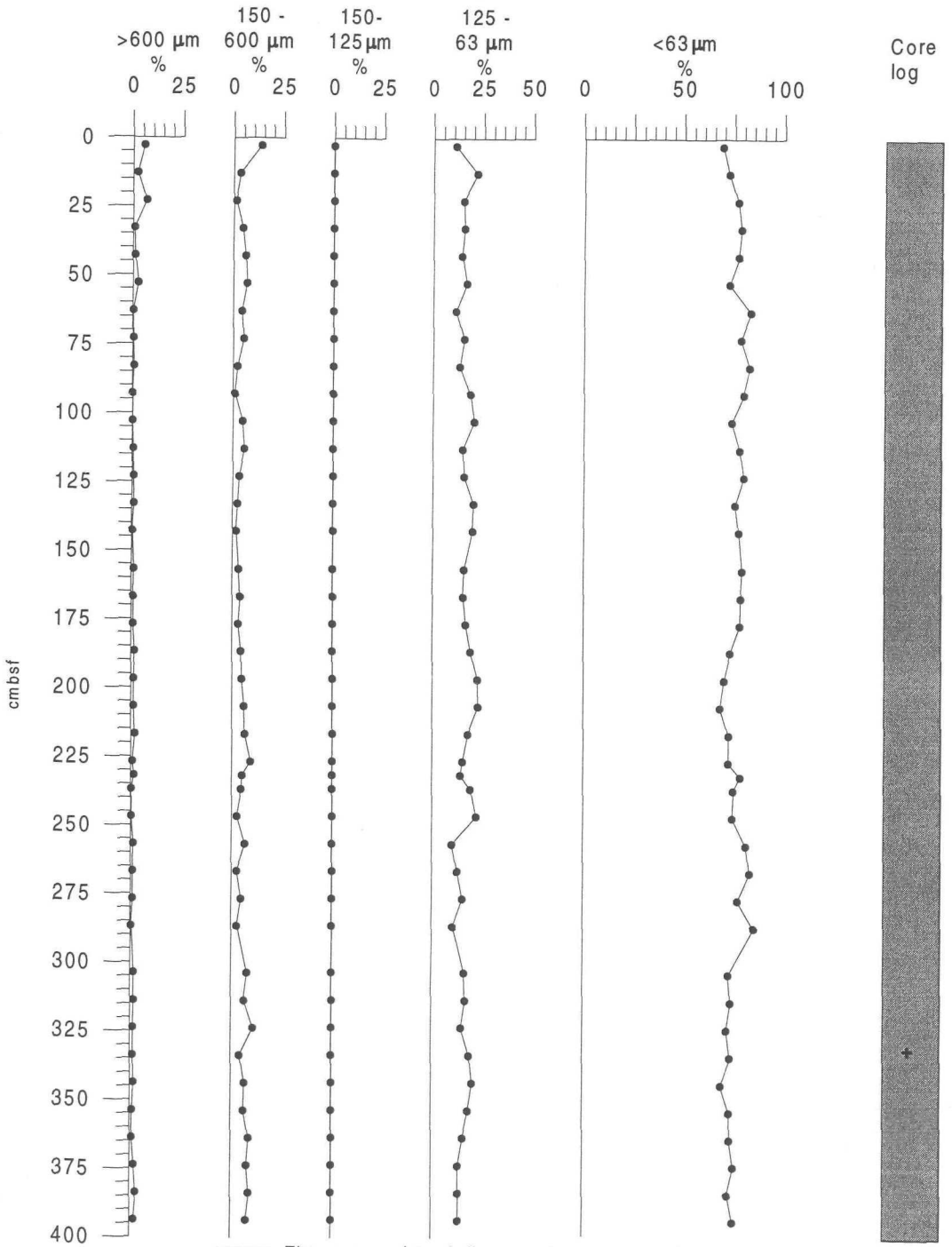

Figure 6.33 **Down-Core Variations in Sediment Grain-Size Classes, Core 1005, Gulf of Aden.**

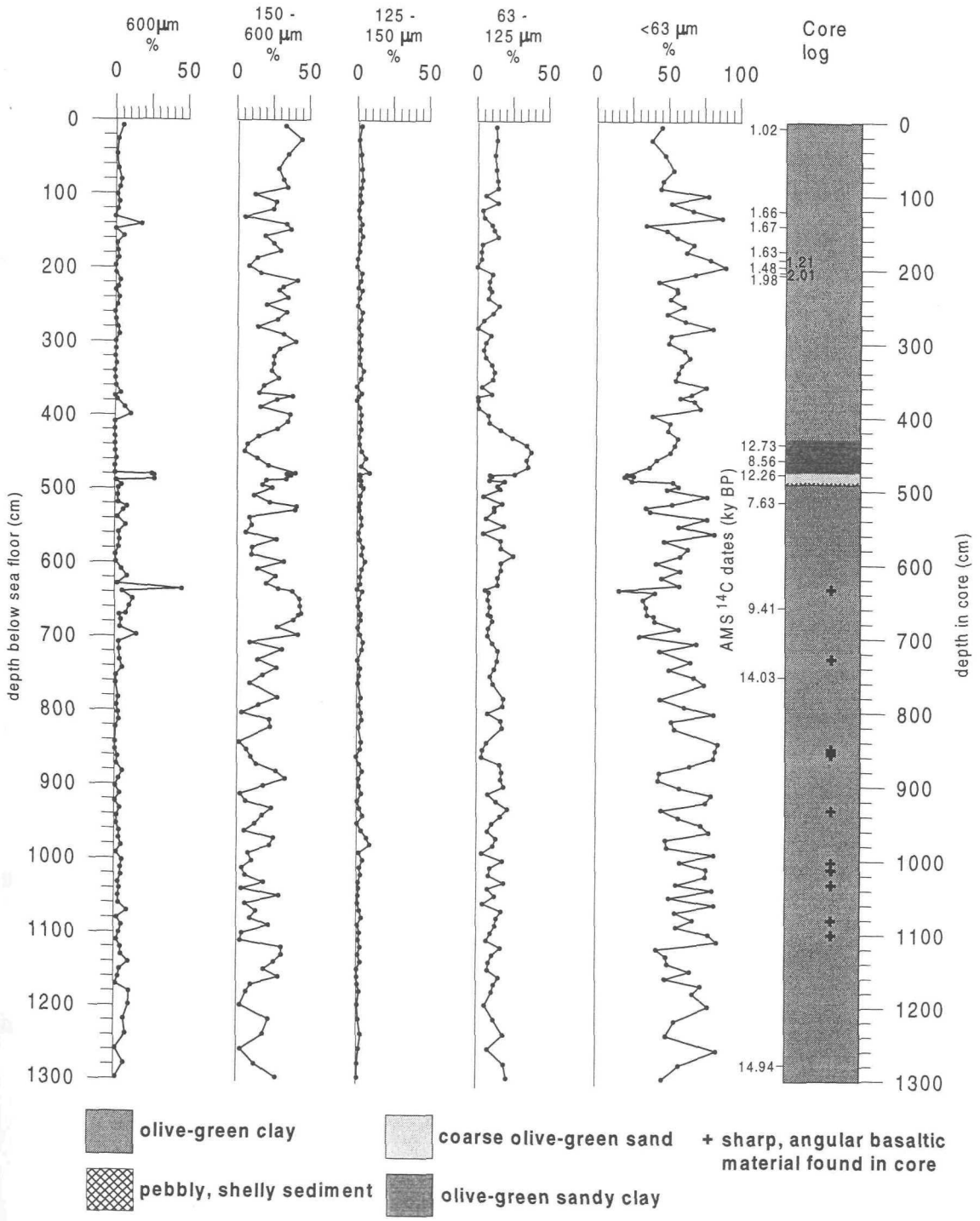

Figure 6.34 **Key down-core variations. Core 1005, Gulf of Aden**

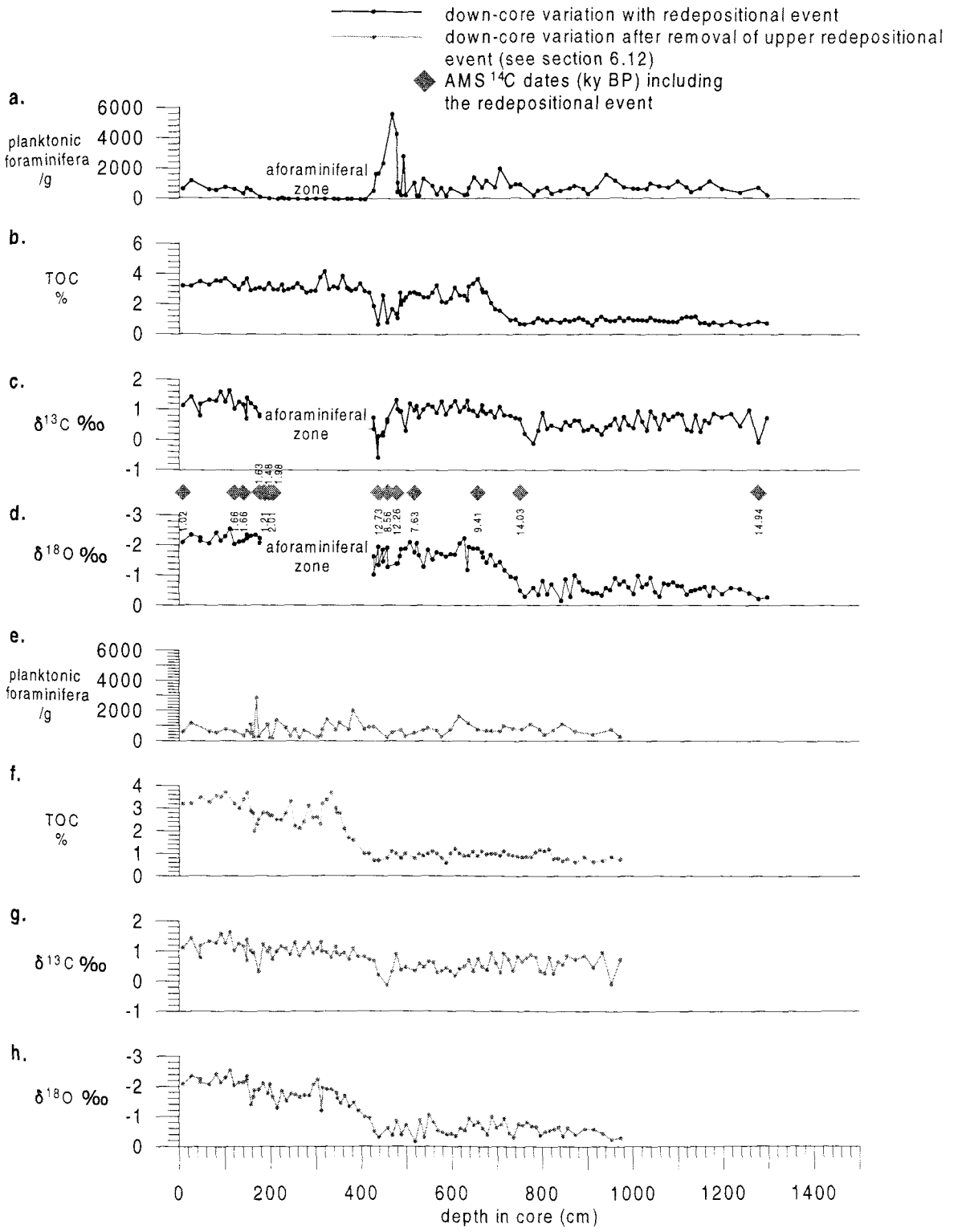

Figure 6.35 **Absolute numbers of planktonic foraminifera. Core 1006, Gulf of Aden.**

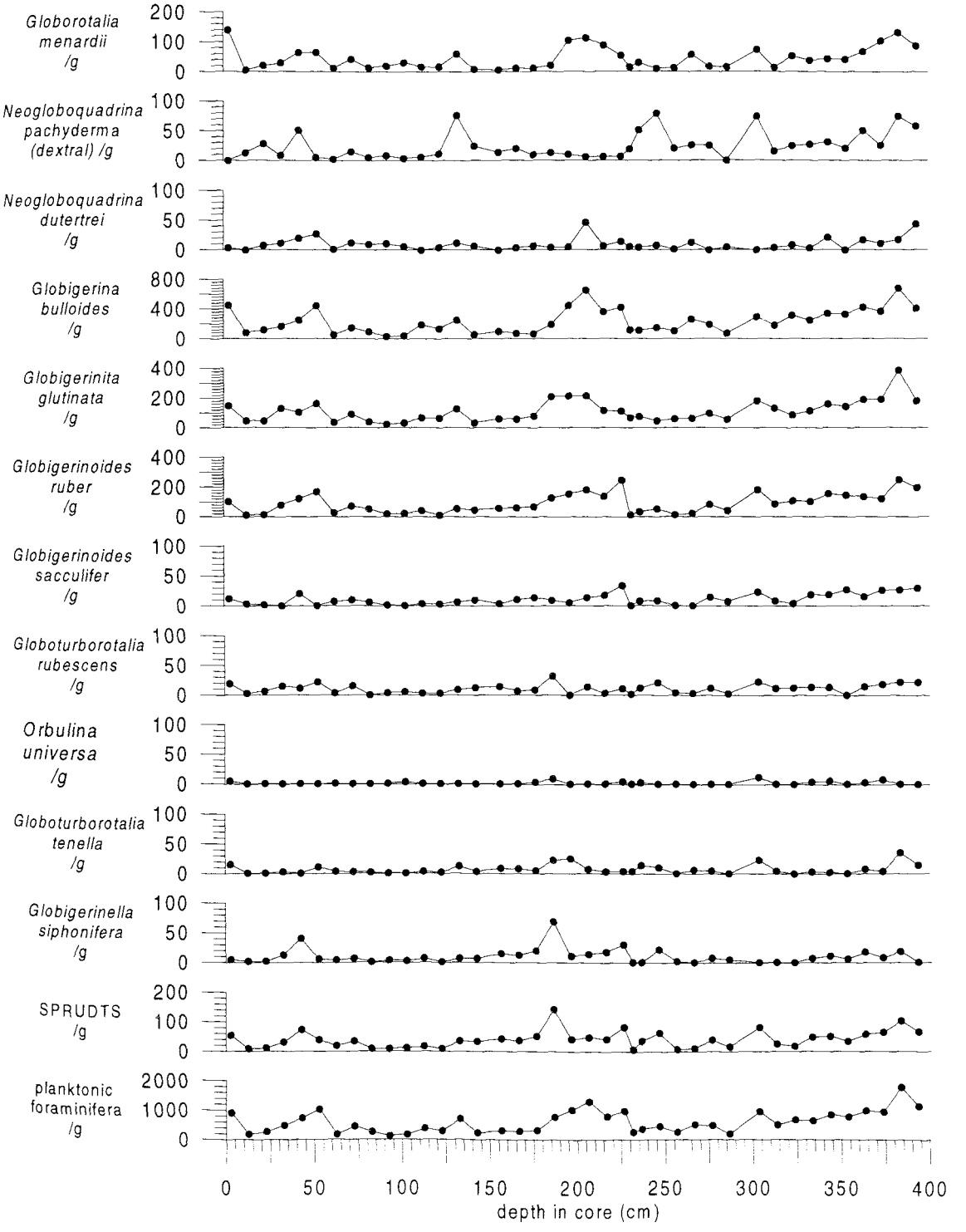

Figure 6.36

Relative numbers of abundant foraminifera.
Core 1006, Gulf of Aden.

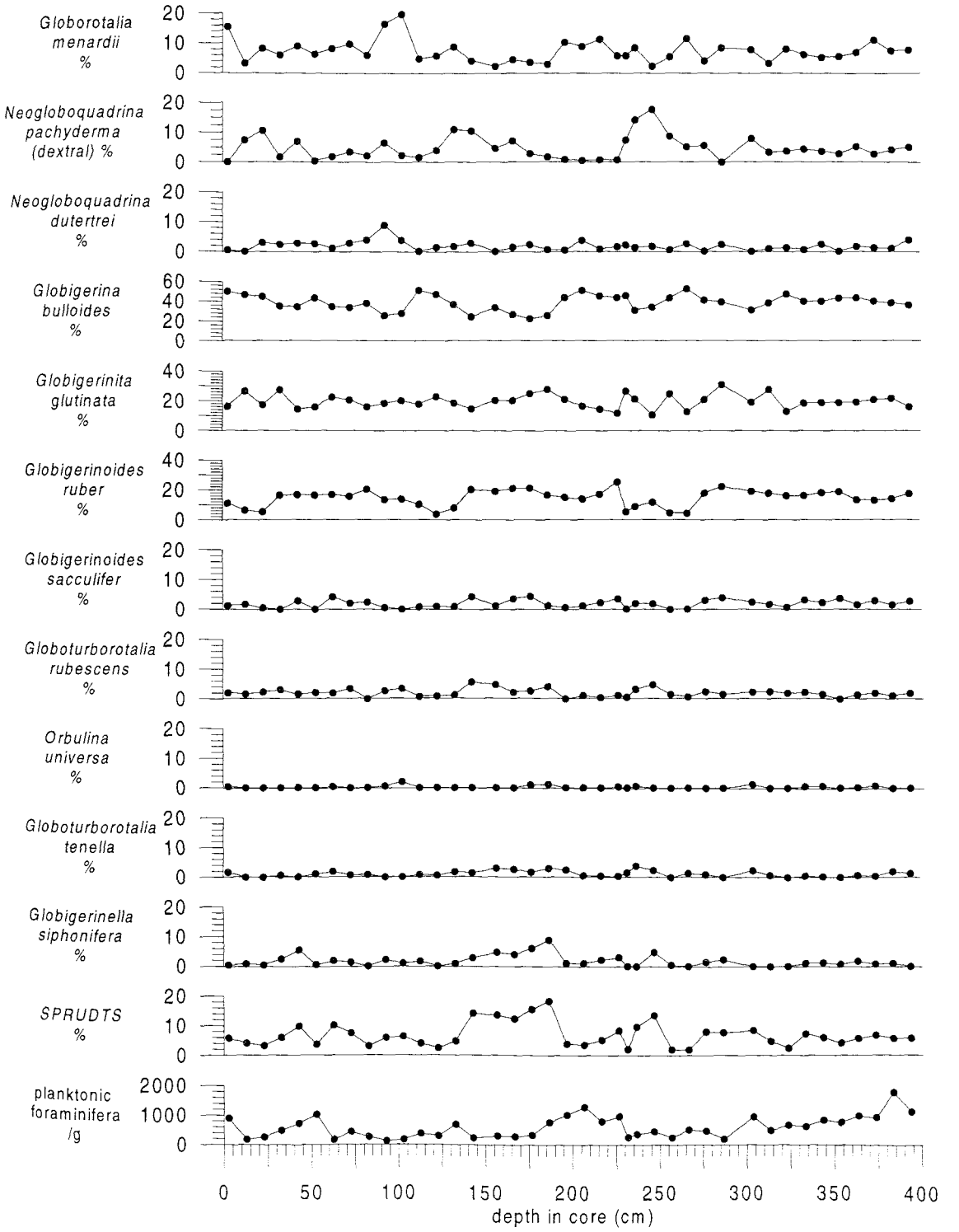

6.34a shows the variation in absolute numbers of planktonic foraminifera in core 1005. Two distinct features are seen:

i) A zone where planktonic, and benthic, foraminifera are mostly absent. Where specimens do occur quantities are negligible. This has been termed the "aforaminiferal zone", and is situated between 410 and 200 cm depth in the core.

ii) A large peak in numbers, up to 5500 planktonic foraminifera, at 450 cm depth.

No significant variation is seen in the remainder of the down-core record. Values become noisy with relatively high amplitude variations between 480 and 520 cm depth. The dominant species found in the core are shown in figures 6.37 and 6.38. The aforaminiferal zone and the anomalous peak in foraminiferal numbers (at 450 cm depth) are clearly reflected through all the species shown (figure 6.37). With the exception of these intervals, the absolute numbers show relatively uniform changes throughout.

Relative abundance curves are shown in figure 6.38. A peak (up to 100 %) in the SPRUDTS group, dominated by *G.siphonifera* and *O.universa* is seen in conjunction with the aforaminiferal zone, but the virtual absence of specimens in the sediment render the peak false. No significant variations in relative abundance of individual species are seen. The dominant species found in the sediments are *G.ruber*, *G.glutinata* and *G.bulloides* (up to approximately 35 % abundance in each case), the same species found to dominate throughout core 1006.

(NB. Figures 6.39 and 6.40 present the down-core planktonic foraminiferal species variations after removal of the redepositional event (section 6.12), in order to show the "true" faunal changes. The lack of significant faunal variation is highlighted.)

6.10 Down-core TOC variations, core 1005.

Figure 6.34b depicts variations in TOC content against depth in core 1005. The overall values show that the organic carbon content (%) in the sediments is very high (up to 4.0 %). From the core base (1300 cm depth) to 750 cm depth values are relatively constant, ranging between 1 and 2 %. However, between 750 and 675 cm depth, values are seen to rise to above 3 %. Values remain steady to core top, ranging between 3 and 4 %, with the exception

Figure 6.37

Absolute numbers of abundant planktonic foraminiferal species. Core 1005, Gulf of Aden.

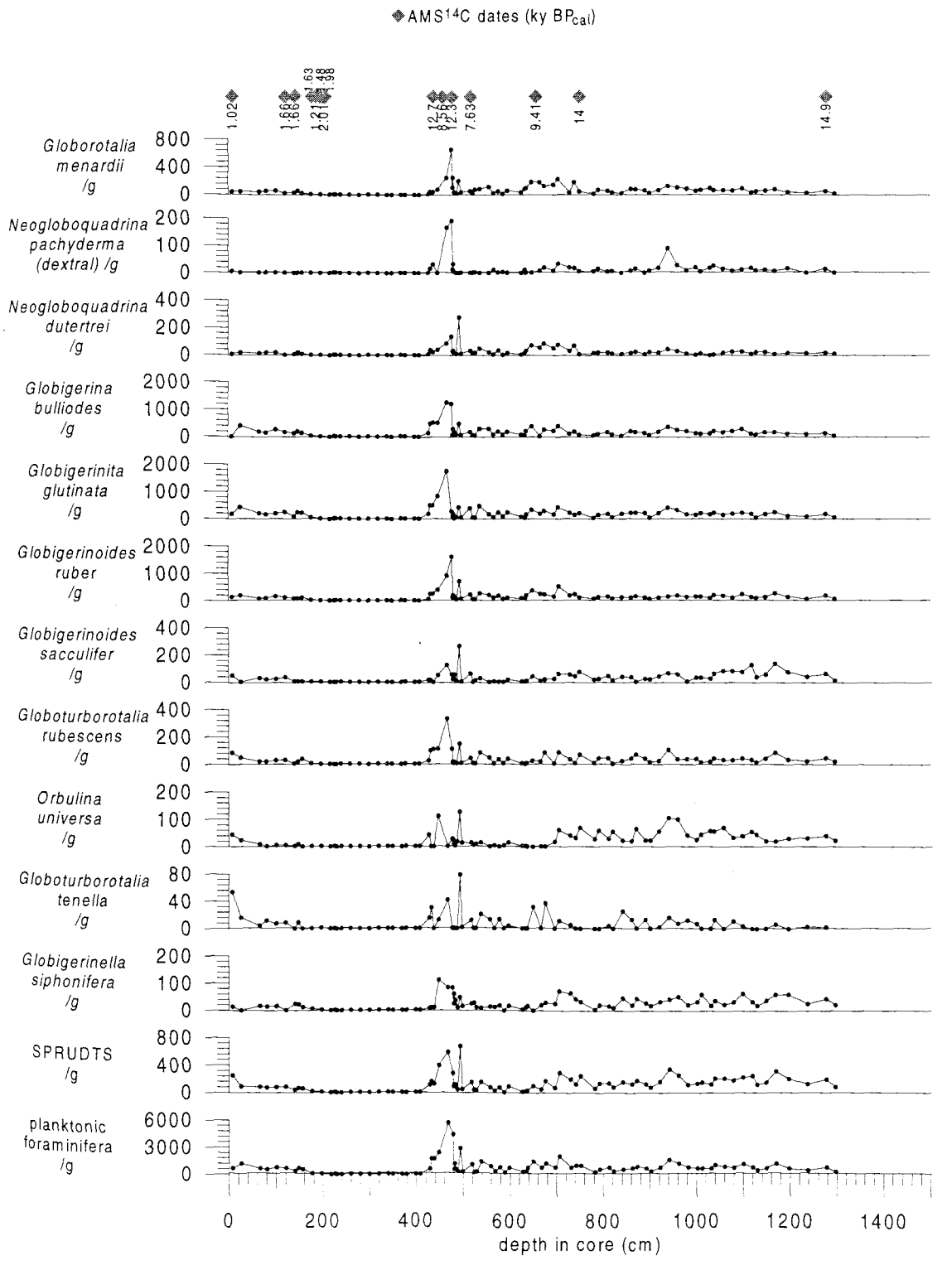

Figure 6.38 **Relative abundance of common planktonic foraminifera. Core 1005, Gulf of Aden.**

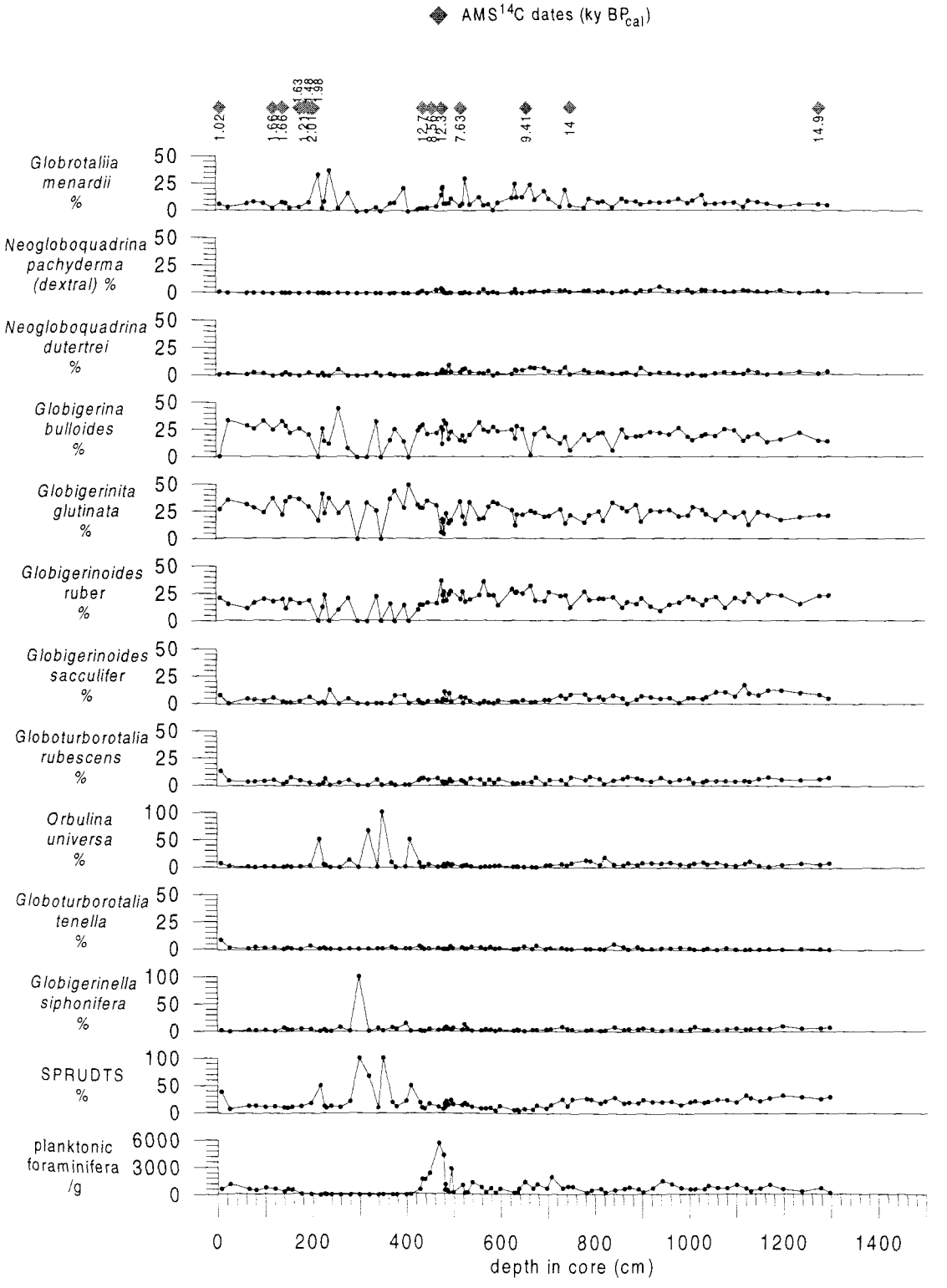

Figure 6.39 **Absolute numbers of abundant planktonic foraminiferal species after removal of the redepositional event (see section 6.12). Core 1005, Gulf of Aden.**

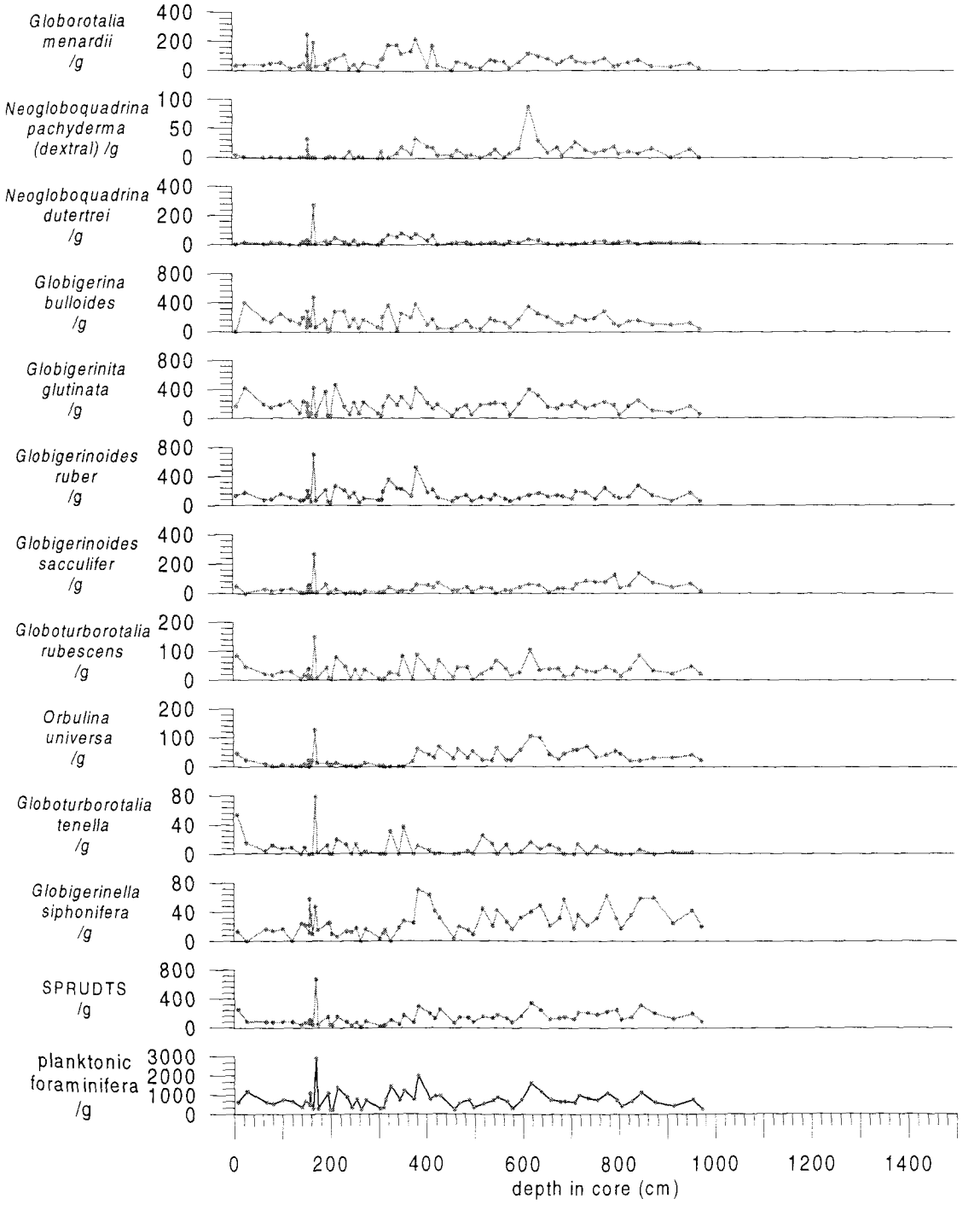

Figure 6.40 **Relative abundance of common planktonic foraminiferal species after removal of the redepositional event (see section 6.12). Core 1005, Gulf of Aden.**

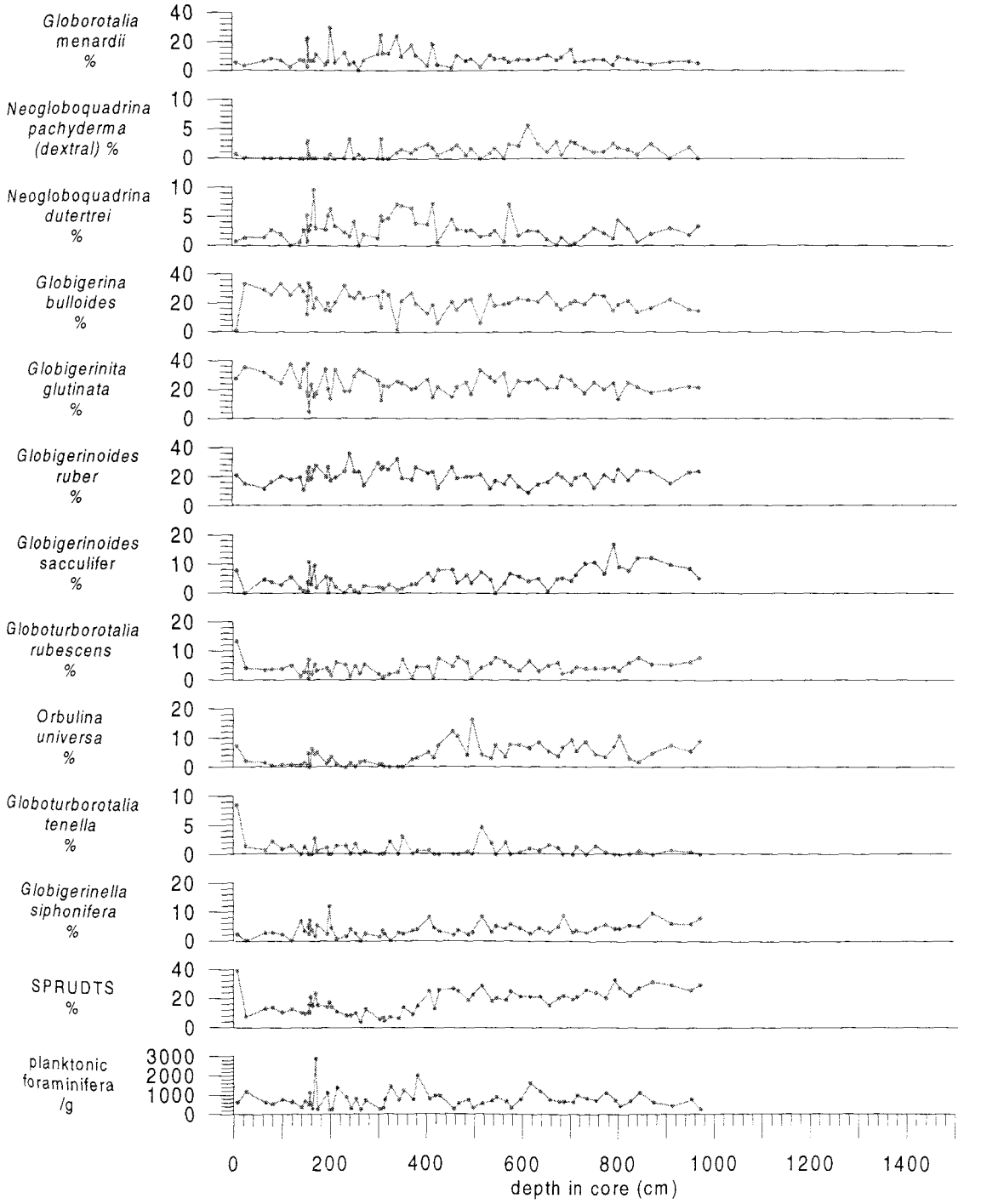

of values between approximately 475 and 425 cm depth, in conjunction with the peak in planktonic foraminiferal concentration. Here the values are mostly between 1 and 2 %. No apparent change in TOC content is noted in association with the aforaminiferal zone.

(NB. Figure 6.34f shows the down-core TOC variation after removal of the redepositional event (section 6.12). The results show the steady rise in TOC content from between 1 and 2 % to 3-4 % around 400 cm depth.. The removal of the "slumped" sediment has removed the low values (1-2 %) previously found between 275 and 425 cm depth.)

6.11 Down-core stable isotope variations, core 1005.

Stable oxygen and carbon isotope data for core 1005 are depicted in figure 6.34c and d. The gaps in the data between 150 to 400 cm depth are due to the lack of planktonic foraminifera in the sediments.

$\delta^{13}C$ (figure 6.34b) shows values between 0.25 and 1.0 ‰ from the core base to 600 cm depth, corresponding to the increase in $\delta^{18}O$. Above 600 cm depth values increase to between 1 and 1.75 ‰. However, a fall in values to approximately -0.75 ‰ is noted around 425 cm depth, coinciding with the peak in planktonic foraminiferal and the fall in TOC concentrations within the sediments.

The down-core $\delta^{18}O$ (figure 6.34d) suggests that core 1005 is representative of stage 1, the Holocene, and part of glacial stage 2. Higher $\delta^{18}O$ values (-1.25 to -0.25 ‰) are apparent in the stage 2 sediments, below 760 cm depth. The last true glacial maximum value is seen at 760 cm depth, suggesting an age of 16-15 ka BP (Martinson et al., 1987). A gradual decrease is noted between 760 and 600 cm depth in the core, reaching values of -2 to -3 in isotope stage 1.

(NB. Figures 6.34g and h present the down-core $\delta^{13}C$ and $\delta^{18}O$ variations for core 1005 after the removal of the redepositional event. The $\delta^{18}O$ record shows the last true glacial maximum value (15-16 ka BP (Martinson et al., 1987) at 440 cm depth.)

6.12 Time-stratigraphic framework for core 1005.

AMS ^{14}C dates have been obtained for 14 samples in core 1005 and corrected to calendar years using the Calib 3.03 program written by Stuiver and Reimer (1993), ((table 6.8, figure 6.41a), revealing unexpected results. The core top sediment was dated at 1.03 ka BP_{cal} and the core base at 14.94 ka BP_{cal}. The curve shows three values at around 438 cm, 458 cm and 478 cm depth, located within a zone of high foraminiferal (figure 6.41b) and lower TOC (figure 6.41c) concentration, which are assigned older dates (12.73, 8.56 and 12.18 ka BP_{cal} respectively) than would be expected, on the basis of a steady, linear sedimentation rate. This suggests the presence of a re-depositional event at this depth and is supported by the fining upwards sequence seen between 490 and 400 cm depth (figure 6.33). Other anomalous dates are highlighted (*) in table 6.8. Oxygen isotope data were used in conjunction with the AMS ^{14}C results (figure 6.41d). The results suggest that the core sediments penetrate stage 2, with the last true glacial value of 16-15 ka BP (Martinson et al., 1987) found at 760 cm depth. This again suggests the possibility of redepositional interference in the lower core, which is also suggested by the presence of angular blocks of basalt at arbitrary depths below 630 cm depth in the core (figure 6.41a).

It is assumed, from the evidence above, that the sediment between 155 and 480 cm depth is an instantaneous redepositional event, and that this interval should, therefore, be removed from the data. Removal of the anomalous data provides the core with a very tentative age-depth relationship (figure 6.42a). Using this relationship, the mean sedimentation rate for the upper 430 cm depth in the core is estimated at around 72 cm ky^{-1}. Below this the sedimentation rate is seen to increase dramatically to 576 cm ky^{-1}. This transition is coincident with the proposed stage 1-2 boundary, indicated by the $\delta^{18}O$ record. However, it seems that the AMS date at 880 cm depth (originally 1278.75 cm depth) is part of another redepositional event, and that the more likely progression of the age-depth relationship is predicted by incorporating the last true glacial oxygen isotope date of 16 ka BP (Martinson et al., 1987) at 440 cm depth (originally 760 cm depth) (figure 6.42a and d). This gives a more likely sedimentation rate of approximately 5 cm ky^{-1} below 440 cm depth in the core.

Table 6.8 AMS ^{14}C data for core 1005, Gulf of Aden. Anomalous dates are highlighted (*).

Depth in core (cm)	**Laboratory reference number UtC**	**AMS 14C dates (ka BP)**	**AMS ^{14}C dates (corrected to calendar ka BP_{cal})**
7.75	5807	1.496 ±0.025	1.03
120.75	Not available	2.149 ±0.045	1.662
140.75	5809	2.092 ±0.032	1.665
176.75	5814	2.087 ±0.041	1.629*
186.75	5813	1.608 ±0.110	1.239*
196.75	5812	1.950 ±0.060	1.498*
202.75	5811	2.390 ±0.160	1.992*
206.75	5810	2.370 ±0.080	1.972*
438.75	Not available	11.200 ±50	12.728*
458.75	Not available	8.250 ±46	8.56*
478.75	5808	10.780 ±0.080	12.177*
518.75	Not available	7.241 ±45	7.629
658.75	Not available	8.790 ±50	9.41
752.75	5806	12.430 ±0.060	14.028
1278.75	Not available	13.090 ±60	14.94

Figure 6.41 **Age-Depth Plot. Core 1005, Gulf of Aden.**

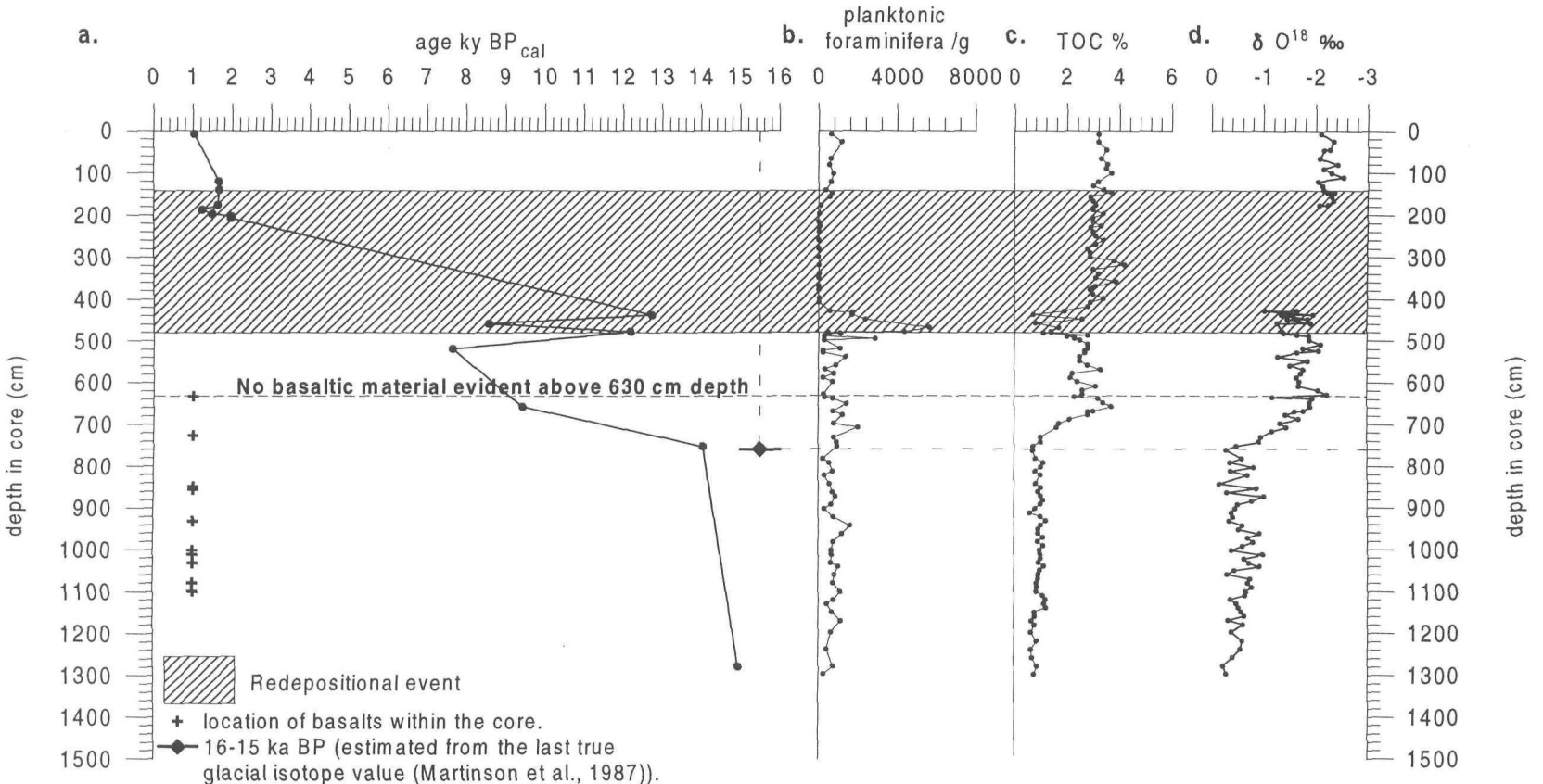

a. AMS ^{14}C dates versus depth in core.
b. variation in planktonic foraminiferal numbers.
c. down-core TOC (%) variation.
d. down-core oxygen isotope variation (gap in data is due to lack of planktonic foraminifera).

Together these records show that core 1005 is representative of the last 15 ky BP. The AMS ^{14}C results, combined with the planktonic foraminifera /g and TOC data, suggest a major redepositional event through the middle section of the core, of around 325 cm thickness.

Figure 6.42 Likely age-depth plot for core 1005, Gulf of Aden

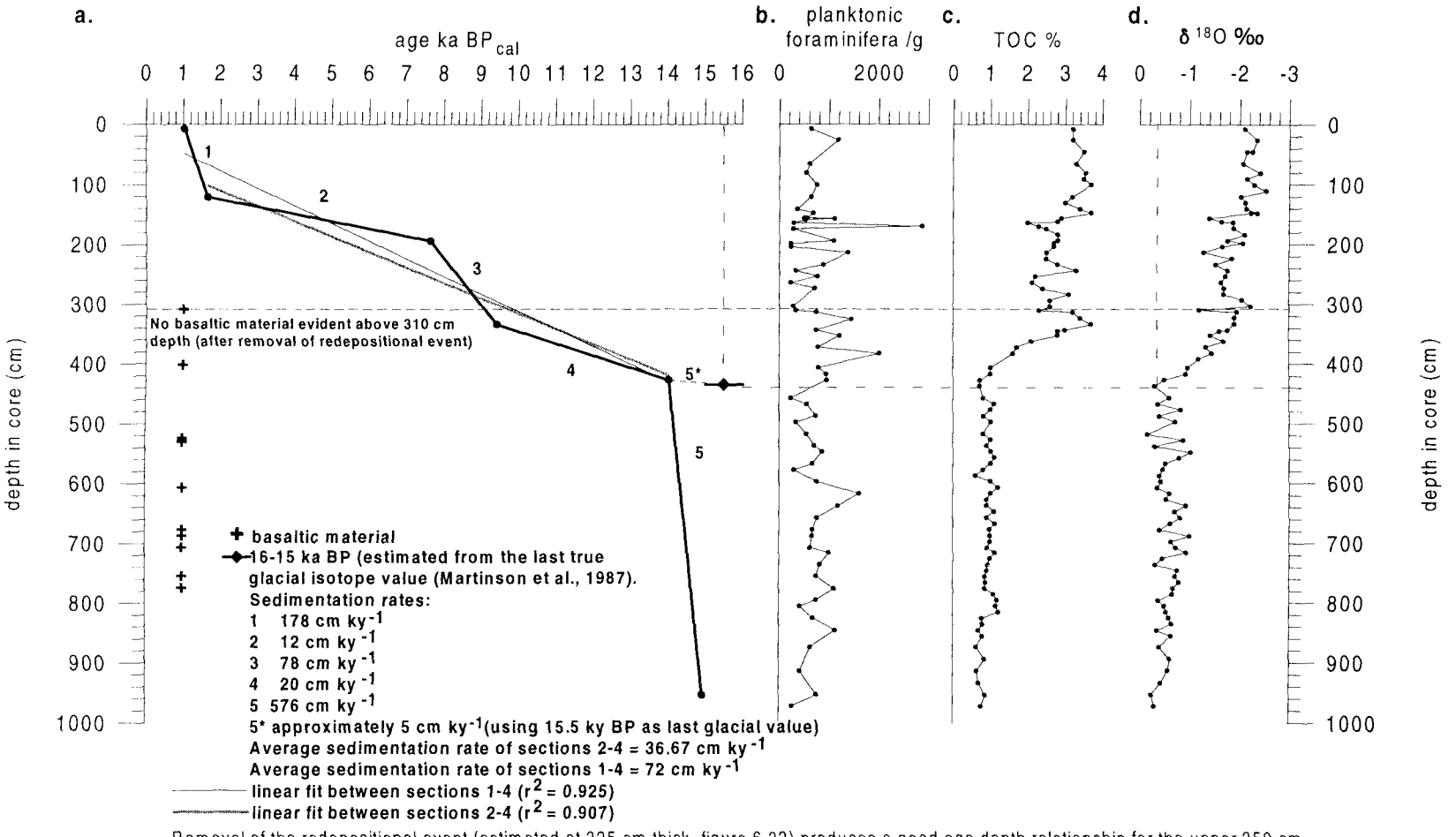

Removal of the redepositional event (estimated at 325 cm thick, figure 6.32) produces a good age depth relationship for the upper 350 cm of the core. Redepositional events are assumed to be geologically instantaneous.
However, below this the sedimentation rate increases greatly from an average of 72 cm ky^{-1} to approximately 576 cm ky^{-1}. It is here suggested that this may be a factor of change in sedimentation during glacial stage 2, or that this is another redepositional event in the core.

6.13 The Gulf of Aden sediments, cores 1006 and 1005.

On the basis of planktonic foraminiferal variations, CLIMAP (1981) suggest that there was no significant change in Gulf of Aden surface water temperature between present day and the LGM. The present study supports this, since core 1006 and in particular, core 1005, show no significant down-core species variation and the consistent abundance of *G.bulloides*, *G.glutinata* and *G.ruber* throughout. Thus, it is impossible to identify the stage 1-2 boundary in cores 1006 and 1005 through faunal variation alone.

No dates were obtained for core 1006 since down-core sedimentary and planktonic foraminiferal variations showed little change. Owing to the short length of this core (4 m) and the extremely high sedimentation rate of the region (implied in core 1005 at around 30 cm ky^{-1}) it is unlikely that core 1006 penetrates isotope stage 2, rendering it of little consequence to this study.

The time-stratigraphic framework for core 1005 suggests that the core is interrupted by redepositional events occurring between 480 and 200 cm depth, and below 650 cm depth in the core. Core 1005 is located on the flanks of the Tadjura trench at 1490 m water depth at the base of a steep slope (chapter 5, figure 5.1, table 5.2). It is proposed that the redepositional events are slumps likely to have been caused by local, nearby tectonic activity, disturbing the sediments on the slope above. This allowed older sediments to be redeposited above those which are younger and explains the occurrence of older AMS ^{14}C dates above those younger in core 1005 (figure 6.41a). Core 1005 did contain angular blocks of basalt of up to 6 cm in diameter, suggestive of recent volcanic/tectonic activity in this region. The Gulf of Aden is a young ocean (initially opening during the Oligocene-Miocene) and is still an active area of sea-floor spreading (Fantozzi, 1996), extruding basaltic material at the spreading centre. Faugères et al. (1983) reported such recent activity in the Gulf of Tadjura, close to the site of core 1005. Thus, it is suggested that tectonic activity in the vicinity of Bab el Mandab is apparent, resulting in frequent slumping events in the region. Owing to its poorly understood time frame, core 1005 will not be considered further in this study.

Chapter 7.

DISCUSSION

Cores 1017 and 1039 have provided detailed records including the last glacial cycle (core 1036 - 160 ky BP), and beyond (core 1017 - 475 ky BP). The main conclusion reached from the data is that the Red Sea displays strong sensitivity to global sea level variation and so is strongly influenced by glacial-interglacial cycles.

7.1 High salinities in the glacial Red Sea.

Evidence for elevated salinities during glacial maxima in the Red Sea is apparent in cores 1017 and 1039. High salinity is held responsible for the aplanktonic zones found in sediments throughout the Red Sea, in accordance with previous work (Ivanova, 1985; Locke, 1984; Locke and Thunnel, 1987; Thunnel, 1988; Almogi-Labin et al., 1991; Hemleben et al., 1996). Surface water temperature variation is unlikely to be a significant factor since sea surface temperature in the Red Sea is thought to have only dropped by approximately 2-3 °C, relative to present day values (25-30 °C), while surface water temperature in the Gulf of Aden remained about the same (25 °C) (CLIMAP, 1981).

The results of cores 1017 and 1039 show great similarity to those of other Red Sea studies (eg. Locke, 1984; Hemleben et al., 1996 and many more), and strongly indicate high salinity events in the basin associated with glacial maxima. Aplanktonic zones had been known already from glacial isotope stages 2 and 6 (Ivanova, 1985; Locke, 1984; Locke and Thunnel, 1987; Thunnel, 1988; Almogi-Labin et al., 1991; Hemleben et al., 1996), however, core 1017 has revealed, for the first time, an additional aplanktonic zone in stage 12 (figure 7.1a). In this study, a systematic succession of species disappearances is noted approaching the aplanktonic zones, a feature not previously addressed. Absence / near absence of *G.ruber* through the aplanktonic zones (figure 7.1b), a species tolerant of up to 49 ‰ salinity (Bé and Hamelin, 1967; Bé and Tolderlund, 1971; Tolderlund and Bé, 1971; Hemleben, 1989), suggests that salinity possibly exceeded this. On the basis of oxygen isotope values, maximum LGM surface water salinity has been estimated at around 53 ‰ (Hemleben et al., 1996).

Figure 7.1 **Evidence for high salinity in the Glacial Red Sea**

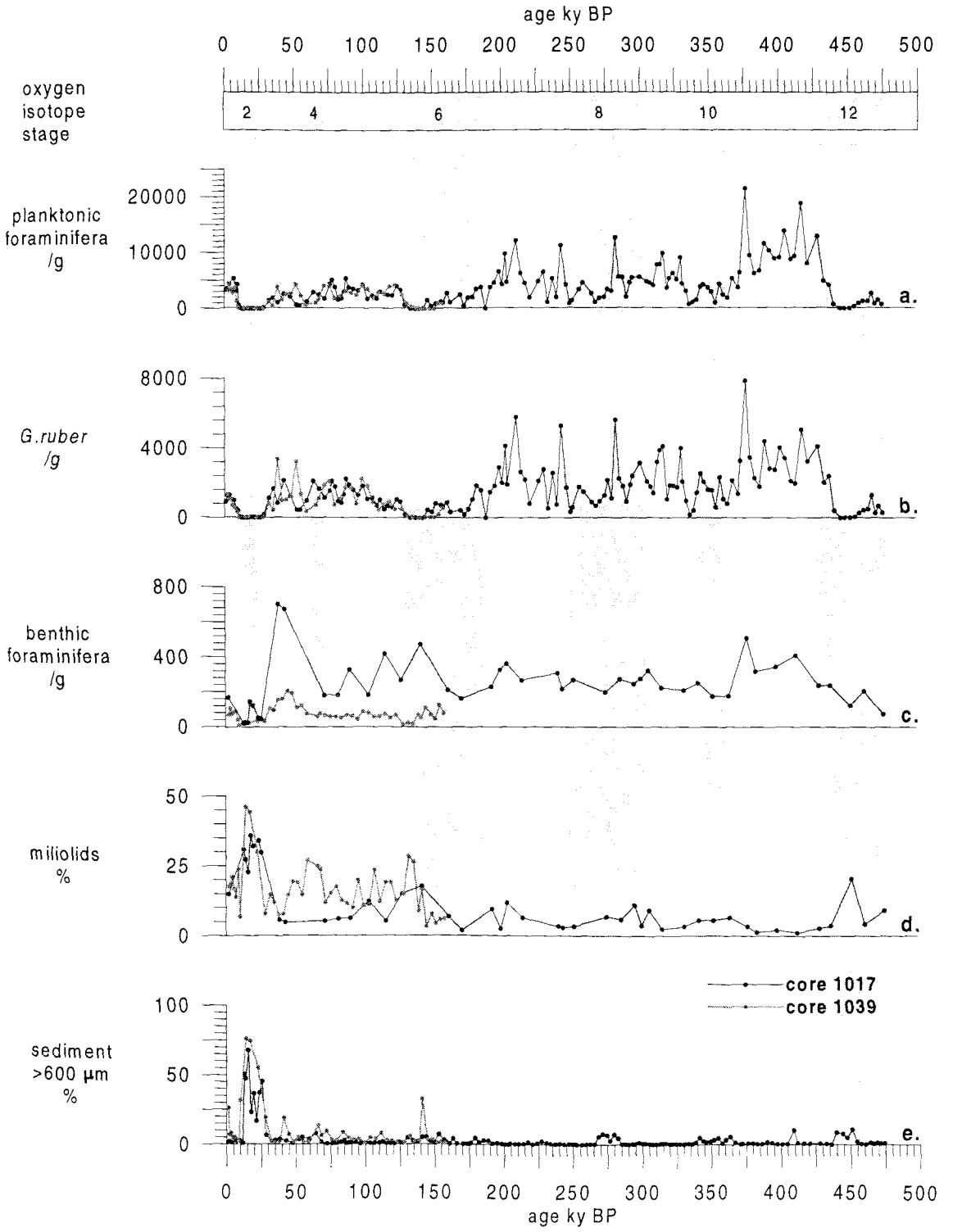

The disappearance of the majority of benthic foraminifera simultaneous with the aplanktonic zones (figure 7.1c) suggests a great change in Red Sea bottom water properties during glacial maxima. The coincident increase in relative abundance of the benthic foraminiferal group, the miliolids, known to dwell in hyper-saline lagoons and shallow water (Halicz and Reiss, 1981), (figure 7.1d), indicates that elevated bottom water salinity is the likely cause. This is most clearly demonstrated in glacial stage 2, the LGM. Locke (1984) showed an increase in miliolid abundance (up to 70 %), associated with the aplanktonic sediments of LGM, and Halicz and Reiss (1981) showed a concurrent increase in miliolid abundance in cores from the northern Red Sea. In each case the elevated abundance was attributed to increased salinity of the bottom waters. Locke (1984) also reported the highest abundance of *Ammonia sp.* at this time, a genus known to dwell in hyper saline lagoons and shallow water (Halicz and Reiss, 1981). Bottom water salinity has been estimated at >55 ‰ using oxygen isotope values from the tests of *Hanzawaia sp.* and *Cibicides mabahethi* (Hemleben et al., 1996).

A monospecific assemblage of pteropod tests of the salinity tolerant epipelagic species *Creseis acicula* were noted to persist throughout the aplanktonic zones in accordance with the results of Almogi-Labin et al. (1986; 1991; 1998). The encrusted state of preservation of these aragonite tests (figure 6.29) provides further evidence for high basinal salinity (Almogi-Labin et al., 1986; 1991). Almogi-Labin et al. (1986; 1991; 1998) attributed the aragonite encrusted pteropod shells found in glacial maximum levels in Red Sea cores MD76-140, KL 13 and KL 11, respectively, to aragonite super-saturation of the bottom waters owing to elevated salinity and/or temperature (Herman, 1965; Chen, 1969; Milliman et al., 1969). Corroborating evidence is provided by an increase in sediment coarseness particularly in stage 2, and to a lesser extent in stage 6, in cores 1017 and 1039, and stage 12 in core 1017 (figures 7.1e). This endorses the observations of LGM intervals of other Red Sea cores (Milliman et al., 1969; Ivanova, 1984; Locke, 1986; Almogi-Labin et al., 1991), attributed to lithification of particles, cemented by inorganically precipitated aragonite. This, again, suggests that bottom waters, and pore waters, were supersaturated with respect to aragonite (Milliman et al., 1969; Ivanova, 1984; Almogi-Labin et al., 1991). Locke (1984) discovered high concentrations of magnesium-carbonate in the fine sediments at this time, supporting this hypothesis.

The continuation of benthic fauna and pteropods throughout glacial maximum sediments indicates that some communication (possibly a seasonal exchange) between the Red Sea and open ocean continued preventing worse salinisation and sterilisation of the basin. Global sea level lowering associated with glacial maxima (Shackleton, 1987; Chappell and Shackleton, 1986; Fairbanks, 1989; Radtke, 1990; Pirazzoli et al., 1993; Bard et al., 1996) is viewed as the driving force behind the elevated glacial Red Sea salinities (Deuser and Ross, 1976; Ivanova, 1985; Locke, 1984; Locke and Thunnel, 1987; Thunnel et al., 1988; Almogi-Labin et al., 1991; Hemleben et al., 1996). Lowering of global sea level would cause a significant reduction in strait dimensions at Bab el Mandab, and since the only significant exchange between Red Sea and Gulf of Aden waters occurs across this Strait, a dramatic reduction in water exchange between the Red Sea and the open ocean occurred. During the LGM, 120 m sea level lowering (Fairbanks, 1989) would have reduced sill depth from the present day value of 137 m (Werner and Lange, 1975) to a minimum of around 17 m at the shallowest point, close to Hanish island, assuming the sill has not been significantly uplifted over the last 18 ky. The width of the channel would also have been reduced from around 112 km today, to approximately 11 km (figure 4.2, chapter 4).

Using the hydraulic model of Assaf and Hecht (1974) with a sill depth of 80 m, Thunell et al. (1988) showed that a reduction in width or depth of the Strait of Bab el Mandab, or an increase in evaporation over the Red Sea, will result in an increase in salinity in the basin. Use of much shallower depths in the hydraulic model, like those suggested for the LGM (17 m), results in a break down in the proposed 2-way flow (Locke, 1984; Thunell et al., 1988; Hemleben et al., 1996). As such Hemleben et al. (1996) suggest that the sill has been tectonically uplifted since the LGM. However, Rohling (1994) suggests that a two way flow system across the sill did exist, despite the shallow sill depth, due to the equilibrium set up between prevailing wind stress, persistent surface water inflow and resultant sea surface slope. Owing to the intensification of the winter NE monsoon during the LGM, the prevailing wind over the Red Sea was southeasterly year-round and regional aridity was possibly enhanced (Duplessy, 1982; Fontugne and Duplessy, 1985; Sirocko et al, 1991; Sirocko and Ittekkot, 1992). This would have sustained a simple, long-term average, two-way exchange in the shallow (minimum possible depth 17 m), narrow (11 km) water column

above the sill throughout the last glaciation, driving the surface current in a northwestward direction (figure 7.2). Continued flow in this direction set up a sea surface slope. When this slope reached equilibrium with the prevailing wind stress, the two-way flow system was set up (Rohling, 1994).

Summarising, the almost complete loss of planktonic foraminifera seen in Red Sea cores 1017 and 1039 was most likely caused by elevated salinities of around 50 ‰ during glacial maxima. The high salinity is a direct result of lower global sea level during these times, causing a severely restricted two-layer exchange of water between the basin and the open ocean, combined with continued high evaporation due to aridity that may have been enhanced over the basin (Duplessy, 1982; Almogi-Labin et al., 1991).

7.2 Successive species disappearance preceding the aplanktonic zones in the Red Sea.

The aplanktonic zones, resulting from extreme salinity, are preceded by a succession of planktonic foraminiferal species disappearances. This succession (figure 6.13 and 6.14, chapter 6) begins with the disappearance of *G.sacculifer* about 15 ky preceding the zones, followed by *G.siphonifera*, *G.rubescens* and *G.tenella*, until finally *G.ruber* and *G.glutinata* disappear at the onset of the aplanktonic zone.

The aplanktonic zones are attributed to extreme salinities (of around 50 ‰) in the Red Sea, beyond the tolerance of planktonic foraminifera. *G.ruber* has the highest salinity tolerance of the foraminifera in the Red Sea, withstanding salinities up to 49 ‰ (Be and Hamelin, 1967; Be and Tolderlund, 1971; Tolderlund and Be, 1971; Hemleben, 1989), explaining its persistence up to the onset, and its rare appearances during the aplanktonic zones. Ecological parameters for *G.sacculifer*, *G.siphonifera*, *G.ruber* and *G.glutinata*; the main species involved in the successional disappearance, have previously been discussed in chapter 3 (and summarised in table 3.1). *G.tenella* and *G.rubescens* were omitted due to their low abundance in the sediments, and lack of information regarding their ecological preferences. The results of laboratory experiments have shown that *G.sacculifer* has a higher salinity tolerance (24-47 ‰) than *G.siphonifera* (27-45 ‰), yet *G.sacculifer* disappears between 5 to

Figure 7.2

Schematic diagram of glacial maximum Red Sea circulation

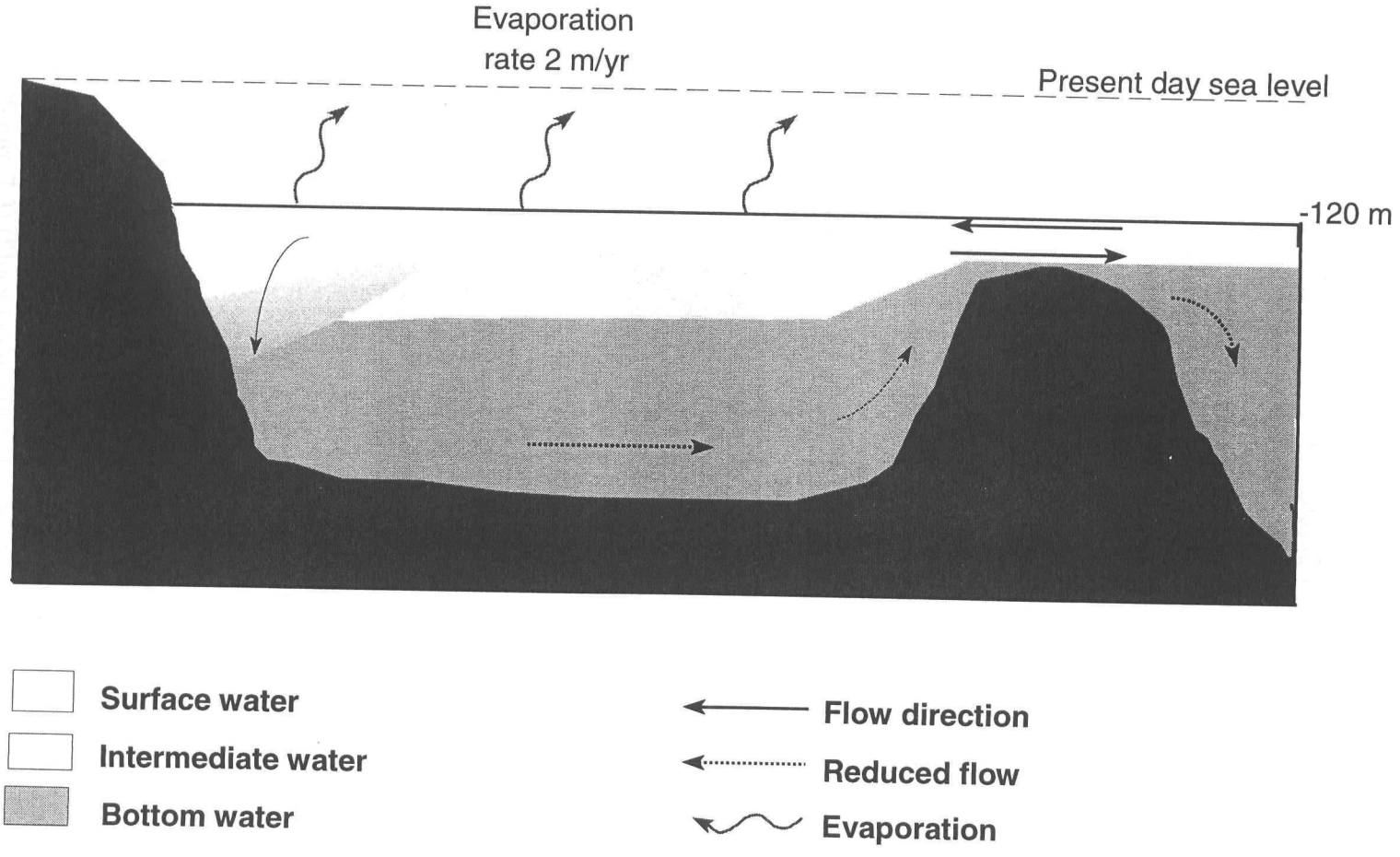

15 ky before the disappearance of *G.siphonifera* in each succession. If the disappearance of these species was attributed to salinity then *G.siphonifera* should die out before *G.sacculifer*. It is also noted that *G.sacculifer* and *G.siphonifera* disappear previous to the onset of glacial stage 4 and do not return until the onset of stage 1. Their absence is also noted in the less severe glacial stages 8 and 10 (Table 7.1).

Table 7.1 Time of species disappearance preceding the aplanktonic zones in cores 1017 and 1039.

Species	***G.sacculifer***	***G.siphonifera***	***G.glutinata***	***G.ruber***
Approximate time of disappearance (ka BP). Core 1017				
stage 2 aplanktonic between 25.5-12 ka BP	☆	☆	26	25.5
stage 4 no aplanktonic zone	68	58	★	★
stage 6 aplanktonic between 143.8-134 ka BP	157.5	152	144	143.8
stage 8 no aplanktonic zone	275	265	★	★
stage 10 no aplanktonic zone	355	340	★	★
stage 12 aplanktonic between 450.5-444 ka BP	464	454.8	451	450.5
Approximate time of disappearance (ka BP). Core 1039				
stage 2 aplanktonic between 27.7-16 ka BP	☆	☆	27.8	27.7
stage 4 no aplanktonic zone	67.5	58.8	★	★
stage 6 aplanktonic between 150.5-139 ka BP	>157.5?	>157.5?	151.5	150.5

☆ No return of species following stage 4.

★ No disappearance of the species.

? Disappearance dates for *G.sacculifer* and *G.siphonifera* in core 1039 preceding stage 6 are uncertain as the record stops at 157.5 ky BP.

Since the Red Sea salinity crises are, in turn, attributed to global sea level lowering, it is noted that sea level was around 70 m below present day sea level at the time of the disappearance of *G.sacculifer* in stage 4, and around 90 m below present sea level at the disappearance in stage 6 (figure 7.3) (Shackleton, 1987; Fairbanks, 1989; Bard et al., 1996). As such, communication was not as severely restricted at Bab el Mandab. Estimated sill depths around 70 m and 50 m and strait widths of around 15 and 13 km, respectively, would

Figure 7.3

Global sea level variation over the last 200 ky

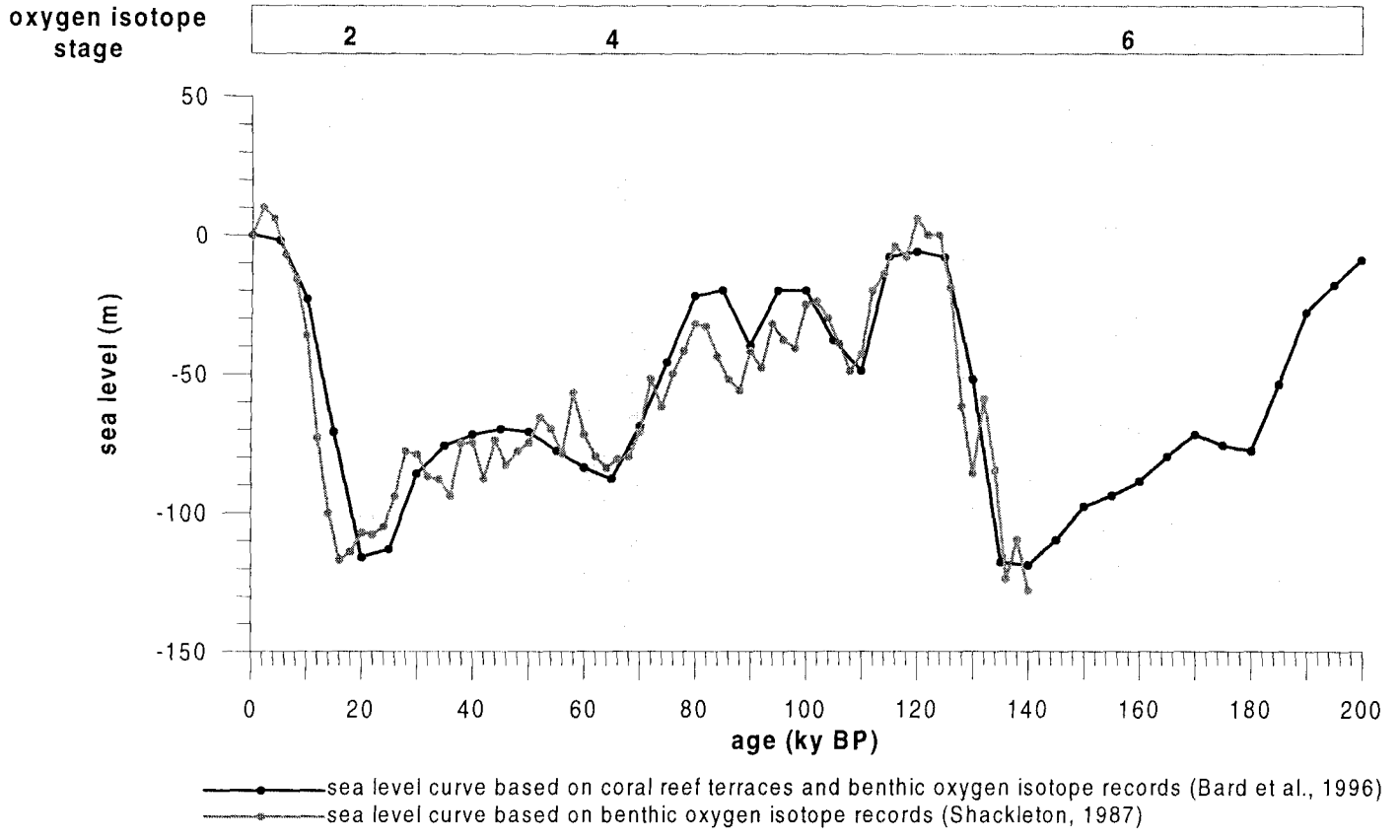

result in relatively good open ocean - basin communication, in comparison to the great restriction caused by the 120 m sea level lowering of the LGM (Fairbanks, 1989). This should present elevated, yet tolerable salinities in the Red Sea at the time of species disappearance in stages 4 and 6.

The above information implies that salinity variation cannot account for the successive disappearance of the planktonic foraminiferal species observed. An alternative explanation to salinity increase must be found for the succession. Here, it is proposed that the successive disappearance of the planktonic foraminiferal species involves their dietary requirements, as discussed in chapter 3, and a link to variation in monsoon intensity.

Today, a pattern of abundance of planktonic foraminifera and prey occurs in the Red Sea (Hemleben et al., 1989). Carnivorous, spinose planktonic foraminiferal species dominate north of latitude 20°N while herbivorous, non-spinose species abundance increases to the south. This boundary is associated with a distinct break in phytoplankton productivity at the surface current convergence zone (chapter 2, 2.3), with zooplankton organisms being more prominent in the north (Hemleben and Spindler, 1983a; Hemleben et al., 1989). The current convergence zone seasonally migrates northward and southward depending on the intensity of the surface wind stress, which in turn depends on the position of the NE and SW monsoon (chapter 2, 2.2.2).

The NE monsoon is dominant in glacial periods owing to prolonged snow cover in Central Asia and the minimum variation in summer insolation at this time (Van Campo et al., 1982; Prell and Van Campo, 1986; Prell et al., 1992; Anderson, 1993). Thus, it follows that there would be prolonged / more intense inflow of Gulf of Aden water into the Red Sea basin, driven by the prolonged southeasterly wind, provided that there was sufficient communication between the basin and the open ocean via the strait of Bab el Mandab. This persistent inflow would allow penetration of Gulf of Aden water northward, pushing the zone of convergence and, consequently, invasion of new plankton species into the Red Sea surface waters, increasing species diversity further north in the basin. As a result the proportion of food for the specialised zooplankton feeders would be reduced and the species would be

phased out in turn, from the most specialised zooplankton feeders (*G.sacculifer*) through those more tolerant of a mixed zooplankton diet (*G.siphonifera*) to those who can efficiently utilize primary producers and thus establish a significant advantage in competing for energy resources in regions of limited productivity (*G.ruber*, *G.glutinata* and other non-spinose species) (figure 7.4).

However, in conjunction with the increasing intensity of the NE monsoon there is gradual lowering of global sea level, causing reduced basin - open ocean communication. This results in a gradual reduction of inflow of Gulf of Aden surface water with time, and increasing salinisation of the basin. Hence at the onset of the aplanktonic zones the emphasis on planktonic foraminiferal species presence has switched from dietary requirements to extreme salinity tolerance, explaining the persistence of the salinity tolerant *G.ruber* up to, and in some cases through, the aplanktonic zones that span the glacial maxima. These extreme conditions, with salinities around 50 ‰, also prevented successful invasion by non-spinose herbivorous foraminifera.

A flaw in this argument is apparent due to the insolation modulator of the precession (1/23 ky cycle) effect on monsoonal intensity which does not reflect in the successional disappearance of the species (for example, *G.sacculifer* and *G.siphonifera* disappear around 5-15 ky preceding glacial stage 4 and do not return until the onset of stage 1). However, the dominance of the NE monsoon over the SW monsoon during stage 3 and leading up to glacial stages (Almogi-Labin et al., 1998) is likely due to the build up of snow and ice cover on the Himalayas and Tibetan Plateau approaching glacial periods, and its continued presence throughout stage 3, reducing sensible heat radiation and creating a high albedo (Barnett, et al., 1988). The combined effect results in a quasistable high pressure system (chapter 2, 2.2.2) and continued dominance of the NE monsoon over the region. In turn, this allows the continued dominance of southerly winds over the southern Red Sea retaining the northerly position of the surface water current convergence zone.

The above hypothesis would imply that the northward penetration of non-spinose Gulf of Aden planktonic foraminiferal species (eg. *G.menardii*, *N.dutertrei*) in the Red Sea may be an

Figure 7.4 Summarised events involved in the successional disappearance of planktonic foraminiferal species in the Red Sea

Winter NE Monsoon

a.

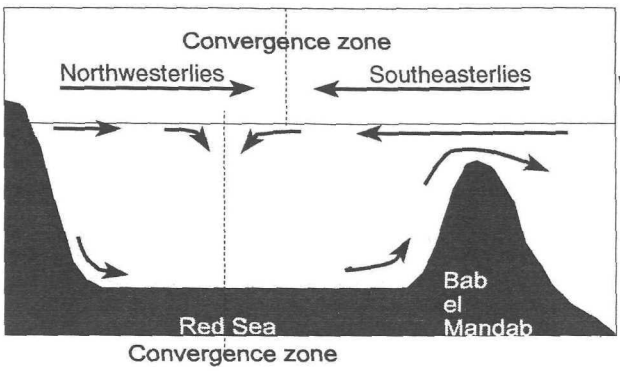

Wind driven circulation

During the NE monsoon the convergence zone reaches its most northerly extent over the basin, allowing Gulf of Aden water to penetrate further into the surface waters of the basin.

b.

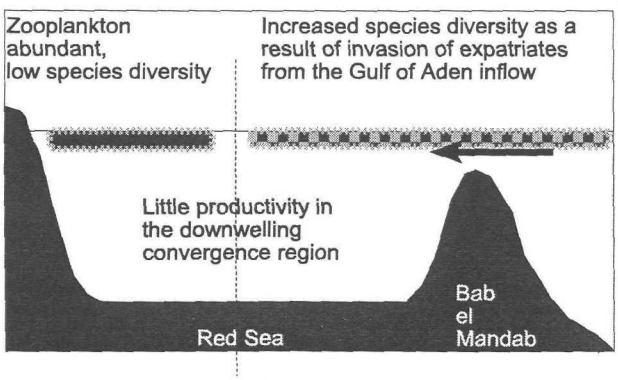

Zooplankton and phytoplankton diversity and distribution

Inflowing Gulf of Aden water introduces more plankton species into the Red Sea surface waters, increasing species diversity. This inhibits more specialised feeders (*G.sacculifer* and *G.siphonifera*) as competition for food becomes more intense, allowing other species with more diverse dietry requirements (*G.ruber*) to move north.

Intensified - prolonged NE monsoon eg.Pre-aplanktonic Red Sea.

c.

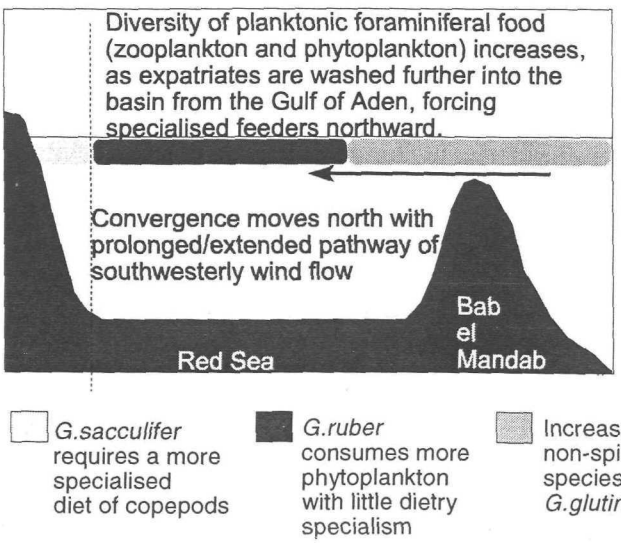

Prolonged inflow of Gulf of Aden water driven by the more intense southerly winds associated with the increased intensity of the glacial NE monsoon would allow the Gulf of Aden water to penetrate further north, forcing the specialised feeders further north again.
During the lead up to the aplanktonic zones this phenomenon is seen, with specialised, carnivorous species being reduced drastically in numbers and those with less carnivorous tendencies flourish.

indication of increased intensity of the NE monsoon. This agrees with the findings of Ganssen and Kroon (1991) who discovered the presence of Gulf of Aden dwelling species *G.menardii* as far north as the Gulf of Suez and *N.dutertrei* up to 18 °N in the Red Sea during the summer of 1985 when the NE monsoon was more intense. During 1984, when "normal" monsoonal conditions prevailed, Ganssen and Kroon (1991) observed that these species were absent from the basin.

To summarise, the monsoon intensity controls the position of the wind convergence zone, which controls the surface current convergence zone in the Red Sea, and this, in turn, controls the distribution of phytoplankton and zooplankton in the basin (chapter 3, figure 3.4). To the north of the current convergence zooplankton is abundant with low species diversity and to the south a higher zooplankton species diversity is apparent. It is the distribution of planktonic foraminiferal food (zooplankton and phytoplankton) which ultimately controls the distribution of planktonic foraminiferal species within the basin. The increasing prevalence of the NE monsoon, in association with glacial periods, ultimately changed the distribution of planktonic foraminiferal food in the Red Sea. The current convergence was pushed northward allowing penetration of imported Gulf of Aden species further north in the basin, and consequently forced the specialised zooplankton-feeders (*G.sacculifer* and *G.siphonifera*) further north. In the sediments this is recorded as a successive disappearance of planktonic foraminiferal species, with the initial absence of the most specialised feeders (*G.sacculifer* followed by *G.siphonifera*) through to planktonic foraminiferal species able to sustain themselves on phytoplankton alone (*G.ruber* and *G.glutinata*). To confirm this theory a detailed investigation of planktonic foraminiferal records of a north-south transect of cores from the Red Sea would be required. Such an investigation should reveal the lack of successive species disappearance in the north, thus establishing the most northerly position of the current convergence zone.

7.3 Evidence for dysoxic-anoxic intervals in the Red Sea.

7.3.1 The sapropelic horizon

The total organic carbon records for cores 1039, and to a lesser extent 1017 (figure 7.5a and b), show a sapropelic horizon deposited around 11 ka BP_{cal}. A similar horizon has been discovered in other cores from throughout the Red Sea, dated around 8 ka BP using AMS ^{14}C (Ivanova, 1984; Locke, 1984). Conversion of this AMS ^{14}C date to calendar years (ka BP_{cal}) using the Calib 3.03 program (written by Stuiver and Reimer, 1993) gives a date of 8.4 ka BP_{cal} for the sapropelic horizon. Clearly there is a discrepancy between the AMS ^{14}C date of Ivanova (1984) and Locke (1984) and those estimates of cores 1039 and 1017 (10.42 and 11.58 ky BP respectively) based on a combination of oxygen isotope data combined with AMS ^{14}C (chapter 6, 6.1). However, it is clear that this horizon is coincident with the rise in global sea level associated with deglaciation (Bard et al., 1987; Fairbanks, 1989; Bard et al., 1996).

Micropalaeontological analysis of the sapropel has shown that benthic foraminifera are almost absent, with absolute numbers falling to <5 benthic foraminifera /g of sediment. The benthic foraminifera found here are infaunal, with the exception of *Eponides punctulatus* which is covered with many pores (plate 17) suggesting a need for good gaseous exchange. The fauna implies a low oxygen environment, which is corroborated by the elevated organic carbon preservation within the sapropelic sediments. Possible causes for low oxygen concentrations in the bottom waters are I) increased surface water productivity, and/or ii) stagnation of the water column.

<u>i) Possible increase in productivity.</u>

An increase in productivity in the surface waters would lead to an increase in export of degradable organic material to the deeper waters, supplying food to the benthic community and increasing deep water oxygen consumption. Evidence for a productivity increase associated with the Red Sea sapropel has not been found in this study. Thunell et al., (1988) suggested the possibility of a productivity increase following the LGM due to rapid lowering of surface salinities aiding the reestablishment of planktonic communities. However, planktonic foraminifera remain absent throughout the sapropelic horizon and no peak in

Figure 7.5

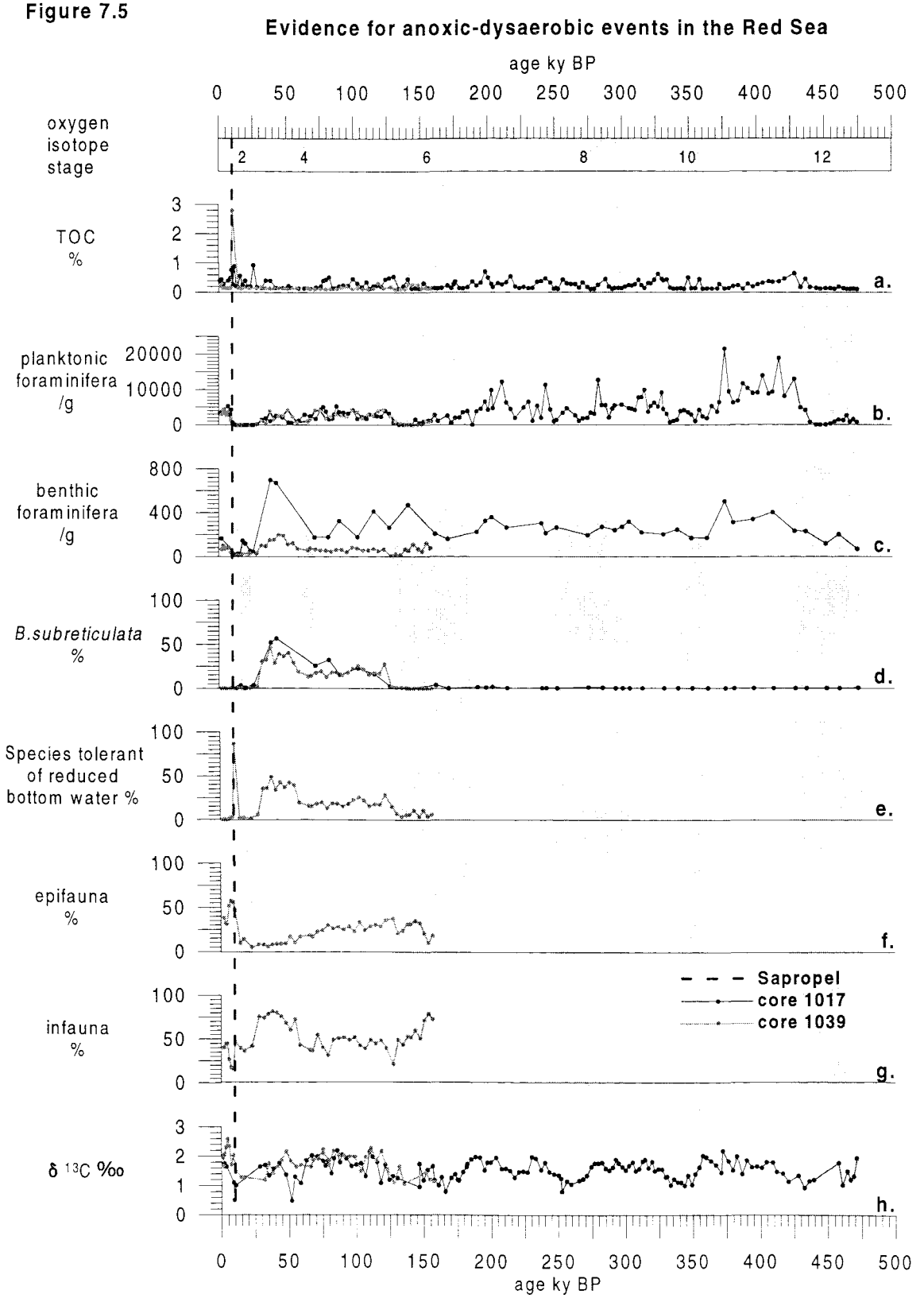
Evidence for anoxic-dysaerobic events in the Red Sea
age ky BP
0 50 100 150 200 250 300 350 400 450 500
oxygen isotope stage
2 4 6 8 10 12
TOC %
3 2 1 0
a.
planktonic foraminifera /g
20000 10000 0
b.
benthic foraminifera /g
800 400 0
c.
B.subreticulata %
100 50 0
d.
Species tolerant of reduced bottom water %
100 50 0
e.
epifauna %
100 50 0
f.
Sapropel
core 1017
core 1039
infauna %
100 50 0
g.
δ 13C ‰
3 2 1 0
h.
0 50 100 150 200 250 300 350 400 450 500
age ky BP

benthic foraminifera is seen either preceding or through the sapropelic sediments (figure 7.5b and c), suggesting that increased productivity was not the cause of the observed enhanced sedimentary TOC levels.

ii) Stagnation of the water column.

Evidence from pteropod studies has shown that only epipelagic species, in particular *Creseis chierchiae*, survived in the Red Sea at the time of sapropel deposition, suggesting that the mixed layer was <50 m deep, with probable oxygen poor waters below (Almogi-Labin et al., 1991; 1998).

It is here suggested that the rapid rise in global sea level, associated with deglaciation, (Bard et al., 1987; Fairbanks 1989, Bard et al., 1996), resulted in a sudden increase in the volume of Gulf of Aden inflow into the Red Sea, washing the broad shallow shelves (<100 m deep) in the south as sea level rose. The coincident increase in intensity of the southwest monsoon (reaching maximum intensity around 8 ka BP (Rossignol-Strick, 1984; Petit-Maire et al., 1994)) caused increased rainfall over the Arabian Peninsula (higher by 100-400 mm than at present), increased humidity over the region, and allowed northwesterly winds to prevail over the Red Sea basin (Prell and Streeter, 1981; van Campo et al., 1982; Fontugne and Duplessy, 1985; Prell an van Campo, 1986; Prell et al., 1992; Petit-Maire et al., 1994). Although input from permanent rivers into the Red Sea is negligible, it has been suggested that land run-off entered the basin via wadi systems on the Arabian Peninsula (Rossignol-Strick, 1984).

The combination of increased relatively fresh inflow from the Gulf of Aden and input of the fresher, nutrient rich water from increased precipitation and land run-off into the basin, at the time of sapropel deposition, caused a great reduction in surface water salinity, and hence density. The lower density of the surface water and dominance of the northwesterly winds would have greatly impeded mixing off the Sinai Peninsula in the north. As a result the production of bottom water would have been reduced, or even ceased. Note that deep water production today is greatly reduced during the summer owing to the prevailing northeasterly winds (Maillard and Soliman, 1986; Cember, 1988; chapter 2). Reduction/cessation of new deep water formation around 11 ka BP would have caused stagnation and depletion of

dissolved oxygen in the deeper water masses. The low oxygen content of the deep waters combined with the continued supply of organic matter from the surface waters may have led to the improved organic matter preservation and formation of sediments with enhanced organic carbon contents (*cf.* Locke, 1984).

To summarise, a stratified, stagnant water column is suggested as the cause for the sapropelic horizon. Circulation at this time is proposed to be mainly in the top 50 m of the water column, with a surface water inflow and a shallow subsurface outflow, above sill depth (figure 7.6).

7.3.2 Dysaerobic environment in the Red Sea basin during isotope stage 3

Globally, benthic foraminifera have been used extensively to reconstruct changes in the marine environment. Concerning the Red Sea basin, detailed studies of benthic foraminiferal ecology have been conducted in the Gulf of Aqaba, and some shallow areas in the northern Red Sea (Said, 1949, 1950a, b; Reiss et al., 1977; Bahafzallah, 1979; Reiss and Hottinger, 1984; Hottinger et al., 1993; Hounold et al., 1997). However, Red Sea deep water benthic foraminifera have not previously been studied in detail. Locke (1984) discussed variations on genus-level since the last glacial maximum, and Gupta (1994) presented a taxonomic study of deep sea benthic foraminifera in the Red Sea, concerning only the Holocene. The, here presented, 160 ky history of deep sea benthic foraminiferal variations in Red Sea core 1039, in combination with the pilot study carried out on core 1017, provides much needed information about the history of change in the bottom water environment through the last glacial cycle.

Gupta (1994) studied present day material from the Red Sea, discovering a rich benthic foraminiferal assemblage primarily composed of calcareous forms. His Red Sea deep water assemblage is confined between 800 and 1800 m and is marked by the dominance of *Bolivina subreticulata* (plates 22 and 23), a species associated with highly saline, low oxygen water. *B.subreticulata* was also found in the benthic faunas of cores 1039 and 1017. It dominates the sediments in stages 5 to 3 only, peaking to approximately 50-60 % of the total fauna in stage 3 (figure 7.5d). A small occurrence is also noted in mid-stage 6. The species is not

Figure 7.6

Schematic circulation in the Red Sea at the time of sapropel formation.

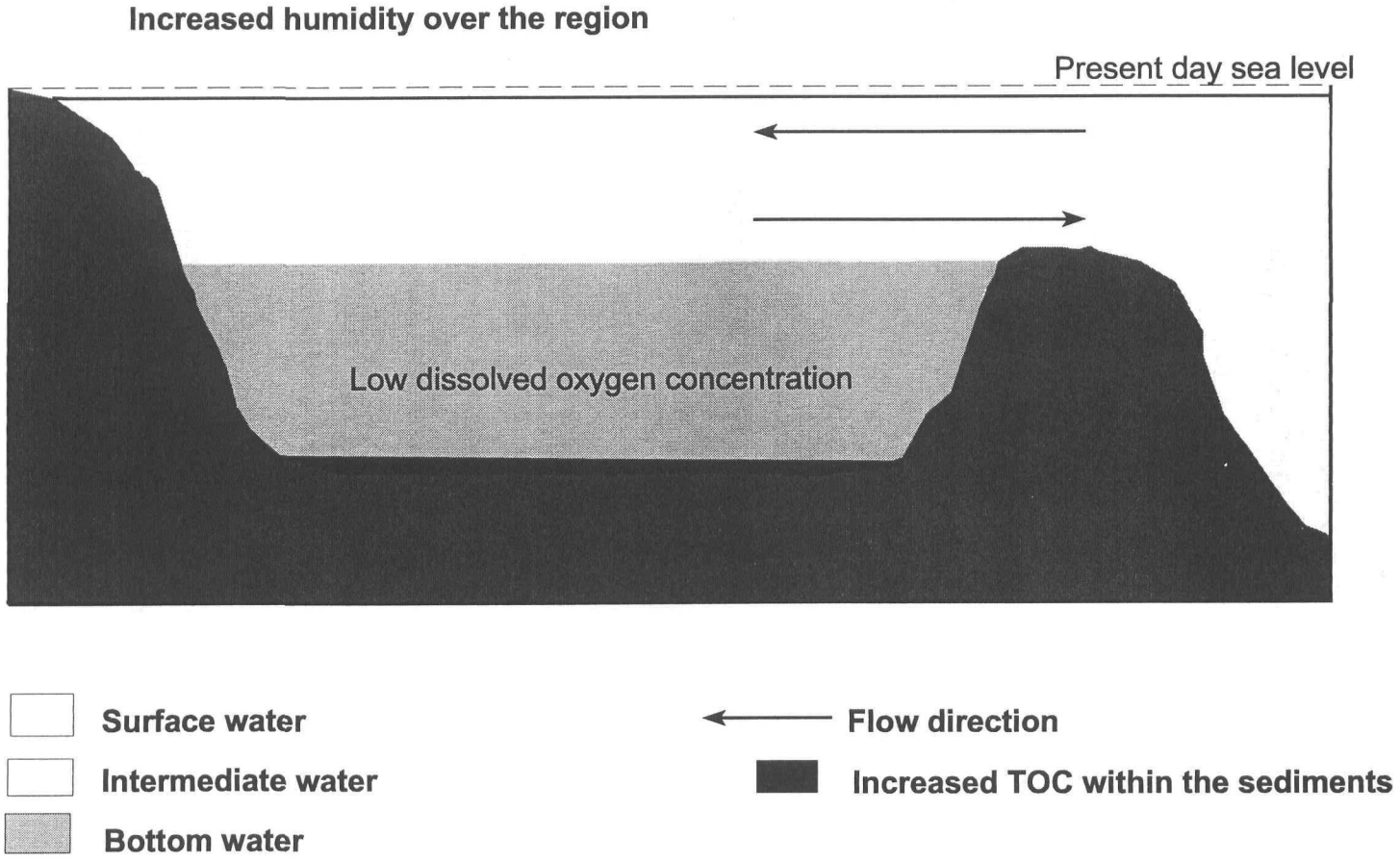

noted at any other time in the sediments. During stage 3, and stage 6, *B.subreticulata* is accompanied by other benthic foraminifera assumed to be tolerant of low oxygen environments owing to their presence, albeit in low absolute abundances, through the sapropelic horizon (chapter 6, figures 6.20 and 6.21). Benthic foraminiferal abundance is highest during stage 3.3 (figure 7.5c) and is clearly associated with the high dominance of species tolerant of low oxygen environments (figure 7.5e), particularly *B.subreticulata*. Stage 3 also contains a fall in the relative abundance of the epifauna and a corresponding increase in the infauna (figure 7.5f and g). This is concurrent with the stage 3 "epifaunal free" interval noted in nearby core KL11 (Hemleben et al., 1996). The lack of epifauna suggests that there was a change in the deep waters of the Red Sea affecting their habitat during stage 3. Almogi-Labin et al. (1996) observed a general decline in agglutinated foraminiferal numbers since 60 ka BP, around the onset of stage 3, suggesting a great alteration in the circulation in the Red Sea at this time. A full recovery of this group was only observed in surface sediments.

Isotopic stage 3 (59-24 ky BP) is known to be a period of low oxygen bottom water in the Red Sea (Almogi Labin et al., 1998). Evidence from pteropods (epipelagic and mesopelagic) has indicated the structure of the surface water column. Epipelagic *Limacina trochoformis* dominated the pteropod assemblage during isotope stage 3 and also during stage 10. Its presence indicates strong surface stratification and lower dissolved oxygen content in the deeper waters below. High abundances were also recorded in parts of isotope stages 5, 6 and 7 (Almogi- Labin et al., 1991; Almogi-Labin et al., 1998). These enhanced abundances of epipelagic pteropods in Red Sea surface waters have been attributed to an enhanced SW monsoon-derived humid climate (Almogi-Labin et al., 1998).

Low oxygen subsurface conditions may result either from high surface water productivity, or from a change in the circulation regime of the basin. Evidence from TOC and $\delta^{13}C$ (measured in planktonic foraminiferal tests), and absolute numbers of planktonic foraminifera records afford no significant evidence of the former associated with stage 3 (figures 7.5a, b and h). Hence, a change in the circulation around this time is proposed. Maximum sea level at the onset of stage 3 was around 70 m below that of present day (Shackleton, 1987; Bard et

al., 1996 (see figure 7.3), exposing the Gulf of Suez, the key source region for Red Sea deep water formation today (Maillard and Soliman, 1986; Cember, 1988; Tragou and Garrett, 1997; chapter 2). The loss of contribution to the bottom water from this well aerated basin would result in sluggish formation of bottom water, relying on surface mixing alone. In turn, however, surface mixing and consequent deep water formation would have been impeded by the more intense SW monsoon regime (Almogi-Labin et al., 1998) with elevated humidity over the region and dominant northeasterly winds over the basin (Maillard and Soliman,1986; Cember, 1988; Tragou and Garrett, 1997). The result would be low oxygen bottom water conditions. The first appearance of *B.subreticulata* along with other low oxygen indicating fauna was around 160 ka, mid-stage 6. It is also attributed to the loss of the Gulf Suez input into the basin when sea level was approximately 90 m below that of present day (Bard et al., 1996, figure 7.3) in combination with a SW monsoon humid climate (Almogi-Labin et al., 1998). No analogue faunal response for stages 8, 10 and 12 was noted in the pilot study of core 1017, indicating the possibility that such low oxygen conditions were not achieved previous to stage 6. A detailed study of the benthic foraminiferal fauna of core 1017 is necessary to form any further conclusions regarding bottom water variations during stages 12 to 6.

The dominant SW monsoon climate with prevailing northeasterly winds and resultant retarded mixing off the Sinai Peninsula (Maillard and Soliman, 1986; Cember, 1988), combined with the loss of well aerated Gulf of Suez source water to the deep Red Sea is therefore suggested as the reason for reduced ventilation of the deep Red Sea during stage 3, and possibly mid-stage 6.

7.4 Rohling, E.J., Fenton, M., Jorissen, F.J., Bertrand, P., Ganssen, G. and Caulet, J.P. July, 1998. Magnitudes of sea-level lowstands of the past 500,000 years. Reprint from *Nature* (Vol. 394, pp162-165).

Magnitudes of sea-level lowstands of the past 500,000 years

E. J. Rohling*, M. Fenton*, F. J. Jorissen†, P. Bertrand†, G. Ganssen‡ & J. P. Caulet§

* *Department of Oceanography, Southampton University, Southampton Oceanography Centre, Southampton SO14 3ZH, UK*
† *Département de Géologie et Océanographie, Université de Bordeaux I, CNRS URA 197, Avenue des Facultés, 33405 Talence Cedex, France*
‡ *Department of Earth Sciences, Free University Amsterdam, De Boelelaan 1085, 1081 HV Amsterdam, The Netherlands*
§ *Laboratoire de Géologie, National Museum for Natural History, CNRS URA 723, 43 Rue Buffon, 75005 Paris, France*

Existing techniques for estimating natural fluctuations of sea level and global ice-volume from the recent geological past exploit fossil coral-reef terraces or oxygen-isotope records from benthic foraminifera. Fossil reefs reveal the magnitude of sea-level peaks (highstands) of the past million years, but fail to produce significant values for minima (lowstands) before the Last Glacial Maximum (LGM) about 20,000 years ago, a time at which sea level was about 120 m lower than it is today[1–4]. The isotope method provides a continuous sea-level record for the past 140,000 years (ref. 5) (calibrated with fossil-reef data[6]), but the realistic uncertainty in the sea-level estimates is around ±20 m. Here we present improved lowstand estimates—extending the record back to 500,000 years before present—using an independent method based on combining evidence of extreme high-salinity conditions in the glacial Red Sea with a simple hydraulic control model of water flow through the Strait of Bab-el-Mandab, which links the Red Sea to the open ocean. We find that the world can glaciate more intensely than during the LGM by up to an additional 20-m lowering of global sea-level. Such a 20-m difference is equivalent to a change in global ice-volume of the order of today's Greenland and West Antarctic ice-sheets.

Our technique relies on evidence of adverse living conditions for planktonic foraminifera in the glacial Red Sea due to extremely high salinities, giving rise to so-called 'aplanktonic' zones. These contain only few specimens (mostly *Globigerinoides ruber*) and are found not only in our core MD921017 (Fig. 1), but throughout the Red Sea[7–11]. Planktonic pteropods[10] and benthic foraminiferal faunas were less affected, although the latter show increased abundances of high-salinity-resistant miliolid taxa (Fig. 1e; also refs 8, 9). Inorganic aragonite coatings, cements and concretions indicative of high salinities are found within the 'aplanktonic' zones of stages 2, 6 and 12 (Fig. 1b), in agreement with previous reports[12,13]. Multidisciplinary studies of the youngest aplanktonic zone (LGM) indicate that Red Sea salinities rose to 50 ± 2 practical salinity units (p.s.u.), that is, 10 ± 2 p.s.u. higher than in the adjacent ocean[9,10,14]. The highest estimate[11] is 55 p.s.u. Similar faunal reductions and compositional changes, as well as distinct aragonite

occurrences, characterize the stage 6 and 12 glacial maxima, reflecting comparable high-salinity conditions (Fig. 1). Continuation of a more diverse, although severely reduced, fauna through stages 10 and 8 suggests less harsh conditions, with those during stage 8 being least restricted.

Arguments for hydraulic control of flow through the Strait of Bab-el-Mandab (SBM) and conservation of mass and salt[14,15] demonstrate that the glacial freshwater deficit was similar to the present ($2\,m\,yr^{-1}$), and that the high salinities resulted from restricted marine exchange through the SBM, which today is only 137 m deep[16]. Continuation of benthic faunas, albeit in reduced numbers and different compositions, indicates that all glacial sea-level drops of the past 500 kyr left sufficient communication between the Red Sea and the open ocean to prevent worse salinization and consequent sterilization (Fig. 1c, e). The calculations[14,15] may be rearranged to find the 'critical' glacial sill depth (H_{crit}) at which salinities would rise to reconstructed LGM values, and so trigger an aplanktonic interval. We use the more common range of estimates for LGM salinities[9,10,14], with a salinity difference (ΔS) across the SBM of 10 ± 2 p.s.u., and in sensitivity tests with $\Delta S = 15$ p.s.u. and $\Delta S = 10 \pm 5$ p.s.u. we evaluate the potential effects of the highest-salinity extreme[11].

A glacial water deficit of $2.0 \pm 0.5\,m\,yr^{-1}$ is used, allowing for uncertainties in sea–air temperature contrasts and freshwater input of a factor of two, and $\pm 2\,m\,s^{-1}$ uncertainty in mean wind speed variations[14]. As glacial exposure of shelves would reduce the Red Sea surface area by 50%, volumes of net glacial evaporation (= area × deficit) amounted to 0.50 ± 0.13 times present-day values. Hydraulic control defines $Q = W0.375H_{crit}(0.375H_{crit}7.4 \times 10^{-3}\Delta S)^{0.5}$ for the maximum exchange solution, while $Q = (3.29\gamma Q_p)/\Delta S$ follows from conservation of mass and salt[14,15]. Here Q is volume of Red Sea outflow, W is the glacial width of the shallow passage of the SBM, and γ is the ratio of glacial to present-day net evaporation; subscript p indicates present-day value.

Consequently, $H_{crit} = 18 \pm 5$ m, for $\Delta S = 10 \pm 2$ p.s.u., $W = 11 \pm 1$ km, $\gamma = 0.50 \pm 0.13$ and $Q_p = 0.32 \pm 0.03$ Sv ($1\,Sv = 10^6\,m^3\,s^{-1}$)[14–17]. Potentially increased mixing of inflow and outflow for reduced sill depths favours values of H_{crit} towards the higher end of its confidence interval over those towards the lower end. We combine the present-day sill depth of 137 m with H_{crit} to estimate past sea-level lowstands, but we first evaluate whether—and to what extent—correction is needed for uplift in the SBM region.

Total planktonic foraminiferal abundances show a distinct decrease over the interglacial periods of the past 500 kyr in core MD921017 (Figs 1b, 2a). A similar trend is seen for the past 380 kyr contained in nearby core KL11[11]. Sedimentation rates throughout MD921017 are very uniform (see Supplementary Information), so that the foraminiferal numbers per gram—based on constant sample thickness—closely approximate true fluxes per unit time.

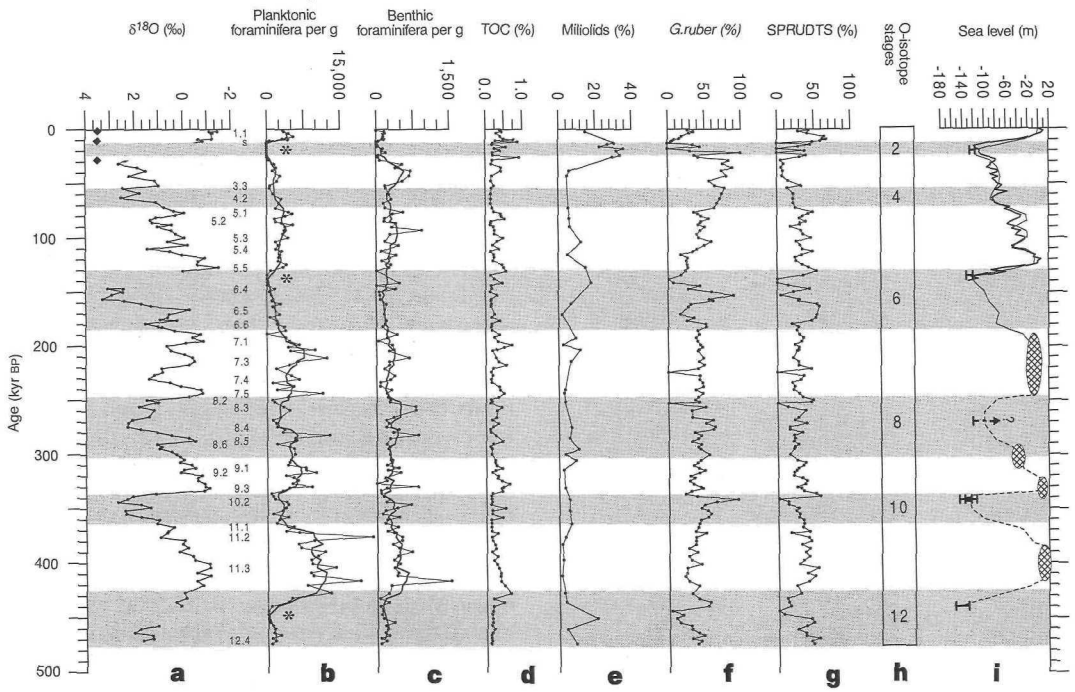

Figure 1 Results for core MD921017, Red Sea (19° 23′ 24″ N, 38° 40′ 84″ E, water depth 570 m). All variables plotted against time in calendar years (kyr BP) according to correlation with SPECMAP[22]. **a**, Oxygen-isotope record (versus PDB standard) for *Globigerinoides ruber* in the 250–350 μm size fraction (filled circles). Numbers refer to SPECMAP events[22]; filled diamonds indicate samples used for AMS radiocarbon dating (1,666 ± 26, 9,681 ± 41 and 25,300 ± 200 radiocarbon years BP, respectively). **b**, Planktonic foraminifera per gram dry weight (thin line). Asterisks highlight true aplanktonic zones of oxygen isotope stages 2, 6 and 12 which contain aragonitic coatings, cement and nodules. Heavy line is five-point moving-average highlighting the general trends. **c**, Benthic foraminifera per gram dry weight (thin line), with five-point moving average (heavy line). We note factor 10 difference between scales in **b** and **c**. **d**, Down-core variation in TOC (%) (LECO 125-CS elemental analyser). Preparation involved removal of carbonate by acidification using dilute hydrochloric acid. **e**, Abundance of miliolids relative to total benthic foraminiferal fauna. Although of lower resolution than the other records, the miliolid percentages do show a general increase in abundance through the record, as well as peaks associated with the aplanktonic zones. **f**, Abundance of *Globigerinoides ruber* relative to total planktonic foraminiferal fauna. **g**, Abundance of SPRUDTS group relative to total planktonic foraminifera. This group represents a cluster of the individually infrequent subtropical species *Globigerinoides sacculifer*, *Hastigerina pelagica*, *Globoturborotalia rubescens*, *Orbulina universa*, *Globigerina digitata*, *Globoturborotalia tenella* and *Globigerinella siphonifera*[18]. **h**, Oxygen isotope stages[22]. **i**, Global sea level record. The heavy solid line through the past 140 kyr is based on benthic isotopes[5] and the thin solid line through the past 200 kyr is based on coral reef terraces and benthic isotopes[4]. Cross-hatched ovals show reported ranges of interglacial sea-level highstands[2–4,21]. Thick error bars in stages 2, 6, 8, 10 and 12 represent ranges of glacial sea-level lowstands according to the model presented here. The dashed line through stages 8–12 shows schematic sea-level fluctuations sketched through the control points following the main trends in the oxygen-isotope record.

Consequently, the decreasing trend in planktonic foraminiferal numbers reflects: (1) a steady decrease in interglacial productivity over the past 500 kyr; or (2) a progressive deterioration of living conditions for foraminifera through increasing isolation of the Red Sea from the open ocean.

Investigation of other parameters for interglacial periods, to detect long-term changes unrelated to glacial cycles, provides no support for the first option. First, the total organic carbon (TOC) record shows only minor, random fluctuations (Fig. 1d). Second, there are no long-term trends in the carbon isotope record. Third, the continuously low-diversity planktonic foraminiferal faunas are totally dominated by relative fluctuations (within a 100% sum) of only two taxonomic groups, *G. ruber* and the SPRUDTS group (see Fig. 1 legend for details), both of which are typical of warm and oligotrophic conditions[18] (Figs 1f, g, 2b). Last, there is only a weak, statistically insignificant, trend in total benthic foraminiferal abundances, whereas a significant decrease would be expected under conditions of decreasing primary/export productivity (= food supply) (Figs 1c, 2a).

The second option—increasing Red Sea 'restriction'— is supported by a steady increase in the abundances of high-salinity resistant[8,9] miliolid species in the benthic foraminiferal fauna over the interglacial periods of the past 500 kyr (Figs 1e, 2c). The increasing restriction would have occurred within a context of already limited exchange with the open ocean, as witnessed by: the lack of successful[19] 'invasions' into the Red Sea by oceanic species like *Globigerina bulloides*, *Globorotalia menardii* and *Neogloboquadrina dutertrei*; the limited and diminishing presence of *Turborotalita quinqueloba* (Fig. 2b) (these four species abound just outside the SBM in core MD921005; 11° 35′ 13″ N, 43° 31′ 84″ E); and the amplified glacial–interglacial contrasts throughout the Red Sea oxygen-isotope record relative to those of the open ocean (Fig. 1a), a typical characteristic of evaporative marginal basins related to their restriction from the world ocean. The inferred slow but progressive isolation of the Red Sea, superimposed on already restricted communication with the open ocean, is best explained by slow and fairly continuous uplift of a shallow sill.

The rate of uplift may be assessed using the present-day sill depth of 137 m (ref. 16) and previous estimates that sea level stood around 125 m below present sea level (b.p.s.l.) during stage 6 (135 kyr BP) (Fig. 1i)[4,5]. Addition of H_{crit} gives an estimated stage 6 sill depth of 143 m b.p.s.l., which implies 6 m uplift in 135 kyr (4.4 cm kyr^{-1}). This rate is a factor of 5–10 smaller than the assumed constant rates of classical reef-terrace-based sea-level studies[1–4]. To account for uncertainties in the derivation of the rate and/or its possible temporal nonlinearities, a 50% confidence interval is added, giving 0.044 ± 0.022 m kyr^{-1}. Our model then back-calculates the stage 6 sea level drop at $137 + (135 \times 0.044) - H_{crit} = 125$ m, with a confidence interval of ±6 m based on propagation[20] of uncertainties in H_{crit} (±5 m) and uplift rate (±0.022 m kyr^{-1}). Validation of the model through determination of the LGM

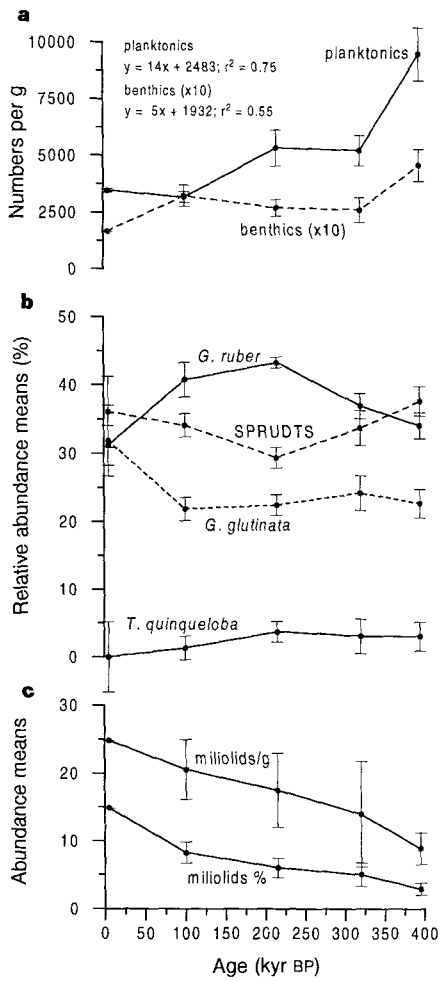

Figure 2 Trends through interglacial stages. **a**, Trends in the numbers of planktonic and benthic foraminifera per gram sediment dry weight, through interglacial stages 11, 9, 7, 5 and 1. Positions on age axis are simple stage mid-points. Stage 3 is excluded as this in fact is a warm interstadial within the last glacial period. Symbols indicate mean values, and error bars an interval of ±1 standard error of the mean. Benthic numbers have been multiplied times 10, to allow plotting on the same scale as planktonic numbers. Equations and r^2 coefficients concern linear fits through the two records. Linear fit for planktonics shows a significant trend ($\alpha = 0.05$), for benthics the trend is weak and statistically insignificant. We emphasise that, as stage 1 is continuing, its values may be less representative than those of the other (completed) interglacial periods. **b**, Mean relative abundances of *Globigerinoides ruber* and SPRUDTS-group (see also Fig. 1), and of *Globigerinita glutinata* and *Turborotalita quinqueloba*, in percentages relative to total planktonic foraminiferal fauna, through interglacial stages 11, 9, 7, 5 and 1. Symbols, error bars and note on stage 3 and 1 values as in **a**. **c**, Trends in high-salinity indicative miliolid benthic foraminifera–both relative to total benthic foraminiferal faunta (%), and as absolute abundances (numbers per gram dry weight)–through interglacial stages 11, 9, 7, 5 and 1. Symbols, error bars and note on stage 3 and 1 values as in **a**.

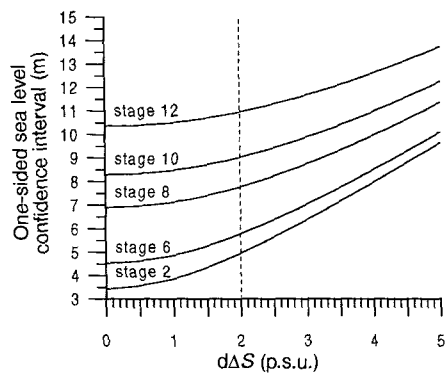

Figure 3 Sensitivity of confidence interval. Changes in the confidence intervals around the reconstructed mean sea level lowstands for glacial stages, 2, 6, 8, 10 and 12, for glacial Red Sea salinity contrast $\Delta S = 10$ p.s.u. ± a variable confidence interval $d\Delta S$. Effects are investigated per glacial stage for a range of $d\Delta S$ values from 0 to 5 p.s.u. Dashed line indicates $d\Delta S = 2$ as used in this Letter. The sea level confidence intervals (*y* axis) essentially change due to modification of the confidence interval around H_{crit}, which by close approximation corresponds to the line marked "stage 2".

(20 kyr BP) sea-level lowstand gives 120 ± 5 m, in agreement with fossil reef results[1] and supporting our mean value for H_{crit}.

To evaluate the dependence of our lowstand reconstructions on the main assumption that previous glacial ΔS values were similar to LGM values of 10 ± 2 p.s.u., we perform two tests based on the highest extreme glacial salinity estimate (55 p.s.u.; ref. 11). One increases ΔS to 15 p.s.u.; the other keeps ΔS at 10 p.s.u. but increases its confidence interval ($d\Delta S$) from ±2 to ±5 p.s.u. In the first test, H_{crit} is smaller, and reconstructed sea level drops are greater, by a maximum of 6 m. In the second test, with $d\Delta S$ increased by a factor of 2.5, the lowstand confidence intervals remain accurate within a factor of 2 (Fig. 3). These results justify the use of the SBM uplift rate with H_{crit} to study pre-stage-6 lowstands, noting that our method is more likely to underestimate rather than overestimate past sea-level drops, by a few metres.

Accounting for uplift since stage 8 (270 kyr BP), sill depth was around 150 m b.p.s.l. Stage 8 does not contain a completely 'aplanktonic' interval. Although the total planktonic foraminiferal numbers are strongly reduced, the main species composition shows little change that might reflect high-salinity stress (Fig. 1). We infer that sill depth remained considerably greater than H_{crit}. To allow continuation of all observed planktonic species, Red Sea salinity should have remained below a maximum of ~45 p.s.u., requiring a minimum sill depth of ~30 m (compare ref. 14). Hence, the maximum conceived stage 8 sea level drop is 150 − 30 = 120 m b.p.s.l.(±8 m).

A similar argument to that for stage 8 may be made for stage 10 (340 kyr BP). However, stage 10 shows a much closer approximation of a complete 'aplanktonic' zone, with disruption of the main species composition. We infer that sill depth was maintained between H_{crit} (18 m) and 30 m, defining a stage 10 lowstand between 134 and 122 m b.p.s.l. (±9 m).

Stage 12 (440 kyr BP) contains a true 'aplanktonic' zone (Fig. 1), suggesting a sill depth around H_{crit} and, consequently, a sea-level lowstand of 139 m b.p.s.l. (±11 m). This mean value implies that global ice-volume during stage 12 exceeded LGM values by some 15%. This independently derived result validates the only previous estimate of stage 12 ice-volume, based on benthic oxygen-isotope records[5].

Our lowstand values allow assessment of sea-level rises during the main deglaciations of the past 500 kyr (Fig. 1i), for comparison with that of 120 m following the LGM[1]. With the maximum stage 5 sea level ~6 m above the present[2,6], the stage 6–5 sea-level rise was around 131 ± 6 m. During interglacial stage 7, sea level remained below the present-day level[4,5], giving a maximum amplitude for the stage 8–7 sea-level rise of 120 m, although the actual rise was probably considerably smaller. The stage 9 highstand reached 0–15 m above the present-day level[4,5], giving a stage 10–9 sea-level rise between 122 and 149 m. The largest sea-level rise of the past 500 kyr followed the stage 12 lowstand of 139 ± 11 m b.p.s.l. and culminated in a maximum stage 11 highstand up to 20 m above present-day sea level[21].

We conclude that the last glacial–interglacial cycle showed ice-volume fluctuations that were more than 10% smaller than those that occurred in three out of four of the immediately preceding main cycles. The stage 12–11 sea level rise implies that over 30% greater ice-volume changes were involved in Quaternary glacial–interglacial cycles than would be expected on the basis of the last cycle alone. □

Received 27 October 1997; accepted 22 April 1998.

1. Fairbanks, R. G. A 17,000 year glacio-eustatic sea level record: Influence of glacial melting rates on the Younger-Dryas event and deep ocean circulation. *Nature* **342,** 637–642 (1989).
2. Radtke, U. & Grün, R. Revised reconstruction of middle and late Pleistocene sea-level changes based on new chronologic and morphologic investigations in Barbados, West Indies. *J. Coastal Res.* **6,** 699–708 (1990).
3. Pirazzoli, P. A. *et al.* A one million-year-long sequence of marine terraces on Sumba Island, Indonesia. *Mar. Geol.* **109,** 221–236 (1993).
4. Bard, E. *et al.* Pleistocene sea levels and tectonic uplift based on dating of corals from Sumba Island, Indonesia. *Geophys. Res. Lett.* **23,** 1473–1476 (1996).
5. Shackleton, N. J. Oxygen isotopes, ice volume and sea level. *Quat. Sci. Rev.* **6,** 183–190 (1987).
6. Chappell, J. & Shackleton, N. J. Oxygen isotopes and sea level. *Nature* **324,** 137–140 (1986).
7. Berggren, W. A. & Boersma, A. in *Hot Brines and Heavy Metal Deposits* (eds Degens, E. T. & Ross, D. A.) 282–298 (Springer, New York, 1969).
8. Halicz, E. & Reiss, Z. Palaeoecological relations of foraminifera in a desert enclosed sea—The Gulf of Aqaba. *Mar. Ecol.* **2,** 15–34 (1981).
9. Locke, S. & Thunell, R. C. Palaeoceanographic record of the last glacial-interglacial cycle in the Red Sea and Gulf of Aden. *Palaeogeogr. Palaeoclimatol. Palaeoecol.* **64,** 163–187 (1987).
10. Almogi-Labin, A., Hemleben, C., Meischner, D. & Erlenkeuser, H. Palaeoenvironmental events during the last 13,000 years in the central Red Sea as recorded by pteropoda. *Paleoceanography* **6,** 83–98 (1991).
11. Hemleben, C. *et al.* Three hundred and eighty thousand year long stable isotope and faunal records from the Red Sea: Influence of global sea level change on hydrography. *Paleoceanography* **11,** 147–156 (1996).
12. Milliman, J. D., Ross, D. A. & Ku, T. L. in *Hot Brines and Heavy Metal Deposits* (eds Degens, E. T. & Ross, D. A.) 724–736 (Springer, New York, 1969).
13. Ku, T. L., Thurber, D. L. & Mathieu, G. G. in *Hot Brines and Heavy Metal Deposits* (eds Degens, E. T. & Ross, D. A.) 348–359 (Springer, New York, 1969).
14. Rohling, E. J. Glacial conditions in the Red Sea. *Paleoceanography* **9,** 653–660 (1994).
15. Rohling, E. J. & Zachariasse, W. J. Red Sea outflow during the last glacial maximum. *Quat. Int.* **31,** 77–83 (1996).
16. Werner, F. & Lange, K. A bathymetric survey of the sill area between the Red Sea and Gulf of Aden. *Geol. Jahrb. D* **13,** 125–130 (1975).
17. Siedler, G. in *Hot Brines and Heavy Metal Deposits* (eds Degens, E. T. & Ross, D. A.) 131–137 (Springer, New York, 1969).
18. Rohling, E. J., Jorissen, F. J., Vergnaud-Grazzini, C. & Zachariasse, W. J. Northern Levantine and Adriatic Quaternary planktic foraminifera; Reconstruction of paleoenvironmental gradients. *Mar. Micropaleontol.* **21,** 191–218 (1993).
19. Ganssen, G. & Kroon, D. Evidence for Red Sea surface circulation from oxygen isotopes of modern surface waters and planktonic foraminiferal tests. *Paleoceanography* **6,** 73–82 (1991).
20. Squires, G. L. *Practical Physics* 3rd edn (Cambridge Univ. Press, 1988).
21. Howard, W. R. A warm future in the past. *Nature* **388,** 418–419 (1997).
22. Imbrie, J. *et al.* in *Milankovitch and Climate* (eds Berger, A. *et al.*) 269–305 (Reidel, Hingham, MA, 1984).

Supplementary Information is available on *Nature*'s World-Wide Web site (http://www.nature.com) or as paper copy from the London editorial office of *Nature*.

Acknowledgements. We thank H. Vonhof, M. Dignan and P. Martinez for assistance with stable-isotope and TOC analyses; J. W. Zachariasse for cooperation within the context of our joint studies of the NW Indian Ocean; NERC for support to M.F., and the National Museum of Natural History in Paris for support to E.J.R. during the planning and sampling phase of this work.

Correspondence and requests for materials should be addressed to E.J.R. (e-mail: E.Rohling@soc.soton.ac.uk).

Chapter 8.

CONCLUSIONS AND FURTHER WORK

This chapter aims to briefly highlight and link the important points raised in this study, and outlines further work which should be carried out in the Red Sea region in order to obtain a fuller understanding of the basin.

8.1 Conclusions

- The results presented for the two high quality cores, MD921017 and MD921039 from the Red Sea show a predominant glacial-interglacial influence in all aspects of the sediments studied (with the exception of TOC). The isolated nature of the Red Sea creates amplified signals in comparison to their equivalent in the open ocean. This is particularly noted in the $\delta^{18}O$ where values vary over 5-6 ‰ in comparison to typical open ocean variations of over 1-2 ‰. This amplification makes the basin ideal for investigation into global climate change.

- Red Sea sediments associated with severe glacial maxima are characterised by the absence of planktonic foraminifera, reduced numbers of benthic foraminifera with increased abundances of salinity tolerant miliolids, lithified sediment secured by an inorganic aragonitic cement and secondary aragonite overgrowth of pteropod tests. These changes are attributed to increased glacial salinities, around 50 ‰ or above. Such salinities are considered to have resulted from low glacial global sea levels causing restricted communication between the Red Sea and open ocean over the shallow sill at Bab el Mandab.

- The aplanktonic zones are preceded by a successive disappearance of species beginning with *Globigerinoides sacculifer*, through *Globigerinella siphonifera*, *Globoturborotalia rubescens*, *Globoturborotalia tenella* and finally *Globigerinoides ruber* and *Globigerinita glutinata*. During the NE monsoon, the current convergence zone reaches its most northerly extent over the basin, allowing more northward penetration of Gulf of Aden water into the basin, increasing the diversity of the zooplankton population in the

basin, and restricting dominance of the more specialised feeders to the northern most Red Sea. It is suggested that prolonged intensity of the NE monsoon associated with glacial maxima may be the cause of the successional disappearance of the planktonic foraminiferal species, with the initial disappearance of specialised carnivorous species through the less specialised feeders until salinity comes into play at the glacial maximum and finishes the omnivores and herbivores.

- Evidence for anoxia in the Red Sea is seen in the deposition of an olive green sediment horizon relatively rich in organic carbon (TOC=2.8 %) around 10 ka BP. The sediment is devoid of planktonic and most benthic foraminifera. Deposition of this sediment took place beneath a stratified water column, coinciding with the final phase of deglaciation and global sea level rise. The elevation of sea level resulted in increased inflow of relatively fresh water from the Gulf of Aden creating a strong density stratification, enhanced by maximum SW monsoon intensity increasing humidity in the region. Rainfall is estimated to have been higher by up to 400 mm over the Arabian Peninsula, and land run-off may have entered the basin via wadi systems. Stratification would have impeded mixing and sinking off the Sinai Peninsula causing stagnation of the bottom waters.

- Benthic foraminiferal records and pteropod data indicate the occurrence of oxygen-poor intervals in the Red Sea during isotope stage 3, and possibly during mid-stage 6. These periods are associated with dominance of SW monsoon humid climates, characteristic of slow deep water formation in the present day basin, and sea level <70 m below present day sea level. Such a low sea level would render the Gulf of Suez as dry land (maximum depth 73 m). Today the Gulf of Suez is regarded as an important source of well oxygenated deep water in the Red Sea (Cember, 1988; Tragou and Garrett, 1997). The loss of this well oxygenated deep water source during stage 3, and possibly stage 6, created poor ventilation in the basin, resulting in an oxygen-poor environment.

- The planktonic foraminiferal fauna shows a general decrease in numbers over the last 500 ky towards present day. This is attributed to deteriorating living conditions in the basin,

owing to increased isolation of the Red Sea due to uplift of the Hanish Sill at a rate of 4.4 cm ky^{-1}. Incorporating this with the sill depth required to create glacial salinities of 50 ‰ in the Red Sea basin (Hcrit=18 ±5 m as calculated combining hydraulic control of flow through the strait with conservation of mass and salt arguments), it is possible to estimate sea level low stands over the last 500 ky. Low stands are estimated at -120 ±5 m during stage 2, -125 ±6 m during stage 6, <-131 ±8 m during stage 8, between -134 and -122 ±9 m during stage 10 and -139 ±11 m during stage 12.

- The sediments in the Gulf of Aden core 1005 were unfortunately disturbed by a large redepositional event, likely to be slumped material. The extremely high sedimentation rate in the region (estimated at around 30 cm ky^{-1}) resulted in extremely short records for both cores, showing very little faunal variation. It is assumed that core 1006 did not even penetrate stage 2 sediments. Both cores proved to be of little consequence to this study, and as a result the emphasis has been placed on the palaeoceanography within the Red Sea basin.

8.2 Further work

8.2.1 Benthic foraminiferal investigation of core 1017.

A detailed investigation of the endemic benthic foraminiferal fauna and their stable isotope variations of core 1017, spanning the last 500,000 years would provide a graphic history of Red Sea bottom water fluctuations. In combination with the results presented in this thesis, the complementary study would provide insight into the impact of sea level and climate change on the basins unique benthic ecosystem. As demonstrated previously, during glacial maxima the Red Sea has experienced great environmental crises directly owing to sea level lowering causing restricted communication between the basin and the open ocean across the shallow Hanish Sill. The proposed study would investigate the relationship between the basin's endemic fauna and these crises; how the fauna reacted, which species survived and why? It is also necessary to assess why an endemic fauna exists in the basin - perhaps because of the isolation of the basin and/or the severity of the environmental crises inflicted at times of low sea level? Studying the mechanisms behind the adaption of the Red Sea fauna to the extreme environmental stress would provide wider implications for monitoring

faunistic responses to ocean water property change, and consequent effects on deep sea faunal diversity, owing to present day (anthropogenic) climate change.

8.2.2 Investigation into the nature of aplanktonic zones in the Red Sea.

It is clear that further investigation into the nature of aplanktonic zones is necessary, in particular the successional species disappearance observed leading up to the complete absence of planktonic foraminifera. As implied in this thesis (chapter 7, section 7.2), the species disappearance cannot be attributed to high salinity in the basin. Instead it is proposed that the disappearances reflect the movement of the surface current convergence zone set up by the convergence in the wind stress over the sea surface. The distribution of planktonic foraminiferal species in the Red Sea is ultimately related to the position of this front, with *G.sacculifer* dominating to the north and *G.ruber* to the south. It is suggested that the increase in NE monsoon intensity drove persistent southeasterly winds over the surface of the southern Red Sea, pushing the current convergence zone northward resulting in the apparent disappearance of the northerly dwelling species (*G.sacculifer*). To assess this further it is necessary to study well dated down-core planktonic foraminiferal variations, particularly around aplanktonic zones, from a north-south transect of locations in the basin. If the present hypothesis is correct one would expect to see no successional disappearance in the most northerly cores.

8.2.3 The Gulf of Aden.

For a detailed study of sediments from the Gulf of Aden, it is necessary to locate cores to the east of the Strait region and away from steep slopes. Sediments on the steep slopes in the west are prone to slumping, possibly triggered by tectonic movement in this young ocean (chapter 6 section 6.8-6.13). A study of both benthic and planktonic fauna should be carried out on the Gulf of Aden sediments as Red Sea outflow appears to be a deeper, mid-depth current (Maillard and Soliman, 1986). Results of this study should aim to provide details of surface water and deep water property changes which may then be related to climatic variation (monsoonal, glacial). Comparison of these results with those presented in Red Sea studies (eg. this thesis) would provide further insight in to the extent of influence of the Gulf of Aden inflow on Red Sea circulation, as well as the fate of Red Sea outflow and its effect

on the Gulf of Aden. At present Red Sea outflow is seasonal, with a much reduced outflow during the summer SW monsoon (Maillard and Soliman, 1986). Although it is unlikely that this seasonal effect would be recorded in the sediments of the Gulf of Aden, the change in monsoonal intensity may be accounted for in the form of benthic foraminiferal variations.

References.

Almogi-Labin, A. 1982. Stratigraphic and palaeoceanographic significance of Late Quaternary pteropods from deep sea cores in the Gulf of Aqaba (Elat) and northernmost Red Sea. *Marine Micropalaeontology. Vol.7, pp.53-72.*

Almogi-Labin, A., Luz, B. and Duplessy, J.C. 1986. Quaternary palaeo-oceanography, pteropod preservation and stable isotope record of the Red Sea. *Palaeogeography, Palaeoclimatology, Palaeoecology. Vol.57, pp.195-211.*

Almogi-Labin, A., Hemleben, C., Meischner, D. and Erlenkeuser, H. 1991. Palaeoenvironmental events during the last 13,000 years in the central Red Sea as recorded by pteropoda. *Palaeoceanography. Vol.6, pp.83-98.*

Almogi-Labin, A., Hemleben, C., Meischner, D. and Erlenkeuser, H. 1996. Response of Red Sea deep-water agglutinated foraminifera to water mass changes during the Late Quaternary. *Marine Micropaleontology. vol.28, pp.283-297.*

Almogi-Labin, A., Hemleben, C. and Meischner, D. 1998. Carbonate preservation and climatic changes in the central Red Sea during the last 380 kyr as recorded by pteropods. *Marine Micropaleontology. Vol.33. pp.87-107.*

Anderson, O.R. 1983. *Radiolaria. Springer, New York. pp352.*

Anderson, D.M. and Prell, W.L. 1992. The structure of the SW monsoon winds over the Arabian Sea during the late Quaternary: observations, simulations and marine geologic evidence. *Journal of Geophysical Research. Vol.97. No.C10. pp.15,481-15,487.*

Anderson, D.M. and Prell, W.L. 1993. A 300-kyr record of upwelling off Oman during the late Quaternary: Evidence of the Asian southwest monsoon. *Palaeoceanography . Vol.8, pp.193-208.*

Assaf, G. and Hecht, A. 1974. Sea straits: A dynamical model. *Deep Sea Research. Vol.21, pp.947-958.*

Auras-Schudnagies, A., Kroon, D., Ganssen, G., Hemleben, C., and van Hinte, J.E. 1988. Biogeographic evidence from planktonic foraminifers and pteropods for Red Sea anti-monsoonal surface currents. In: *Brummer, G-J.A., and Kroon, D. 1988. Planktonic foraminifers as tracers*

of ocean-climate history. pp203-227

Auras-Schudnagies, A., Kroon, D., Ganssen, G., Hemleben, C. and Van Hinte, J.E. 1989. Distributional pattern of planktonic foraminifers and pteropods in surface waters in surface waters and top core sediments of the Red Sea, Gulf of Aden and western Arabian Sea, controlled by the monsoonal regime and other ecological factors. *Deep Sea Research. Vol.36, pp.1515-1533.*

Bahafzallah, A.B.K. 1979. Recent benthic foraminifera from Jiddah Bay, Red Sea (Saudi Arabia). *Neues Jahrb. Geol. Paläontol. Montash. Vol.7. pp.385-398.*

Bally, A.W. 1979. Continental margins, geological and geophysical research needs and problems. *Bally, A.W., Chairman, and other panel members. Washington D.C. National Academy of Sciences.*

Bandy, O.L. 1960a. General correlation of foraminiferal structure with environment. *Rept. 21st Int. Geol. Congr., Norden. Vol. 22, pp.7-19.*

Bard, E., Arnold, M., Duprat, J., Moyes, J. and Duplessy, J-C. 1987. Reconstruction of the last deglaciation: deconvolved records of δ18O profiles, micropaleontological variations and accelerator mass spectrometric ^{14}C dating. *Climate Dynamics. Vol. 1, pp.101-112.*

Bard, E., Jouannic, C., Hamelin, B., Pirazzoli, P., Arnold, M., Faure, G., Sumosusastro, P and Syaefudin. 1996. Pleisocene sea levels and tectonic uplift based on dating of corals from Sumba Island, Indonesia. *Geophysical Research Letters. Vol.23. pp.1473-1476.*

Barnett, T.P., Dumenil, L. Schlese, U. and Roeckner, E. 1988. The effect of Eurasian snow cover on global climate. *Science. Vol. 239. pp. 504-507.*

Bé A.W.H. and Hamlin, W.H. 1967. Ecology of Recent planktonic foraminifera. Part 3 - Distribution in the North Atlantic during the summer of 1962. *Micropaleontology. Vol.13, no.1, pp.87-106.*

Bé, A.W.H. and Tolderlund, D.S. 1971. Distribution and ecology of living planktonic foraminifera in surface waters of the Atlantic and Indian Oceans. *In: Funnell, B.M. and Riedel, W.R. (eds.). The micropaleontology of the oceans. London: Cambridge Univ. Press. pp.105-149.*

Belkin, I.M., Emelianov, M.V., Kostianoy, A.G. and Fedorov, K.N. 1986. Thermohaline structure of intermediate waters of the ocean and intrathermocline eddies. *In: Intrathermocline*

eddies in the ocean. Fedorov, K.N. (ed.). Institute of Oceanology. Moscow. pp.8-34.

Berggren W.A. and Boersma, A. 1969. Late Pliestocene and Holocene planktonic foraminifera from the Red Sea. *Hot brines and heavy metal deposits in the Red Sea. E.T. Degens and D.A. Ross (eds.) Springer / Verlag Berlin / Hiedelberg / New York. pp.282-298.*

Berggren W.A. 1969. Micropalaeontologic investigations of Red Sea cores - summation and synthesis of results. *Hot Brines and recent heavy metal deposits in the Red Sea. Springer / Verlag Berlin / Heidelberg / New York. pp329-335.*

Beydoun, Z.R. 1982. The Gulf of Aden and Northwest Arabian Sea. *In: Nairn, A.E.M. and Stehli, F.G. (eds.) 1982. The Ocean Basins and Margins, Vol. 6. pp253-313.*

Boltovskoy, E. 1972. Nota sobre los valores minimos de origenación que pueden soportar los foraminiferos bentónics. *Boln. Soc. Biol. Concepción. Vol. 44, pp135-143.*

Boltovskoy, E., Scott, D.B. and Medioli, F.S. 1991. Morphological variations of benthic foraminiferal tests in response to changes in ecological parameters: a review. *Journal of Paleontology. Vol.65, No.2, pp. 175-185.*

Brasier, M.D. 1975c. Morphology and habitat of living benthonic foraminiferids from Carribean carbonate environment. *Revista Española de Micropaleontología. Vol.7, pp.567-569.*

Burgess, M.V. And Schnitker, D. 1990. Morphometry of *Bulimina aculeata* d'Orbigny and *Bulimina marginata* d'Orbigny. *Journal of Foraminiferal Research. Vol. 20, pp. 37-49.*

Caulet, J.P., Celment, P. and Giannesini, P.J. 1992. GEOCORES: Inventèire informatise des roches et sèdiments marins conservès au Museum National d'Histoire Naturelle. *Bulitin Museum National d'Histoire Naturelle, Paris. Vol.14, section C, No.1. pp93-136.*

Cember, P.R. 1988. On the sources, formation, and circulation of Red Sea Deep Water. *Jn. Geophysical Research. Vol.93, No. C7. pp8175-8191.*

Chappell, J. and Shackleton, N.J. 1986. Oxygen isotopes and sea level. *Nature. Vol.324. pp.137-140.*

Chen, C. 1969. Pteropods in the hot brine sediments of the Red Sea. *Hot Brines and recent heavy metal deposits in the Red Sea. Springer / Verlag Berlin / Heidelberg / New York. pp313-316*

CLIMAP. 1981. Seasonal reconstructions of the Earths surface at the last glacial maximum. Geol. Soc. Am. Map and Chart series.

Colom, G. 1970. Estudio de los foraminíferos de muestras de fondo de la costa de Barcelona. *Investigación Pesquera. Vol. 34, pp.355-384.*

Cooksa, V.I. 1972. Some peculiarities of the formation and distribution of intermediate layers in the Indian Ocean. *Okeanologia. Vol.12. pp.26-37.*

Craig, H. 1966. Isotopic composition and origin of the Red Sea and geothermal brines. *Science. Vol. 154, pp.1544-1584.*

Craig, H. 1969. Geochemistry and origin of the Red Sea brines. *Hot Brines and recent heavy metal deposits in the Red Sea. Springer / Verlag Berlin / Heidelberg / New York. pp.208-242.*

Craig, H. and Lupton, J.E. 1981. Helium-3 and mantle volatiles in the ocean and the oceanic crust. *The Sea, Vol. 7. The Oceanic Lithosphere. Emiliani, C. (Ed). Wiley Interscience. New York, Chichester, Brisbane, Toronto. pp391-428.*

Currie, R.I., Fisher, A.E. and Hargreaves, P.M. 1973. Arabian Sea Upwelling. *In: The Biology of the Indian Ocean. Zeitzchel, B. (ed). Springer-Verlag, New York. pp.37-53.*

Curry, W.B., Osterman, D.R., Gupta, M.V.S., and Ittekkot, V. 1992. Foraminiferal production and monsoonal upwelling in the Arabian Sea: Evidence from sediment traps. *In: Upwelling Systems: Evolution since the early Miocene. (Summerhayes, C.P., Prell, W.L. and Emeis, K.C. eds.). Geological Society Special Publication. Vol.64. pp.93-106.*

Davis, J.C. 1986. *Statistics and data analysis in geology (2nd edition). Wiley. New York. pp.550*

Deuser W.G. and Degens E.T. 1969. O18/O16 and C13/C12 ratios of fossils from the hot bring deep area of the central Red Sea. *Hot brines and recent heavy metal deposits in the Red Sea. Springer-Verlag New York. pp.336-347.*

Deuser, W.G. Ross, E.H. and Waterman, L.S. 1976. Glacial and pluvial periods: their relationship revealed by Pleistocene sediments of the Red Sea and Gulf of Aden. *Science. Vol.191, pp.1168-1170.*

Deuser, W.G., Ross, E.H. and Mlodzinska, Z.J. 1978. Evidence for the rate of denitrification

in the Arabian Sea. *Deep Sea Research. Vol.25. pp.431-445.*

Duplessy, J.C. 1982. Glacial to interglacial contrasts in the northern Indian Ocean. *Nature. Vol.295, pp.494-498.*

Dyer, K.R. 1973. *Estuaries: a physical introduction. John Wiley & sons, London. 140pp.*

Ellis, B.F. and Messina, A.R., 1968. Catalogue of foraminifera. *American Museum of Natural History*

Eshel, G., Cane, M.A. and Benno Blumenthal, M. 1994. Modes of subsurface, intermediate, and deep water renewal in the Red Sea. *Journal of Geophysical Research. Vol. 99, No. C8. pp. 15,941-15,952.*

Fantozzi, P.L. 1996. Transition from continental to oceanic rifting in the Gulf of Aden: Structural evidence from field mapping in Somalia and Yemen. *Tectonophysics. Vol.259. pp.285-312.*

Faugères, J.C., Duprat, E., Gonthier, E. and Peypouquet, J.P. 1983. La sédimentation marine holocene dans le Ghubbet el Kharab (territoire des Afars et Issas): importance du contexte régional. *Oceanologica Acta. Vol.7. No.1. pp5-12.*

Fairbanks, R.C. 1989. A 17,000 year glacio-eustatic sea level record: Influence of glacial melting rates on the Younger Dryas event and deep ocean circulation. *Nature. Vol.342, pp.637-642.*

Fedorov, K.N. 1976. Thermohaline finestructure of the ocean. *Gidrometeoizdat. Leningrad. pp.184.*

Fleisher, R.L. 1974. Preliminary report on the late Neogene Red Sea foraminifera Deep Sea Drilling Project. *In: Initial reports of the Deep Sea Drilling Project. Leg 26. Ludendyk, B.P, and Davis, T.A. eds. U.S. Government Printing Office, Washington. pp.985-1012.*

Fontugne, M.R. and Duplessy, J.C. 1986. Variations of the monsoon regime during the Upper Quaternary: Evidence from carbon isotopic record of organic matter in north Indian Ocean sediment cores. *Palaeogeography, Palaeoclimatology, Palaeoceanography. Vol.56, pp.69-88.*

Ganssen, G. and Kroon, D. 1991. Evidence for Red Sea surface circulation from oxygen isotopes of modern surface waters and planktonic foraminiferal tests. *Palaeoceanography. Vol.6(1), pp.73-82.*

Goll, R.M. 1969. Radiolaria: the history of a brief invasion. *Hot brines and recent heavy metal deposits.... pp.306-312.*

Grasshoff, K. 1969. *'Meteor' Forschungsergebnisse. Gebruder Borntraeger, Berlin, Reihe A. No. 6, pp. 76.*

Grasshoff, K. 1975. The hydrochemistry of landlocked basins and fjords. *In: Chemical Oceanography. Riley, J.P, and Skirrow, G. eds. Academic, San Diego, California. Vol.2, pp.455-597.*

Green, E.J. and Carritt, D.E. 1967. Oxygen solubility in sea water: thermodynamic influence of sea salt. *Science. Vol.157. pp.191-193.*

Greiner, G.O. 1974. Environmental factors controlling distributions of Recent foraminifera. *Brevoria, Museum of Comparative Zoology, Harvard University. Vol. 420, pp. 1-35.*

Gupta, A.K. 1994. Holocene deep-sea benthic foraminifera and watermasses in the Indian Ocean and the Red Sea. *Journal Geological Society of India. Vol.43, pp.691-703.*

Halicz, E. and Reiss, Z. 1981. Palaeoecological relations of foraminifera in a desert enclosed sea - The Gulf of Aqaba. *Marine Ecology. Vol.2, pp.15-34.*

Halim, Y. 1984. Plankton of the Red Sea and the Arabian Gulf. *Deep Sea Research. Vol.31. pp.969-982.*

Haunold, T.G., Baal, C. and Piller, W.E. 1997. Benthic foraminiferal associations in the northern bay of Safaga, Red Sea, Egypt. *Marine Micropaleontology. vol. 29, pp.185-210.*

Haynes, J.R. 1981. *Foraminifera. Macmillan Publishers LTD. London and Basingstoke. 433pp.*

Hemleben, C. and Spindler, M. 1983. Recent advances in research on living planktonic foraminifera. *Utrecht Micropaleontology Bulletin. Vol.30. pp. 141-170.*

Hemleben, C. Spindler, M. and Anderson, O.R. 1989. *Modern planktonic foraminifera. Springer-Verlag, New York. 363pp.*

Hemleben, C., Meischner, D., Zahn, R., Almogi-Labin, A., Erlenkeuser, H. and Hiller, B. 1996. Three hundred eighty thousand year long stable isotope and faunal records from the Red Sea:

Influence of global sea level change on hydrography. *Paleoceanography. Vol. 11, No.2, pp.147-156.*

Herman, Y. 1965. Evidence of climatic changes in Red Sea cores. *In: Means of Correlations of Quaternary succession. Congress of the International Association of Quaternary Research. Vol.8(VII), pp.325-348.*

Herman, Y. and Rosenberg, P.E. 1969. Mineralogy and micropalaeontology of a geothite bearing core. *Hot Brines and recent heavy metal deposits in the Red Sea. Springer / Verlag Berlin / Heidelberg / New York. pp448-459.*

Hottinger, L., Halicz, E. And Reiss, Z. 1993. *Recent foraminiferida from the Gulf of Aqaba, Red Sea. Dela Slovenska Akad. Znanosti in Umetnosti, Razred za Naravoslovne vede, Classis IV: Historia Naturalis. Vol.33. pp.179.*

Howard, W.R. 1997. A warm future in the past. *Nature. Vol.388. pp.418-419.*

Imbrie, J., Shackleton, N.J., Pisias, N.G., Morely, J.J., Prell, W.L., Martinson, D.G., Hays, J.D., McIntyre, A. and Mix, A.C. 1984. The orbital theory of Pleistocene climate: support from a revised chronology of the marine $\delta^{18}O$ record. *In Milankovitch and Climate (Berger et al., eds.). D. Reidel, Hingham, Mass. pp.269-305.*

Ivanova, E.V. 1985. Late Quaternary biostratigraphy and palaeotemperatures of the Red Sea and Gulf of Aden based on planktonic foraminifera and pteropods. *Marine Micropalaeontology. Vol.9, pp.335-364.*

Jasper, J.P. and Deuser, W.G. 1993. Annual cycles of mass flux and isotopic composition of pteropod shells settling into the deep Sargasso Sea. *Deep Sea Research I. Vol.40. No.4. pp.653-669.*

Jones, R.W., 1994. The *Challenger* Foraminifera. *Oxford Science Publ. The Natural History Museum. 149pp.*

Kennett, J. 1982. *Marine Geology. Prentice-Hall. 813pp.*

Kleijne, A., Kroon, D. and Zevenboom, W. 1988. Phytoplankton and foraminiferal frequencies in Northern Indian Ocean and Red Sea surface waters. In: *Brummer, G-J.A., and Kroon, D. 1988. Planktonic foraminifers as tracers of ocean-climate history. pp271-283.*

Kolla, V. and Biscaye, P.E. 1977. Distribution and origin of quartz in the sediments of the Indian Ocean. *Journal of Sedimentary Petrology. Vol.47. pp.642-649.*

Kossina, E. 1921. Die treifen des weltmeeres. *Verhöff. Inst. Meeresk. Univ. Berlin. Reihe A. No.9. pp.63.*

Krause, G. 1968. Struktur und verteilung des wassers aus dem Roten Meer im Nordwesten des Indischen Ozeans. *Meteor Forschungsevgebnisse. Reihe A. No.4. pp.77-100.*

Kroon, D. 1988. Distribution of extant planktic foraminiferal assemblages in Red Sea and northern Indian Ocean surface waters. *In: Planktonic foraminifers as tracers of ocean-climate history. Brummer, G.-J. A, and Kroon, D. eds. PhD Thesis, Free University of Amsterdam. pp.229-267.*

Kroon, D. and Darling. 1995. Size and upwelling control of stable isotope composition of N.dutertrie (d'Orbigny), G.ruber (d'Orbigny) and G.bulloides d'Orbigny: examples from the Panama basin and Arabian Sea. *Journal of Foraminiferal Research. Vol.25. No.1. pp.39-52.*

Ku, T.L., Thurber, D.L. and Mathieu, G.G. 1969. Radio carbon chronology of Red Sea sediments. *Hot brines and recent heavy metal deposits in the Red Sea. Degens, E.T, and Ross, D.A. eds. Springer-Verlag, New York. pp.348.*

Kuntz, R. 1985. Bestimmung der Tiefenwasserzirkulation des Rotten Meers anhand einer boxmodellauswertung von tritium , H^3 und salinitatsdaten. *PhD thesis, Ruprecht Karls Univ., Heidelberg. 76pp.*

Lamb, J.L. and Miller T.H. 1984. Stratigraphic significance of uvigerinid foraminifers in the western hemisphere. *University of Kansas, Paleontological Contributions. Article 66, pp. 1-32.*

Levanon-Spanier, I., Padan, E. and Reiss, Z. 1979. Primary production in a desert enclosed sea - The Gulf of Elat (Aqaba), Red Sea. *Deep Sea Research. Vol.26, 673-685.*

Libes, S.M. 1992. *An introduction to marine biogeochemistry. John Wiley and Sons Inc. New York, Chichester, Brisbane, Toronto, Singapore. pp.734.*

Loeblich, A.R. and Tappan, H., 1988. Foraminiferal genera and their classification. *van Nostrand, Reinhold. 970pp.*

Locke, S.M. 1984. The palaeocenographic record of the last glacial-interglacial cycle in the Red

Sea and Gulf of Aden. *Masters thesis.*

Locke, S.M. and Thunnel, R.C. 1987. Palaeoceanographic record of the last glacial-interglacial cycle in the Red Sea and Gulf of Aden. *Pal. Pal.Pal. 64. pp.163-187*

Lupton, J.E., Weiss, R.F. and Craig, H. 1977. Mantle helium in the Red Sea brines. *Nature. Vol. 266. pp.244-246*

Luz, B. and Riess, Z. 1983. Stable carbon isotopes in Quaternary foraminifera from the Gulf of Aqaba (Elat), Red Sea. *Utrecht Micropaleontological Bullitin. Vol.30, pp.129-140.*

Luz, B., Heller-Kallai, L. and Almogi-Labin, A. 1984. Carbonate mineralogy of late pleistocene sediments from the northern Red Sea. *Isreal Journal of Earth Science. Vol.33, pp.157-166.*

Maillard, C. and Soliman, G. 1986. Hydrography of the Red Sea and exchanges with the Indian Ocean in summer. *Oceanologica Acta Vol.9 No.3 pp249-269.*

Manins, P.C. 1973. A filling box model of the deep circulation of the Red Sea. *Mem. Soc. R. Sci. Lieges. Tome VI, pp. 153-166.*

Martinson, D.G., Pisias, N.G., Hays, J.D., Imbrie, J., Moore, T.C and Shackleton, N.J. 1987. Age dating and the orbital theory of the Ice Ages: development of a high resolution 0-300,000 year chronostratigraphy. *Quaternary Research. Vol.27. pp.1-29.*

McCulloch, I., 1977. Qualitative observations on recent foraminiferal tests with emphasis on the Eastern Pacific. *PhD Thesis, University of Southern California, Los Angeles, California 90007. 676pp.*

McIntyre, A. 1969. The coccolithophorida in Red Sea sediments. *Hot brines and recent heavy metal deposits.... pp299-305.*

Meyer, W.C. 1973. Late Pleistocene and Holocene palaeoceanography of the Red Sea. *Thesis Fac. Grad. School, University of Southern California, Los Angeles. pp118.*

Milliman, J.D., Ross, D.A. and Ku, T.L. 1969. Precipitation and lithification of deep-sea carbonates in the Red Sea. *Journal of Sedimentary Petrology. Vol.39, pp.724-736.*

Morcos, S. A. 1970. Physical and chemical oceanography of the Red Sea. *Oceanography and Marine Biology Ann. Rev. Vol. 8. pp.73-202.*

Muromtsev, A.M. 1960. A contribution to the hydrology of the Red Sea. *Doklady Acadamy of Nauk SSSR. Vol.134. pp.1443-1446.*

Murray, C.N. and Riley, J.P. 1969. The solubility of gases in distilled water and seawater - II. Oxygen. *Deep Sea Research. Vol.16. pp.297-310.*

Murray, J.W. 1991. Ecology and palaeoecology of benthic foraminifera. *Longman. Harlow. 397pp.*

Naquvi, S.W.A. and Fairbanks, R.G. 1996. A 27,000 year record of Red Sea outflow: Implication for timing of post-glacial monsoon intensification. *Geophysical Research Letters. Vol.23. No.12. pp1501-1504.*

Neumann, A.C. and McGill, D.A. 1962. Circulation of the Red Sea in early summer. *Deep Sea Res. 8. pp223-235.*

Olson, D.B., Hitchcock, G.L., Fine, R.A. & Warren, B.A. 1993. Maintenance of the low-oxygen layer in the central Arabian Sea. *Deep Sea Research 2. Vol 40, No. 3. pp.673-685.*

Parisi, E. 1983. Distribuzione dei foraminiferi bentonici in una carota della Dorsale Mediterranean (Pleistocene medio e superiore). *Rivista Italiana di Paleontologia e Stratigrafia. Vol. 88, pp. 641-677.*

Patzert, W.C. 1974. Wind induced reversal in Red Sea circulation. *Deep Sea Res. Vol.21. pp109-121.*

Pedgley, D.E. 1974. An outline of the weather and climate of the Red Sea. *L'oceanographie physique de la Mer Rouge. Publications du Centre National pour l'exploitation des Oceans (C.N.E.X.O.). No. 2. pp9-21.*

Pendlebury, D.C. 1974. Recent sediments, shelly fauna and foraminifera of the Malin Sea. *PhD thesis Univ. College of Wales, Aberystwyth.*

Petit-Maire, N., Sanlavill, P. and Zhong-Wei, Y. 1994. Changements globaux et paléosoussons: la zone de transition afro-asiatique au cours des derniers 140,000 ans. *Geochronique. vol. 50, pp. 16-19.*

Pirazzoli, P.A, Radtke, U., Hantoro, W.S., Jouannic, C., Hoang,C.T., Causse, C. and Borel Best, M. 1993. A one-million year long sequence of marine terraces on Sumba Island, Indonesia.

Marine Geology. Vol.109. pp.221-236.

Pflum, C.E. and Frerichs, W.E. 1976. Gulf of Mexico deep water foraminifers. *Cushman Foundation for Foraminiferal Reasearch, Special Publication. Vol. 14, pp1-108.*

Prell, W.L. 1984. Monsoonal climate of the Arabian Sea during the late Quaternary: A response to changing solar radiation. *In: Milankovitch and Climate, Part 1. Berger, A.L. (ed.) Reidel, Hingham, Mass. pp. 349-366.*

Prell, W.L. et al. 1991. *Proceedings of the Ocean Drilling Programme, Scientific Results. College Station, Texas. Vol.117. pp.638.*

Prell, W. L., Murray, D. W. and Clemens, S.C. 1992. Evolution and variability of the Indian Ocean Summer Monsoon: Evidence from the Western Arabian Sea Drilling Program. *In: R. A. Duncan et. al. (eds.). Synthesis of results from scientific drilling in the Indian Ocean. Geophysical Monograph 70. pp.447-469.*

Prell, W.L. and Streeter, H.F. 1981. Temporal and spatial patterns of monsoonal upwelling along Arabia: A modern analogue for the interpretation of Quaternary SST anomalies. *Journal of Marine Research. Vol. 40, pp.143-155.*

Prell, W.L. and van Campo, E. 1986. Coherent response of Arabian Sea upwelling and pollen transport to late Quaternary monsoonal winds. *Nature. Vol. 323, pp.526-528.*

Quadfasel, D. and Baudner, H. 1993. Gyre scale circulation cells in the Red Sea. *Oceanologica Acta. Vol. 16, No. 3. pp.221-229.*

Radtke, U. and Grün, R. 1990. Revised reconstruction of middle and late Pleistocene sea-level changes based on new chronologic and morphologic investigations in Barbados, West Indies. *Journal of Coastal Research. Vol. 6. pp.699-708.*

Reiss, Z., Halicz, E. and Perelis, L. 1974. Planktonic foraminiferida from recent sediments in the Gulf of Elat. *Isreal Journal of Earth Science. Vol.23, pp.69-105.*

Reiss, Z. and Hottinger, L. 1984. The Gulf of Aqaba. Ecological Micropalaeontology. *Ecological Studies. Vol.50. Springer-Verlag, New York. pp.354.*

Reiss, Z., Luz, B., Almogi-Labin, A., Halicz, E., Winter, A., Wolf, M. and Ross, D.A. 1980. Later Quaternary palaeoceanography of the Gulf of Aqaba (Elat), Red Sea. *Quaternary*

Research. Vol.14, pp.294-308.

Risch, H. 1976. Microbiostratigraphy of core-sections of the Red Sea. *Geologisches Jahrbuch. Vol.17, pp.3-14.*

Rochford, D.J. 1964. Salinity maximum in the upper 1000 meters of the north Indian Ocean. *Australian Journal of Marine Freshwater Research. Vol.15. pp.1-24.*

Rohling, E.J., Jorissen, F.J., Vergnaud-Grazzini, C. and Zachariasse, W.J. 1993. Northern Levantine and Adriatic Quaternary planktic foraminifera; Reconstruction of paleoenvironmental gradients. *Marine Micropaleontology. Vol. 21. pp. 191-218.*

Rohling, E.J. 1994. Glacial conditions in the Red Sea. *Palaeoceanography. Vol.9. No.5. pp.653-660.*

Rohling, E.J. and Zachariasse, W.J. 1996. Red Sea outflow during the last glacial maximum. *Quaternary International. Vol.31. pp.77-83.*

Rohling, E.J., Fenton, M., Jorissen, F.J., Bertrand, P., Ganssen, G. and Caulet, J.P. 1998. Glacial sea level low stands of the last 500,000 years. Nature. Vol.394. pp.162-165.

Rollinson, H.R. 1993. *Using geochemical data: evaluation, presentation and interpretation. Longman Singapore Publishers (Pte) Ltd. pp.352.*

Rose, P.R. And Lidz, B. 1977. Diagnostic foraminiferal assemblages of shallow-water modern environments: South Florida and the Bahamas. *Sedimenta. Vol. VI, pp. 1-55.*

Ross, D.A and Schlee, J. 1973. Shallow structure and geologic development of the southern Red Sea. *Geological Society America Bulletin. Vol.84. pp.3827-3848.*

Rossignol-Strick, M. 1985. Mediterranean Quaternary sapropels, an immediate response of the African monsoon to variation of insolation. *Palaeogeography, Palaeoclimatology, Palaeoecology. Vol. 49, pp.237-263.*

Sabinin, K. 1964. The layers of high salinity in the north Indian Ocean. *Trudy Instituta Okeanologii. Vol.64. pp.51-58.*

Said, R. 1949. Foraminifera of the northern Red Sea. *Cushman Lab. Foram. Research, Special publication. Vol.26, pp.1-44.*

Said, R. 1950a. Additional foraminifera from the northern Red Sea. *Contrib. Cushman Found. Foram. Res. Vol.1, pp.4-9.*

Said, R. 1950b. The distribution of foraninifera in the northen Red Sea. *Contrib. Cushman Found. Foram. Res. Vol.1, pp.9-29.*

Sarkar, A., Ramesh, R., Bhattacharya, S.K. and Rajagopalan, G. 1990. Oxygen isotope evidence for a stronger winter monsoon current during the last glaciation. *Nature. Vol. 343, pp.549-551.*

Schlich, R. 1982. The Indian Ocean, aseismic ridges, spreading centres, and oceanic basins. *In: The ocean basins and margins (Indian Ocean). Nairn, A.E.M. and Stehli, F.G. (eds.). Plenum. New York. Vol.6. pp51-147.*

Schoell, M., and Risch, H. 1976. Oxygen and carbon isotope analyses on planktonic foraminifera of core VA 01-188 P (Southern Red Sea). *Geologisches Jahrbuch. Vol.D17, pp.15-32.*

Shackleton, N.J. 1974. Attainment of isotopic equilibrium between ocean water and the benthonic foraminifera genus, *Uvigerina*; isotopic changes in the ocean during the last glacial. *Fr. Cent. Natl. Rech. Sci. Colloq. Int. Vol. 219, pp. 203-210.*

Shackleton, N.J. 1987. Oxygen isotopes and sea level. *Quaternary Science Reviews. Vol. 6. pp. 183-190.*

Shapiro, G. I. and Meschanov, S. L. 1991. Distribution and spreading of Red Sea water and salt lens formation in the North West Indian Ocean. *Deep Sea Research. Vol. 38. No. 1. pp. 21-34.*

Showers, W.J. 1980. Biometry of the foraminifer *Rosalina globularis* (d'Orbigny) in Antarctic environment. *Journal of Foraminiferal Research. Vol. 10, pp. 61-74.*

Siedler, G. 1968. Conditions of layering and water movements in the entrance of the Red Sea.(summary). *Sonderdruch ains, METFOR " FORSCHUNGSERGERNISSE " Reite A, Heft 4 GEBRUDER BORNTRAEGER. BERLIN STUTTGART.*

Siedler, G. 1969. General Circulation of water masses in the Red Sea. *In: Degens, E. T. & Ross, D. A. (eds.) Hot Brines and recent heavy metal deposits in the Red Sea. Springer / Verlag Berlin / Heidelberg / New York. pp.131-137.*

Sirocko, F. and Ittekkot, V. 1992. Organic carbon accumulation rates in the Holocene and glacial Arabian Sea: implications for O_2-consumption in the deep-sea and atmospheric CO_2

variations. *Climate Dynamics. Vol. 7, pp.167-172.*

Siroko, F., Sarnthein, M., Lange, H. and Erlenkeuser, H. 1991. Atmospheric summer circulation and coastal upwelling in the Arabian Sea during the Holocene and the last glaciation. *Quaternary Research. Vol. 36, pp.72-93.*

Smith, P.B. 1964. Ecology of benthonic species. *U.S. Geological Survey, Professional Paper 429-A pp. A1-A39.*

Spindler, M., Hemleben, C., Salomons, J.B. and Smit, L.P. 1984. Feeding behaviour of some planktonic foraminifers in laboratory cultures. *Journal of Foraminiferal Research. Vol.14. No.4. pp.237-249.*

Squires, G.L. 1988. *Practaical Physics, 3rd ed. with rev. Cambridge Univ. Press, Cambridge, UK, pp. 213.*

Stuiver, M. And Brazunias, T.F. 1993. *Radiocarbon. Vol.31. No.1. pp137-189.*

Thunnel, R.C., Locke, S.M. and Williams, D.F. 1988. Glacio-eustatic sea-level control on Red Sea salinity. *Nature Vol.334. pp601-604.*

Tolderlund, D.S. and Bé, A.W.H. 1971. Seasonal distribution of planktonic foraminifera in the western North Atlantic. *Micropaleontology. Vol.17, no.3, pp.297-329.*

Tragou, E. and Garrett, C. 1997. The shallow thermohaline circulation of the Red Sea. *Deep Sea Research 1. Vol.44. No.8. pp.1355-1376.*

van Campo, E., Duplessy, J.C. and Rossignol-Strick, M. 1982. Climatic conditions deduced from a 150-kyr oxyen isotope - Pollen record from the Arabian Sea. *Nature. Vol.296, pp.56-59.*

van Couwelaar, M. 1997. Zooplankton and micronekton biomass off Somalia and in the Southern Red Sea during the SW monsoon of 1992 and the NE monsoon of 1993. *Deep Sea Research II. Vol.44. No.6-7. pp.1213-1234.*

van Leeuwen, R.J.W., 1989. Sea-floor distribution and late Quaternary faunal patterns of planktonic and benthic foraminifers in the Angola Basin. *PhD Thesis, Utrecht Micropaleontological Bulletin. vol. 38, pp.288.*

Vangriesheim, A. 1974. Structure hydrologique et dynamique du Golfe d'Aden d'aprés la V^{e}

campagne du "Robert Giraud". *Rapp. Int. Mus. Hist. Nat., Paris. 31pp.*

Vergnaud-Grazzini, C., Caulet, J-P. and Vénec-Peyré, M-T. 1995. Index de fertilité et mousson dans le bassin de Somali. Evolution au Quaternaire supérieur. *Bull. Soc. Géol. France. Vol.166. No.3. pp.259-270.*

Verhallen, P.J.J.M., 1991. Late Pliocene to early Pleistocene Mediterranean mud-dwelling foraminifera; influence of a changing environment on community structure and evolution. *PhD Thesis, Utrecht Micropaleontological Bulletin vol.40, pp.220.*

Wall, D. and Warren, J.S. 1969. Dinoflaggelates in Red Sea piston cores. *Hot Brines and recent heavy metal deposits in the Red Sea. Springer / Verlag Berlin / Heidelberg / New York. pp317-328.*

Warren, B.A. 1992. Circulation of north Indian deep water in the Arabian Sea. In: *Desai, B.N. (ed). 1992. Oceanography of the Indian Ocean. New Delhi: Oxford and IBH Publishing Co. pp. 575-582.*

Warren, B.A. 1994. Context of the suboxic layer in the Arabian Sea. *Proceedings of the Indian Academy of Sciences. (Earth and Planetary Sciences.) Vol. 103, No. 2. pp. 301-314.*

Weiss, R.F. 1970. The solubility of nitrogen, oxygen and argon in water and seawater. *Deep Sea Research. Vol.17. pp.721-735*

Werner, F. and Lang, K. 1975. A bathymetric survey of the sill area between the Red Sea and Gulf of Aden.

Wiebinga, C.J., Veldhuis, M.W.J. and De Baar, H.J.W. 1997. Abundance and productivity of bacterioplankton in relation to seasonal upwelling in the northwest Indian Ocean. *Deep Sea Research I. Vol.44. No.3. pp.451-476.*

Winter, A., Almogi-Labin, A., Erez,Y., Halicz, E., Luz, B. and Reiss, Z. 1983. Salinity tolerance of marine organisms deduced from Red Sea Quaternary record. *Marine Geology. Vol.53, pp.17-22.*

Wyrtki, K. 1971. Oceanographic atlas of the international Indian Ocean science expedition. *National Science Foundation. Washington D.C. pp.531.*

Wyrtki, K. 1974. On the deep circulation of the Red Sea. In: *La formation des eaux oceaniques*

profondes. CNRS, Paris. pp. 91-106.

SPECIES, PLATES AND TAXONOMY

1. List of foraminiferal species discovered in cores.

Planktonic foraminifera:

Globigerina bulloides d'Orbigny, 1826 (plate 12).

Globigerinella (Beella) digitata (Brady), 1879.

Globigerinella siphonifera (d'Orbigny), 1939a (plate 6).

Globigerinita glutinata (Egger), 1893 (plate 7).

Globigerinoides conglobatus (Brady), 1879.

Globigerinoides ruber (d'Orbigny), 1839 (plate 1).

Globigerinoides sacculifer (Brady), 1877 (plates 2 and 3).

Globorotalia anfracta (Parker), 1967 (plate 8).

Globorotalia crassaformis (Galloway and Wissler), 1927.

Globorotalia menardii (Parker, Jones and Brady), 1865 (plate 13).

Globorotalia scitula (Brady) 1882.

Globorotaloides hexagonus (Natland), 1938.

Globoturborotalia rubescens Hofker, 1956 (plate 4).

Globoturborotalita tenella (Parker), 1958 (plate 5).

Neogloboquadrina dutertrei (d'Orbigny), 1839a (plate 11).

Neogloboquadrina pachyderma (Ehrenberg), 1861 (plate 10).

Orbulina universa d'Orbigny, 1939a.

Pulleniatina obliquiloculata (Parker and Jones), 1865.

Turborotalia quinqueloba (Natland), 1938 (plate 9).

Benthic foraminifera:

Alliatinella gedgravensis (Carter), 1957.

Amphycorine scalaris (Batsch) Parr, 1950.

Anomalina ammonoides (Reuss) var. *umbilicatula* Vasilenko and Myatliuk, 1447 (plate 27).

Astacolus crepidulatus (de Montfort), 1808.

Astrononion echolsi Kennett, Corlis, 1979 (plate 32).

Biloculinella irregularis d'Orbigny, 1839 (plate 45).

Bolivina albatrossi Cushman, 1922.

Bolivina subreticulata Parr, 1932 (plates 22 and 23).

Bolivina subspathulata Boomgaart, 1949 (plate 36).

Bolivina italica Cushman, 1936 (plate 15).

Bolivina amygdalaeformis (Brady), 1881.

Bolivina earlandi (Parr), 1950.

Bolivina spathuloides Hofker, 1956 (plate 14).

Bolivinita quadrilatera (Schwager) 1866.

Bulimina marginata (d'Orbigny) 1826 (plate 18).

Cancris auriculus (Fichtel and Moll) 1798 (plate 16).

Cassidulina laevigata (d'Orbigny), 1826 (plate 20).

Cassidulina subglobosa (Brady), 1881.

Cibicides kullenbergi Parker, 1953.

Cibicides refulgens (de Montfort) 1808.

Cibicides ungerianus (d'Orbigny), 1846 (plate 24).

Cushmanina striatopunctata Parker and Jones, 1865.

Cyclogyra lata Scott, 1974.

Dentalina baggi Galloway and Wissler, 1927.

Dentalina drammenensis Feyling-Hanssen, 1964.

Dentalina subsoluta Cushman, 1923.

Dentalina trondheimensis Feyling-Hanssen, 1964.

Dentalina bradyensis (Dervieux) 1894.

Dentalinoides canulina Marie, 1941.

Rosalina elegans Hansen, 1970 (plate 35).

Ehrenbergina trigona (Goes), 1896 (plate 21).

Eponides punctatus LeRoy, 1941 (plate 17).

Glandulina laevigata d'Orbigny, 1846 (plate 28).

Gyroidina altiformis (R.E. & K.C. Stewart), 1958 (plate 29).

Gyroidina orbicularis d'Orbigny, 1826.

Gyroidina subsoldanii (McCulloch), 1977 (plate 38).

Gyroidina umbonata (Silvestri), 1898 (plate 37).

Hanzawaia boueana (d'Orbigny), 1846.

Hoeglundina elegans (Brotzen), 1948.

Hyalinea balthica (Hofker), 1951 (plate 26).

Lagena laevis (Montagu) var. *baggi* Cushman and Gray, 1946.

Lagena striata (d;Orbigny) var. *basisenta* Cushman and Stainforth, 1947.

Lagena vulgaris Williamson var. *spinoso-marginata* Jones, 1874.

Lenticulina calcar (Linne) 1767.

Loxostomina limbata (Brady), 1881.

Miliolina caucasica Bogdanovich, 1947.

Miliolina reussi Bogdanovich, 1947.

Miliolinella subrotunda (Montagu), 1803 (plate 41).

Nodosaria d'Orbigny, 1826.

Oolina apiculata Reuss, 1851.

Oolina cf. *squamosa* (Montagu) McCulloch, 1977.

Procerolagena gracillima Williamson, 1848.

Pseudofissurina mccullochae R.W. Jones, 1984.

Pyrgo depressa d'Orbigny, 1826.

Pyrgo laevis Defrance, 1824.

Pytine parthenopeia Moncharmont Zei and Sgarrella, 1978.

Quinqueloculina elongata Natland, 1938.

Quinqueloculina lamarckiana d'Orbigny, 1839 (plate 43).

Quinqueloculina multimarginata Said, 1949 (plate 42).

Robertina bradyi Cushman and Parker, 1936.

Rosalina globularis d'Orbigny, 1826.

Sigmoilina tenuis (Čžjžek) 1847.

Sigmoilopsis schlumbergeri Finlay, 1947.

Sphaeroidina bulloides d'Orbigny, 1826.

Spirillina vivipara Ehrenberg, 1843.

Spiroloculina communis (plate 39)

Spiroloculina depressa d'Orbigny, 1826 (plate 40).

cf. Suggrunda porosa Hoffmeister and Berry, 1937.

Siphotextularia sp. (plate 30).

Textularia fistulosa (plate 34)

Textularia pseudocarinata Cushman, 1921.

Triloculina tricarinata d'Orbigny 1826 (plate 44).

Uvigerina hollicki (Thalmann) 1950 (plate 19).

Uvigerina porrecta (Brady), 1879 (plate 33).

Uvigerina proboscidea Schwager, 1866 (plate 25).

Vaginulinopsis reniformis (d'Orbigny), 1846.

Vaginulinopsis tasmanica (Parr), 1950.

2. List of plates (species listed in order of mention in chapter 6 (results).

Planktonic foraminifera

1. *Globigerinoides ruber* (d'Orbigny), 1839.
2. *Globigerinoides sacculifer* (Brady), 1877 (without sac)
3. *Globigerinoides sacculifer* (Brady), 1877 (with sac).
4. *Globoturborotalia rubescens* Hofker, 1956.
5. *Globoturborotalita tenella* (Parker), 1958.
6. *Globigerinella siphonifera* (d'Orbigny), 1939a.
7. *Globigerinita glutinata* (Egger), 1893.
8. *Globorotalia anfracta* (Parker), 1967.
9. *Turborotalia quinqueloba* (Natland), 1938.
10. *Neogloboquadrina pachyderma* (Ehrenberg), 1861.
11. *Neogloboquadrina dutertrei* (d'Orbigny), 1839a.
12. *Globigerina bulloides* d'Orbigny, 1826.
13. *Globorotalia menardii* (Parker, Jones and Brady), 1865.

Benthic foraminifera

14. *Bolivina spathuloides* Hofker, 1956
15. *Bolivina italica* Cushman, 1936
16. *Cancris auriculus* (Fichtel and Moll) 1798
17. *Eponides punctatus* LeRoy, 1941

18. *Bulimina marginata* (d'Orbigny) 1826
19. *Uvigerina hollicki* (Thalmann) 1950
20. *Cassidulina laevigata* (d'Orbigny), 1826
21. *Ehrenbergina trigona* (Goes), 1896
22. *Bolivina subreticulata* Parr, 1932
23. *Bolivina subreticulata* Parr, 1932
24. *Cibicides ungerianus* (d'Orbigny), 1846
25. *Uvigerina proboscidea* Schwager, 1866
26. *Hyalinea balthica* (Hofker), 1951
27. *Anomalina ammonoides* (Reuss) var. umbilicatula Vasilenko and Myatliuk, 1447
28. *Glandulina laevigata* d'Orbigny, 1846
29. *Gyroidina altiformis* (R.E. & K.C. Stewart), 1958
30. *Siphotextularia sp.*
31. *Astrononion echolsi* Kennett, Corlis, 1979
32. *Uvigerina porrecta* (Brady), 1879
33. *Textularia fistulosa*
34. *Rosalina elegans* Hansen, 1970
35. *Bolivina subspathulata* Boomgaart, 1949
36. *Gyroidina umbonata* (Silvestri), 1898
37. *Gyroidina subsoldanii* (McCulloch), 1977
38. *Spiroloculina communis*
39. *Spiroloculina depressa* d'Orbigny, 1826
40. *Miliolinella subrotunda* (Montagu), 1803
41. *Quinqueloculina multimarginata* Said, 1949
42. *Quinqueloculina lamarckiana* d'Orbigny, 1839
43. *Triloculina tricarinata* d'Orbigny 1826
44. *Biloculinella irregularis* d'Orbigny, 1839

Plates

Species relevant to the study are presented here.

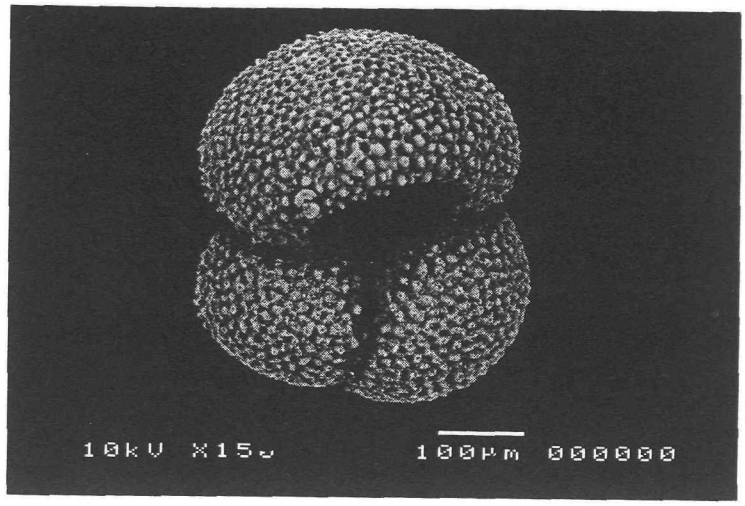

1. *Globigerinoides ruber*

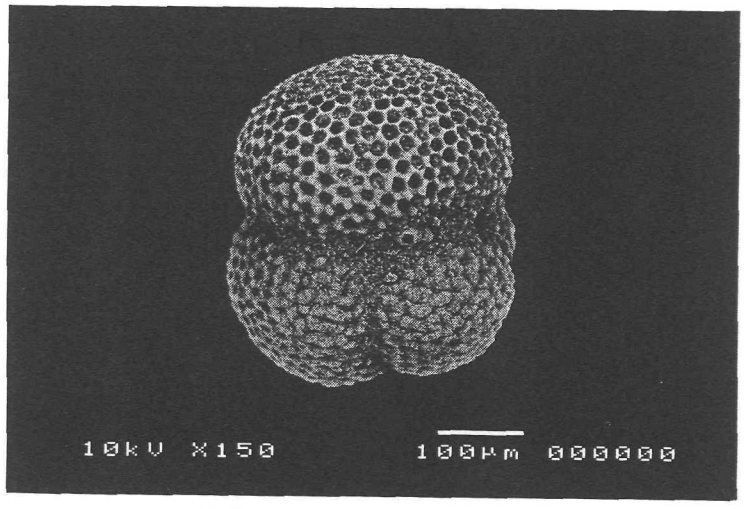

2. *Globigerinoides sacculifer*
(without sac)

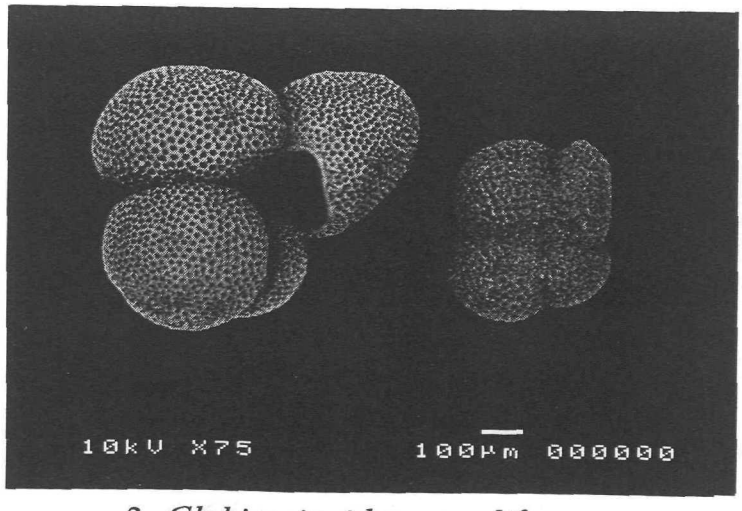

3. *Globigerinoides sacculifer*
(with sac)

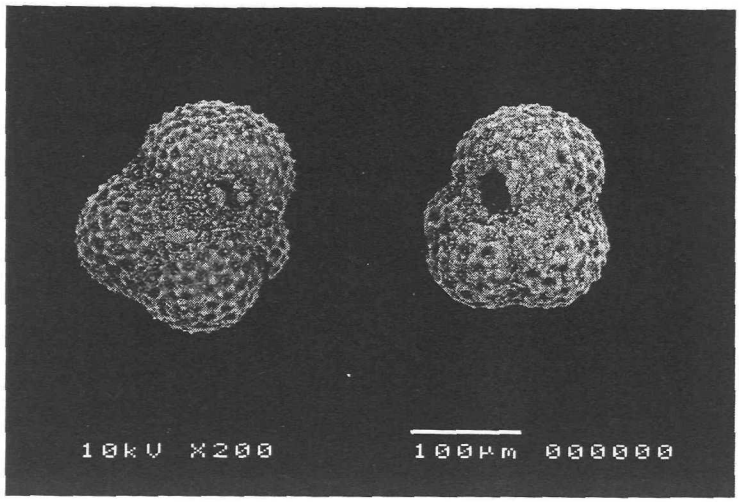

4. *Globoturborotalia rubescens*

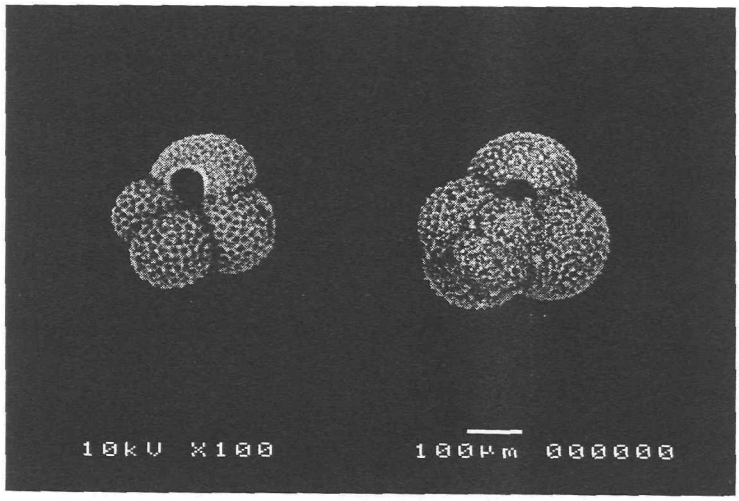

5. *Globoturborotalia tenella*

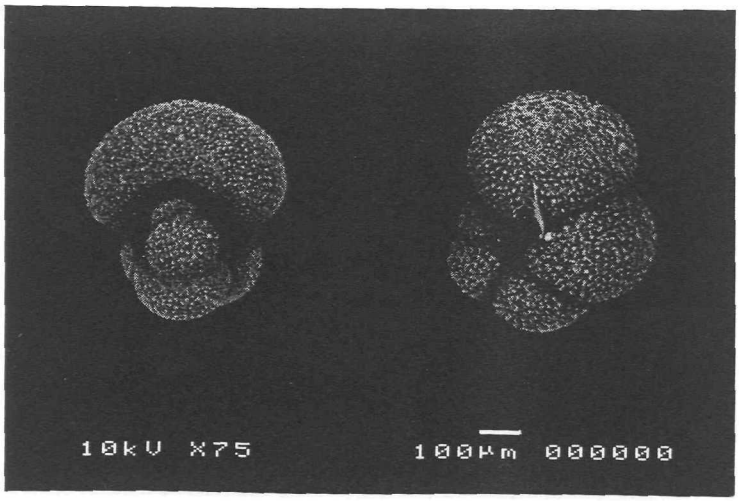

6. *Globigerinella siphonifera*

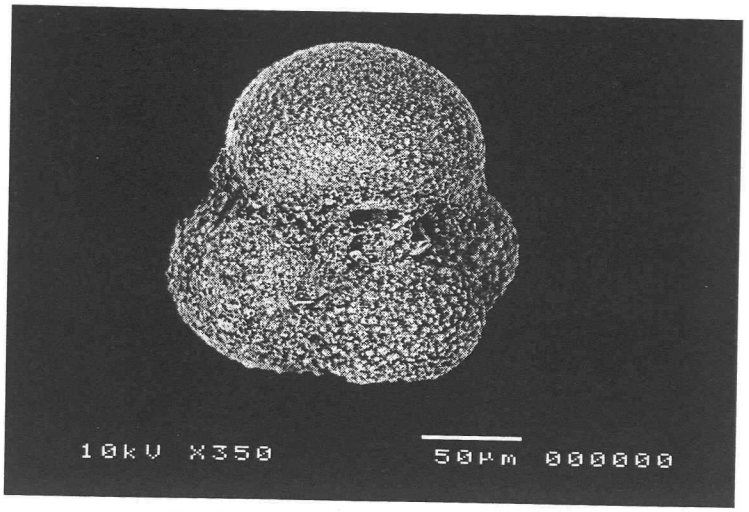

7. *Globigerinita glutinata*

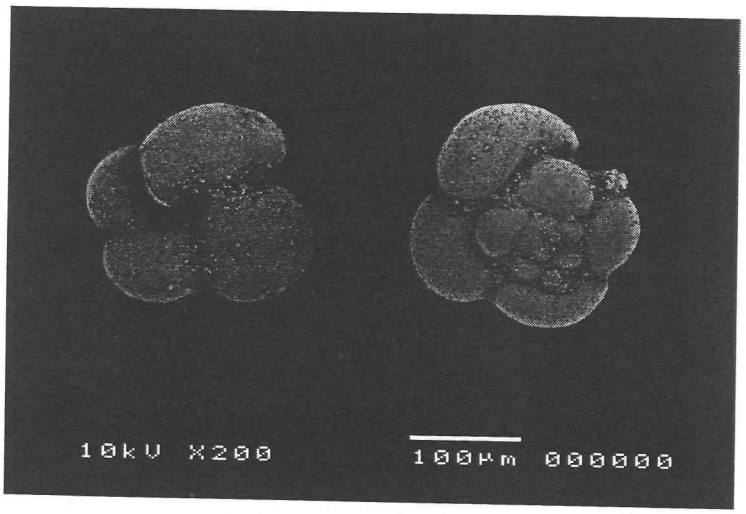

8. *Globoturborotalia anfracta*

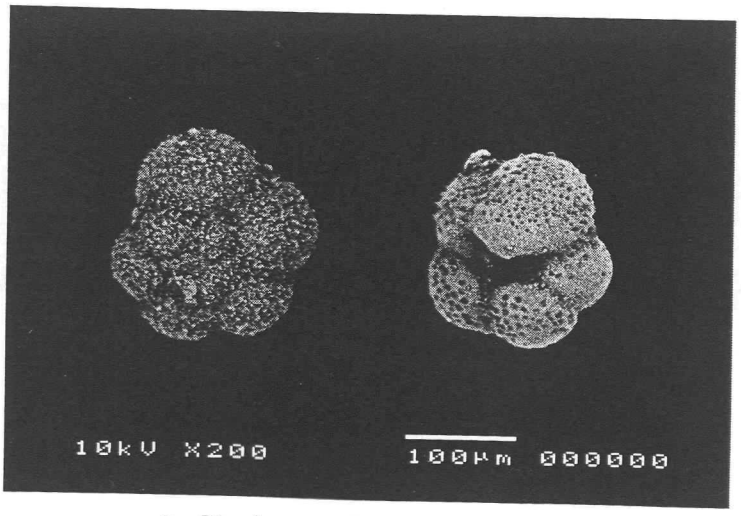

9. *Turborotalia quinqueloba*

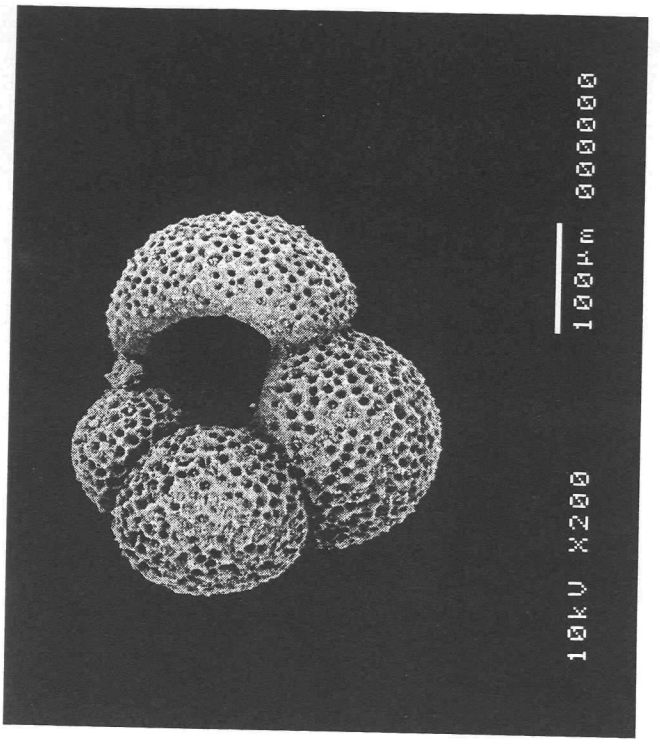

12. *Globigerina bulloides*

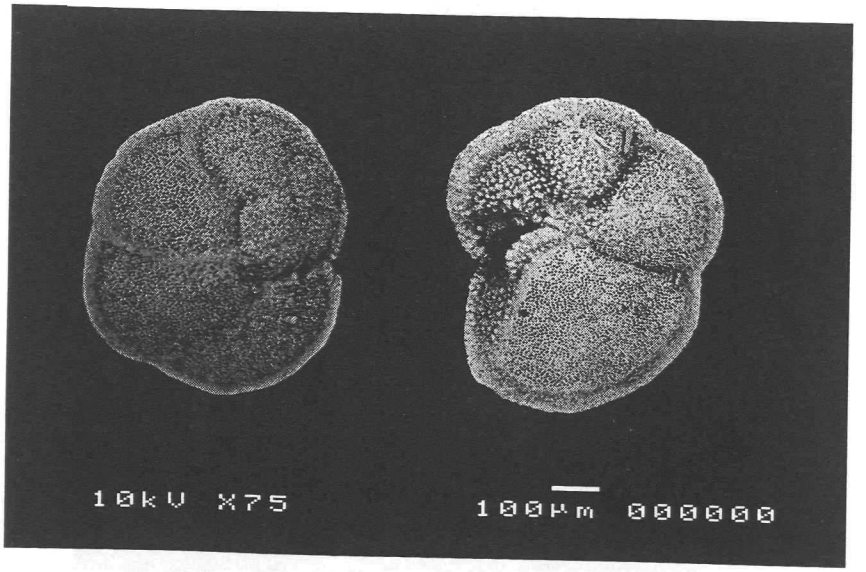

13. *Globorotalia menardii*

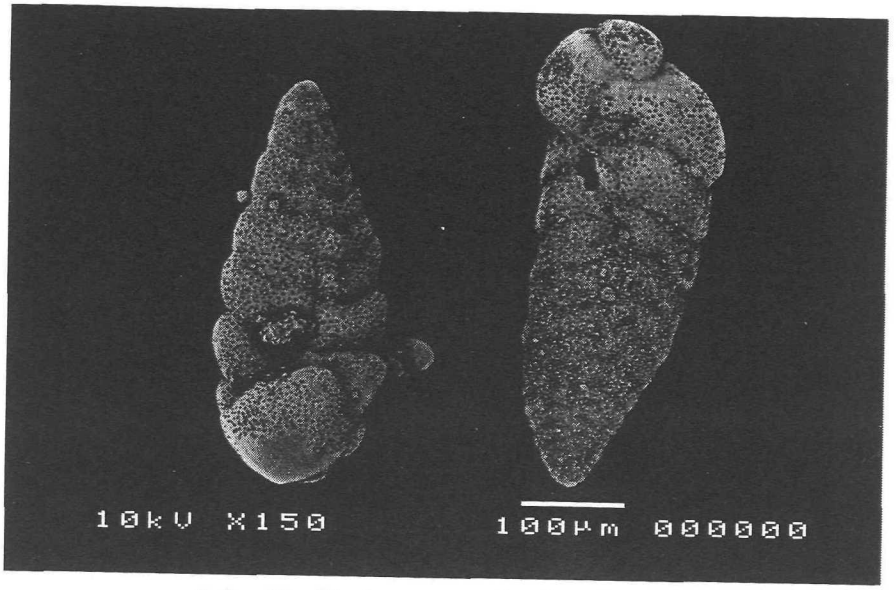

14. *Bolivina spathuloides*

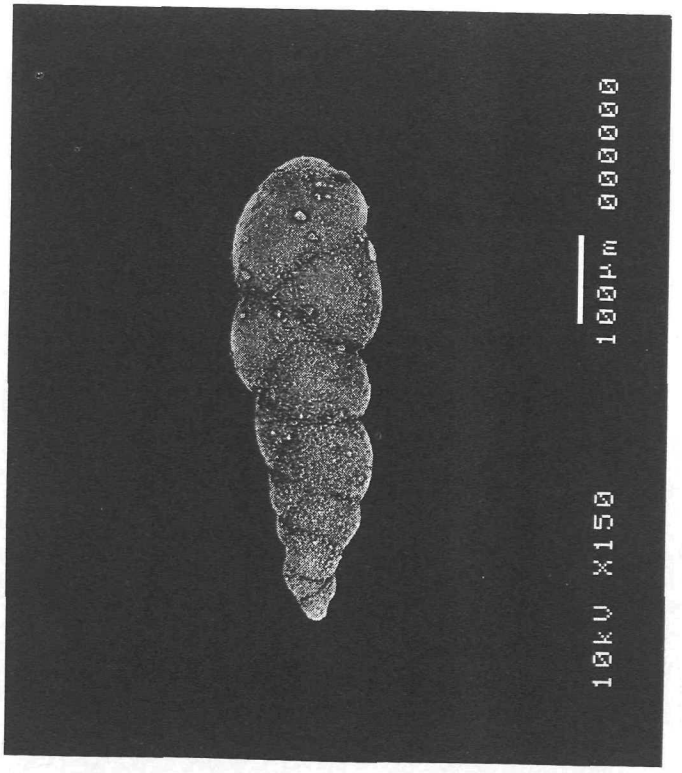

15. *Bolivina italica*

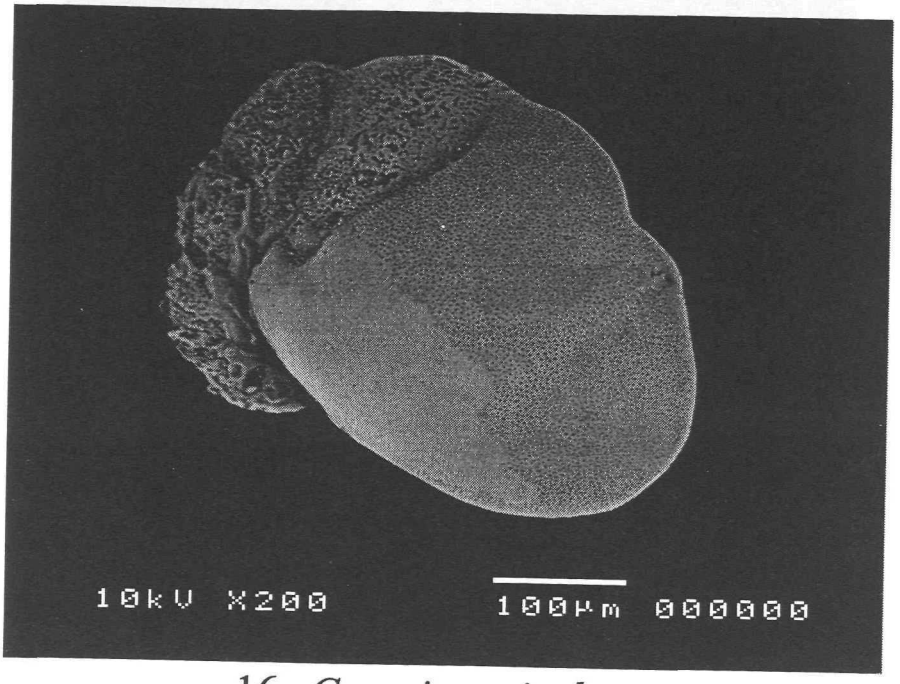

16. *Cancris auriculus*

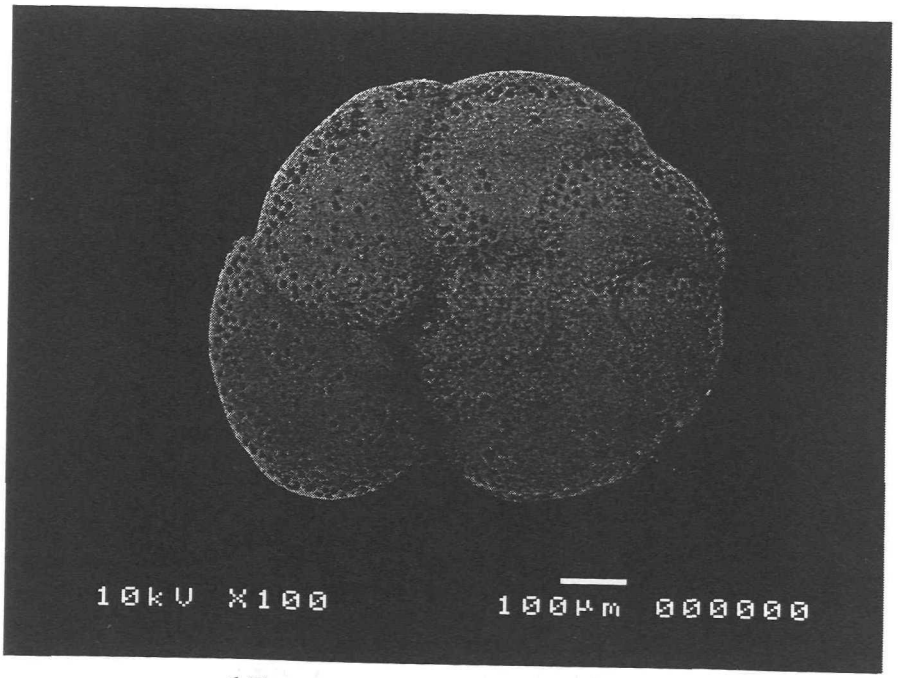

17. *Eponides punctatus*

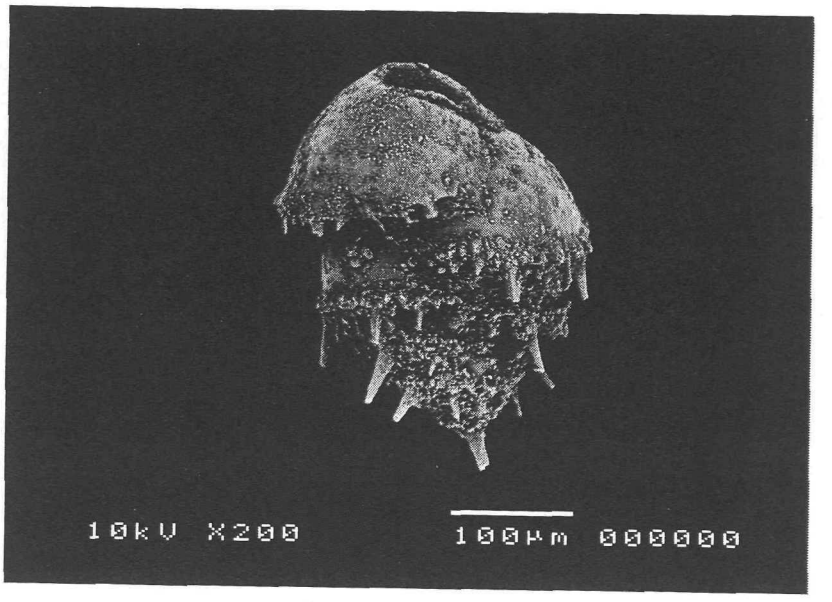

18. *Bulimina marginata*

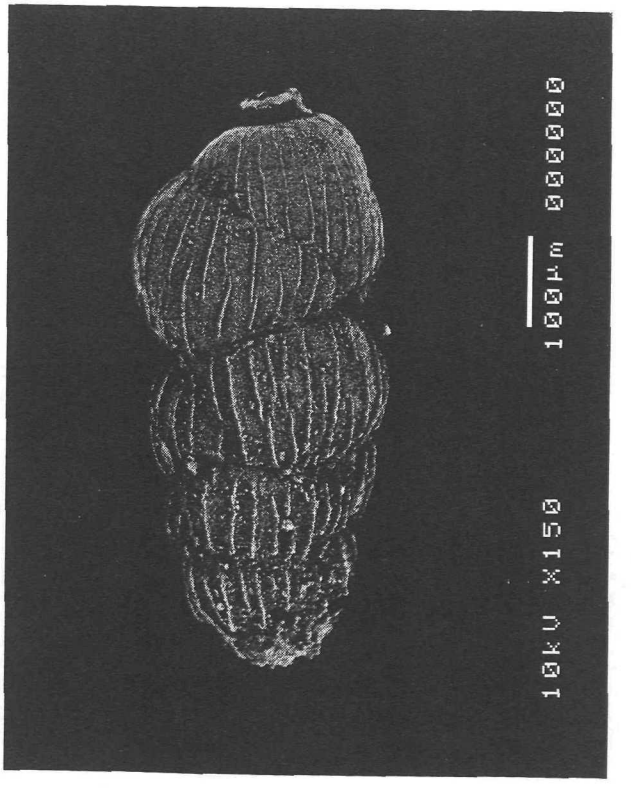

19. *Uvigerina hollicki*

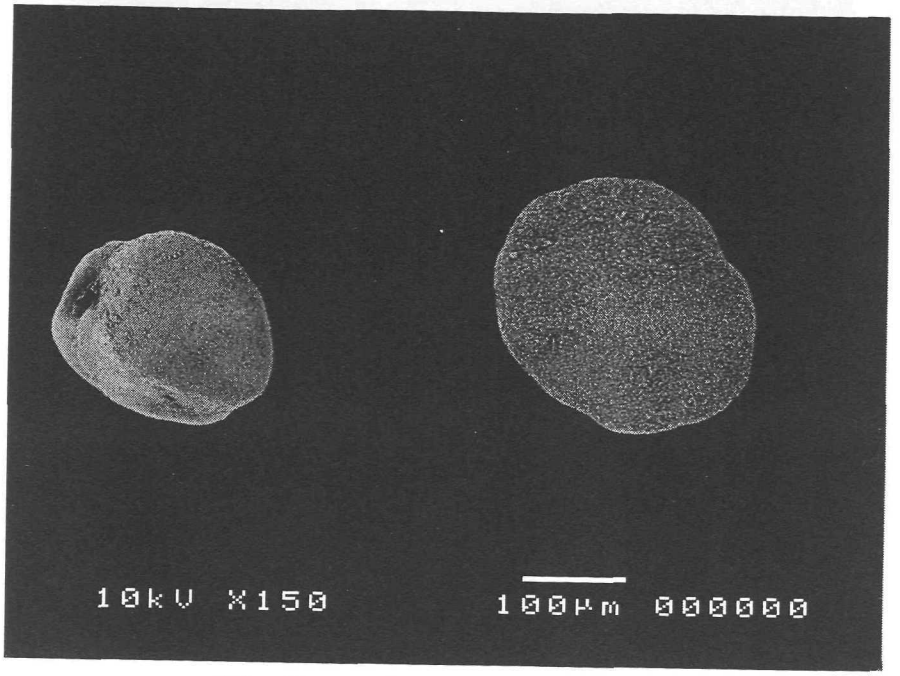

20. *Cassidulina laevigata*

21. *Ehrenbergina trigona*

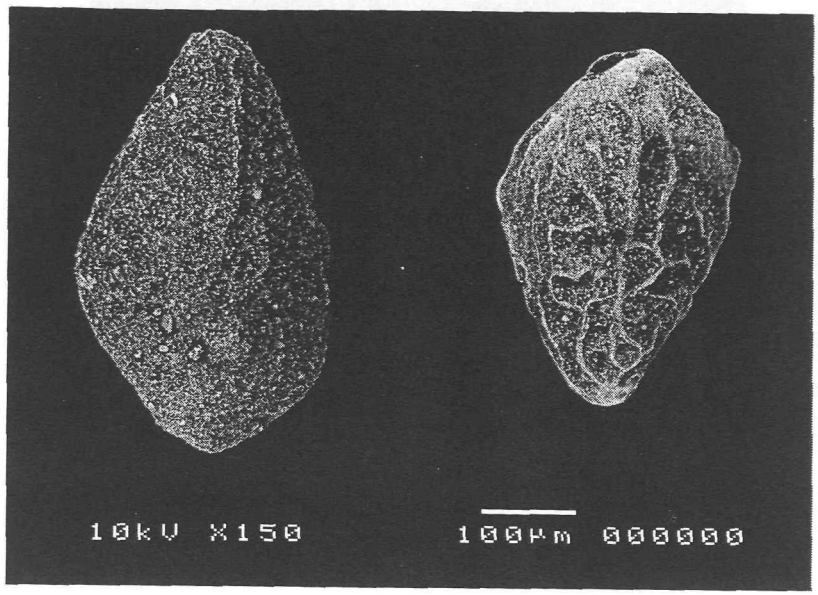

22. *Bolivina subreticulata*

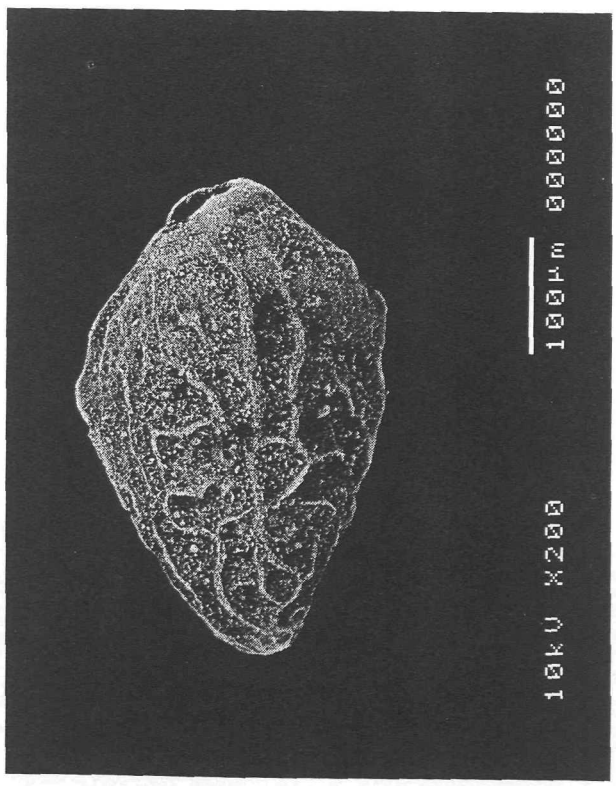

23. *Bolivina subreticulata*

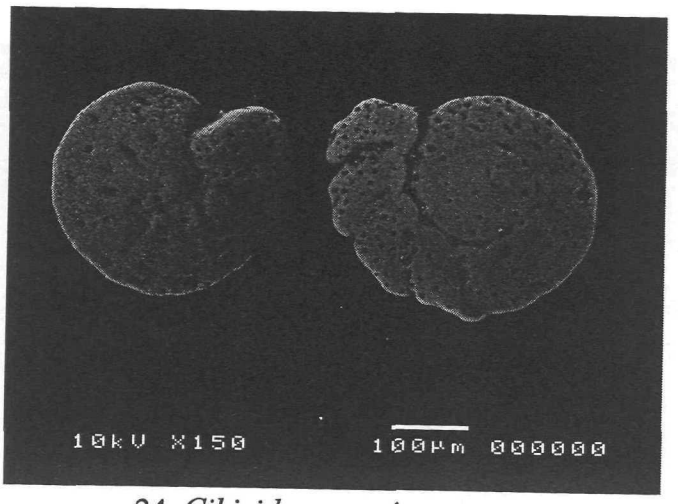

24. *Cibicides ungerianus*

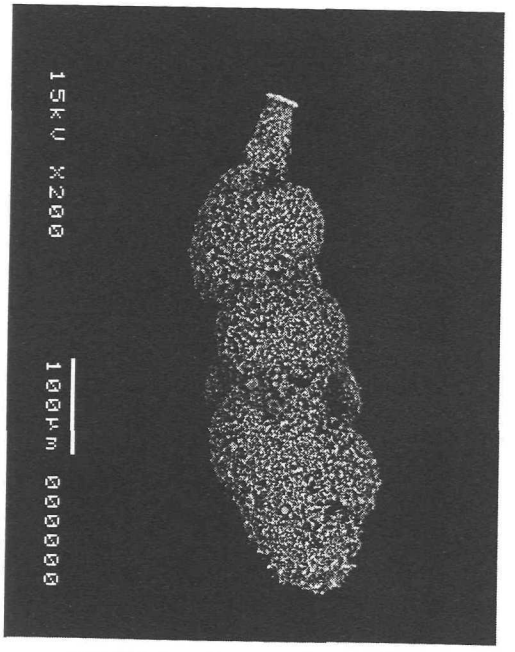

25. *Uvigerina proboscidia*

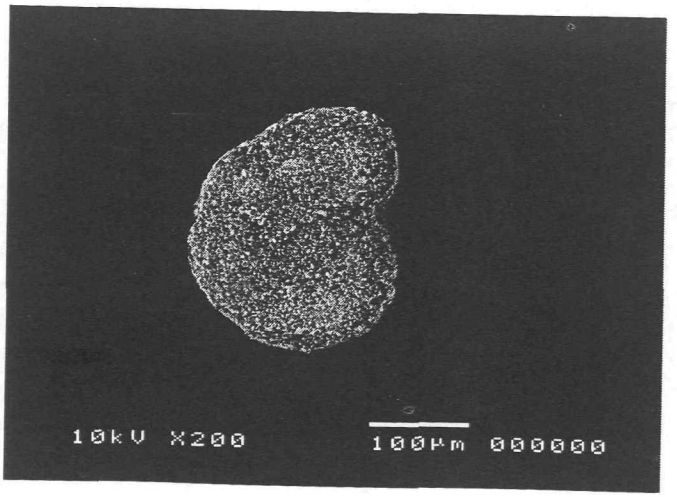

26. *Hyalinea balthica*

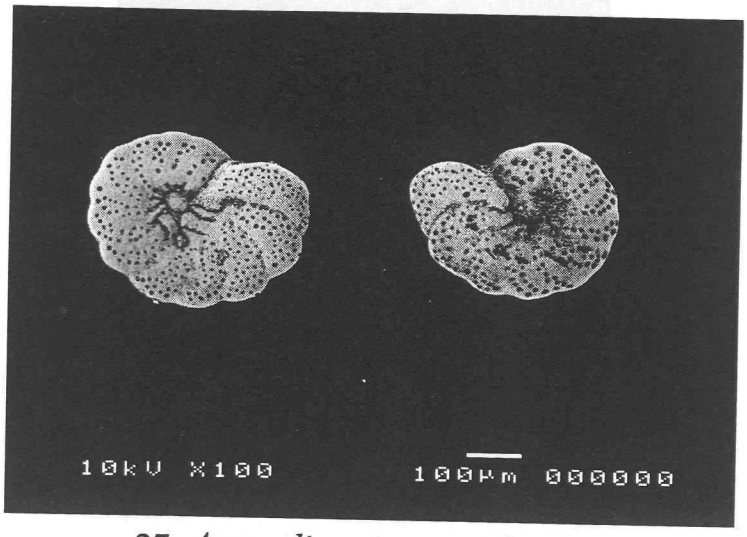

27. *Anomalina ammonoides*

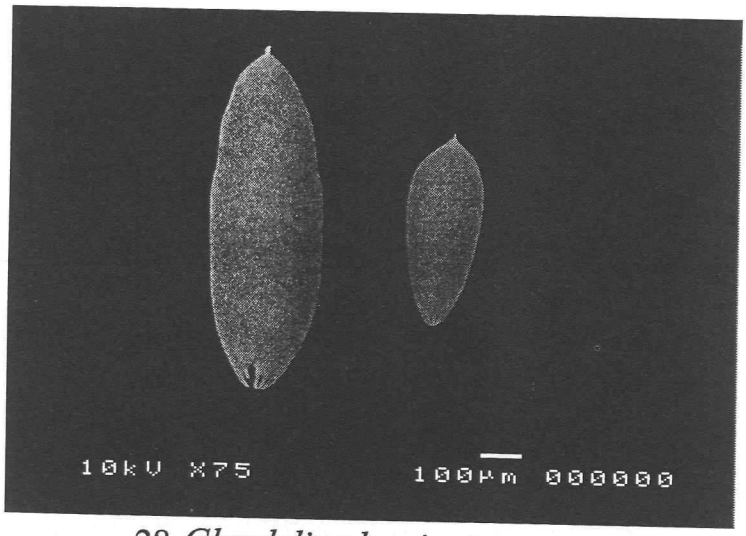

28. *Glandulina laevigata*

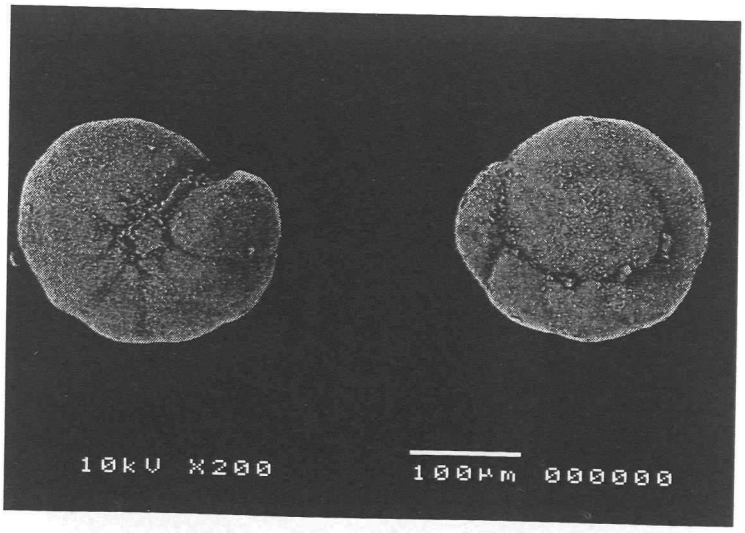

29. *Gyroidina altiformis*

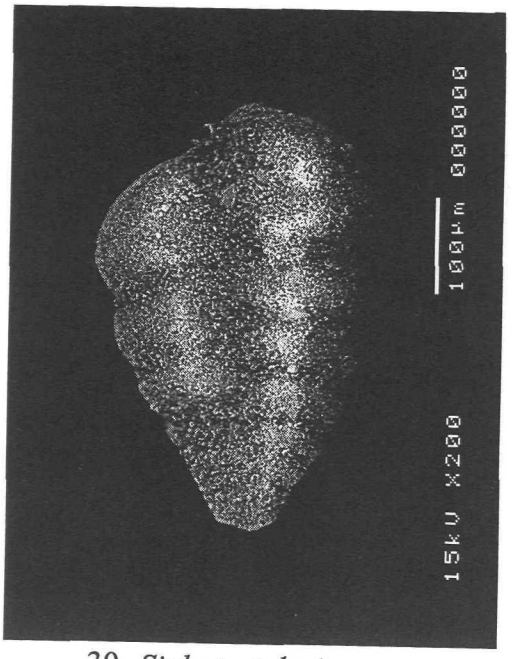

30. *Siphotextularia sp.*

31. *Siphotextularia sp.*

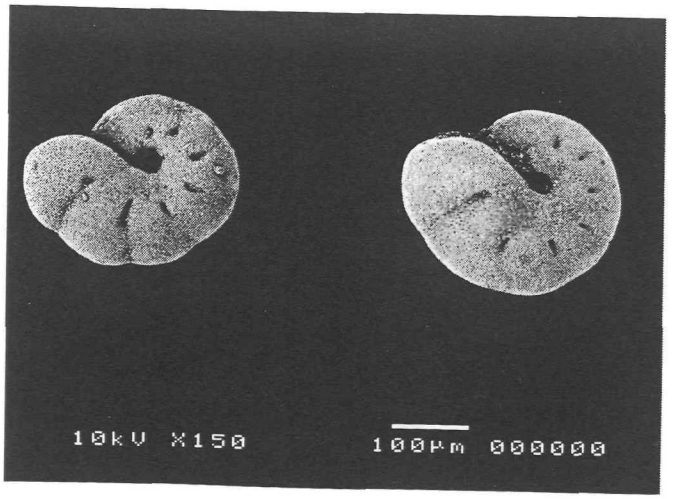

32. *Astrononion echolsi*

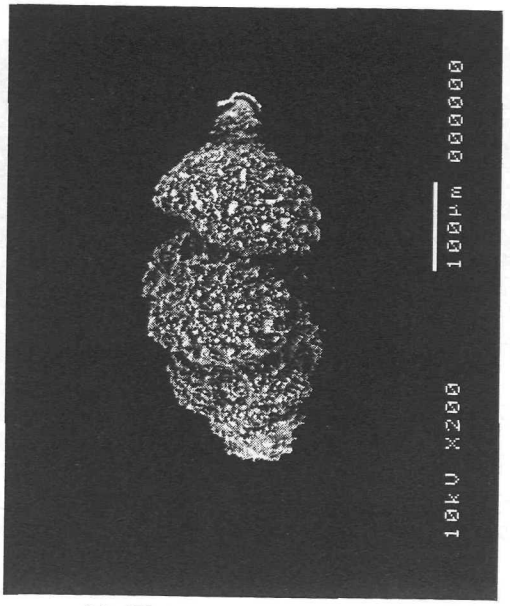

33. *Uvigerina porrecta*

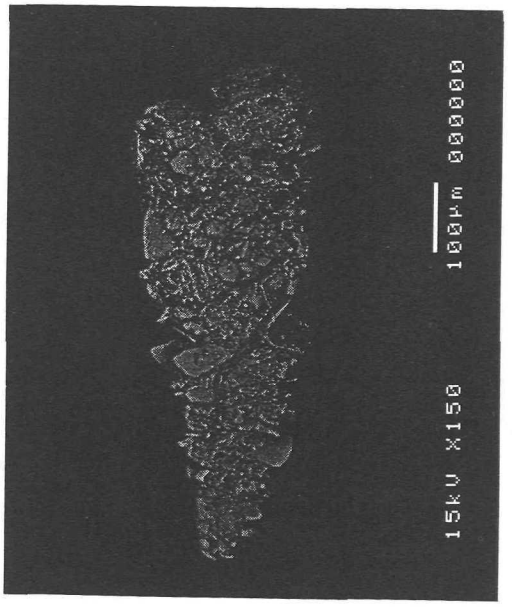

34. *Textularia fistulosa*

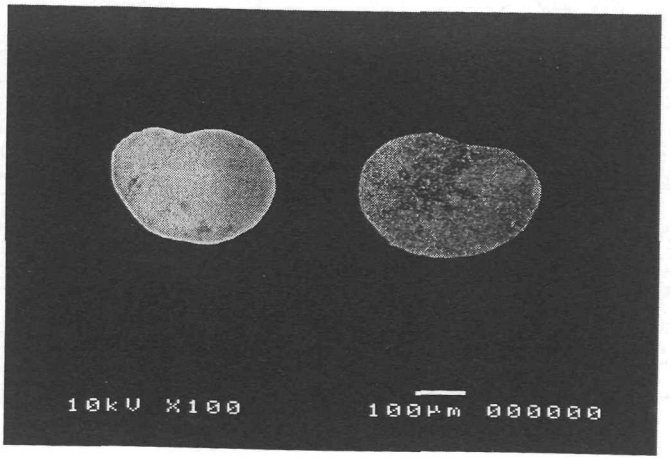

35. *Rosalina elegans*

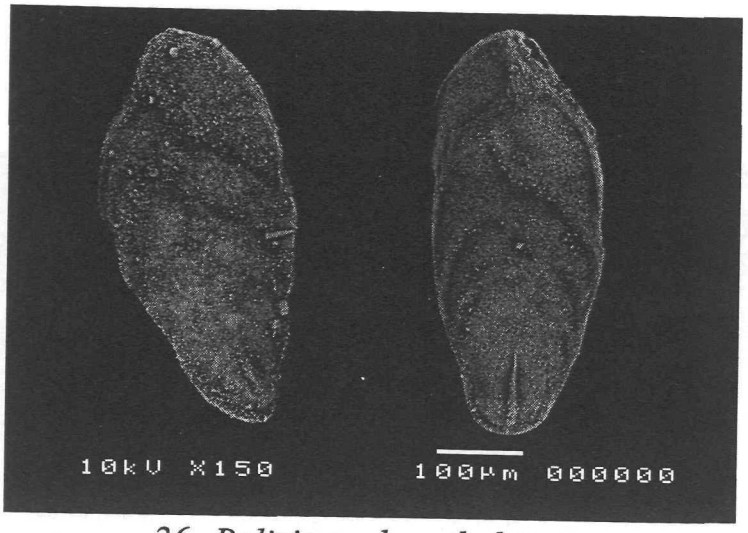

36. *Bolivina subspathulata*

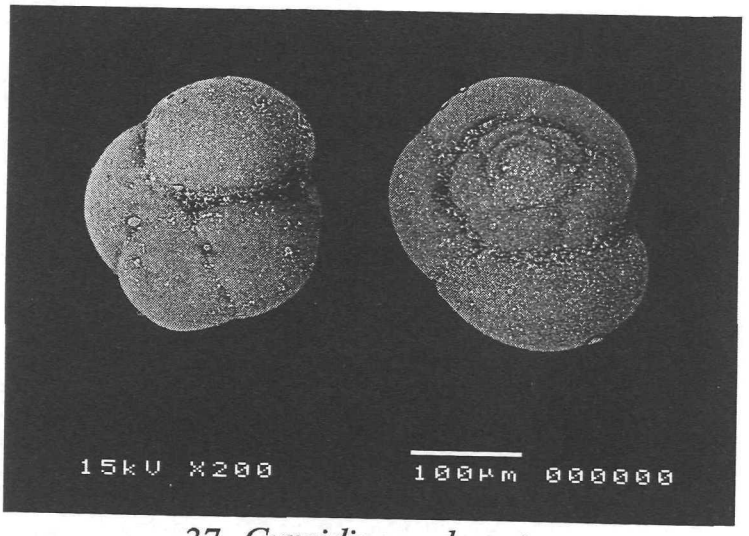

37. *Gyroidina umbonata*

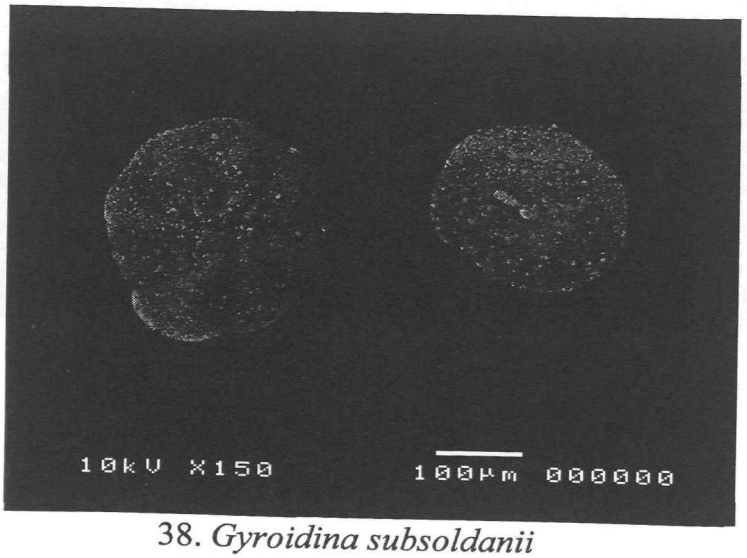

38. *Gyroidina subsoldanii*

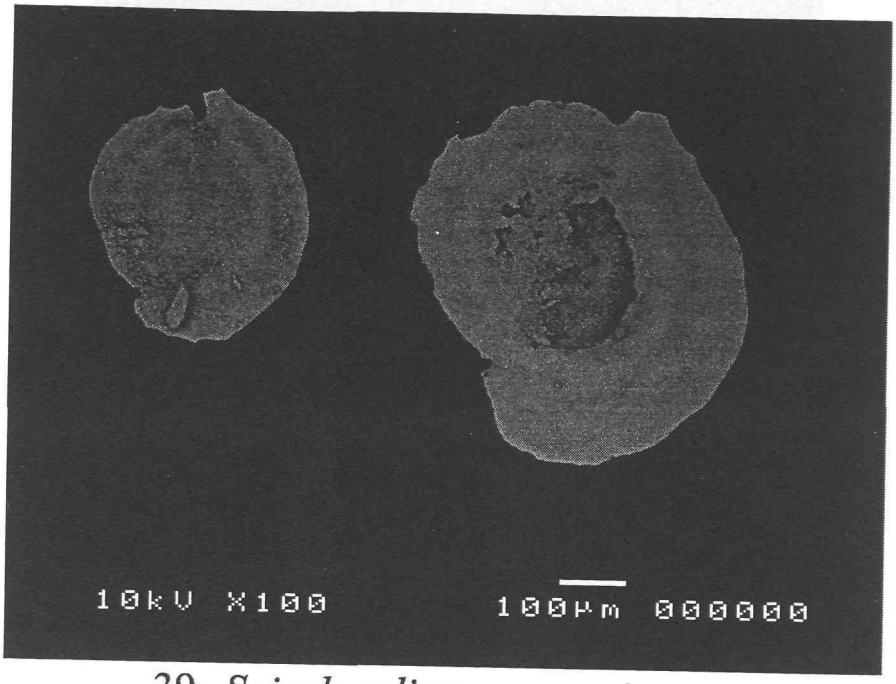

39. *Spiroloculina communis*

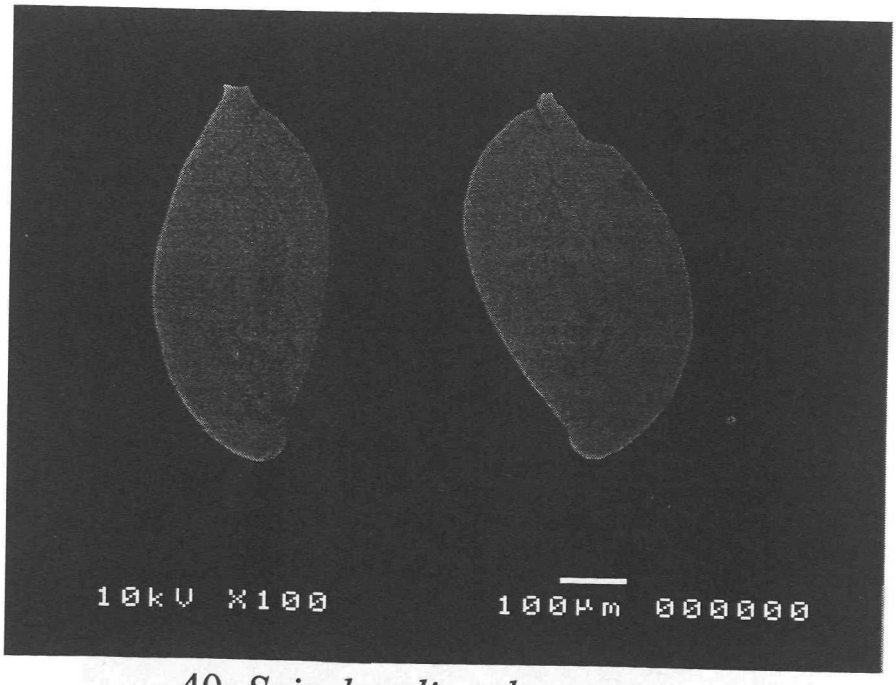

40. *Spiroloculina depressa*

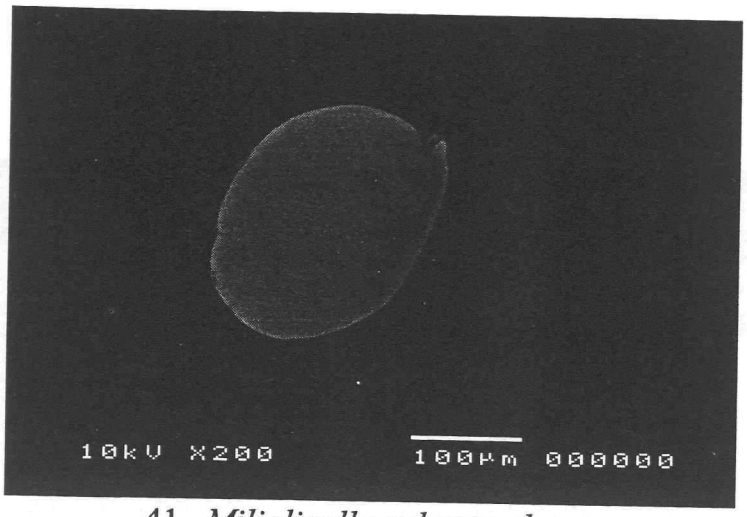

41. *Miliolinella subrotunda*

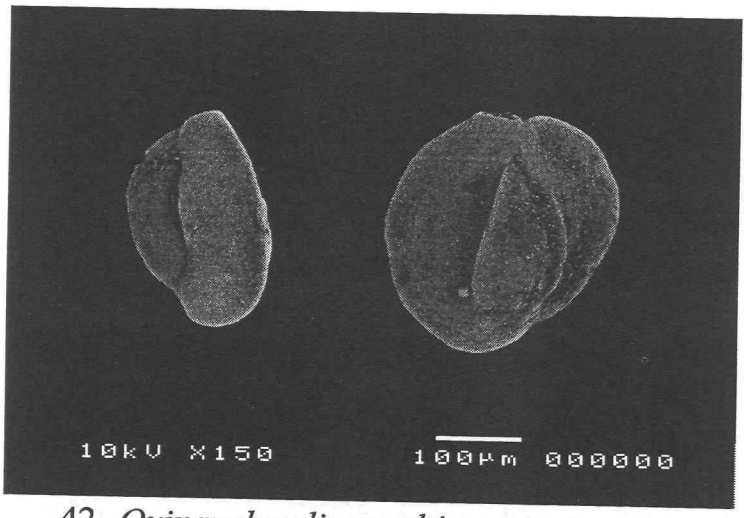

42. *Quinqueloculina multimarginata*

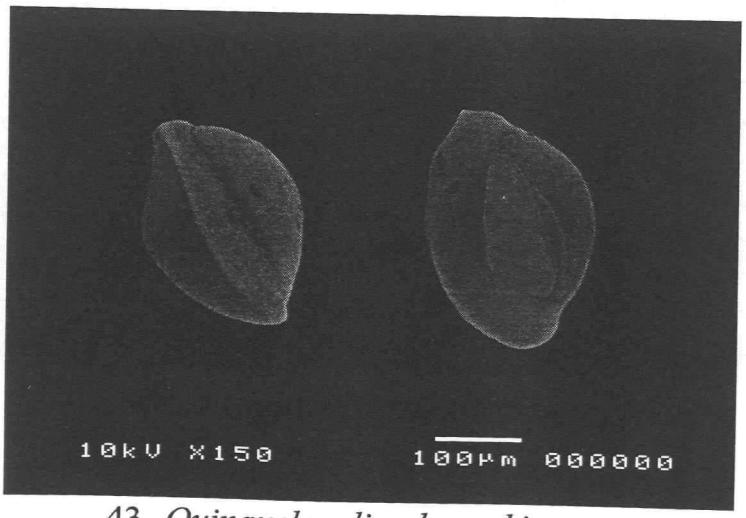

43. *Quinqueloculina lamarkiana*

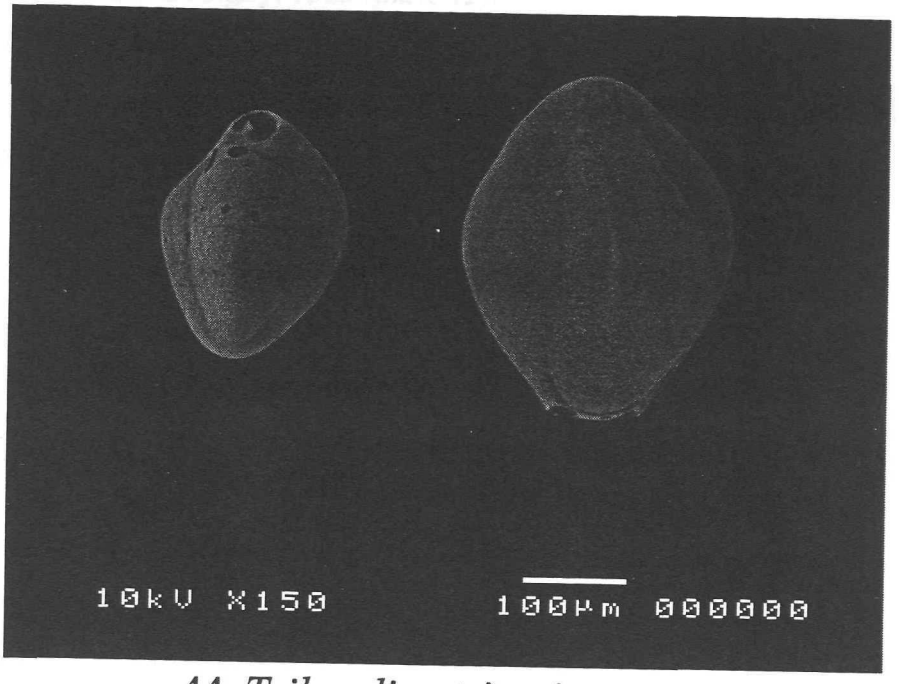

44. *Triloculina tricarinata*

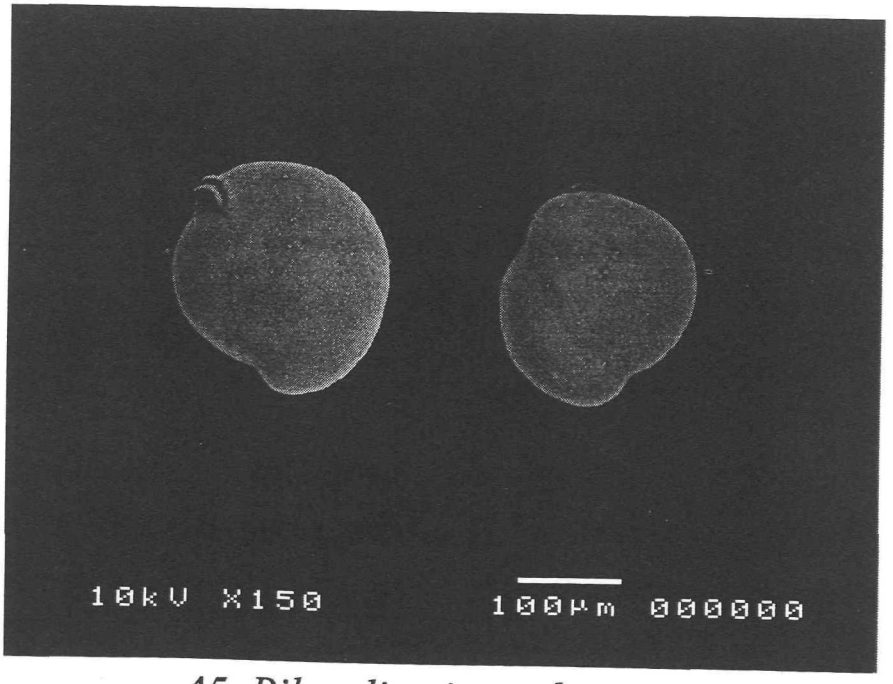

45. *Biloculina irregularis*

3. Ecology of the main planktonic foraminiferal species

***Globigerina bulloides* d'Orbigny, 1826 (plate 12).**

Typical transitional to polar species. Also characteristic of upwelling situations, regardless of their geographic position. Found mainly in and above the thermocline, and throughout the water column above 400 m (Hemleben et al., 1988).

***Globigerinella siphonifera* (d'Orbigny), 1939a (plate 6).**

[=*Globigerinella aequilateralis* (Brady), 1897]

[Other generic assignment: *Hastigerina*]

This species possesses two different symbiont types, both belonging to the chrysophytes. *G.siphonifera* has been often taxonomically misplaced in the genus *Hastigerina*, because of it's late adult planispirality, although the wall structure, spine morphology, cytoplasmic occurrence and presence of symbionts are different. This species is rather variable and shows several ecophenotypes (Parker, 1962). Its salinity and temperature tolerance have been determined as 27‰-45‰ and 11°-30°C respectively (Hemleben et al., 1988).

***Globigerinita glutinata* (Egger), 1893 (plate 7).**

[Other genus assigned: *Globigerina*, *Tinophodella*, *Globigerinoides*]

Juveniles are characterised by a planispirally coiled test with an equatorial aperture provided with a pronounced flange. During the neanic stage the aperture migrates to an umbilical position while the umbilicus closes rapidly. Terminal stages typically develope an umbilical bulla. *G.glutinata* occurs abundantly in tropical/subtropical to polar surface waters, and is the most widely distributed living species. It can tolerate a wide range of temperatures and salinities (Hemleben et al., 1988).

***Globigerinoides ruber* (d'Orbigny), 1839 (plate 1).**

G.ruber exhibits two varieties, a pink and a white form. Generally the pink form, pigmented by a reddish colour, is larger than the white one. The white form prefers lower temperatures. The symbionts are dinoflagellates similar to those occurring in the other *Globigerinoides* species and *O.universa*. *G.ruber* seems to be the shallowest dwelling species and, thus, it is very suitable for isotopic temperature investigations to estimate past sea surface temperature

and salinity. Its salinity and temperature tolerance are estimated as 22‰-49‰ and 16°-31°C, respectively (Hemleben et al., 1988).

***Globigerinoides sacculifer* (Brady), 1877 (plates 2 and 3).**

[=*Globigerinoides trilobus* (Reuss); *G.quadrilobatus*]

Tropical species. It lives in the photic zone, bears dinoflagellate symbionts, feeds mostly on calanoid copepods, exhibits a lunar reproductive cycle, and is most variable in its terminal chamber morphology. *G.sacculifer* is a euryhaline species which withstands salinities in a range of 24‰-47‰ and tolerates temperatures of 14°-31°C. This species includes specimens with a sac-like ultimate chamber (Hemleben et al., 1988).

***Globorotalia menardii* (Parker, Jones and Brady), 1865 (plate 13).**

[=*Globorotalia cultrata* (d'Orbigny)]

Tropical species characterised by the amount of its highly variable calcite crust; the test can be smooth without any additional calcite, or can be obscured by a thick calcite crust. G.menardii changes its habitat (eg. from shallow to deep water) during ontogeny. Omnivore, preferring phytoplankton (Hemleben et al., 1988).

***Globoturborotalia rubescens* Hofker, 1956 (plate 4).**

[Other generic assignment: *Globigerina*]

This species occurs in warm through temperate waters and occasionally rather frequently. In recent samples it is easily distinguished by its reddish pigment distributed throughout its test. This is in contrast to G.ruber where only the inner whorl is red (Hemleben et al., 1988).

***Globoturborotalita tenella* (Parker), 1958 (plate 5).**

[Other generic assignment: *Globigerinoides*]

This species is similar to *G.rubescens*, except for the pigmentation of the test and the secondary aperture on the last chamber. Pre-adult stages are difficult to distinguish from *G.rubescens* and *G.ruber* (Hemleben et al., 1988).

***Neogloboquadrina dutertrei* (d'Orbigny), 1839a (plate 11).**

[=*Globigerina eggeri*, Rhumbler]

[Other genera assigned: *Globigerina*, *Globoquadrina*]

Wide variation in number of chambers per whorl; the highest number are found in tropical waters and the fewest in transition regions. It lives almost exclusively on phytoplankton of which unicellular chrysophytes are very common. It tolerates salinities and temperatures of 25‰-46‰ and 13°-33°C respectively (Hemleben et al., 1988).

***Neogloboquadrina pachyderma* (Ehrenberg), 1861 (plate 10).**

[Other genera assigned: *Globigerina*, *Globoquadrina*, *Globorotalia*, *Turborotalia*]

Left coiling variety inhabits polar and subpolar regions. It lives within the sea ice and tolerates salinities up to 82‰ (Hemleben et al., 1988). The right coiling variety inhabits warmer regions and is discovered in the Gulf of Aden cores in this study.

***Orbulina universa* d'Orbigny, 1939a.**

O.universa is widely distributed from the tropics to sub-polar regions. It's size is correlated with temperature as well as food (nutrients). *O.universa* is carnivorous, especially in its spherical adult phase. It's ontogeny is rather peculiar as it passes through at least five different generic stages: 1) *Turborotalita?* during the juvenile stage; 2) *Globigerina* during the neanic stage; 3) *Globigerinoides* during the adult stage; 4) *Orbulina* (spherical) during the terminal stage, and perhaps 5) we could add the Biorbulina form as an ecotypic final stage. When sinking into deeper water *O.universa* forms a calcite crust. Reproduction follows the lunar period. It tolerates 23‰-46‰ salinity and 12°-31°C temperature (Hemleben et al., 1988).

***Turborotalia quinqueloba* (Natland), 1938 (plate 9).**

[Other generic assignment: *Globigerina*]

T.quinqueloba bears symbionts and lives mostly in the photic zone. The abundance of this species seems to decrease from higher to lower latitudes; simultaneously the pore distribution changes from more evenly distributed to more peripherally distributed. This spinose species is rather small and difficult to distinguish from other small species when observed at the neanic or early stage Hemleben et al., 1988).

4. Ecology of the main benthic foraminiferal genera and the Miliolids

Bolivina

Bolivina species are infaunal (Murray, 1991). They are found in cold, temperate and warm waters (Haynes, 1981; Murray, 1991). *Bolivina* species will tolerate oxygen levels as low as <0.1 $ml.l^{-1}$ (Boltovskoy, 1972). Bolivina are generally restricted to the neritic-mid bathyal depth (30-2000 m), with most highly ornamented forms concentrated in the neritic environments. However, some costate species do extend over the entire depth range (Pflum and Frerichs, 1976). The tests become larger with increased depth (Bandy, 1960). Pflum and Frerichs (1976) suggest that the test of *Bolivina albatrossi* increases in length and width ratio with increased depth. Some *Bolivina* species are also tolerant of high salinity eg. *Bolivina subreticulata* in the Red Sea (Gupta, 1994).

Brizalina

Brizalina species are infaunal (Murray, 1991). They are found in cold, temperate and warm waters (Haynes, 1981; Murray, 1991) and will tolerate oxygen levels as low as <0.1 $ml.l^{-1}$ (Boltovskoy, 1972). The tests become larger and more ornamented with increased depth (Bandy, 1960).

Bulimina

Bulimina species are infaunal, and are found in cold and temperate waters (Haynes, 1981; Murray, 1991). A study by Burgess and Schnitker (1990) suggests that temperature has an effect on the morphotype *Bulimina* aculeata-marginata complex. It appears that *B.marginata* dominates in cooler water, while *B.aculeata* dominates in warmer water. The tests become larger and more ornamented with increased depth (Bandy, 1960).

Cancris

Cancris species are motile either on or within soft muddy substrates. Shelf dwelling species tend to be compressed and sharp edged, however, deeper dwellers tend to be rounded and globose (Bandy, 1960a). They are typically found in temperate and subtropical waters (Murray, 1991).

Cassidulina

Cassidulina species are infaunal (Murray, 1991). They are also considered to be indicative of cold water (eg. *Cassidulina laevigata* (Pendlebury, 1974)) and will tolerate sub-zero temperatures. They are most common in temperate and high latitude environments (Haynes, 1981; Murray, 1991). Limbate, sharp-edged species of *Cassidulina*, typical of the inner shelf, are replaced by large, globose species at greater depths. In the bathyal zone the test tends to uncoil giving rise to *Cassidulinoides* and *Ehrenbergina* (Bandy, 1960). Smith (1964) suggests that *Cassidulina laevigata* will develop a carina with increased water depth.

Cibicides

Cibicides species are generally found in muddy/silty-sand substrate on the shelf (Haynes, 1981). They are infaunal and are typical of cold or temperate waters (Haynes, 1981; Murray, 1991).

Eponides

Eponides species are typically found in clear water, with a shelly-sandy substrate, or in a reef or shallow open-marine environment (Rose and Lidz, 1977; Haynes, 1981). They are epifaunal and are generally found in cold or temperate waters (Haynes, 1981; Murray, 1991).

Gyroidina

Gyroidina species have mobile habitats either on or within soft muddy substrates (Haynes, 1981). Shelf dwelling species tend to be compressed and sharp edged, however, deeper dwellers tend to be rounded and globose (Bandy, 1960a). They are typically found in cold waters (Murray, 1991).

Hyalinea

Hyalinea species have mobile habitats either on or within soft muddy substrates (Haynes, 1981). Shelf dwelling species tend to be compressed and sharp edged, however, deeper dwellers tend to be rounded and globose (Bandy, 1960a). They are typically found in cold and temperate waters (Murray, 1991). *Hyalinea balthica* displays a size decrease and becomes less ornate in a deeper water environment (Colom, 1970).

Uvigerina

Uvigerina species are infaunal (Murray, 1991) and are generally considered to be indicative of cold water and will tolerate sub-zero temperatures (Haynes, 1981; Murray, 1991). They will also tolerate low oxygen levels (<0.14 $ml.l^{-1}$), although the fauna may be impoverished and stunted showing deformities of the test (Lutze, 1978). The tests become larger and more ornamented with accentuation of spines and costae in deeper water environments (Bandy, 1960; Lamb and Miller, 1984). *Uvigerina* species build their test in isotopic equilibrium with sea water (Shackleton, 1974) making them useful for palaeoenvironmental interpretation.

The Miliolids

Miliolids flourish at shallow to abyssal depths. They display a broad temperature tolerance occupying niches in cold, temperate and tropical environments (Murray, 1991). This group is also found to occupy normal marine and hypersaline (up to 70 ‰) conditions (Haynes, 1981). Miliolids tend to dominate the microfaunas in tropical carbonate environments eg. Persian Gulf and Carribean (Greiner, 1969). *Pyrgo* and *Biloculinella* species occur at abyssal depths and may have infaunal habitat here. It is also suggested that *Pyrgo* is tolerant of low oxygen concentrations (Parisi, 1983). *Quinqueloculina* and *Triloculina* are typical of shallow water environments. The specimen *Triloculina tricarinata* is suggested to be larger in cold water than in warm (Boltovskoy *et al.*, 1991). Species may live on sea grass and graze on unicellular algae and bacteria, or live within a stable sedimentary substrate. Few species will dwell in sediment that is too clean and active to provide food. *Miliolinella* is considered as an epiphyte and is indicative of cooler water (Brasier, 1975c).

5. Taxonomy of planktonic foraminifera

***Globigerina bulloides* d'Orbigny, 1826 (plate 12).**

Test is globular and trochospirally enrolled with spherical to ovate chambers, enlarging rapidly as added, with commonly only 3 to 5 in the last whorl. Sutures are distinct and depressed. The umbilicus is open, and the periphery rounded with a lobulate peripheral outline. Wall is calcareous and perforate with cylindrical pores. In life, the surface has numerous long slender, round spines of circular cross section. The short blunt spine remnants result in a hispid wall surface. The primary aperture is a high umbilical arch that may be bordered by an imperforate

rim or narrow lip, no secondary apertures are found (Loeblich and Tappan, 1988).

***Globigerinella (Beella) digitata* (Brady), 1879.**

G.digitata with its extreme digitate chambers occurs rather often in the Mediterranean but seems to be restricted to deeper water.

The test is trochospirally coiled, with a strongly convex spiral side. Early chambers are globular and increase rapidly in size as added. Those of the final whorl are radially elongated and subconical. Sutures are radial and depressed. The umbilicus is open, and the periphery rounded with a lobulate to stellate peripheral outline. The wall is calcareous and perforate. The pores may be grouped in clusters, and the surface between the pores is covered by irregular ridges or costellae that may represent spine bases. The aperture is umbilical in position forming a wide open arch which is bordered by a recurved lip (Loeblich and Tappan, 1988).

***Globigerinella siphonifera* (d'Orbigny), 1939a (plate 6).**

[=*Globigerinella aequilateralis* (Brady), 1897]

[Other generic assignment: *Hastigerina*]

The test is a low trochospiral coil in the early stage, becoming nearly planispiral and evolute in later life. The globular to ovate chambers enlarge rapidly, with about four to six in the final whorl. The sutures are radial and depressed. The periphery is rounded with a lobulate peripheral outline. The wall is calcareous and densely perforate with numerous circular pores in slight depressions of the surface. The interpore areas are smooth and set with numerous fine elongate spines that are circular in section at the base. Shorter spines remain circular in section but more elongate ones become triradiate distally, with a smooth and unbarbed surface. The aperture is interiomarginal, a large open equatorial arch that may be asymmetrical with respect to the plane of coiling (Loeblich and Tappan, 1988).

***Globigerinita glutinata* (Egger), 1893 (plate 7).**

[Other genus assigned: *Globigerina*, *Tinophodella*, *Globigerinoides*]

Microperforate test. Test small low to medium trochospiral, equatorial periphery lobulate,

chambers spherical to subglobular, three to four in the last whorl, increasing rapidly in size; sutures nearly radial, depressed; surface smooth with irregularly distributed fine perforations largely covered by small, subconical tubercles or crystallites; primary aperture interiomarginal, umbilical, a low arch with a thin lip. In some individuals covered bu an irregular bulla expanding along the earlier sutures with numerous infra laminal supplementary apertures bordered by tiny arched or tubulose openings

***Globigerinoides conglobatus* (Brady), 1879.**

G.conglobatus occurs in medium abundances in subtropical waters. It lives in the photic zone as it is associated with dinoflagellate symbionts of the same type as the ones that occur in *G.ruber*, *G.sacculifer*, and *O.universa*. This is the only *Globigerinoides* species known to form a calcite crust. Its ontogeny is more comparable to *O.universa* and *G.siphonifera*; whereas the surface morphology, including the spines, is similar to other globigerinoids.

Test large, tightly coiled trochospiral subglobular to subquadrate, three - three and a half chambers in the last whorl increasing very slowly in size as added; sutures distinctly depressed, almost radial; surface coarsely perforated with spines and spine bases; umbilicus narrow; primary aperture interiomarginal, umbilical, a long, low asymmetric arch bordered by a thin rim; sutural supplementary apertures, small, irregular on thew spiral side

***Globigerinoides ruber* (d'Orbigny), 1839 (plate 1).**

Test medium low to high trochospiral with three subspherical chambers in the final whorl, increasing moderately in size; sutures radial, distinctly depressed; surface coarsely perforate; thin secondary calcite crusts surround the spine bases; calcite crust developing between the spine bases form a honeycomb-shaped surface; umbilicus narrow, primary aperture interiomarginal, umbilical with a wide arched opening bordered by a rim, with two supplementary sutural apertures situated opposite sutures of earlier chambers (van Leeuwen, 1989).

***Globigerinoides sacculifer* (Brady), 1877 (plates 2 and 3).**

[=*Globigerinoides trilobus* (Reuss); *G.quadrilobatus*]

Test medium sized with a low spire, periphery rounded and lobulate with four more or less irregular chambers forming basal contour. The wall is coarsely punctate, reticulate and thick. Chambers rapidly increase in size with a spiral organization. A secondary apertural formation of adults sharply defined on the dorsal side. Sutures are deeply depressed. The umbilicus is prominent in both edge and ventral views (van Leeuwen, 1989; McCulloch, 1977).

***Globorotalia anfracta* (Parker), 1967 (plate 8).**

[Other genus assigned: *Turborotalita*, *Tenuitella*]

Non spinose, with normal sized pores. This species is separated from *Globorotalia* because of its streptospiral coiling during the juvenile stage and the presence of unique pustules, resembling shark teeth, in front of the aperture (Hemleben et al., 1988).

Test small, very low trochospiral, spiral side almost flat, lobulate in equatorial profile; axial profile rounded, the final chamber somewhat compressed; chambers inflated four to five in the final whorl, increasing slowly as added; sutures on spiral side and umbilical side radial and depressed; surface smooth, translucent, covered with fine pustules. Aperture a low arch with a broad lip.

***Globorotalia crassaformis* (Galloway and Wissler), 1927.**

[=*Globorotalia punctulata*]

[Other genus assigned: *Globorotalia crotonensis* Conato and Follador, 1967; *G.crassula* Cushman, Stewart and Stewart, 1930]

This species has rarely been observed in the living state (Hemleben et al., 1988).

Test low trochospiral, spiral side almost flat, umbilical side strongly convex, equatorial periphery slightly lobulate, subquadrate; axial periphery planoconvex, subacute to subrounded; chambers compressed, four in the final whorl, increasing rapidly in size; sutures on the spiral side curved, depressed,; on umbilical side almost radial, depressed; surface finely perforate, pustulate on umbilical as well as spiral side; umbilicus narrow, deep; aperture interiomarginal, extraumbilical, a low - arched slit bordered by a lip.

***Globorotalia menardii* (Parker, Jones and Brady), 1865 (plate 13).**

[=*Globorotalia cultrata* (d'Orbigny)]

The test is calcareous, compressed, biconvex and trochospiral with a strongly lobulate periphery. The wall is white to opaque to semihyaline finely perforate. The dorsal side is evolute and slightly depressed centrally presenting two whorls of arcuate chambers increasing rapidly in size with variable in height. Four or five chambers in the last formed whorl. The sutures are dorsally limbate, broad and slightly depressed curved bands continuous with peripheral carina. The ventral side is involute. The sutures are depressed and radiate. The aperture is interiomarginal with an extraumbilical arch lip (McCulloch, 1977).

***Globorotalia scitula* (Brady) 1882.**

[Other genus assigned: *Globorotalia bermudezi* Roegl and Bolli, 1973]

Occurs in some temperate regions and at times with high frequency. It appears always as a very thin shelled specimen living at spring time close to the surface and then sinks to deep water (Hemleben et al., 1988).

The test is small, calcareous, biconvex and trochospiral, with a lobulate acute to rounded periphery. The wall is semihyaline and prominently perforate. The dorsal side is evolute with about three whorls of subsemicircular inflated chambers rapidly increasing in size. There are five chambers in last formed whorl. The sutures are dorsally curved and depressed. Ventral sutures are radiate and depressed. The ventral side is involute. The aperture is interiomarginal, extraumbilical with a sutural shallow triangular lip and a short narrow umbilical flap (McCulloch, 1977).

***Globorotaloides hexagonus* (Natland), 1938.**

[Other assigned genus: *Globoquadrina*]

Non spinose species. Indo-Pacific (Hemleben et al., 1988).

Test very low trochospiral, spiral side almost flat; equatorial periphery lobulate, axial periphery broadly rounded; chambers spherical, five in the final whorl, increasing rapidly in size a s added; sutures on both spiral and umbilical sides slightly curved to nearly radial,

depressed; surface distinctly cancellate, with large pores set in deep hexagonal funnel like pore pits; umbilicus fairly wide, partly covered by apertural plate; aperture interiomarginal, umbilical-extraumbilical, a very low arch bordered by a distinct apertural plate or thick rim.

***Globoturborotalia rubescens* Hofker, 1956 (plate 4).**

[Other generic assignment: *Globigerina*]

Test trochospiral with globular chambers, closely appressed and enlarging rapidly. Few chambers per whorl. The sutures are radial to curved and depressed. Periphery is rounded, and the peripheral outline is lobulate. Wall is calcareous and perforate, the pores with distinct pore pits resulting in a cancellate surface. True spines of circular cross section. The aperture is umbilical, a small to high arch bordered by a distinct rim (Loeblich and Tappan, 1988).

***Globoturborotalita tenella* (Parker), 1958 (plate 5).**

[Other generic assignment: *Globigerinoides*]

This species is similar to *G.rubescens*, except for the pigmentation of the test and the secondary aperture on the last chamber. Pre-adult stages are difficult to distinguish from *G.rubescens* and *G.ruber* (Hemleben et al., 1988).

***Neogloboquadrina dutertrei* (d'Orbigny), 1839a (plate 11).**

[=*Globigerina eggeri*, Rhumbler]

[Other genera assigned: *Globigerina*, *Globoquadrina*]

The non-spinose test is medium to large in size, the largest diameter, measured roughly parallel to the suture between the ultimate and penultimate chamber, is generally more than 0.30 mm. Chambers are coiled in a low to moderately high trochospire and their number in the last whorl varies between 4 and 7. Aperture is umbilical to umbilical-extraumbilical and a toothplate may be present. Coiling is dextral (van Leeuwen, 1989).

***Neogloboquadrina pachyderma* (Ehrenberg), 1861 (plate 10).**

The non-spinose test is compact (almost square in shape), small-sized, low trochospiral, with the largest diameter generally less than 0.30 mm. Generally four to five chambers in the last whorl. The aperture is umbilical to umbilical/extraumbilical, which is usually bordered by a

rim-like lip (van Leeuwen, 1989).

***Orbulina universa* d'Orbigny, 1939a.**

The test is spherical in shape. The wall is calcareous and perforate with 2 pore classes, the more numerous smaller ones interspersed among the fewer considerably larger ones. The earliest whorl non spinose and without sutural apertures. Later chambers and adult test have long monocrystalline, circular section, spines arising from a terraced base. The primary aperture in the young stage is interiomarginal and umbilical, with an irregular imperforate bordering lip. The final chamber has sutural supplementary openings, the larger series of pores possibly also representing an areal aperture (Loeblich and Tappan, 1988).

***Pulleniatina obliquiloculata* (Parker and Jones), 1865.**

Non spinose. This species is similar to *G.inflata* in relation to the adult wall structure. A final covering forms a smooth veneer on top of the calcite crust. The veneer is thin and finely crystalline, whereas the calcite crust itself can be very thick and coarsely crystalline. However, pre-adult and early adult stages suggest a closer relationship to *Neogloboquadrina spp* (Hemleben et al., 1988).

Test medium, initially trochospiral, later streptospiral, equatorial periphery slightly lobulate, axial periphery broadly rounded, chambers subspherical, about five to six in the final whorl, increasing slowly in size except for the last chamber, which is abruptly more embracing; sutures weak, on spiral side curved, gently depressed; on umbilical side radial, depressed; surface smooth, covered with thick cortex, granular open early chambers facing the aperture; umbilicus covered by last chamber; aperture interiomarginal, extraumbilical-umbilical, a rather medium arch along the base of the final chamber extending up to the periphery of the preceding whorl

***Turborotalia quinqueloba* (Natland), 1938 (plate 9).**

[Other generic assignment: *Globigerina*]

Spinose species, rather small. Abundance of the species decreases from high to low latitudes. Test small, slightly compressed, trochospiral, five chambers in the final whorl, rapidly

increasing in size as added; chambers inflated, subglobular; final chamber distinctly spinose, early chambers with reticulate ridges and pore pits; sutures radial, depressed; aperture an elongate slit often at the end of flap like extension of the final chamber (McCulloch, 1977).

6. Taxonomy of Benthic Foraminifera.

***Alliatinella gedgravensis* (Carter), 1957.**

{=*Fawcettia panayensis* McCulloch, 1977; *Subcushmanella differens* McCulloch, 1977; *Subcerobertina simplissima* McCulloch, 1977}

Test articulate in outline, somewhat compressed and biconcave, resembling *Alliatinella* but distinctly trochospiral, small accessory chambers developed over the sutures on the umbilical side, reflecting the position of attachment of the internal partition of inverted V shape, crossing the chamber obliquely to attach to the interior wall of the septal face where its position is marked externally by a groove from the areal opening to the proximal chamber margin near the umbilicus, then extending back to attah to the base of the previous septum, sutures distinct, white in colour, later ones slightly depressed, periphery broadly rounded; wall aragonitic, finely perforate, lamellar; aperture a low interiomarginal and equatorial slit, with a rounded areal aperture as in *Alliatinella* but slightly offset towards the umbilical side, aperture sealed in the final chamber by a thin calcareous plate that is resorbed when new chamber is added to leave a functional areal foramen (Loeblich and Tappan, 1988; Ellis and Messina, 1968).

***Amphycorine scalaris* (Batsch) Parr, 1950.**

Test short and thick, subcylindrical, usually consisting of two or three chambers, each about as long as broad, broadening in the later chambers; surface ornamented by numerous strong costae, most of which extend the full length of the test, overhanging the apiculate base as a series of irregular spines; apertural end produced, annulate, the aperture terminal and circular (Ellis and Messina, 1968)

***Anomalina ammonoides* (Reuss) var. *umbilicatula* Vasilenko and Myatliuk, 1447 (plate 27).**

{*Rosalina ammonoides* Reuss Beissel, 1891; *Anomalina ammonoides* (Reuss) Dain, 1934.}

This form is characterised by the subinvolute test, consisting of two and one-half to three narrow whorls, with a rather flat dorsal side and an inflated ventral side. The final whorl consists of eleven to thirteen convex chambers. A deep, broad umbilicus is situated in the centre of the ventral side, a characteristic feature of this species. Sutures raised, limbate, not very broad. Periphery rounded. Wall matte (Ellis and Messina, 1968).

***Astacolus crepidulatus* (de Montfort), 1808.**

{=*Nautilus crepidula* Fichtel and Moll, 1798; *Cochlidion alexandrae* Zalessky, 1926; *Polymorphinoides spiralis* Cushman and Hanzawa, 1936; *Saccullariella ensis* Wedekind, 1937; *Cristellaria hermanni* Andreae, 1898; *Cristellaria recta*, d'Orbigny, 1840.
Astacolus = *Chrysolus* de Montfort, 1808; *Crepidulina* de Blainville, 1824; *Cochlidion* Zalessky, 1926, *Polymorphinoides* Cushman and Hanzawa, 1936; *Saccullariella* Wedekind, 1937; *Gladiaria* Wick, 1939; *Enantiovaginulina* Marie, 1941; *Lenticulina (Astacolus)* Barnstein, 1948.}

Test elongate to ovate in outline, flattened, chambers numerous, broad and low, added on a slightly curved axis or may be distinctly enrolled in the very early stage, later uncoiling, with strongly oblique, straight to curved or sinuate sutures, periphery rounded to angular; wall calcareous, perforate, radial in structure, surface smooth; aperture radiate, at the dorsal angle. L. Jurassic to Holocene; cosmopolitan (Loeblich and Tappan, 1988).

***Astrononion echolsi* Kennett, Corlis, 1979 (plate 32).**

{*Astrononion sp.* van Leeuwen, 1989}

Test moderately compressed and small, maximum diameter generally less than 0.32 mm. The last whorl is composed of seven or eight chambers, which increase gradually in size. The periphery is (broadly) rounded and slightly lobulate. The aperture is a low opening at the base of the last chamber and extends from umbilicus to umbilicus; the apertural face is broader than high and distinctly convex. The complex of chamber flaps and secondary chamberlets is distinctly developed. The secondary openings are pits in the sutures, which are placed closer to the umbilicus than to the periphery of the test. The sutural areas in between these openings and the centre are covered by imperforate umbilical flaps. Beyond the openings, the sutures are somewhat depressed, broad and imperforate (van Leeuwen, 1989).

***Biloculinella irregularis* d'Orbigny, 1839 (plate 45).**

{=*Pyrgoella irregularis* d'Orbigny, 1839; *Biloculina* Brady, 1884; *Nummoloculina* Thalmann, 1932, Barker, 1960, Hofker, 1976, and van Marle, 1991.} (Jones, 1994)

***Bolivina albatrossi* Cushman, 1922.**

Only the lower part of the test is covered with a reticulate network; in most individuals the later chambers have a smooth outer surface. Elongated test form, rounded in transection (Verhallen, 1991).

***Bolivina subreticulata* Parr, 1932 (plates 22 and 23).**

{=*Brizalina subreticulata* (Parr) Parr, 1932, Belford, 1966, and van Marle 1991; *Bolivina reticulata* Brady, 1884; *Latibolivina subreticulata* (Parr) Srinivasan 1966.}

Test small, in front view rhomboid, thickest along the median line and with sharp edges; chambers numbering about fourteen in the megalospheric form, but more in the microspheric form, much longer than wide, slightly inflated in the later portion of the test; sutures distinct, limbate, sinuous, with processes of varying length on the posterior margin; wall calcareous, finely perforate, and ornamented in the early part of the test with a few irregular costae, later with a network of raised lines formed by the projecting processes extending more or less across the face of each chamber; aperture bolivine, elongate-oval (Jones, 1994; Ellis and Messina, 1968).

***Bolivina subspathulata* Boomgaart, 1949 (plate 36).**

Test elongate, rather strongly compressed, about two and a half times as long as broad, regularly tapering to the subacute initial end; greatest breadth nearest the apertural end; periphery acute or even slightly keeled, chambers eight pairs, distinct, much broader than high, rapidly increasing in size, the youngest chamber tending to become uniserial; sutures distinct, slightly limbate, but with triangular widened portions alternating on either side of the median line, curved, especially toward the periphery; wall smooth, distinctly perforate; aperture narrow, elongate, reaching the inner margin of the last former chamber (Ellis and Messina, 1968).

***Bolivina italica* Cushman, 1936 (plate 15)**

Elongated test, numerous small, inflated chambers covered with pustules or blunt spines. Test elongate, somewhat fusiform, greatest breadth usually somewhat below the last formed chambers, in adult slightly compressed, periphery broadly rounded, initial end typically with a short, stout spine; chambers distinct, inflated, about as high as broad, increasing rather uniformly in size; sutures distinct, very strongly depressed throughout, nearly horizontal or forming a slight angle; wall coarsely perforate, otherwise smooth; aperture very broadly rounded, often nearly circular with a slight lip (Verhallen, 1991; Ellis and Messina, 1968).

***Bolivina amygdalaeformis* (Brady), 1881.**

{= *Saidovina amygdalaeformis* Brady, 1881

Bolivina = *Loxostomum* Barker, 1960.}

Test oval, compressed, almond shaped; ends obtuse or rounded, periphery rounded. Segments few, septation obscured by a surface ornamentation of stout, branching, longitudinal costae. Terminal chamber nearly smooth and conspicuously perforated; aperture central, of long oval form, slightly constricted at the middle (Jones, 1994; Ellis and Messina, 1968).

***Bolivinita quadrilatera* (Schwager) 1866.**

{= *Textularia quadrilatera* Schwager, 1866; *Bolivinita quadrilatera* (Schwager) Cushman, 1927;

Textularia (Bolivinita) Yabe and Hanzawa, 1929}

Test elongate, cuneiform in outline, compressed, sides flat, margins truncate and flaring in the microspheric generation, slowly diverging to subparallel in the megalospheric one, angles carinate, proloculus commonly apiculate, chambers of somewhat greater breadth than height, biserial in arrangement, sutures oblique, flush on the flat sides, slightly indented on the margins; wall calcareous, thin, optically radial, perforate, completely covered with fine pores but with some interspersed larger ones, surface smooth, slightly nodose or with a few short longitudinal ribs in the early stage, secondary calcite encrustation may form a thin veneer or may be localised as domelike mounds around the pores; aperture basal, elliptical, extending up the apertural face, one margin bending inward to form a folded toothplate that extends to the previous foramen, free part of the toothplate narrow and projecting through the aperture,

continuing as a rim bordering the opening. Mid Miocene to Holocene; Atlantic, Pacific, Indo-Pacific (McCulloch, 1977; Loeblich and Tappan, 1988; Jones, 1994).

***Bolivina earlandi* (Parr), 1950.**

{=*Bolivina punctata* (d'Orbigny) Brady, 1884; *B. beyrichi* (Reuss) Thalmann, 1932; *Brizalina. earlandi* (Parr) Barker, 1960.}

Test elongate, slender, about four and a half times as long as broad, oval in traverse section; chambers up to twelve in number, distinct, slightly inflated, in the adult about as twice as high as broad; sutures strongly curved, distinct, very slightly depressed; wall smooth, finely perforate, translucent; aperture a narrow, comma-shaped lit, at the inner margin of the lats formed chamber (Ellis and Messina, 1968; Jones, 1994).

***Bolivina spathuloides* Hofker, 1956 (plate 14).**

{= *Textularia variabilis* var. *spathulata* Williamson 1858; *Brizalina spathulata* (Williamson) 1858; *Bolivina dilatata* (Reuss)Brady, 1884; *B. beyrichi* (Reuss) Thalmann, 1932; *B. spathulata* (Williamson) Thalmann ,1932, Barker, 1960, van Marle, 1991; *B. (Brizalina) spathulata* (Williamson) Haynes 1973a.}

Test long and slender, much compressed, with sharp carinate margin, about three times as long as broad. Walls smooth and hyaline, with fine but distinct pores. These pores are found in the microspheric form only at the initial sutures of each chamber, mostly in a single row, but in the last formed chambers in several rows. In the megalospheric form the restriction of the basal suture to possess pores is gradually given up, and the last formed chambers are nearly totally covered with pores. Since the microspheric form always shows the more primitive characteristics it is obvious that the typical characteristic is the possession of pores at the initial suture. Chambers very numerous, about ten sets of biserial chambers in the megalospheric, thirteen of them in the microspheric generation. The chambers are low, and tend to grow backward near the margin with a sharp angle. Sutures strongly oblique, slightly depressed, somewhat more in the microspheric form than in the megalospheric form. As each chamber overgrows the former in the central line, The sutures show a sharp angle here. In the last formed chambers the aperture tends to become terminal, but it never abandons the inner suture. It is a narrow and low slit. The tooth is very slightly protruding from the aperture.

The free part of the tooth plate is reduced to a short tooth, with a sharp point, having only half of the height of the whole plate (Ellis and Messina, 1968; Jones, 1994).

***Bulimina marginata* (d'Orbigny) 1826 (plate 18).**

Test elongate ovate to subcylindrical, chambers triserially arranged, but later ones may be nearly centred as if tending to become uniserial, septa distinct, depressed; wall calcareous, finely to coarsely perforate, optically radial, surface smooth, but lower margin of chambers may be carinate, fimbriate, or spinose; aperture a loop extending up the face from the base of the last chamber, a free border having an elevated rim, and a fixed border continuous with an internal folded tooth plate that attaches to the inside chamber wall below the aperture, and has a smooth to dentate, flaring to enrolled and almost tubular free shank. Paleocene to Holocene; cosmopolitan (Ellis and Messina, 1968; Jones, 1994).

***Cancris auriculus* (Fichtel and Moll) 1798 (plate 16).**

{=*Cancris auriculatus* de Montfort, 1808; *Nautilus auricula* (Fitchel and Moll) Thalmann, 1932; *Pulvinulina oblonga* (Williamson) Brady, 1884; *C. oblongus* (Williamson) Barker, 1960}

Test elongate ovate to auriculate in outline, lenticular in section, periphery angled to carinate, chambers increasingly rapidly in breadth as added in a flaring trochospiral coil, sutures depressed, arched on the spiral side, nearly radial around the open umbilicus on the opposite side; wall calcareous, optically radial, perforate, but with an imperforate area above the apertural flap, surface smooth other than the peripheral keel; aperture a low interiomarginal opening on the umbilical side, with a broad apertural flap that begins at the base of the imperforate area extending across the opening to project over the umbilicus. Eocene to Holocene; cosmopolitan (Ellis and Messina, 1968; Jones, 1994).

***Cassidulina laevigata* (d'Orbigny), 1826 (plate 20).**

{*Cassidulina*, d'Orbigny 1826 = *Entrochus*, Ehrenberg, 1843; *Selenostomum*, Ehrenberg, 1858; *Lernina*, Khusid 1973; *Lernina*, Saidova 1975;

=*Entrochus septatus*, Ehrenberg, 1843; *Lernina micae*, Saidova, 1975}

Test lenticular to flattened and ovoid, periphery subangular to carinate, chambers biserially

arranged and plane of biseriality planispirally enrolled, commonly with umbonal boss of clear calcite, sutures radial to oblique, straight to curved, flush; wall calcareous, hyaline, optically granular, perforate, surface smooth, polished; aperture a narrow arched slit at the base of the apertural face and parallel to the peripheral margin, partially closed by an apertural plate, no internal tooth plate. Upper Eocene to Holocene; cosmopolitan (Loeblich and Tappan, 1988).

***Cassidulina subglobosa* (Brady), 1881.**

{*Cassidulina* Brady 1884, Thalmann, 1932, Barker, 1960 =*Globocassidulina* Voloshinova, 1960, Belford, 1966, Hermelin, 1989, Van Marle, 1991; *Bradynella* Saidova 1975.}
Test globular to lenticular, periphery rounded to acute, and may be carinate, chambers biserially arranged and enrolled, with zig-zag suture along the periphery, sutures radial to oblique, slightly depressed; wall calcareous, optically granular, perforate, surface smooth and polished or less commonly with low reticulations or papillae; aperture oval, slit like or curved, extending up the apertural face at an angle to the base, apertural tooth plate on posterior side, with cristate tooth projecting through the opening and with external apertural ridge. Upper Eocene to Holocene; cosmopolitan (Ellis and Messina, 1968; Jones, 1994).

***Cibicides kullenbergi* Parker, 1953.**

Test is large and biconvex, the spiral side being generally less elevated. the periphery is formed by a thickened imperforate rim, which is bluntly angled or rounded. Sutures are slightly depressed or flush with the surface. At the spiral side, they run obliquely and are nearly straight; at the umbilical side, they are radial, somewhat curved and meet in the centre of the test in an imperforate area. The last whorl is composed of ten to seventeen chambers, but in the smallest specimens there may be as few as eight (van Leeuwen, 1989).

***Cibicides refulgens* (de Montfort) 1808.**

{=*Cibicides* de Montfort, 1808, ref 2176 p.122.
=*Storilus* de Montfort, 1808, ref 2176 p. 130; type species: *Storilus radiatus* de Montfort, 1808.
=*Truncatulina* d'Orbigny, 1826, ref 2303 p. 278; type species: obj.; SD Galloway and Wissler, 1927, ref 1209 p.63

=*Planorbulina* (Truncatulina) Reuss, 1874, ref 2592 p. 113 (nom. transl.).

=*Truncatulina* (Cibicides) Yabe and Hanzawa, 1929, ref 3410 p. 142 (nom transl.).

Test attached to substrate, trochospiral and planoconvex, spiral side flat to concave, evolute, sutures thickened and may be elevated, strongly convex and involute umbilical side with depressed sutures, apertural face angular, periphery carnate; wall calcareous, optically radial, spiral side coarsely perforate, the pores being filled in earlier chambers by lamellar thickening of the wall, umbilical side finely perforate and apertural face and peripheral keel imperforate, surface smooth; aperture a low interiomarginal equatorial opening that extends a short distance onto the umbilical side but continues along the spiral suture on the spiral side. Paleocene to Holocene; cosmopolitan (Loeblich and Tappan, 1988).

***Cibicides ungerianus* (d'Orbigny), 1846 (plate 24).**

{*Rotalina ungeriana* d'Orbigny, 1846; *Anomalina wullerstorfi* Schwager, 1866; *Cibicides ungerianus* (d'Orbigny) Marks, 1951; *Cibicidoides ungerianus* (d'Orbigny) Agip Mineraria, 1982}

Test ventro-convex to biconvex, relatively thin, hyaline test wall, coarse perforation at the dorsal side. The chamber sutures are typically bent backwards near the periphery at the ventral side. The spiral suture is visible throughout its length; it is not obscured by dorsally secreted calcite (Verhallen, 1991).

***Cushmanina striatopunctata* Parker and Jones, 1865.**

{=*Lagena sulcata* var. *striatopunctata* Parker and Jones, 1865; *Lagena* Brady, 1884, Thalmann, 1932; *Oolina* Barker, 1960, van Marle, 1991.}(Jones, 1994)

***Cyclogyra lata* Scott, 1974.**

{=*Cyclogyra sp.* Sliter, 1968}

Planispiral, calcareous, tubular test, not divided into chambers after the proloculus. Slightly involute, each whorl being overlapped about 15% of its breadth by succeeding whorl. Whorls rapidly-enlarging, smooth, porcelaineous. Aperture simple, unmodified end of tube. Weak constrictions, or, in some specimens, faint growth-lines, may occur parallel to former apertural positions (Ellis and Messina, 1968).

***Dentalina baggi* Galloway and Wissler, 1927.**

{= Nodosaria pauperata d'Orbigny, Brady, 1884; Dentalina baggi Galloway and Wissler, Barker, 1960.}

Test elongate, slightly curved, circular in cross section, the initial chamber round, somewhat larger than those immediately succeeding; chambers inflated, closely appressed, somewhat irregularly increasing in size; sutures depressed, limbate, slightly curved; wall smooth, very finely perforate; aperture terminal, produced, round, radiate, situated near the concave side of the test (Ellis and Messina, 1968; Jones, 1994).

***Dentalina drammenensis* Feyling-Hanssen, 1964.**

{=*Dentalina californica* (Cushman and Gray), Cushman and McCulloch, 1950

=*Dentalina sp.*, Feyling-Hansses, 1954

=*Dentalina californica* Cushman and Gray, 1946}

Test small, elongate, circular in section, of nearly uniform diameter throughout, initial end with a very short spine; chambers few, 2-5, elongate, pyriform, uniserially arranged, latest chamber longer than the other, nearly three times as long as broad, initial chamber usually shorter than the other; sutures distinct, depressed, slightly oblique; wall calcareous, hyaline, finely and densely perforate; aperture terminal, eccentric, radiate with the slits slightly diverging at the end of the test; colour glassy to grayish (Ellis and Messina, 1968).

***Dentalina subsoluta* Cushman, 1923.**

{=*Nodosaria subsoluta* Cushman, 1923; *Nodosaria (Dentalina) soluta* Reuss Brady, 1884; *Dentalina soluta* (Reuss) Thalmann, 1932; *D. subsoluta* (Cushman) Barker, 1960, van Marle, 1991; *Nodosaria subsoluta* Cushman Hofker, 1976 (Jones, 1994).

***Dentalina trondheimensis* Feyling-Hanssen, 1964.**

Test elongate, often almost straight in the early portion, becoming arcuate and lobulate in the later, somewhat compressed laterally, more so in the early part than in the later, initial chamber terminating in a short spine or point which may be divided into two or three; chambers 6-10, uniserially arranged, of approximately equal height and breadth in the early

half of the test, later chambers becoming elongated and inflated, proloculus subglobular; sutures distinct, limbate, moderately oblique, flush with the surface in the early part of the test, depressed in the later; wall calcareous with radiate structure, translucent to hyaline, finely perforate, more densely in the later chambers than in the earlier, in an area around the aperture the wall seems to be almost imperforate and glassy; aperture terminal, at the peripheral angle, radiate with the relatively long slits somewhat divergent projecting (Ellis and Messina, 1968).

***Dentalina bradyensis* (Dervieux) 1894.**

{=*Nodosaria inornata* var. *bradyensis* Dervieux, 1894; *Nodosaria (Dentalina) communis* d'Orbigny Brady, 1884; *Dentalina communis* d'Orbigny Thalmann, 1932; *Nodosaria inornata* var. *bradyensis* Dervieux Thalmann, 1942; *Dentalina* cf. *communis* d'Orbigny Leroy, 1944a; *D. inornata* var. *bradyensis* (Dervieux) Barker, 1960; *D. bradyensis* (Devreiux) Hofker, 1976 (Jones, 1994).

***Dentalinoides canulina* Marie, 1941.**

Test elongate, straight to slightly arcuate, uniserial, circular in section, sutures horizontal; wall calcareous, hyaline radial in structure, with secondary lamination, perforate, surface smooth; aperture terminal, large, round, slightly eccentric in position and opening toward the concave side of the test (Loeblich and Tappan, 1988).

***Rosalina elegans* Hansen, 1970 (plate 35).**

Test trochospiral, planoconvex to concavoconvex. Spiral side convex. Umbilical side flat or concave, Umbilicus open and deep. 6-7 chambers in final whorl. Chambers somewhat inflated on both sides, especially on the umbilical side. General outline subcircular and slightly lobate. Periphery subacute to rounded. Sutures on the spiral side narrow, depressed and irregularly curved. Spiral suture depressed. Sutures on the umbilical side depressed, curved with the strongest sinus about midway between the umbilicus and the periphery. Aperture interiomarginal umbilical and confined to the umbilical side. It extends from near the periphery into the umbilicus below umbilical flaps which are somewhat twisted so that each flap covers the distal part of the preceding flap. Older apertures remain open into the umbilicus. There are sutural slits present in the umbilical area representing remnants of older

apertures. The flaps have slightly crenulate lips. Test wall composed of radiate, perforate calcite. The septa are monolamellar (Ellis and Messina, 1968; Jones, 1994).

***Ehrenbergina trigona* (Goes), 1896 (plate 21).**

{= *Ehrenbergina serrata* var. *trigona* Goes, 1896; *Ehrenbergina serrata* (Reuss) Brady, 1884, Leroy, 1944b; *E. bradyi* (Cushman) Thalmann, 1932; *E.serrata* var. *trigona* (Goes) Barker, 1960.}

Test differing from the typical with a much more compressed form of the test, the whole being very thin and broad, the angles at the sides are well developed and spinose, usually with numerous short spines below the main one at the angle, the early portion of the test often covered with numerous short spinose projections, wall rather coarsely perforate, test translucent (Ellis and Messina, 1968).

***Eponides punctatus* LeRoy, 1941 (plate 17)**

Test small, unequally biconvex, dorsally more convex than ventrally, periphery sharply rounded; chambers distinct, six or seven in last-formed whorl, enlarge very gradually as added; sutures distinct, slightly depressed, somewhat oblique both ventrally and dorsally; wall finely punctate on ventral side, coarser on dorsal side; aperture at base of last chamber midway between periphery and umbilicus (Ellis and Messina, 1968).

***Glandulina laevigata* d'Orbigny, 1846 (plate 28).**

{=*Nodosaria* (les Glandulines) *laevigata* d'Orbigny 1826; *Nodosaria (Glandulina)* d'Orbigny, 1839; *Nodosaria* (les Glandulines) d'Orbigny, 1826; *Glandulina* d'Orbigny, 1849; *Atractolina* von Schlicht, 1870; *Psecadium ellipticum* Neugeboren, 1856}

Test elongate, ovate, tapering at each end, circular in section, microspheric generation with tiny and biserially arranged early chambers and uniserial and rectilinear later chambers, megalospheric test uniserial throughout, chambers increasing rapidly in size as added, strongly overlapping previous chambers, septa commonly resorbed, possibly as each new chamber is added or at the time of reproduction, leaving only a single internal open cavity, external sutures distinct, flush; wall calcareous, radial, commonly opaque except for a narrow hyaline and translucent band just below the aperture, surface smooth or less commonly finely striate;

aperture terminal, radiate, provided with a short, straight entosolenian tube. Paleocene to Holocene; cosmopolitan (Loeblich and Tappan, 1988). May develope an apical spine at greater water depths (Bandy, 1963).

***Gyroidina altiformis* (R.E. & K.C. Stewart), 1958 (plate 29).**

{=*Gyroidina soldanii* d'Orbigny, var. *altiformis* R.E. & K.C. Stewart, Jour. of Pal. 1904, vol. 4 no. 1, p. 67, pl. 9, fig. 2

=*Gyroidina altiformis* R.E. & K.C. Stewart, Resiz Micropal. vol. 4, no. 3, 1958, p. 306.}

Test free, calcareous, circular in contour, trochoid, planoconvex to slightly biconvex; periphery gently lobulate, bluntly angled; wall smooth, finely perforated, polished; spiral side evolute, flattened, almost three whorls of comparatively small chambers with raised curved sutures; umbilical surface elevated, involute, one whorl of nine uniform chambers, sutures radiate, flush,; umbilical area depressed, filled with shell and lobed, medial ends of chambers dipping into depressed area, apparently covering small slits, secondary apertures; primary aperture in form of a low arch beginning about one third of distance above periphery and continuing almost to umbilicus (McCulloch, 1977).

***Gyroidina orbicularis* d'Orbigny, 1826.**

{=*Gyroidina* cf. *G. neosoldanii* not Brotzen Parker, 1958.}

Broadly rounded periphery, like G. umbonata, but axially compressed test and more than 7 chambers per whorl. The sutures are not at all incised, giving the test a perfectly smooth appearance (Verhallen, 1991).

***Gyroidina subsoldanii* (McCulloch), 1977 (plate 38).**

Test free, calcareous, circular in contour, trochoid, symmetrically biconvex; periphery gently lobulated, rounded; wall smooth, glossy, semihyaline, finely perforated; spiral side centrally in form of glossy mound, detailed structure lacking, last formed whorl showing about ten small chambers, sutures slightly depressed, radiate; umbilical side less opaque, involute; sutures radiate, curved slightly, flush; umbilicus closed, clearing solution outlines sharply the over lapping internally to present a stellate outline externally; primary aperture closer to periphery than umbilical area (McCulloch, 1977).

***Gyroidina umbonata* (Silvestri), 1898 (plate 37).**

{=*Rotalia soldanii* d'Orbigny var. *umbonata* Silvestri, 1989; *Gyroidina umbonata* (Silvestri) Parker, 1958, Wright, 1978, Agip Mineraria, 1982}

Small sized *Gyroidina* with short spiral, only 4-6 chambers per whorl and a well rounded periphery. Slightly incised sutures. Points of junction of chamber sutures and spiral suture and somewhat depressed, giving the impression of secondary apertures, as in *Oridosalis*. Actual openings, however, cannot be traced (Verhallen., 1991).

***Hanzawaia boueana* (d'Orbigny), 1846.**

{=*Truncatulina boueana* d'Orbigny, 1846; *Cibicides boueana* (d'Orbigny) Marks, 1951; *Hanzawaia boueana* (d'Orbigny) Wright, 1978, Van der Zwaan, 1982.}

Plano-convex test form, dorsal side sometimes slightly concave. Coarse pores, in most specimens only dorsally present. Hyaline sutures and keel, the latter strongly developed. The youngest chamber is often disproportionally volumous (Verhallen, 1991).

***Hoeglundina elegans* (Brotzen), 1948.**

{= *Rotalia elegans* d'Orbigny, 1826; *Epistomina (Hoeglundina)* Salaj, 1984}

Test trochospiral, close coiled, biconvex, chambers enlarging gradually, eight or nine in the final whorl, internal partition flat, earlier ones resorbed as new chambers are added so that only the final chamber contains an intact partition, sutures curved backward at the periphery on the spiral side, straight and oblique on the umbilical side, periphery subacute, carinate; wall calcareous, aragonitic, radial, lamellar, finely perforate, surface smooth; aperture lateromarginal and slitlike, parallel to the peripheral keel and opening on the umbilical side, those of earlier chambers commonly closed by shell material, may have a secondary interiomarginal aperture, intercameral foramen interiomarginal. Paleocene to Holocene; cosmopolitan (Loeblich and Tappan, 1988).

***Hyalinea balthica* (Hofker), 1951 (plate 26).**

{=*Nautilus balthicus* Schroter, 1783

Hyalinea Hofker 1951=*Hofkerinella* Bermudez, 1952; *Hyalinia* Agassiz, 1837; *Hyalina* Schumacher, 1817}

Test discoidal, very low trochospiral to nearly Planispiral, semi-evolute on both sides, about two slowly enlarging whorls, eight to ten chambers in the final whorl, umbilical margin of the chambers with a small umbilical flap, sutures radial, slightly curved, limbate, elevated, the thickened sutures grading into the broad imperforate peripheral carina, periphery angular; wall calcareous, optically radial, finely perforate, surface smooth, except for the elevated imperforate septa and keel and occasional pustules in the umbilical region; aperture a low equatorial and interiomarginal arch, bordered above by a narrow lip, a low slit continuing laterally beneath the folium in the umbilical region and around the spiral suture on both sides of the test, chamber lumen communicating with the exterior through a small rounded opening beneath the folium, apertures remaining open for a few chambers before being closed by lamellar thickening. Pleistocene to Holocene; Atlantic; Pacific; Mediterranean; Europe; USA (Loeblich and Tappan, 1988).

***Lagena laevis* (Montagu) var. *baggi* Cushman and Gray, 1946.**

Variety differing from the typical in the more nearly spherical body of the test, shorter neck, and distinct lip. This variety is even more common than the typical form (Ellis and Messina, 1968).

***Lagena striata* (d;Orbigny) var. *basisenta* Cushman and Stainforth, 1947.**

{=Lagena strumosa Reuss 1874}

Variety differing from the typical form in having the costae near the base ending in short, spinose projections (Ellis and Messina, 1968).

***Lagena vulgaris* Williamson var. *spinoso-marginata* Jones, 1874.**

Shell sub-globular, lenticular, or ovoid, smooth, densely foraminated. External neck long, straight, and narrow, passing abruptly from the upper end of the structure, and patulous, lipped and sometimes 'scalloped' round its outer rim. The peripheral margin of the shell is ornamented with a wide single or double layer of shell substance, which passes two-thirds up the neck, and becomes incorporated in its walls. This band is single, and of film like transparency, and is strengthened by a series of long, slender, straight spines, which radiate from the circumference of the shell, and form a single and parallel row round the flask. At the

middle of this base these spines become rather longer and somewhat bent; and at the anterior extremity, near the point of insertion of the neck tube, they are deficient, their place being supplied by long filamentous appearances, which are apparently minute canals. The walls are very coarsely foraminated, and the tubular neck considerably elongated, being about once and a half the length of the ovoid portion (Ellis and Messina, 1968).

***Lenticulina calcar* (Linne) 1767.**

{=*Nautilus calcar* Linne, 1767;

Lenticulina = *Cristellaria* Brady, 1884; *Robulus* Thalmann 1932 and Leroy 1944b; *Lenticulina* Barker, 1960, Hofker, 1976 and van Marle, 1991.}

Test subcircular in outline, lenticular in side view, closely coiled, distinctly umbonate; periphery sharply angled with keel, with a short spine projecting from each chamber 5-6 chambers in last whorl; suture gently curved, slightly limbate; wall smooth; aperture radiate, with a ventral slit (Jones, 1994).

***Loxostomina limbata* (Brady), 1881.**

{=*Bolivina limbata* Brady, 1881, Thalmann, 1932, 1933a; *Loxostomum* Thalmann, 1942, Barker, 1960; *Loxostomoides* Barker, 1960; *Rectobolivina* Belford, 1966, van Marle, 1991.}

Test elongate, tapering, compressed, more or less twisted, margin angular or only slightly rounded, sinuate. Sutures irregularly curved, limbate, especially near the points of contact of the two series of segments on both faces of the shell (Ellis and Messina, 1968; Jones, 1994).

***Miliolina caucasica* Bogdanovich, 1947.**

{=Tschokrakella Bogdanovich, 1969, 1965.}

Test narrow, elongate, chambers one-half coil in length, early chambers in quinqueloculine arrangement, then planispiral or with planes slightly more than 180° apart to result in a sigmoid appearance in section, chambers strongly produced at the aperture, resulting in a very long elongate test; wall calcareous, porcelaineous, surface smooth to coarsely costate; aperture terminal at the end of the elongate neck, ovate to slit like, without a tooth Loeblich and Tappan, 1988).

***Miliolina reussi* Bogdanovich, 1947.**

{=Varidentella Łuczkowska, 1972.}

Test ovate in outline, chambers one-half coil in length, early stage quinqueloculine to cryptoquinqueloculine, axis of coiling may change by 90° after the early stage but later return to the original axis, three, four, or five chambers may be visible from the exterior, chambers without a floor; wall calcareous, imperforate, porcelaineous; aperture rounded to slit like, with narrow to broad tooth, or none (Loeblich and Tappan, 1988).

***Miliolinella subrotunda* (Montagu), 1803 (plate 41).**

{=*Vermiculum subrotundum* Montagu, 1803; *Miliolinella* Wiesner, 1931; *Renoidea glabra* Brown, 1977; *Pateoris* Loeblich and Tappan, *1953; Quinqueloculina subrotunda* (Montagu) forma *hauerinoides* Rhumbler, 1936=*Miliolinella subrotunda* (Montagu); *Scutuloris* (Miliolinella) Cherif, 1973; *Pippinoides perplexa* McCulloch, 1977; *Neophthalmina oregonensis* McCulloch, 1977}

Test ovate in outline, flattened, periphery rounded, early stage quinqueloculine, later planispiral, chambers without a floor, added alternately as in Massalina or may have slightly more than two chambers in the final whorl, from four or five to as many as seven chambers visible from exterior; wall calcareous, imperforate, porcelaineous; aperture an arch, terminal on the final chamber, with a broad and low apertural flap. M. Miocene to Holocene; cosmopolitan (Loeblich and Tappan, 1988).

***Nodosaria* (les Dentalines) *cuvieri* d'Orbigny, 1826.**

{= *Dentalina* Risso, 1826; *Nodosaria* (les Dentalines) d'Orbigny 1826; *Nodosaria (Dentalina)* d'Orbigny 1839.}

Test elongate, arcuate, uniserial, proloculus apiculate, chambers cylindrical to ovate, enlarging gradually as added, sutures horizontal; wall calcareous, hyaline, radial in structure, with secondary lamination, surface with numerous longitudinal costae; aperture terminal, radiate. L. Cretaceous to Holocene; cosmopolitan (Loeblich and Tappan, 1988)

***Oolina apiculata* Reuss, 1851.**

{=*Lagena (Reussoolina)* Colom, 1956; *Reussoolina* R.W. Jones, 1984.}

Test unilocular, ovate; wall calcareous, hyaline, optically radial, surface smooth but may have an apiculate base; aperture rounded, bordered by radial grooves, slightly produced but without a distinct neck. L.Jurassic to Holocene; cosmopolitan (Loeblich and Tappan, 1988).

***Oolina* cf. *squamosa* (Montagu) McCulloch, 1977.**

Test free, calcareous, globulose to pyriform and flask-shaped, sometimes slightly compressed; initial end usually broadly rounded with greatest width below or at midpoint; apertural end drawn out or otherwise; globulose form usually more areolar in its ornamentation with flask-shaped forms more and smaller intra-areolar spaces tending to become organized into more nearly vertical columns suggesting "fish scales". The reticular network has a hyaline plate-like margin with bases becoming slightly thicker; entosolenian tube centred, straight, diameter small, length less than half that of cavity; aperture small round with reticular network or a narrow smooth hyaline area immediately below opening (McCulloch, 1977).

***Procerolagena gracillima* Williamson, 1848.**

{=*Lagena gracilis* Williamson, 1848

=*Procerolagena* Puri, 1953}

Test elongate, fusiform, highly drawn out on both sides; with a long neck and expanded lip, without an entosolenian tube; aperture terminal. Surface of the test ornamented with strong longitudinal striations, ribs or ridges (Ellis and Messina, 1968).

***Pseudofissurina mccullochae* R.W. Jones, 1984.**

Test small, rounded to ovate in outline, slightly compressed, but with low convex sides and carinate periphery, commonly tricarinate, with the median keel being most prominent; wall calcareous, perforate, hyaline radial, surface smooth and unornamented other than the peripheral keels; aperture subterminal, crescentic, one margin somewhat produced but does not form a hood like that of Parafissurina, internally provided with a long entosolenian tube attached to the dorsal wall and extending back nearly to the base of the chamber before flaring terminally. Oligocene to Holocene; cosmopolitan (Loeblich and Tappan, 1988).

***Pyrgo depressa* d'Orbigny, 1826.**

(var. tomiyensis)

Test in front view nearly circular, compressed, toward the periphery extending out into a thin carina, in end view ellipsoid, the edge angled and drawn out into the carina; ventral chamber is very small, about two-fifths as large as dorsal chamber, not circular; wall smooth, dull white; aperture broad, without a neck, the tooth on ventral side wide, extending nearly the whole width of the aperture, and in end view nearly filling the opening, leaving the actual aperture but a narrow slit-like opening (Ellis and Messina, 1968).

***Pyrgo laevis* Defrance, 1824.**

{= *Biloculina bulloides* d'Orbigny, 1826, Cushman, 1917; *Pseudobiloculina* Cherif, 1970; *Biloculina oblonga* d'Orbigny, 1839; *Pyrgoides* Hofker, 1976; *Biloculina ringens* (Lamarck) var. *denticulata* Brady, 1884}

Test ovate in outline, compressed through the midpoint of the opposing chambers one-half coil in length, microspheric generation with nearly quinqueloculine to cryptoquinqueloculine arrangement, adult biloculine; wall calcareous, imperforate, porcelaineous; aperture at the end of the final chamber, ovate, with a short bifid tooth. U.Eocene to Holocene; cosmopolitan (Loeblich and Tappan, 1988).

***Pytine parthenopeia* Moncharmont Zei and Sgarrella, 1978.**

Test unilocular, ovate to pyriform, circular in section, with distinct neck; wall calcareous, hyaline, optically radial, translucent, double, with inner thicker, smooth layer and outer layer consisting of long flat strips or ribs supported by pillars perpendicular to the wall surfaces; elongate apertural neck is an extension from the inner wall layer, and the outer layer may not continue onto the neck, or only a few of the longitudinal ribs of the outer layer may continue up the neck to the ringlike apertural rim, the longitudinal ribs on the neck connected and supported by traverse plates that occupy the position of the pillars of the main chamber wall; aperture rounded, at the end of the elongate neck. Plaistocene to Holocene; Mediterranean; Pacific (Loeblich and Tappan, 1988).

***Quinqueloculina elongata* Natland, 1938.**

Test twice as long as broad; chambers with concave sides bluntly keeled; walls smooth, porcelaineous; sutures depressed, distinct; apertural end slightly extended to form small circular opening with a small bifid tooth (Ellis and Messina, 1968).

***Quinqueloculina lamarkiana* d'Orbigny, 1839 (plate 43).**

Test elliptical, somewhat triangular in cross section; periphery angular. Chambers somewhat angled, slightly concave, earlier chambers strongly overlapping, quinqueloculine throughout. Sutures distinct, slightly depressed. Surface smooth, matte. Aperture small and somewhat rounded, with a bifid tooth (Ellis and Messina, 1968).

***Quinqueloculina multimarginata* Said, 1949 (plate 42).**

Test short and broad, oval in outline; chambers angular, usually all peripheral edges of the chambers of the last whorl with distinct thin keels; sutures very indistinct, curved; wall smooth, polished, occasionally with fine irregular costae over part of the test; aperture terminal, rounded, without a neck or lip, with a short tooth (Ellis and Messina, 1968).

***Robertina bradyi* Cushman and Parker, 1936.**

{=Bulimina subteres Brady,1884}

Test somewhat longer than broad, fusiform, initial end bluntly pointed, apertural end broadly rounded; chambers slightly inflated, 4-5 pairs in the last formed whorl, increasing rapidly in size as added, the next to the last chamber in the series with the apertural one meeting the median line; sutures distinct, slightly depressed, strongly limbate; wall smooth, polished, fairly thick; aperture very elongate, open, only slightly curved in the median line of the axis, supplementary axis short, fairly high (Ellis and Messina, 1968).

***Rosalina globularis* d'Orbigny, 1826.**

{=*Rosalina* d'Orbigny, 1826; *Turbinolina* d'Orbigny, 1839; *Pararosalina densitiva* McCulloch, 1977}

Test planoconvex to concavoconvex, trochospiral, chambers broad, low, and crescentic and all visible on the flat to concave spiral side, subtriangular and strongly overlapping on the

gently convex umbilical side, sutures of early chambers thickened and flush, later ones depressed, strongly oblique on the spiral side, curved and nearly radial on the umbilical side, umbilicus closed, periphery carinate; wall calcareous, surface smooth; aperture a low interiomarginal arch in a slight re-entrant at the base of the final chamber midway between the umbilicus and periphery on the flattened spiral side. Holocene; Pacific Ocean (Loeblich and Tappan, 1988). The test of Rosalina globularis becomes more rounded in low nutrient environments. Where nutrients are in abundance the test is more oval in shape (Showers, 1980).

***Sigmoilina tenuis* (Cžjžek) 1847.**

{=*Quinqueloculina tenuis* Cžjžek, 1847; *Sigmoilina tenuis* Cžjžek, 1892.}

Test much compressed, broadly fusiform, periphery rounded; length about twice width, thickness less than one-third width; wall polished, porcelaineous, imperforate, thin, semihyaline in part; quinqueloculine organisation of initial chambers produces a slightly biconvex end view; sutures depressed; basal end of test extended to narrowly rounded, anterior end tapered into a short neck or a flush to oblique end; no visible tooth observed (McCulloch, 1977).

***Sigmoilopsis schlumbergeri* Finlay, 1947.**

{=*Sigmoilina schlumbergeri* Silvestri, 1904.}

Test ovate in outline, chambers one-half coil in length, with rapidly changing planes in the early stage resulting in two spiralling series that appear sigmoid in section, gradually becoming planispiral in the adult, chambers with floors, chamber lumen narrow; wall thick, porcelaineous but enclosing a large quantity of agglutinated quartz particles, sponge spicules, and shell fragments; aperture terminal, rounded, with a small tooth. Miocene to Holocene; Europe; Atlantic; Caribbean; Australia; New Zealand (Loeblich and Tappan, 1988).

***Sphaeroidina bulloides* d'Orbigny, 1826.**

{=*Sexloculina haueri* CžJžek, 1848}

Test subglobular, coiling variable, depending on position of aperture, each of the few hemispherical and strongly embracing chambers centred over the preceding aperture, median

plane of later chambers diverging from that of earlier ones, either in an alternating manner or in a relatively regular spiral; wall calcareous, very finely perforate, optically radial, surface smooth; aperture a crescentic opening near the base of the chamber, commonly above the junction of three earlier chambers, bordered by a narrow lip, and may have a simple flaplike or bifid tooth. U. Eocene to Holocene; cosmopolitan (Loeblich and Tappan, 1988).

***Spirillina vivipara* Ehrenber, 1843.**

{=*Spirillina* Ehrenberg, 1843; *Spirulina* Bory, 1826; *Spirulina* Ehrenberg, 1841; *Arspirillinum* Rhumbler, 1913.}

Test discoidal, globular proloculus followed by a gradually enlarging enrolled, undivided tubular second chamber, earliest few whorls may be in a low trochospiral, later ones planispiral, commonly four to nine closely appressed whorls, tubular chamber may not be entirely cylindrical but lies against the periphery of the preceding whorl, and final part of the last whorl may bend at a right angle so that the aperture opens into the umbilical depression, asexually formed gamont with smaller test and smaller proloculus than those of sexually produced agamont; wall calcareous, hyaline, appearing optically as a single calcite crystal with c-axis oriented perpendicular to the plane of coiling or less commonly parallel to this plane, others may have a transitional orientation with the c-axis at first perpendicular to the coiling axis and becoming progressively oblique to this in successive whorls, or may have a heicoidal structure, with c-axis at an angle of about 45° to the radii from the centre of the test, or may consist of a mosaic of crystals in which the c-axes a variously oriented, the calcite being deposited over an organic membrane; surface commonly with numerous pores or pseudopores of limited distribution; aperture rounded to crescentic, at the open end of the tubular chamber; gamont individuals uninucleate, agomont multinucleate, asexual multiple fission occurs within a reproductive cyst formed by the animal, during sexual reproduction two or three individuals are enclosed within a fertilization cyst, the syzygy ensuring gemetic fusion. U.Triassic to Holocene; cosmopolitan (Loeblich and Tappan, 1988).

***Spiroloculina depressa* d'Orbigny, 1826 (plate 40).**

Test ovate to fusiform in outline, with flattened sides and truncate periphery, microspheric proloculus followed by planispirally wound tubular second chamber of one whorl in length,

later part of microspheric test and all of megalospheric test with chambers one-half length added in a single plane; wall calcareous, imperforate, porcelaineous; aperture at the open end of the final chamber, with simple or bifid tooth, commonly slightly produced on a short neck. U. Cretaceous to Holocene; cosmopolitan (Loeblich and Tappan, 1988).

***cf. Suggrunda porosa* Hoffmeister and Berry, 1937.**

Test small, tapering, biserial throughout, chambers broad and low, enlarging gradually as added, lower margin abruptly angled, overhanging the slightly oblique and depressed sutures; wall calcareous, optically granular, finely perforate, somewhat larger pores near the basal margin of the chambers, surface smooth but with pustulose to spinulate lower margin; aperture an asymmetrical hooklike to comma shaped opening (Loeblich and Tappan, 1988).

***Textularia pseudocarinata* Cushman, 1921.**

{=*Textularia carinata* Brady, 1884}

The carina is broad and has very prominent denticulations and a heavy layer of agglutinated material above the sutures connecting across the middle and united with the material of the carina at either side (Ellis and Messina, 1968).

***Triloculina tricarinata* d'Orbigny 1826 (plate 44).**

The test is as long as broad and triangular in end view. Three arcuate chambers are triloculine internally, broadest at the middle, and becoming narrow towards the proximal and distal ends. The depressed sutures are distinct. The periphery is angled. The smooth porcelaineous wall is polished. The distal end of the last chamber is produced typically to form a cylindrical neck with a phialine lip and oval to rounded aperture (Ellis and Messina, 1968).

***Uvigerina hollicki* (Thalmann) 1950 (plate 19).**

{= Uvigerina tenuistriata (Reuss) Brady 1884, Thalmann 1932; U. hollicki (a new name for U. peregrina var. bradyana Cushman 1923, not U. bradyana Fornasini 1900); U. cushmani (Todd) Barker, 1960}(Jones, 1994).

***Uvigerina porrecta* (Brady), 1879 (plate 33).**

{= *Siphouvigerina cf. porrecta* Brady 1879; *Uvigerina porrecta* (Brady) var. *fimbriata* Sidebottom, 1918}

Test elongate , early chambers triserially arranged and closely appressed, later loosely triserial and then biserial, upper chamber surface broadly domed to a carinate margin and sharply undercut chamber base a slight distance above the preceding suture, resulting in a series of umbrella like and loosely appressed chambers, each attached just above the preceding apertural neck, sutures constricted; wall calcareous, perforate, surface smooth other than the fimbriate carina at the lower, border of the chambers; aperture terminal and rounded, at the end of a short tubular neck and bordered with a phialine lip (Loeblich and Tappan, 1988).

***Uvigerina proboscidea* Schwager, 1866 (plate 25).**

{*Uvigerina asperula* var. *ampullacea* Brady, 1884}

Hispid to pustulous ornamentation. Most typical, however, is the flask-like shape of the chambers, especially those in the upper part of the test. The chamber form of *U. proboschidea* remarkably resembles the aberrant pigmea (hispid, flask-shaped) end-chamber occurring in *U. peregrina* (Verhallen, 1991).

***Vaginulinopsis reniformis* (d'Orbigny), 1846.**

{=*Cristellaria reniformis* d'Orbigny 1846

Vaginulinopsis = *Cristellaria* Brady, 1884; *Lenticulina* Thalmann, 1932; *Astacolus* Thalmann, 1933a and Barker, 1960.}(Jones, 1994).

***Vaginulinopsis tasmanica* (Parr), 1950.**

{= *Cristellaria schloenbachi* (Reuss) Brady, 1884; *Lenticulina schloenbachi* (Reuss) Thalmann, 1932; *Astacolus schloenbachi* (Reuss) Thalmann, 1933a; *Vaginulinopsis tasmanica* (Parr) Barker, 1960.

Test elongate, slipper-shaped to vaginuliniform, variable in width, moderately compressed, ovoid in transverse section with the inner side the broader; early chambers in an open coil, later chambers becoming uncoiled and inflated, increasing rapidly in size as added; in the longer specimens the last three or four chambers are of nearly equal height and oblique,

parallel to one another; sutures distinct, slightly depressed in the later stages; wall smooth, of medium width, and finely perforate; aperture radiate and sometimes elongate instead of round (Ellis and Messina, 1968; Jones, 1994).